UNIVERSIDADE FEDERAL DE SÃO CARLOS
CENTRO DE CIÊNCIAS BIOLÓGICAS E DA SAÚDE
Programa de Pós-Graduação em Genética Evolutiva e Biologia Molecular

EFICÁCIA DO [10]-GINGEROL CONTRA METÁSTASES DE CÂNCER DE MAMA: ESTUDOS *IN VITRO* E *IN VIVO* EM CAMUNDONGOS

ANA CAROLINA BAPTISTA MORENO MARTIN

SÃO CARLOS
2015

EFICÁCIA DO [10]-GINGEROL CONTRA METÁSTASES DE CÂNCER DE MAMA: ESTUDOS *IN VITRO* E *IN VIVO* EM CAMUNDONGOS

UNIVERSIDADE FEDERAL DE SÃO CARLOS
CENTRO DE CIÊNCIAS BIOLÓGICAS E DA SAÚDE
Programa de Pós-Graduação em Genética Evolutiva e Biologia Molecular

EFICÁCIA DO [10]-GINGEROL CONTRA METÁSTASES DE CÂNCER DE MAMA: ESTUDOS *IN VITRO* E *IN VIVO* EM CAMUNDONGOS

Tese de doutorado apresentada ao Programa de Pós-Graduação em Genética Evolutiva e Biologia Molecular, do Centro de Ciências Biológicas e da Saúde da Universidade Federal de São Carlos, como parte dos requisitos para a obtenção do título de Doutor em Genética Evolutiva e Biologia Molecular.

ANA CAROLINA BAPTISTA MORENO MARTIN

SÃO CARLOS
2015

Ficha catalográfica elaborada pelo DePT da Biblioteca Comunitária UFSCar
Processamento Técnico
com os dados fornecidos pelo(a) autor(a)

M379e

Martin, Ana Carolina Baptista Moreno
Eficácia do [10]-gingerol contra metástases de câncer de mama : estudos in vitro e in vivo em camundongos / Ana Carolina Baptista Moreno Martin. -- São Carlos : UFSCar, 2015.
108 p.

Tese (Doutorado) -- Universidade Federal de São Carlos, 2015.

1. Câncer de mama. 2. Gingerol. 3. Metástase. 4. Cérebro. 5. Resveratrol. I. Título.

UNIVERSIDADE FEDERAL DE SÃO CARLOS

Centro de Ciências Biológicas e da Saúde
Programa de Pós-Graduação em Genética Evolutiva e Biologia Molecular

Folha de Aprovação

Assinaturas dos membros da comissão examinadora que avaliou e aprovou a Defesa de Tese de Doutorado da candidata Ana Carolina Baptista Moreno Martin, realizada em 20/03/2015:

Profa. Dra. Heloisa Sobreiro Selistre de Araujo
UFSCar

Profa. Dra. Márcia Regina Cominetti
UFSCar

Profa. Dra. Fernanda de Freitas Anibal
UFSCar

Prof. Dr. Andrei Leitão
IQSC/USP

Profa. Dra. Enilza Maria Espreafico
USP

Profa. Dra. Iracilda Zeppone Carlos
UNESP

“O período de maior ganho em conhecimento e experiência é o período mais difícil da vida de alguém.”

Dalai Lama

Life is short, enjoy it!

Carpe Diem!

Dedico este trabalho em especial ao meu pãe, minha irmã Patrícia, meu irmão Fernando e minha querida mãedrasta Darlene!

Dedico também a minha segunda família, meus queridos amigos/irmãos Bruna e Diogo.

Amo todos vocês.

AGRADECIMENTOS

Primeiramente gostaria de agradecer todo o suporte e apoio de minha família: Ao meu pai que na verdade representa também a minha mãe, por isso, carinhosamente o chamo de pãe!

A minha nova mãe Darlene, que me ajuda de todas as formas possíveis... não poderia pedir por uma mãedrasta melhor.

Aos meur irmãos, Paty e Fernando, que sempre estão presentes me escutando e me ajudando.

Ao meu cunhado querido Ale, que conseguiu me ajudar até na tese! E a Vic por ser essa menina tão meiga e fazer meu irmão feliz, assim como o Ale faz para Paty.

Não posso deixar de agradecer minha mãe que mesmo ausente sempre me incentivou a fazer o que gostava...

A meus avós, Vó Ana, Vô e Vó Dirce, que sempre me apoiaram me perguntando como estava a escola! =)

Agradeço também a minha eterna chefe-mor, Helo, por ter me aceitado há dez anos e me aguentar até hoje, sem contar por todo o conhecimento passado e sua amizade.

A Márcia, minha chefinha, que me orienta também há dez anos, por todos os perrengues que passamos e por toda alegria que nossa amizade trouxe! Meu mais sincero, Obrigada!

Ao laboratório de metástase no Peter MacCallum, Melbourne – Austrália! Por terem me acolhido tão bem e me feito me sentir em casa mesmo tão distante... Meu obrigada ao meu querido e mais recente chefe Norm! My special thanks for all the beers and knowledge that you passed me...

And thanks for everyone in the lab: Robin, the big boss, Phoebe, Soo, Gen, Lara, Selda, Ash, Cameron, Fabian, Tonje, Kara, Kathryn, Jess, Judy, Allan, Anannya, Matt. But specially, thank you Agi and Ryan for your friendship.

A Rebeka, ou melhor, Rebeskoviski, obrigada por tudo! Por essa pessoa honesta, sincera, ingênua, inteligente, por tudo... me faz acreditar cada dia mais como a pesquisa pode ser bem feita. Não poderia pedir por uma melhor companheira de lab no outro lado do mundo e uma melhor roommate!Obrigada!

A Bela e Lucas, pela amizade sem querer, por causa de um elevador e a mesma língua... Muito obrigada, Melbourne não teria sido tão bom quanto foi se não fosse pela amizade de vocês...

A Bruna e Diogo, meus amigos, irmãos por escolha... sem o apoio de vocês eu não seria quem eu sou. Muito, mas muuuuuito obrigada! Amo vocês! E que venham mais 15 anos de amizade.

Aos meus segundos pais, Tio Mauro e Tia Walkíria, palavras não descrevem o carinho que tenho por vocês, simplesmente, Obrigada!

A minha segunda família: todos do camping! Em especial a Angela que também se tornou uma segunda mãe!

Aos meus amigos Carinna, Dani e sua família por me acolherem tão bem em São Carlos, a Elaine querida amiga e seu marido e irmão, obrigada!

A república do Cogu: Djava, Giz e Gustavo, simplesmente por me aguentarem nessa reta final do doc. Mas meu especial obrigada ao Gu, que me ajudou, me ouviu falar, reclamar, chorar e se tornou essa pessoa tão especial, Obrigada!

Aos amigos e colegas de Departamento: Leo (Xuleu), Keico (parceira de bar e viagens), Charles, Salsicha, Anderson, Fabio, Ju, Val, Victor, Karina, Bruna, Dai, Luciane, Luisa, Marina, Cris, Tereza, Izabella, Bárbara, Carla, Tiago e aos professores Verzola e Gerson.

Ao LBBM pelos 10 anos de amizade e trabalho: Sabrina (mais nova parceira e ouvinte, uma pessoa que me ajudou demais nessa fase final, te admiro muito, obrigada!), Monica, Milene, Tais, Gra, Uliana, Rafa, Leo, Kelli, Paty loca, Patty e Bete! E ao meu escravinho Antonio, você tem um futuro brilhante a sua frente, obrigada!

Ao LABEN que me ajudou tanto nessa empreitada de produtos naturais, muito obrigada! Um especial obrigado à Mandinha, quem admiro muito e me ajudou em todos os momentos.

Ivanildes, secretária da pós, meu obrigada por toda ajuda e cafés nesses últimos anos!

Aos meus queridos amigos, Aninha, Du e Wesley, obrigada pela nossa amizade que mesmo estando longes nada mudou!

Marcelo, obrigada pela ajuda, almoços, jantares, pela parceria... Bio-04!

Aos amigos da velha guarda, João Gu, Renan, Lamer, Ligia, Con, Erica e Tuts; obrigada pela amizade incondicional apesar da distância e falta de tempo!

Agradeço também ao apoio financeiro do CNPq no Brasil, A CAPES que me proporcionou um sonho, morar "overseas" e trabalhar em um laboratório de ponta.

Obrigada!

Obrigada!!!

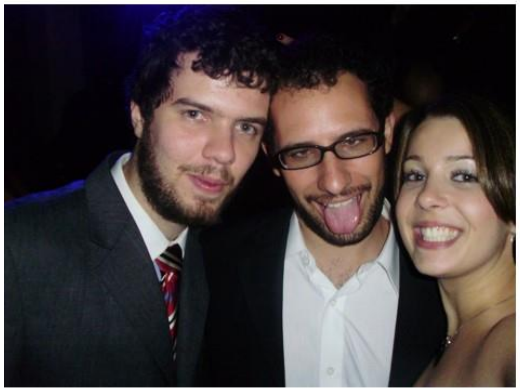

RESUMO

O câncer de mama é o que mais afeta as mulheres no Brasil e no mundo, entre os tipos de câncer de mama, o triplo negativo TNBC (*Triple Negative Breast Cancer*), que não expressa nenhum receptor hormonal, corresponde a 20% dos casos e apresenta recidivas em três anos. Entretanto, a maior causa de morte no câncer é devido a formação de metástases. O TNBC possui uma maior propensão a metástases pulmonares e cerebrais. Além disso, atualmente poucos tratamentos estão disponíveis. Buscas para novos medicamentos alvo para o TNBC e com menos efeitos colaterais são de grande importância para o tratamento dessa doença. Produtos naturais são fontes ricas em moléculas com atividades antitumorais, dentre elas os gingeróis, presentes no gengibre e o resveratrol (RSVT), presente nas uvas. Entretanto, pouco se sabe da atividade antitumoral do [10]-gingerol (10G). Este trabalho teve como objetivo investigar o potencial uso do 10G como molécula antimetastática em experimentos *in vitro* e *in vivo*. Neste trabalho verificou-se a atividade antiproliferativa do 10G e do RSVT em diversas linhagens de câncer de mama (4T1BM2, 4T1BM2 shRNAβ3, 4T1Br4, MDA-MB-231, MDA-MB-231 BrM) e um controle de célula normal, a bEnd.3. Os produtos naturais (PNs) usados afetam a morfologia celular nas células tumorais e o RSVT é capaz de inibir a adesão e migração via vitronectina. O 10G induziu apoptose da linhagem 4T1Br4 através da via extrínseca, com o aumento da expressão de casspase-9, -3 e -7; induziu a parada do ciclo celular nas fases G1 e sub G0. Em modelos de metástase *in vivo* o 10G inibiu o crescimento do tumor primário e de metástases pulmonares, além de inibir metástases ósseas e cerebrais. Portanto, este trabalho foi capaz de fornecer dados de como o 10G atua nas células tumorais e sua possível aplicação clínica.

Palavras-chave: Câncer, Metástase, Produto Natural, [10]-gingerol, Resveratrol, cérebro.

ABSTRACT

Breast cancer is the leading cause of death in Brazil and worldwide, between the types of cancer, triple negative TNBC (Triple Negative Breast Cancer), which do not express hormone receptors, represents 20% of the cases and presents relapses within 3 years. However, the major cause of death in cancer is due the formation of metastasis. The TNBC has a greater propensity to form lung and brain metastasis. Furthermore, currently few treatments are available. Search for new target treatments, with fewer side effects is very important to treat this disease. Natural products are rich sources of molecules with antitumoral activity; among them are the gingerols, from ginger and resveratrol, from grapes. Nevertheless, not much is known about antitumor activity of [10]-gingerol (10G). Therefore, the aim of this work was to investigate the potential use of 10G as an antimetastatic molecule in *in vitro* and *in vivo* experiments. In this work, 10G had antiproliferative activity on several breast cancer cell lines (4T1BM2, 4T1BM2 shRNAβ3, 4T1Br4, MDA-MB-231, MDA-MB-231 BrM) and on a normal cell line, bEnd.3. The natural compounds affected tumor cell morphology and RSVT was able to inhibit cell migration and adhesion through vitronectin. 10G induced apoptosis via the extrinsic pathway through the increase of caspase-9, -3 and -7 expression and decrease of Bcl-2 expression, induced cell cycle arrest in G1 and subG0 phase. In *in vivo* models, 10G inhibited primary tumor growth and lung metastasis, as well as bone and brain metastasis. Therefore, this study was able to provide new data as 10G can be acting in tumor cells and its possible clinical application.

Keywords: Cancer, Metastasis, Natural Product, [10]-gingerol, Resveratrol, Brain.

LISTA DE FIGURAS

Figura 1 – Sobrevivência dos pacientes com câncer nos EUA. 19
Figura 2 – Progressão do câncer de mama. 20
Figura 3 – Passos da cascata metastática. 21
Figura 4 – Estrutura das integrinas e combinações das cadeias α e β para formar as integrinas e seus possíveis ligantes da MEC. 25
Figura 5 – *Hallmarks* do câncer. 26
Figura 6 – Tratamentos indicados para TNBC e suas vias de ação. 27
Figura 7 – Vias de sinalização da apoptose. 29
Figura 8 – Tratamento simultâneo em diferentes vias da apoptose para evitar a resistência das células tumorais. 30
Figura 9 – Fases do ciclo celular e seus pontos de checagem. 32
Figura 10 – Relação de drogas na sua totalidade e de drogas antitumorais entre os anos 1940-2002. 33
Figura 11 – Modelos de metástase *in vivo*. 37
Figura 12 – Esquema das linhagens celulares de câncer de mama com diferentes potenciais metastáticos. 37
Figura 13 – Seleção da linhagem de células de tumor de mama murino 4T1Br4. 38
Figura 14 – Estrutura química dos produtos naturais utilizados neste estudo: [10]-gingerol (A) e Trans-resveratrol, RSVT (B). 42
Figura 15 – Ciclo da Reação de PCR em tempo real. 51
Figura 16 - Modelo ortotópico singênico de metástase espontânea sem cirurgia do tumor primário com tratamento diário com [10]-gingerol. 53
Figura 17 – Figura representativa do modelo *in vivo* de metástase espontânea com cirurgia do tumor primário. 56
Figura 18- Protocolo do modelo de metástase experimental. 57
Figura 19 - Protocolo do modelo de metástase experimental com pré-tratamento com [10]-gingerol. 58
Figura 20 – Cálculo do IC_{50} nas diferentes linhagens celulares do [10]-gingerol. 60
Figura 21 - Cálculo do IC_{50} nas diferentes linhagens celulares do resveratrol. 61
Figura 22 - Ensaio de inibição da adesão na linhagem 4T1Br4 pelo [10]-gingerol e RSVT. 62
Figura 23 - Ensaio de inibição da adesão na linhagem MDA-MB-231 BrM pelo [10]-gingerol e RSVT. 64

Figura 24 - Toxicidade e Morfologia de células da linhagem 4T1Br4 quando incubadas com o [10]-gingerol. 66
Figura 25 - Toxicidade e Morfologia de células da linhagem MDA-MB-231 BrM quando incubadas com o [10]-gingerol. 67
Figura 26 - Toxicidade e Morfologia de células da linhagem 4T1Br4 quando incubadas com o RSVT. 68
Figura 27 - Toxicidade e Morfologia de células da linhagem MDA-MB-231 BrM quando incubadas com o RSVT. 69
Figura 28 – Ensaio de migração celular hapoptática e quimiotática na linhagem 4T1Br4 na presença de [10]-gingerol e RSVT. 70
Figura 29 – Ensaio de proliferação de 5 dias na linhagem 4T1Br4 e MDA-MB-231 BrM. 71
Figura 30 – Ensaio clonogênico sem radiação. 72
Figura 31 - Ensaio clonogênico com radiação. 73
Figura 32 – Ensaio clonogênico associado a radiação. 74
Figura 33 - Ensaio clonogênico associado a radiação. 75
Figura 34 - Ensaio de condensação nuclear. 76
Figura 35 - Ensaio colorimétrico de TUNEL. 77
Figura 36 – Ensaio de ciclo celular. 78
Figura 37 – Atividade de caspases. 79
Figura 38 – Expressão de genes relacionados a apoptose em células 4T1Br4 tratadas com [10]-gingerol por 6h. 80
Figura 39 - Expressão de genes relacionados a apoptose em células 4T1Br4 tratadas com [10]-gingerol por 18h. 81
Figura 40 – Modelo de formação de metástase espontânea IMFP (*Intramammary Fat Pad*): impactos do tratamento com o [10]-gingerol sobre parâmetros morfométricos. 82
Figura 41 – Análise da *Relative Tumor Burden* (RTB) no modelo de formação de metástase espontânea IMFP (*Intramammary Fat Pad*) com tratamento do PN. 83
Figura 42 – Imagem representativa das metástases pulmonares e do tamanho dos baços. 84
Figura 43 - Modelo de formação de metástase espontânea IMFP (*Intramammary Fat Pad*) seguido de cirurgia: impactos do tratamento com o [10]-gingerol sobre parâmetros morfométricos. 85
Figura 44 - Análise da RTB (*Relative Tumor Burden*) no modelo de formação de metástase espontânea IMFP (*Intramammary Fat Pad*) com tratamento do PN após cirurgia do tumor primário. 85

Figura 45 - Imagens fluorescentes dos cérebros do grupo controle. 86
Figura 46 - Imagens dos cérebros do grupo tratado com [10]-gingerol. 87
Figura 47 –Incidência de metástases cerebrais no modelo de metástase espontânea. 87
Figura 48 – Modelo de metástase experimental com tratamento do [10]-gingerol após a injeção intracardíaca (IC). 88
Figura 49 - Modelo de metástase experimental com tratamento do [10]-gingerol antes e após a injeção IC. 89
Figura 50 – Resumo da atuação do [10]-gingerol *in vitro* e *in vivo*. 98

LISTA DE TABELAS

Tabela 1 –Sequências dos primers utilizados e suas concentrações na reação final da PCR em tempo real. 50
Tabela 2 – Componentes da PCR. 51
Tabela 3 – *Primers* e *probes* utilizados no experimento de PCR em tempo real para determinação do *Relative Tumor Burden* (RTB). 54
Tabela 4 – Componentes da PCR em tempo real Taqman para os ensaios *in vivo*. 55

LISTA DE ABREVIATURAS

BCA – Ácido Bicincrônico (***BiC****inchoninic* ***A****cid*)

BSA – Soro Albumina Bovina (***B****ovine* ***S****erum* ***A****lbumin*)

CDKs – Kinases Dependentes de Ciclinas (***C****yclin-****D****ependent* ***K****inase*)

cDNA - Ácido desoxirribonucléico complementar

Ct – Ciclo Limiar (***C****ycle* ***T****hreshold*)

DAB – Diaminobenzidina (*diaminobenzidine*)

DAPI - *4',6-Diamidino-2-Phenylindole, Dihydrochloride*

DISC – Complexo de sinalização induzido por morte (***D****eath-****I****nducing* ***S****ignalig* ***C****omplex*)

DMEM - Meio Dulbecco modificado (***D****ulbecco's* ***M****odified* ***E****agle* ***M****edium*)

DMSO – Sulfóxido de Dimetil (***D****imethyl* ***S****ulfoxide*)

DNA – Ácido desoxirribonucléico

DNAg – DNA gênomico

dNTPs – desoxirribonucleotídeos fosfatados

DPX – Distireno **P**lastificante **X**ileno

DTT - Ditiotreitol

EMT – Transição Epitelial-Mesenquimal (***E****pithelial-****M****esenchymal* ***T****ransition*)

ER – Receptor de Estrógeno (***E****strogen* ***R****eceptor*)

FBS – Soro Fetal Bovino (***F****etal* ***B****ovine* ***S****erum*)

FITC - Isotiocianato de fluoresceína (***F****luorescein* ***I****so****T****hiocyanat****e***)

HER-2 – Receptor do fator de crescimento humano 2 (***H****uman* ***E****pidermal Growth Factor* ***R****eceptor-2*)

HIF – Fato Induzido por Hipóxia (***H****ipoxya-****I****nducible* ***F****actor*)

HR – Receptor de hormônio (***H****ormone* ***R****eceptor*)

HRP - ***H****orseradish* ***P****eroxidase*

HUVEC – Células endoteliais humanas da veia umbilical (***H****uman* ***U****mbilical* ***V****ein* ***E****ndothelial* ***C****ells*)

IC – Intra**c**ardíaca

IC_{50} – Concentração **I**nibitória

IMFP – Intra**m**ammary **F**at **P**ad

IP - Intra**p**eritoneal

LMN-511 – Laminina-511

MEC – Matriz **E**xtra**c**elular

M-MLV - Vírus da Leucemina murina de Moloney (***M****oloney* ***M****urine* ***L****eukemia* ***V****irus*)

MMP – Metalopeptidases de **M**atriz (***M****atrix* ***M****etallo****p****roteinases*)

MTT - *3-(4,5-dimethylthiazol-2-yl)-2,5-diphenyl tetrazolium bromide*

Nec-1 – Necrostatina-1

PBS – Tampão fosfato-Salino (***P****hosphate* ***B****uffered* ***S****aline*)

PCR – Reação em cadeoa da Polimerase (***P****olymerase* ***C****hain* ***R****eaction*)

PI – Iodeto de propídeo (***P****ropidium* ***I****odide*)

PN – Produto **N**atural

PR – Receptor de Progesterona (***P****rogesteron* ***R****eceptor*)

RIP1 – Receptor de interação da protepina 1 (***R****eceptor* ***I****nteracting* ***P****rotein* ***1*****)**

RNA – Ácido ribonucleico

RSVT - Resveratrol

RTB – Carga tumoral Relativa (***R****elative* ***T****umor* ***B****urden*)

rTdT – ***r****ecombinant* ***T****erminal* ***D****eoxynucleotidyl* ***T****ransferase*

RT-PCR – PCR-Transcriptase Reversa (***R****everse* ***T****ranscriptase* ***PCR***)

SDS – Sulfato Dodecil de Sódio (***S****odium* ***D****odecyl* ***S****ulphate*)

SDS-PAGE - ***S****odium* ***D****odecyl* ***S****ulphate* ***P****olyacrylamide* ***G****el* ***E****lectrophoresis*

SRB - *Sulforodamine B*

TAMs – Macrófagos associados ao Tumo (***T****umour* ***A****ssociated* ***M****acrophages*)

TCA – Ácido Tricloroacético (***T****ri****c****hloroacetic* ***A****cid*)

TN – Triplo Negativo (***T****riple* ***N****egative*)

TNBC – Câncer de mama triplo negativo (***T****riple* ***N****egative* ***B****reast* ***C****ancer*)

TNF – Fator de necrose tumotal (***T****umor* ***N****ecrosis* ***F****actor*)

TUNEL - ***T****erminal deoxynucleotidyl transferase d****U****TP* ***N****ick* ***E****nd* ***L****abeling*

VEGF – Fator de crescimento vascular endotelial (***V****ascular* ***E****ndothelial* ***G****rowth* ***F****actor*)

VEGF-R – Receptor de Fator de crescimento vascular endotelial (***V****ascular* ***E****ndothelial* ***G****rowth* ***F****actor* ***R****eceptor*)

VN - Vitronecti**n**a

SUMÁRIO

1 INTRODUÇÃO 18

1.1 CÂNCER DE MAMA 18
1.2 A EVOLUÇÃO DO CÂNCER E METÁSTASE 20
1.2.1 PASSOS DA METÁSTASE 22
1.3 TRATAMENTOS NO CÂNCER DE MAMA TRIPLO NEGATIVO 26
1.4 APOPTOSE E CICLO CELULAR 28
1.5 PRODUTOS NATURAIS 32
1.6 MODELOS DE METÁSTASE IN VIVO 36

2 JUSTIFICATIVAS 39

3 OBJETIVOS 41

4 MATERIAIS E MÉTODOS 42

4.1 PRODUTOS NATURAIS: RESVERATROL E [10]-GINGEROL 42
4.2 LINHAGENS E CULTIVOS CELULARES 42
4.3 DETERMINAÇÃO E CÁLCULO DA IC_{50} 43
4.4 INIBIÇÃO DA ADESÃO CELULAR 44
4.5 CITOTOXICIDADE E MORFOLOGIA CELULAR 44
4.6 ENSAIOS DE MIGRAÇÃO CELULAR 45
4.6.1 MIGRAÇÃO QUIMIOTÁTICA 45
4.6.2 MIGRAÇÃO HAPTOTÁTICA 45
4.7 ENSAIO DE PROLIFERAÇÃO – 5 DIAS 46
4.8 ENSAIO CLONOGÊNICO COM/ SEM RADIO-SENSIBILIZAÇÃO 46
4.9 ENSAIO DE CONDENSAÇÃO NUCLEAR 47
4.10 TUNEL 47
4.11 ANÁLISE DO CICLO CELULAR 48
4.12 ATIVIDADE DAS CASPASES-3 E -7 48
4.13 EXPRESSÃO GÊNICA 49
4.13.1 TRATAMENTO DAS CÉLULAS E EXTRAÇÃO DO RNA 49
4.13.2 SÍNTESE CDNA 49
4.13.3 REAÇÃO DE PCR EM TEMPO REAL E ANÁLISE 50
4.14 MODELOS IN VIVO DE METÁSTASE 51

4.14.1 MODELO DE FORMAÇÃO DE METÁSTASE ESPONTÂNEA IMFP (INTRAMAMMARY FAT PAD) SEM CIRURGIA DO TUMOR PRIMÁRIO 52
4.14.2 MODELO DE FORMAÇÃO DE METÁSTASE ESPONTÂNEA IMFP (INTRAMAMMARY FAT PAD) COM CIRURGIA 55
4.14.3 MODELO DE FORMAÇÃO DE METÁSTASE EXPERIMENTAL POR INJEÇÃO INTRACARDÍACA (IC) E TRATAMENTO DO [10]-GINGEROL PÓS INJEÇÃO 57
4.14.4 MODELO DE FORMAÇÃO DE METÁSTASE EXPERIMENTAL COM INJEÇÃO INTRACARDÍACA (IC) COM PRÉ-TRATAMENTO DO [10]-GINGEROL 58
4.15 DETERMINAÇÃO DA CONCENTRAÇÃO PROTÉICA 59
4.16 ANÁLISE ESTATÍSTICA 59

5 RESULTADOS 60

5.1 DETERMINAÇÃO DO IC_{50} 60
5.2 INIBIÇÃO DA ADESÃO CELULAR A DIFERENTES COMPONENTES DA MEC 61
5.3 TOXICIDADE CELULAR E MORFOLOGIA 65
5.4 MIGRAÇÃO CELULAR 70
5.5 ENSAIO DE PROLIFERAÇÃO CELULAR- 5 DIAS 71
5.6 ENSAIO CLONOGÊNICO 72
5.7 ENSAIO DE CONDENSAÇÃO NUCLEAR 75
5.8 TUNEL 77
5.9 ANÁLISE DO CICLO CELULAR 78
5.10 ATIVIDADE DE CASPASES 78
5.11 EXPRESSÃO GÊNICA 79
5.12 MODELO DE FORMAÇÃO DE METÁSTASE ESPONTÂNEA IMFP (INTRAMAMMARY FAT PAD) SEM CIRURGIA DO TUMOR PRIMÁRIO 82
5.13 MODELO DE FORMAÇÃO DE METÁSTASE ESPONTÂNEA IMFP (INTRAMAMMARY FAT PAD) COM CIRGUGIA 84
5.14 MODELO DE FORMAÇÃO DE METÁSTASE EXPERIMENTAL, INJEÇÃO INTRACARDÍACA (IC) COM TRATAMENTO DO [10]-GINGEROL PÓS INJEÇÃO 88
5.15 MODELO DE FORMAÇÃO DE METÁSTASE EXPERIMENTAL COM INJEÇÃO INTRACARDÍACA (IC) COM PRÉ-TRATAMENTO DO [10]-GINGEROL 88

6 DISCUSSÃO 90

7 CONCLUSÕES 97

8 PERSPECTIVAS FUTURAS ____ 99

9 REFERÊNCIAS BIBLIOGRÁFICAS ____ 100

ANEXOS ____ 108

1 INTRODUÇÃO

1.1 Câncer de mama

A palavra “câncer” descreve mais de 100 tipos de doenças que possuem em comum o crescimento desordenado de células anormais com potenciais invasivos ou não, e que quando invasivos, podem se espalhar pelo organismo. O tumor primário e/ou suas metástases podem resultar em morte. O câncer é uma doença heterogênea, com diferentes aspectos, características moleculares, comportamentos e respostas a terapias. Mesmo pacientes com características tumorais similares apresentam diferentes respostas aos tratamentos, e este pode ser causado por fatores genéticos, ambientais e epigenéticos (AMERICAN CANCER SOCIETY, 2014; CHATTERJEE; MCCAFFREY, 2014; INCA, 2014).

As estimativas no Brasil para 2014/2015 preveem que ocorram 570 mil novos casos de câncer. O câncer de pele do tipo não melanoma será o de maior incidência, seguido pelo câncer de mama e colo de útero nas mulheres e o câncer de próstata em homens. A expectativa é de que em 2030 ocorram 21,4 milhões de novos casos no mundo com cerca de 13,2 milhões de mortes (INCA, 2014).

Apesar da alta incidência dessa doença, com o passar dos anos houve uma melhoria nos métodos de diagnósticos do câncer e de seu tratamento, portanto, existe um grande esforço entre os profissionais da área para o desenvolvimento de novos tratamentos e fármacos (LIVES, 2012). Tais dados podem ser observados na figura abaixo, em que apesar do crescimento da população, houve uma grande melhoria no número de sobreviventes (Figura 1).

Figura 1 – Sobrevivência dos pacientes com câncer nos EUA.

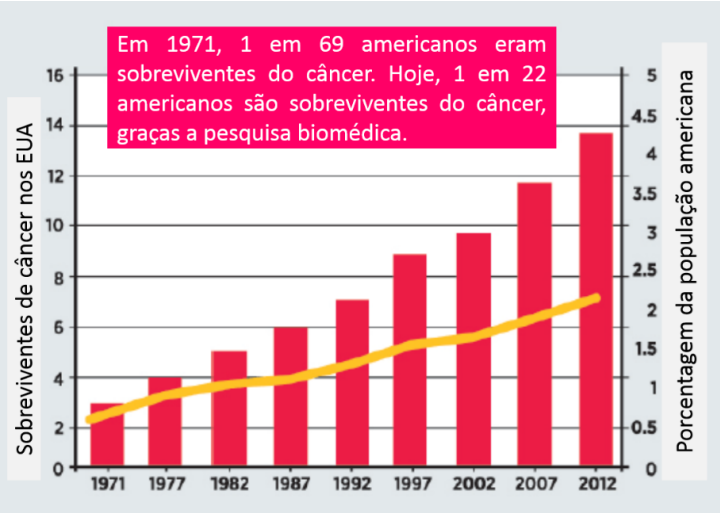

A taxa de sobreviventes com câncer triplicou com relação ao crescimento da população Americana nos anos de 1971 até 2012. Gráfico traduzido do relatório de progresso da AACR (LIVES, 2012).

O câncer de mama pode ser classificado em três grandes grupos baseados em biomarcadores moleculares, como a expressão de receptores hormonais (HR: ***H****ormone* ***R****eceptors*) ou sua ausência na superfície celular. Entre estes grupos estão os que i) apresentam receptores de estrógeno (ER+) ou receptores de progesterona (PR+), ii) os que apresentam receptor HER-2 (***H****uman* ***E****pidermal Growth Factor* ***R****eceptor-2*) com ou sem o receptor ER+ e iii) o subtipo triplo negativo, que não possui os três receptores embora possa apresentar uma baixa expressão de HER-2 (TNBC: ***T****riple* ***N****egative* ***B****reast* ***C****ancer*) (CRISCITIELLO et al., 2012). Mais recentemente, um trabalho propôs a divisão dos grupos de câncer de mama baseado na expressão de HER2 e taxa de proliferação em: ER+/PR/HER2+ (*Triple Positive*), subtipo ER+/PR+/HER2 e TN (VICI et al., 2014). Os tumores HR+ e HER2- são os de maior incidência entre as mulheres e apresentam melhor prognóstico devido a resposta à terapia hormonal. Entretanto, tumores que apresentam HR+/HER+ acometem 6% das mulheres, e estes possuem uma resistência elevada à terapia hormonal e à quimioterapia. Os tumores triplo negativos (TN) possuem um mau prognóstico com relação a cura e sobrevivência geral da doença, acometem de 9-16% da população, e atualmente não possuem terapias-alvo (ENGEBRAATEN; VOLLAN; BØRRESEN-DALE, 2013; RAKHA; CHAN, 2011).

Esta classificação pode predizer a resposta dos pacientes ao tratamento e que tipo de tratamento deverá ser utilizado. Além disso, tumores TN possuem uma propensão à metástase principalmente pulmonar e cerebral mais do que ossos e linfonodos, tornando o tratamento mais difícil que outros tipos de câncer de mama (BEASLEY; TOMS, 2011).

1.2 A evolução do câncer e metástase

A maior causa de morte por câncer de mama não é devido ao tumor primário em si, mas sim devido a formação de metástases em órgãos distantes em 90% dos casos (PERRET; CRÉPIN, 2008; SCULLY et al., 2012).

A glândula mamária consiste em uma camada de células luminais polarizadas e uma outra camada que a envolve, de células mioepiteliais que faz contato com a membrana basal. O câncer de mama se inicia com a formação de uma atipia epitelial benigna ou hiperplasia ductal que pode progredir para um carcinoma *in situ*, que por sua vez pode se transformar em um carcinoma invasivo, como demonstrado na Figura 2. A hiperplasia e a atipia epitelial são lesões precursoras clonais que possuem como principal característica uma taxa de proliferação celular exacerbada, formando um ducto constituído de multicamadas celulares. Durante este processo as células normais se transformam em células tumorais devido a mutações, fatores epigenéticos e/ou intrínsecos que regulam vias essenciais, gerando esta proliferação descontrolada (CHATTERJEE; MCCAFFREY, 2014).

Figura 2 – Progressão do câncer de mama.

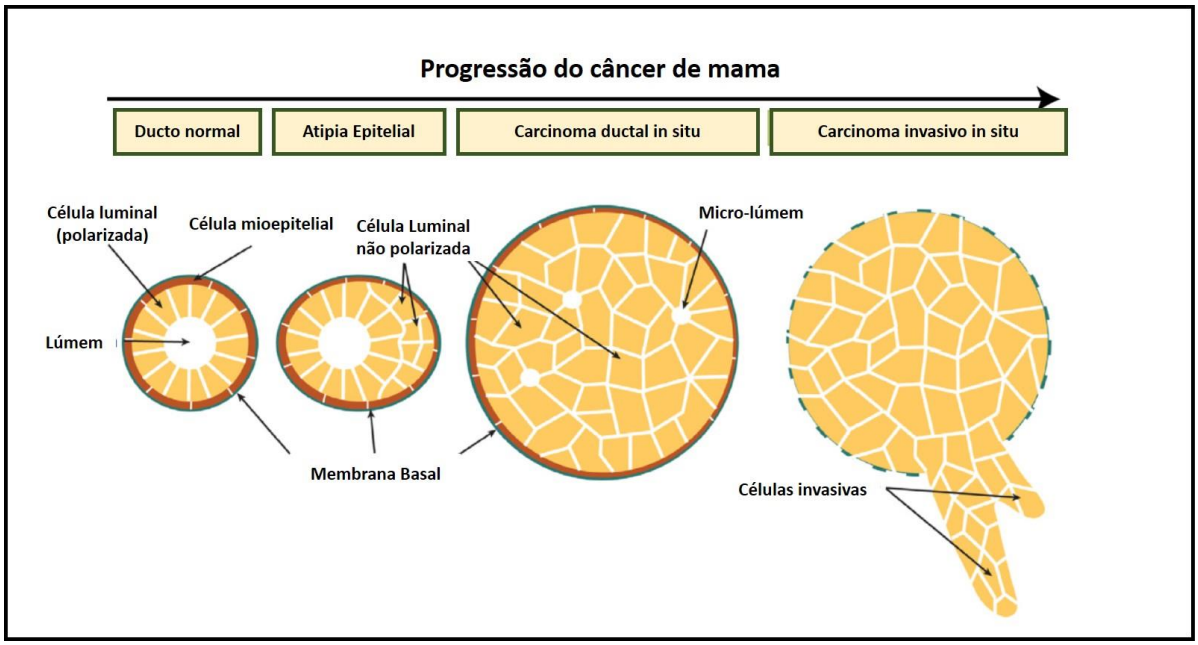

Progressão tumoral indicando os passos desde a estrutura de uma glândula mamária normal até a formação de um carcinoma invasivo em que as células se dissociam do tumor primário para os tecidos adjacentes, iniciando o processo metastático (adaptado de CHATTERJEE; MCCAFFREY, 2014).

A partir dessa regulação descontrolada da proliferação celular, as células tumorais podem se dissociar do tumor primário e invadir tecidos adjacentes e distantes. Este processo é

conhecido como metástase e pode ser descrito como uma cascata de eventos. As células transformadas interagem intensamente com células de seu microambiente tumoral, como células endoteliais, fibroblastos e macrófagos, formando uma estrutura complexa e heterogênea, junto com a indução da formação de novos vasos sanguíneos e linfáticos (JOYCE; POLLARD, 2009). Um importante passo durante a tumorigênese e consequentemente a formação de metástases, é a angiogênese no tumor primário. Este processo é descrito como a formação de novos vasos sanguíneos a partir de vasos pré-existentes. (PERRET; CRÉPIN, 2008). Sem a formação de novos vasos o tumor ficaria restrito a um tamanho microscópico e as células não conseguiriam entrar na circulação para popular novos sítios. Durante a proliferação exacerbada das células tumorais o ambiente celular se torna hipóxico, com isso há a ativação do HIF (*Hipoxya-Inducible Factor*) que estimula células tumorais e células associadas ao tumor a produzirem VEGF (*Vascular Endothelial Growth Factor*) que é uma molécula chave para o início da angiogênese, atendendo então, as exigências de oxigênio do tumor (FOLKMAN, 2003; KUBOTA, 2012).

O processo metastático pode ser descrito portanto por eventos de dissociação, invasão, intravasamento, extravasamento e dormência (Figura 3) (ALIZADEH; SHIRI; FARSINEJAD, 2014).

Figura 3 – Passos da cascata metastática.

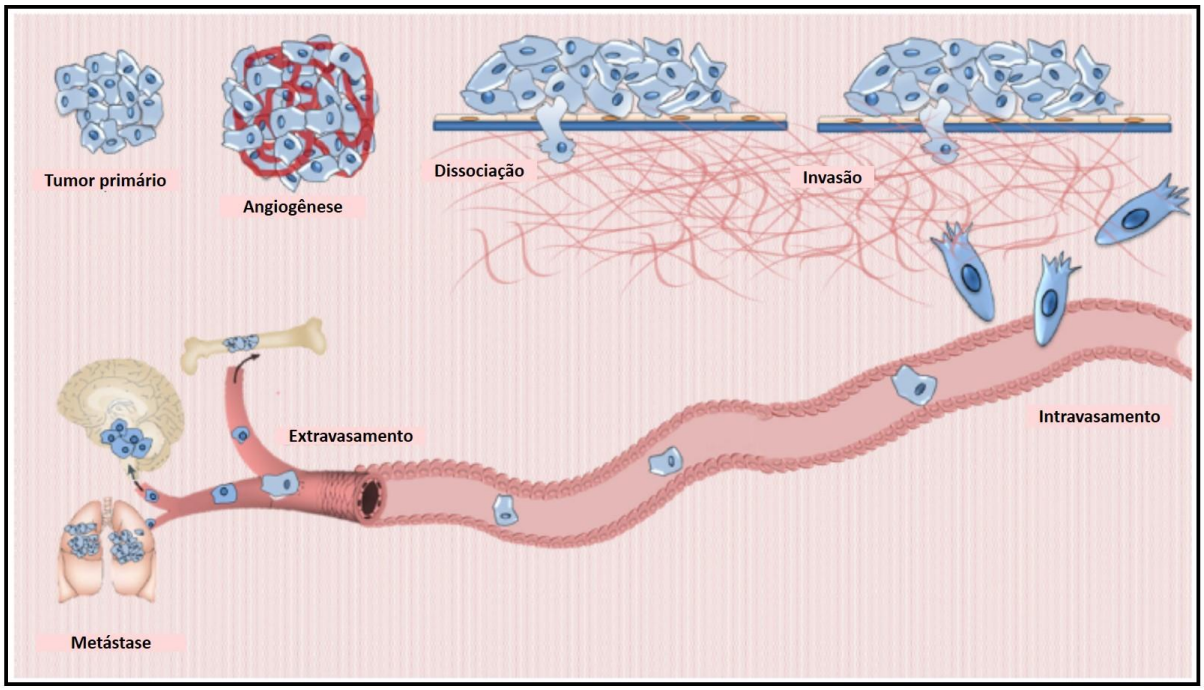

A cascata metastática é iniciada após a formação da massa tumoral em que algumas células do tumor primário se dissociam invadindo os tecidos adjacentes, em seguida ocorre o intravasamento destas células nos vasos

sanguíneos e/ou linfáticos fazendo com que entrem na circulação. Estas células, quando atingem seu sítio secundário, extravasam do vaso chegando ao seu novo ambiente, onde podem entrar em um estado de dormência ou proliferar para a formação da metástase. Modificado de Alizadeh *et al.* 2014 (ALIZADEH; SHIRI; FARSINEJAD, 2014).

1.2.1 Passos da metástase

Dissociação: Nesta fase, células do tumor primário se dissociam para invadir os tecidos adjacentes. Para isso, as células tumorais perdem suas adesões célula-célula. Durante este passo, as células sofrem mudanças na sua expressão gênica tornando-se capazes de aderir a matriz extracelular (MEC), degradá-la e migrar localmente. Como durante esse processo as células devem perder suas adesões célula-célula e célula-MEC, proteínas de adesão celular são de extrema importância, tais como, caderinas, integrinas, selectinas e imunoglobulinas (ALIZADEH; SHIRI; FARSINEJAD, 2014; WOLF; FRIEDL, 2006)

Invasão: Primeiramente as células sofrem mudanças em seu citoesqueleto, em seguida migram de forma individual, perdendo contato com as células do tumor primário, ou de forma coletiva migrando em conjunto sem perder as adesões célula-célula. Durante a migração individual as células perdem suas características epiteliais e adquirem características mesenquimais, este processo é denominado transição epitelial-mesenquimal (**EMT**: ***E**pithelial **M**esenchymal **T**ransition*). Na migração coletiva, as células requerem força para migrar e uma célula será responsável por liderar esta migração. Além dessas duas formas de migração, ainda existe a migração amebóide que não requer a degradação da matriz extracelular por meio de proteases, como as metaloproteases de matriz (MMPs). Neste tipo de migração as células perdem sua polaridade e migram rapidamente. As outras formas de migração requerem a atividade de MMPs (ALIZADEH; SHIRI; FARSINEJAD, 2014; YILMAZ; CHRISTOFORI; LEHEMBRE, 2007).

Intravasamento: É o processo pelo qual as células tumorais invadem localmente os vasos linfáticos ou sanguíneos para atingir seus sítios secundários. Este é um passo limitante da metástase, pois é nele que ocorre a regulação de quantas células tumorais irão circular na corrente sanguínea e consequentemente popular os tumores secundários. O intravasamento nos vasos, sejam linfáticos ou sanguíneos, é conhecido como transmigração endotelial. Para que isso ocorra, as células devem sofrer mudanças drásticas no seu citoesqueleto, morfologia celular e quebrar suas ligações com a matriz e/ou células tumorais (ALIZADEH; SHIRI; FARSINEJAD, 2014; GEIGER; PEEPER, 2009). Esse passo também é limitante, pois uma

vez que as células entram na circulação sanguínea, estas sofrem um grande estresse podendo acarretar na sua morte, porém as plaquetas presentes na circulação possuem um papel protetor em conjunto com o fibrinogênio, atuando como um escudo e impedindo que essas células sejam atacadas pelo sistema imune (COUPLAND; PARISH, 2014).

Extravasamento: Durante o extravasamento as células tumorais saem da corrente sanguínea ou linfática em direção ao sítio secundário onde irão formar as metástases. Para isso, as células devem atravessar o endotélio da vasculatura, invadir o tecido adjacente e se estabelecer neste novo ambiente. Umas das hipóteses que tentam explicar como se dará a nova localização das células tumorais no sítio secundário é a teoria do "*seed and soil*" proposta por Stephen Paget em 1889,a qual pressupõe que as células tumorais (*seed*) só se desenvolverão aonde exista um ambiente propício para seu estabelecimento (*soil*), (MENDOZA; KHANNA, 2009). Atualmente, sabe-se que as células tumorais realmente possuem uma propensão a metastatizar para órgão específicos, e isso ocorre devido a formação do nicho pré-metastático. A formação do nicho prémetastático se inicia pela chegada de células hematopoiéticas da medula óssea que expressam receptores de fatores de crescimento endoteliais, como o VEFGR-1, e precedem a chegada das células tumorais a sítios distantes do tumor primário. Há um aumento de expressão de fatores de crescimento e fibronectina no local, e esses eventos em conjunto resultam na formação do nicho pré-metastático, em que células não neoplásicas marcam o futuro sítio metastático das células tumorais. (PEINADO; LAVOTSHKIN; LYDEN, 2011, 2011).

Dormência e formação das metástases: Quando as células tumorais atingem seu sítio secundário, estas podem entrar num estágio de dormência e permanecer dessa forma por longos períodos de tempo. Entretanto, esta fase pode não ocorrer e as células podem entrar no processo de colonização deste novo ambiente e estabilização da metástase. O final da fase de dormência está altamente relacionado a formação de novos vasos, conhecido como "*angiogenic switch*", quando há inibidores de angiogênese estas células permanecem dormentes, portanto, para estas células escaparem da dormência deve haver um balanço angiogênico positivo nos tumores, este mecanismo também pode ocorrer no tumor primário (ALIZADEH; SHIRI; FARSINEJAD, 2014; GEIGER; PEEPER, 2009; POLLARD et al., 2009).

Durante os passos da metástase, fica clara a importância da interação das células tumorais com a MEC. A MEC é o componente não celular dos tecidos, composta de uma

parte fibrosa e uma não fibrosa, e sua relação determina as propriedades fisiológicas e particulares da MEC (TANZER, 2006). Sua função é promover suporte e força para o desenvolvimento dos tecidos. A MEC em mamíferos é composta por mais de 300 proteínas incluindo os colágenos, proteoglicanos, glicoproteínas, fibronectinas, lamininas e polissacarídeos (BERRIER; YAMADA, 2007; FRANTZ; STEWART; WEAVER, 2010). Entre esses compontentes estão presentes mais de 43 subunidades de colágenos, 36 proteoglicanos e cerca de 200 complexos de glicoproteínas. A principal proteína presente na MEC são os colágenos fibrilares, que proporcionam força e elasticidade ao tecido, e formas não fibrilares. Os proteoglicanos conferem hidratação e as glicoproteínas, tais como, as lamininas e fibronectinas, são responsáveis pela interação célula-MEC através de receptores conhecidos como integrinas. Além disso, proteínas associadas a MEC como fatores de crescimento, citocinas entre outros, também estão presentes e são de grande importância no remodelamento da MEC (BONNANS; CHOU; WERB, 2014; HYNES; NABA, 2012).

Para que as células possam migrar sobre a MEC, estas devem ser capazes de degradá-la através de proteases, principalmente pelas MMPs. As MMPs são responsáveis pelo remodelamento da MEC, liberação de fatores de crescimento e de moléculas de adesão e representam algumas das principais mediadoras das alterações do microambiente tumoral, dentre elas estão a MMP-2 e MMP-9 (FRANTZ; STEWART; WEAVER, 2010; GIALELI; THEOCHARIS; KARAMANOS, 2011; KESSENBROCK; PLAKS; WERB, 2010). A MMP-2 é conhecida como gelatinase A e MMP-9 como gelatinase B, ambas degradam colágenos (IV, V, VII entre outros), gelatina, fibronectina entre outros componentes da MEC. A MMP-2 e -9 são consideradas metaloproteases chaves na invasão e formação de metástases (AMĂLINEI et al., 2010).

Durante a migração, as células tumorais interagem com a MEC através de receptores celulares conhecidos como integrinas (FRIEDL; BRÖCKER, 2000). As integrinas pertencem à superfamília de receptores de adesão celular que reconhecem a MEC e ligantes da superfície celular. São receptores de membrana e sua estrutura é caracterizada pela presença de duas cadeias heterodiméricas, uma cadeia α e uma cadeia β. Já foram descritas 18 cadeias α e 8 cadeias β, que podem se combinar e formar 24 dímeros, apresentando propriedades de ligação diferentes. Essas diferentes combinações acarretam em ligações a diferentes componentes da MEC, como demonstrado na Figura 4. Portanto, as integrinas funcionam como uma conexão entre a MEC e o citoesqueleto celular, regulando diferentes processos biológicos tais como, sobrevivência celular, proliferação, migração e diferenciação celular (BERRIER; YAMADA, 2007; KAPP et al., 2013; TAKADA; YE; SIMON, 2007).

Figura 4 – Estrutura das integrinas e combinações das cadeias α e β para formar as integrinas e seus possíveis ligantes da MEC.

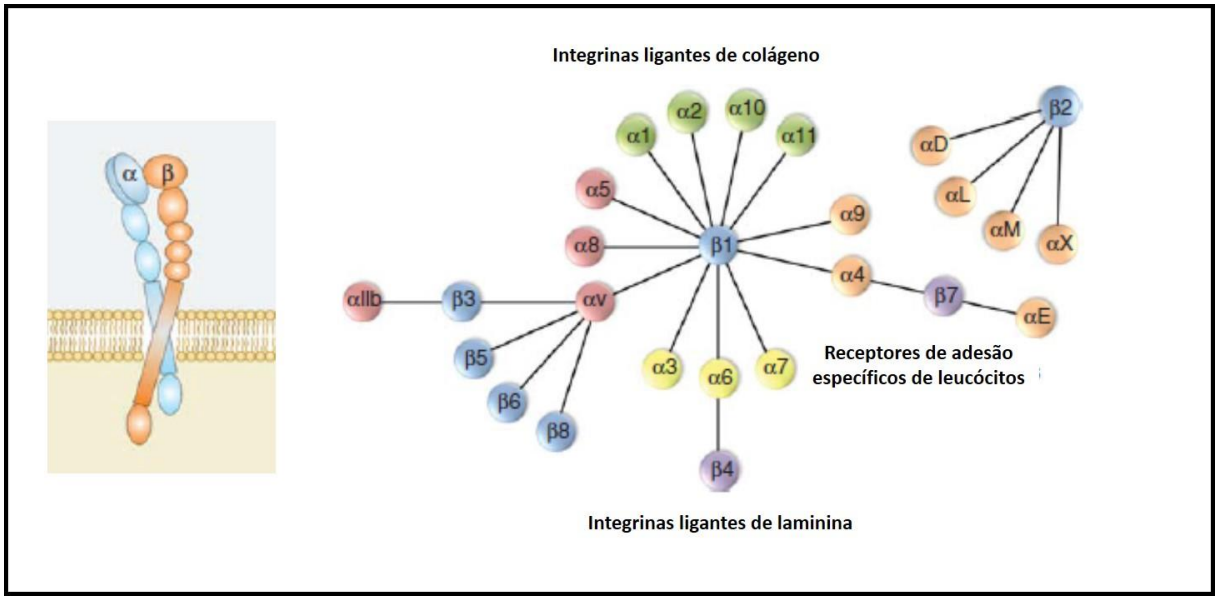

Modificado de Kapp *et al.* (KAPP et al., 2013).

As integrinas contribuem com a progressão tumoral e apresentam diferentes perfis de expressão nos tumores. Integrinas como α6β4, α6β1, αvβ5, α2β1, α3β1 apresentam expressão alterada em tumores, auxiliando na adesão e migração celular, entre outros. Normalmente esta expressão alterada está associada a uma menor sobrevida dos pacientes (DESGROSELLIER; CHERESH, 2010; HOOD; CHERESH, 2002).

Além do conjunto de fatores descrito, o microambiente tumoral é de grande importância para a formação de metástases, assim como o sistema imune, pois as células próximas ao tumor, que fazem parte do estroma normal, participam da tumorigênese e metástase, regulando todos esses processos (MENDOZA; KHANNA, 2009). Células do sistema imune, como os macrófagos associados ao tumor (TAMs – *Tumour Associated Macrophages*), auxiliam as células tumorais na invasão e no comportamento migratório destas, pois secretam MMPs auxiliando as células tumorais a invadirem os tecidos adjacentes, e além disso, atuam como quimioatraente de monócitos que adentram o tumor nas regiões de hipóxia estimulando angiogênese e a progressão tumoral (ECKHARDT et al., 2005, 2012).

Para resumir a complexidade presente na formação de neoplasias e por conseguinte, na formação de metástases, Hanahan e Weinberg definiram algumas caraterísticas do câncer que permitem e contribuem para que todo esse processo ocorra, e as denominaram de "*hallmarks*" do câncer (

Figura 5). Os *hallmarks* são: sinalizações que sustentam a proliferação exacerbada das células tumorais, "fuga" de supressores do crescimento e do sistema imune, replicação

imortal, promoção da inflamação que contribui para o estabelecimento do tumor e formação de mutações que aceleram a evolução genética do tumor, invasão e metástase, indução da angiogênese, instabilidade genômica e desregulação energética das células (HANAHAN; WEINBERG, 2011).

Figura 5 – *Hallmarks* do câncer.

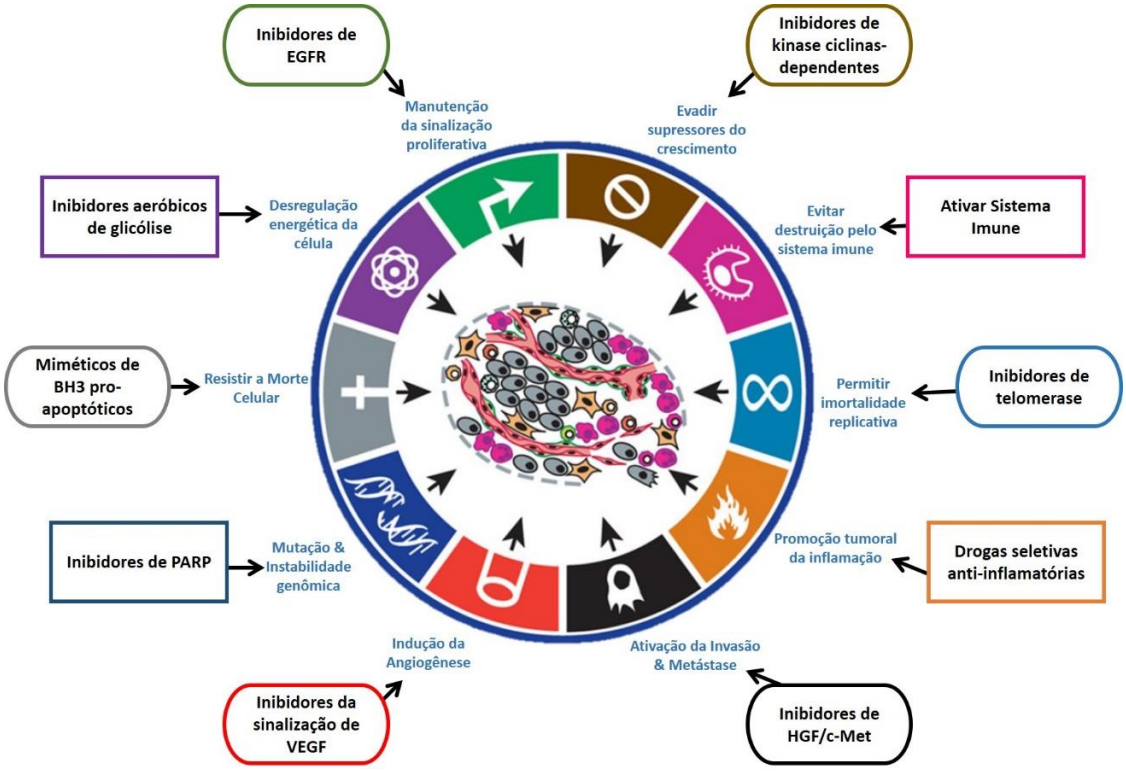

Esta figura ilustra os *hallmarks* do câncer, que são características do tumor que permitem sua progressão e ao redor destes, estão as possíveis formas de intervenção para cada *hallmark*.Modificado de Hanahan & Weinberg, 2011.

1.3 Tratamentos no câncer de mama triplo negativo

Vista a complexidade da cascata metastática, torna-se um desafio a compreensão dos mecanismos envolvidos neste processo. Atualmente, um dos primeiros passos para o tratamento do câncer de mama é a cirurgia para retirada do tumor primário, seguida de quimioterapia, radioterapia e terapia-alvo dependendo do tipo de câncer de mama. Entretanto, os tratamentos atuais apresentam severos efeitos colaterais (NAMBIAR; RAJAMANI; SINGH, 2011).

Para os cânceres de mama positivos para receptores de hormônio, atualmente além dos tratamentos usuais, como cirurgia e radioterapia, existem terapias-alvo que permitem uma maior sobrevida do paciente e até mesmo a cura da doença. Terapias-alvo incluem terapia

hormonal, terapia imunológica e terapia antiangiogênica. Entre estas, o Tamoxifo é um agente bloqueador de ER, assim como o Letrozol e o Anastrozol. O Trastuzumab é um anticorpo monoclonal que se liga seletivamente ao HER2 bloqueando a proliferação de tumores que super-expressam HER2. Outra terapia já em uso é o Bevacizumab, que é um anticorpo monoclonal, que tem como alvo isoformas de VEGF-A (***V**ascular **E**ndothelial **G**rowth **F**actor-**A***) que inibe a proliferação de células endoteliais e como consequência, o fornecimento de nutrientes ao tumor (SCULLY et al., 2012; VICI et al., 2014).

O TNBC está associado a mulheres com menos de 40 anos e mulheres afro-americanas, e é caracterizado pela recorrência da doença entre o primeiro e terceiro ano depois do diagnóstico e recaídas raras até 8-10 anos depois, portanto, apresentam alta taxa de recaída e mau prognóstico. As metástases provenientes desse tipo de câncer são mais agressivas que os outros subtipos e são mais prováveis de ocorrer no pulmão e cérebro do que nos ossos (CRISCITIELLO et al., 2012; NIIKURA et al., 2014).

Terapias atuais para o TNBC são basicamente a cirurgia para remoção do tumor primário, radioterapia e quimioterapia. Atualmente não há tratamentos-alvo disponíveis e os agentes citotóxicos mais usados são as Antraciclinas e Taxanos (antibiótico e produto natural, respectivamente) e também agentes contendo platina, como a cisplatina. Estes agentes são os mais indicados para o tratamento de TNBC pois interagem com o DNA tumoral e mostraram ter melhores respostas que outros tipos de tratamento, como o tratamento hormonal (ENGEBRAATEN; VOLLAN; BØRRESEN-DALE, 2013). Os tratamentos mais usados para TNBC estão indicados na Figura 6, assim como sua forma de ação.

Figura 6 – Tratamentos indicados para TNBC e suas vias de ação.

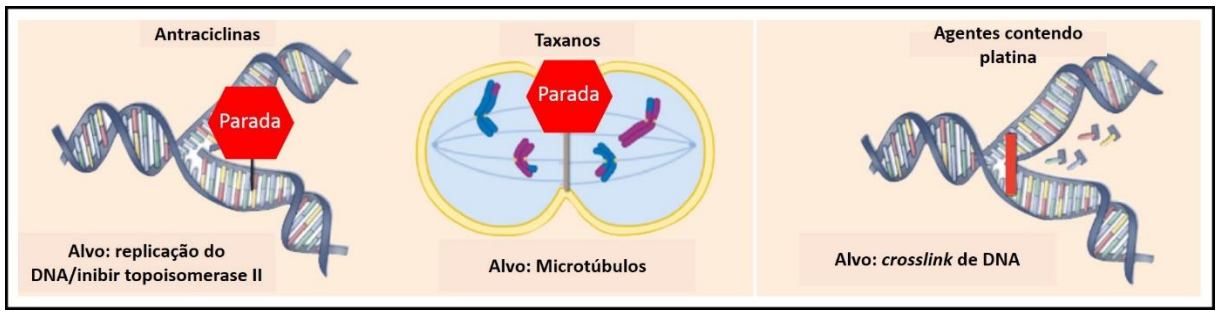

Modificado de Engebraaten *et al.* (ENGEBRAATEN; VOLLAN; BØRRESEN-DALE, 2013).

As metástases provenientes do TNBC não são curáveis e a principal terapia é o re-estabelecimento da qualidade de vida desses pacientes. Como citado acima, a maior incidência de metástases nesse subtipo de câncer de mama são os pulmões e cérebro em vez

de linfonodos, ossos e fígado, e isso ocorre pois as células tumorais tendem a se espalhar preferencialmente via sistema sanguíneo e menos pelo sistema linfático (RAKHA; CHAN, 2011).

1.4 Apoptose e ciclo celular

Atualmente há uma busca de fármacos que consigam tratar o TNBC de forma eficaz e com o mínimo de efeitos colaterais. Sabendo-se da melhor eficácia de agentes citotóxicos para o tratamento do TNBC há a necessidade da compreensão dos mecanismos envolvidos na apoptose e ciclo celular para encontrarmos moléculas que atuem nestas vias (SHASTRY; YARDLEY, 2013).

A apoptose, conhecida como morte celular programada, é um programa celular fundamental inerente a todas as células do corpo humano. A apoptose desempenha um papel crítico durante diversos processos fisiológicos, assim como em condições patológicas. A morte celular programada mantém a homeostase pela eliminação controlada das células que não são mais necessárias ou que sofreram algum dano, entrando então no processo de apoptose (HASSAN et al., 2014; SAYERS, 2011). A apoptose em condições normais é um mecanismo que previne a tumorigênese, portanto, uma vez que este controle é perdido, as células perdem o controle na proliferação, formando os tumores. Consequentemente este processo participa também na progressão tumoral e a resistência ao tratamento do câncer (FULDA, 2014a).

Durante a apoptose ocorrem algumas mudanças morfológicas tais como o encolhimento celular, formação de vesículas, formação de corpos apoptóticos no citoplasma, ausência de sinais inflamatórios, degradação da membrana celular e condensação da cromatina. Assim que as células produzem os corpos apoptóticos, estes são englobados e digeridos por células do sistema imune como os macrófagos (ELMORE, 2007).

A morte celular programada possui duas vias principais, a extrínseca e a intrínseca. A via extrínseca é conhecida também por ser a via ativada por receptores de morte, TRAIL e TNF, os quais recrutam moléculas adaptadoras como a Fas e FADD, que por sua vez se associam com a pro-caspase-8. Uma vez que essas moléculas se associam, há a formação de um complexo conhecido como indutor da morte DISC (DISC: ***D**eath-**I**nducing **S**ignalig **C**omplex*). Nesse processo, a caspase-8 é então ativada e consequentemente, recruta e ativa as caspases efetoras-3 e -7. A caspase-8 também pode mediar a clivagem de Bid em tBid interligando as vias extrínseca e intrínseca, pois a tBid induz a ativação de Bax, membro da

família Bcl-2, importante na via intrínseca (FULDA, 2014b). Pela via intrínseca, também conhecida como mitocondrial, proteínas da família Bcl-2, tais como Bax e Bak (proteínas pró-apoptóticas) são ativadas e induzem a permeabilização da membrana da mitocôndria, e assim moléculas como o **citocromo c** e Smac são também ativadas. Em seguida, o **citocromo c** ativa a pro-caspase-9 e Apaf-1, a caspase-9 é clivada e então ativa as caspases efetoras 3 e 7, consequentemente, ocorrendo a apoptose. Esta via também pode ser regulada pela Bcl-2, uma proteína antiapoptótica, que inibe a Bax (SAYERS, 2011). As vias intrínsecas e extrínsecas (via TRAIL) podem ser visualizadas na Figura 7.

Figura 7 – Vias de sinalização da apoptose.

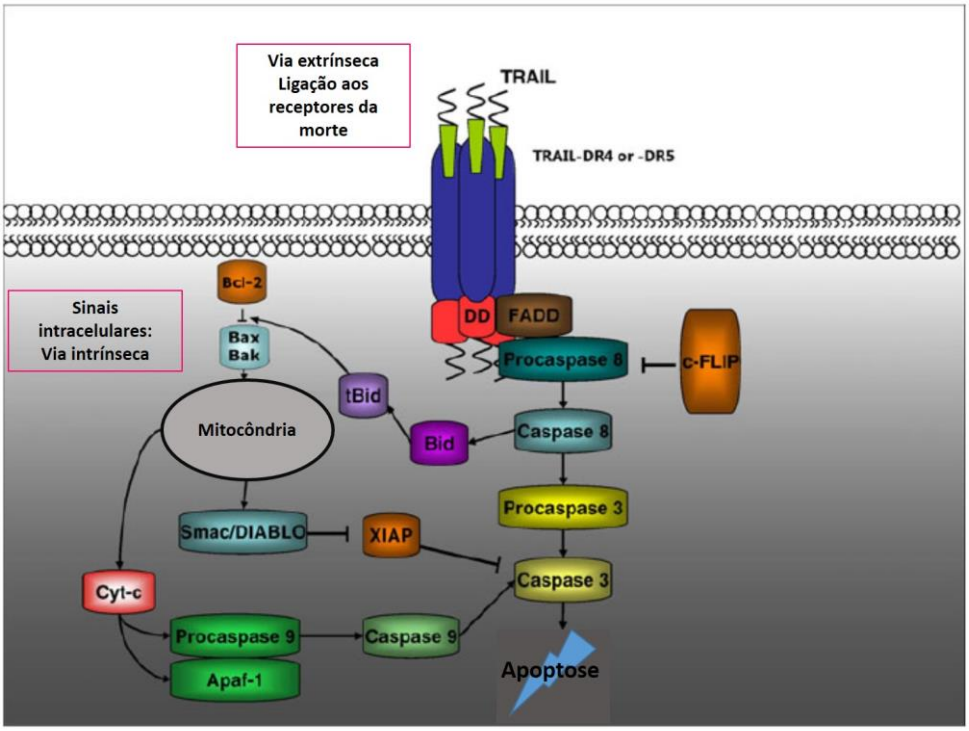

Modificado de Sayers 2011(SAYERS, 2011).

A via intrínseca é estimulada por sinais intracelulares que agem diretamente em eventos iniciados pela mitocôndria. Os sinais variam desde a radiação, toxinas, hipóxia, infecções virais até a presença de radicais livres. Quando esta via é ativada por esses estímulos, o citocromo c é ativado e consequentemente ativa a caspase-9 e Apaf-1 formando o apoptossomo, e consequentemente ativando as caspases efetoras como descrito acima (ELMORE, 2007).

A apoptose não é o único mecanismo que regula a morte celular. A necrose também pode ocorrer, e esta tem sido descrita tradicionalmente como uma morte passiva, mas

atualmente sabe-se que parte dessa morte pode ocorrer através de um mecanismo conhecido como necroptose ou necrose programada. A necroptose pode ser ativada pelos mesmos ligantes da apoptose, como o TNF-α, Fas e TRAIL. Entretanto, a via ativada é através da RIP1 (*Receptor interacting protein 1*) que é considerada a molécula chave na necroptose. A RIP1 é então ativada e se associa com a RIP3 formando o complexo necroptótico IIb, induzindo a necroptose. Sabe-se da existência de um inibidor da formação do complexo IIb conhecido como Nec-1 (Necrostatina-1), entretanto, pouco se sabe sobre qual via será ativada através dos receptores da morte (CHRISTOFFERSON; YUAN, 2010; GALLUZZI; KROEMER; VILLEJUIF, 2008).

Sabe-se que células tumorais podem ser resistentes aos tratamentos. Um trabalho recente descreveu que quando o tratamento é caracterizado por fármacos que induzem apoptose, algumas células podem se tornar resistentes. Isto também acontece em tratamentos que utilizam fármacos que ativam a necrose (outra forma de morte celular), portanto, é necessário o uso de tratamentos que atuem via apoptose, necroptose e uma terceira via de morte celular, como inibição do ciclo celular, para eliminar células com dupla-resistência (HU; XUAN, 2008). Este mecanismo pode ser melhor compreendido observando-se a Figura 8.

Figura 8 – Tratamento simultâneo em diferentes vias da apoptose para evitar a resistência das células tumorais.

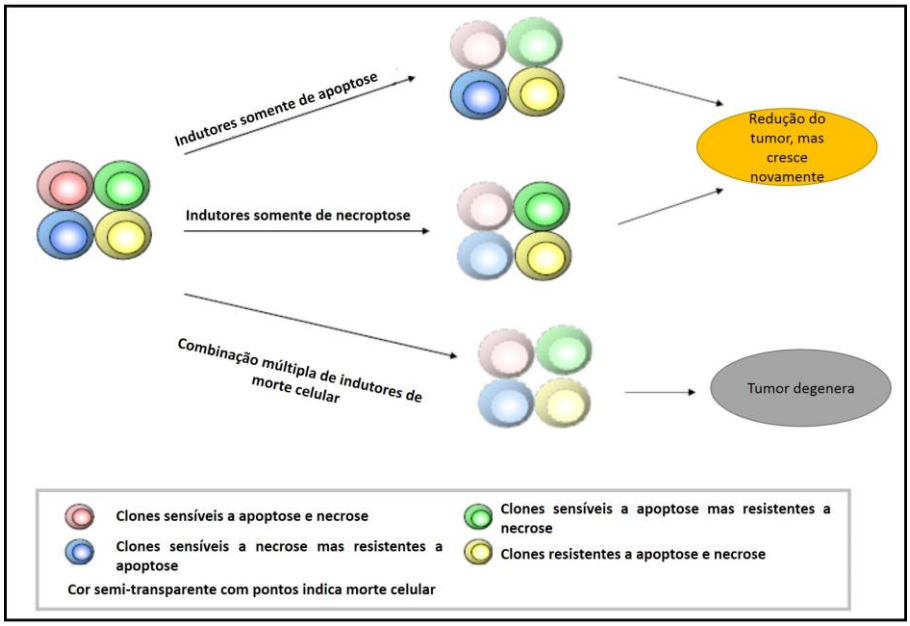

Modificado de Hu & Xuan 2008 (HU; XUAN, 2008).

O ciclo celular é um conjunto de eventos monitorados e extremamente organizados, responsáveis pela divisão celular adequada em duas células-filha. É um processo que demanda altos níveis de energia e requer uma série de eventos que garantem a correta duplicação e segregação do genoma. Esse processo ocorre em 4 fases que vai da dormência ou descanso (fase G0) até a proliferação, dividida em G1, S, G2 e M, e volta ao seu estado de descanso. O ciclo também pode ser dividido em interfase (G1, S e G2) e mitose (M) (DIAZ-MORALLI et al., 2013).

As células podem sair de sua fase de dormência, G0, e entrar na primeira fase do ciclo, G1, se estiverem proliferando. Nesta primeira fase a célula prepara seu DNA para síntese, seguida da fase S, onde ocorre efetivamente a síntese do DNA. Em seguida, a fase G2 caracteriza-se pela preparação da célula para a mitose, esta acontece na fase M. As células podem durante G1 entrar no estado de descanso e permanecer na fase G0, fase em que a célula não cresce e não prolifera no organismo (VERMEULEN; VAN BOCKSTAELE; BERNEMAN, 2003). Este processo é regulado por complexos chamados ciclinas-CDKs (que são ciclinas e kinases dependentes de ciclinas). A transição de uma fase para outra é monitorada por mecanismos chamados *checkpoints* (pontos de checagem) para manutenção dessa sequência de eventos, que fazem com que a próxima fase somente ocorra quando a anterior esteja totalmente completa. Além disso, esse mecanismo tem como objetivo final detectar e reparar danos do DNA, prevenir divisão celular descontrolada e garantir que as duas células-filhas contenham todo o material genético presente na célula-mãe. Os pontos de checagem são ativados quando um erro é detectado e a célula para seu ciclo celular até que o problema se resolva, caso contrário a célula entra em senescência ou apoptose (DIAZ-MORALLI et al., 2013). As fases do ciclo celular e seus pontos de checagem podem ser visualizados na Figura 9.

Figura 9 – Fases do ciclo celular e seus pontos de checagem.

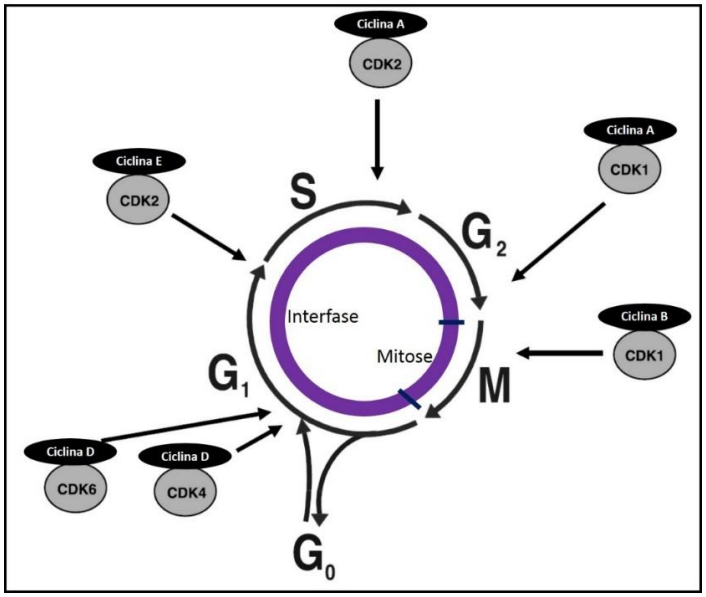

Modificado de Vermeulen e colaboradores 2003 (VERMEULEN; VAN BOCKSTAELE; BERNEMAN, 2003).

Células tumorais apresentam modificações que são reguladas pelo ciclo celular e consequentemente, pela falta de regulação das CDKs: a proliferação exacerbada, a instabilidade genômica e cromossômica, resultando na divisão descontrolada dessas células e portanto, na formação dos tumores (LAPENNA; GIORDANO, 2009; MALUMBRES; BARBACID, 2009). Assim sendo, novos fármacos que atuem induzindo a apoptose ou inibindo o ciclo celular são de grande importância para o tratamento do TNBC.

1.5 Produtos Naturais

Apesar da terapia contra o câncer através de cirurgia e radioterapia ser a mais usual, quando as células se espalham para outros órgãos o tratamento mais usado é a quimioterapia. O tratamento quimioterápico consiste em medicamentos que atuam de forma sistêmica e não somente sobre as células tumorais. Porém, estes medicamentos apresentam efeitos colaterais severos, e portanto, devem ser usadas em níveis subótimos para redução desses efeitos. A baixa eficácia no tratamento de metástases pela quimioterapia faz necessário o desenvolvimento de novos agentes quimioterápicos, principalmente para os TNBC que não possuem terapias-alvo (MARTIN-CORDERO et al., 2012a; NAMBIAR; RAJAMANI; SINGH, 2011).

Com o começo da revolução industrial e introdução de drogas modernas, o uso de plantas medicinais foi abandonado por um período, mas com o surgimento de novas técnicas de extração e separação de compostos houve um aumento no estudo e nas descobertas de

novos produtos com atividade medicinal (SAFARZADEH; SHOTORBANI; BARADARAN, 2014). O interesse no uso de drogas medicinais é proveniente de estudos populacionais que mostraram que pessoas que vivem em países asiáticos têm menor risco de desenvolveram câncer de colo, gastrointestinal, próstata e mama quando comparados com países ocidentais. Habitantes de países orientais cuja dieta é rica em gengibre, soja, cebola, tomate, pimentas e chá verde apresentam menor incidência desses tumores (DORAI; AGGARWAL, 2004). Esses alimentos e seus componentes ativos são conhecidos como produtos naturais. Durante o período de 1981-2002, 48% dos medicamentos antitumorais produzidos foram derivados de produtos naturais ou drogas sintéticas que mimetizam produtos naturais e seus compostos (Figura 10) (NEWMAN; CRAGG; SNADER, 2007). Entre 1981 e 2008, 6% das drogas antitumorais eram produtos naturais não modificados, e somente 37% dos medicamentos não eram relacionados a produtos naturais (MARTIN-CORDERO et al., 2012b).

Figura 10 – Relação de drogas na sua totalidade e de drogas antitumorais entre os anos 1940-2002.

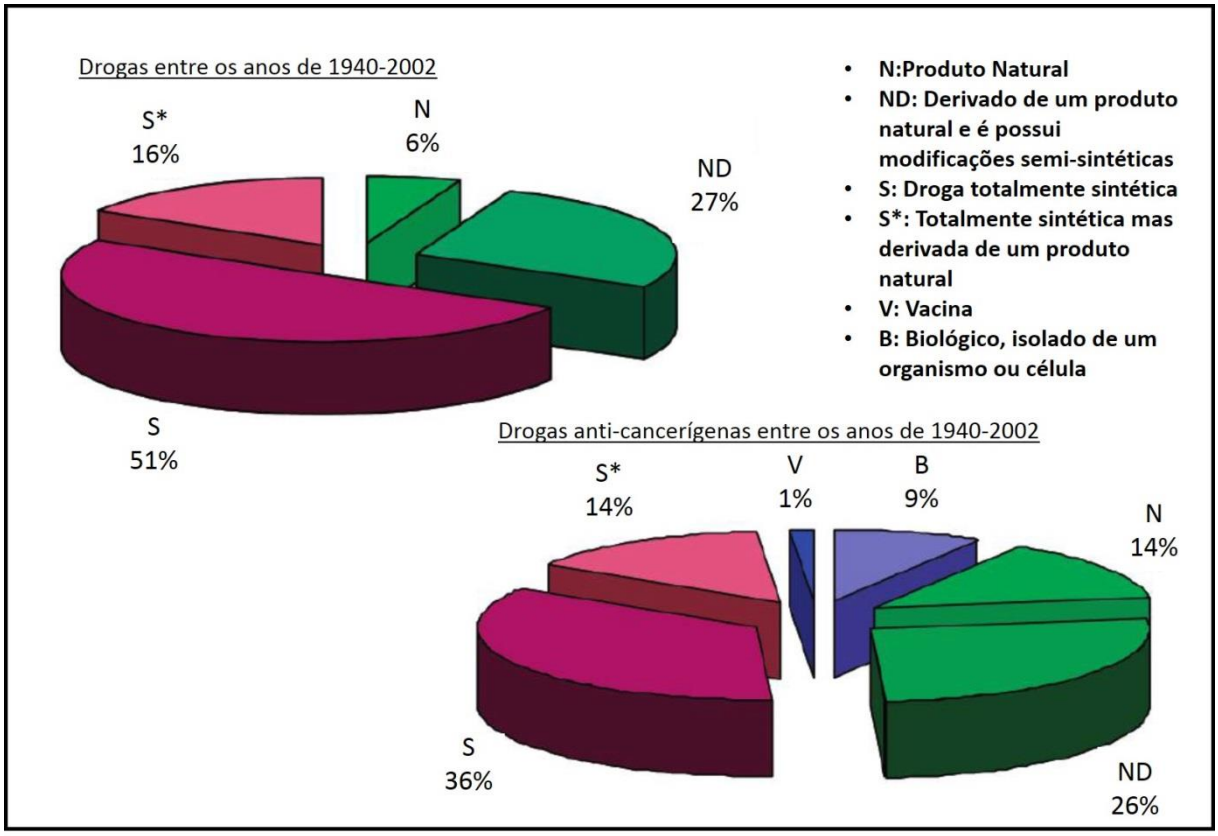

Modificado de Newman e colaboradores, 2007 (NEWMAN; CRAGG; SNADER, 2007).

Os primeiros compostos naturais a avançarem clinicamente como antitumorais foram a vimblastina e a vincristina, assim como o taxol (chamado também de Paclitaxel) e seus análogos (docetaxel). Esses produtos atuam nos microtúbulos e na DNA toposiomerase II, além de aturarem na formação de espécies reativas de oxigênio (ROS) (SAFARZADEH; SHOTORBANI; BARADARAN, 2014). O taxol foi isolado primeiramente da casca da árvore *Taxus brevifolia*, mas pode também ser sintetizado nas folhas da árvore. O taxol é usado no tratamento de câncer de mama, ovário e pulmão. O docetaxel, um derivado semi-sintético do taxol é usado primariamente no tratamento de câncer de mama (PRAKASH et al., 2013).

Os produtos naturais podem agir como radiomoduladores, atuando como radioprotetores, protegendo as células normais ao redor das células normais, e radiosensibilizadores, tornando as células tumorais mais sensíveis à radiação ou a quimioterapia (quimiosensibilização). Portanto, o uso destes compostos em conjunto com as terapias usuais pode aumentar a potência destas e consequentemente diminuir os efeitos colaterais provenientes desses tratamentos, pois a dose da radiação ou quimioterapia pode ser menor em associação com os produtos naturais, tendo o mesmo efeito final, ou até mesmo melhor (NAMBIAR; RAJAMANI; SINGH, 2011).

Compostos fenólicos são originados a partir de umas das maiores classes de metabólitos secundários das plantas. Um desses metabólitos é o resveratrol (RSVT), um dos produtos naturais mais conhecidos e descritos na literatura. Este composto faz parte do grupo dos estilbenos e é um polifenol natural isolado da helebore branca, uvas e amendoim. O RSVT é conhecido por suprimir proliferação e invasão celular e induzir apoptose em diferentes linhagens tumorais. Seu alto poder inibitório contra a progressão tumoral sugere ser um importante agente quimiopreventivo contra o câncer (WENG; YEN, 2012).

O RSVT é considerado um fitoestrógeno e sua estrutura é muito semelhante ao hormônio estrógeno. Apesar do RVST possuir uma menor especificidade ao receptor nuclear de estrógeno, foi demonstrado que esta molécula de liga a integrina αvβ3 e sua atuação é independente do receptor de estrógeno (ER), pois age em linhagens celulares ER+ e ER- (LIN et al., 2006). O trans-RSVT possui maior atividade antitumoral comparado à sua isoforma cis-RSVT, inibindo a proliferação celular de células endoteliais e a formação de vasos *in vivo* (BELLERI et al., 2008). Outros estudos mostraram um efeito inibitório do RSVT na migração celular de células MDA-MB-231 (células tumorais de mama humana) e 4T1 (células tumorais de mama de camundongo), além disso, foi capaz de inibir a expressão de MMP-9 pelas células 4T1 e sua colonização nos pulmões em camundongos Balb/c (SOOK; HA; KIM,

2012), mostrando ser um importante produto natural para a prevenção e tratamento de câncer de mama.

O gengibre pertence à família tropical e subtropical Zingiberaceae, originada do sul e leste da Ásia, entretanto foi introduzido em diversas partes do mundo e é cultivado há milhares de anos como especiaria e com propósitos medicinais. O extrato do gengibre foi descrito por possuir um efeito antiemético em pacientes tratados com quimioterapia diminuindo náusea e vômitos (HANIADKA et al., 2012). O gengibre é constituído por óleos voláteis que contribuem para o aroma e sabor do gengibre e por compostos pungentes não voláteis que constituem os compostos ativos, tais como gingeróis, shogaóis, paradóis e zingeronas, os quais são responsáveis pela sensação de calor na boca quando consumidos. Os gingeróis representam uma série de produtos químicos que diferem pelo número de cadeias alquil e são os compostos mais ativos desta raiz (SHUKLA; SINGH, 2007).

Foram descritos a existência do: [6]-, [8]-, [10]-gingerol, que diferem entre si, pelo tamanho da cadeia de alquil, apresentando 10, 12 e 14 carbonos, respectivamente (SILVA et al., 2012). O [6]-gingerol é o composto mais estudado e encontrado em maior abundância no gengibre, seguido pelo [8]- e [10]-gingerol. O [6]-gingerol inibe a migração, invasão e a atividade da MMP-2/9 em células tumorais humanas de mama MDA-MB-231 *in vitro* (LEE et al., 2008), e ainda é capaz de inibir a proliferação de células endoteliais HUVEC (*Human Umbilical Vein Endothelial Cells*) induzidas por VEGF (KIM et al., 2005). Recentemente, pesquisadores demonstraram que o [6]-gingerol induz a apoptose em células HeLa (câncer cervical) através da fragmentação do DNA, perda do potencial de membrana mitocondrial, além de aumentar a expressão de Caspase-3 (CHAKRABORTY et al., 2012).

Em um trabalho desenvolvido por nosso grupo demonstrou o [10]-gingerol é o que possui menor IC_{50} entre os gingeróis; [6], [8] e [10], em linhagem tumoral de câncer de mama, MDA-MB-231. Além disso, usando-se a mesma concentração em todos o gingeróis, o [10]-gingerol foi o que mais inibiu a proliferação da linhagem tumoral de mama MDA-MB-231 sem afetar a proliferação de uma linhagem normal, fibroblastos humanos (SILVA et al., 2012), sugerindo-se uma atividade seletiva por células tumorais. Um trabalho recente de Ibrahim e colaboradores (2014), demonstrou que o [6]-gingerol possui atividade antitumoral superior ao CDF (5-Fluorouracil), um agente quimioterápico já usado clinicamente, com um IC_{50} de 30,4µM. Ainda, modificações semissintéticas mostraram que a presença de um grupo hidroxil na cadeia lateral é essencial para sua atividade antitumoral, assim como, a perda do anel aromático. Reduções no comprimento da cadeia lateral e a metilação no grupo fenólico

reduziram sua atividade anticancerígena, enfatizando a importância da estrutura dessas moléculas (IBRAHIM et al., 2014).

Um recente trabalho publicado por Ryu & Chung, demonstrou que em células de câncer de colo humano o [10]-gingerol possui uma atividade antitumoral maior que o [6]-gingerol. E que o [10]-gingerol possui uma atividade antiapoptótica, com aumento da expressão da caspase-9, -3, PARP, Bax, fosforilação de JNK, ERK e MAPK; além da redução de Bcl-2; ressaltando seu papel antitumoral (RYU; CHUNG, 2014). Contudo, pouco se sabe sobre a atividade antitumoral e mecanismos de ação do [8]- e principalmente do [10]-gingerol *in vitro* e *in vivo* no câncer de mama.

1.6 Modelos de metástase in vivo

Para estudar a atividade desses produtos naturais, alguns modelos animais podem ser utilizados para mimetizar o que ocorre em uma mulher com câncer de mama. Foram descritos dois modelos animais utilizados na literatura: o modelo de metástase experimental e o modelo de metástase espontâneo (ECKHARDT et al., 2012; PEARSON; POULIOT, 2012). O modelo espontâneo é caracterizado pela formação do tumor primário com consequente entrada das células tumorais na corrente sanguínea para formar metástases em órgãos distantes. Neste modelo podemos estudar drogas que atuem no tumor primário e também na inibição da metástase já que há a formação do tumor e as células são capazes de se estabelecer em outros órgãos. Uma modificação desse modelo pode ser realizada pela remoção do tumor primário, e se o tratamento for iniciado após a cirurgia, avaliar é possível avaliar se realmente o medicamento testado atua somente na inibição da metástase. No modelo experimental, por sua vez não há a formação do tumor primário e as células são injetadas diretamente na corrente sanguínea, onde irão migrar para seus sítios metastáticos. Portanto, este modelo tem maior utilidade para estudo da inibição de metástases comparado com o crescimento tumoral primário (ECKHARDT et al., 2012).

O modelo singênico é aquele em que as células tumorais usadas são da mesma espécie do animal, e xenográficos, em que as células usadas são de uma espécie diferente do animal (ex.: uso de células ou tecidos humanos em camundongos). Ainda, os modelos ortotópicos utilizam células da mesma origem aonde serão injetados (ex.: células de mama injetadas na mama do animal) e os ectotópicos, utilizam linhagens de origens diferentes (ex.: células tumorais de mama injetadas no coração) (PEARSON; POULIOT, 2012). Os modelos de metástase podem ser melhor visualizados na figura abaixo:

Figura 11 – Modelos de metástase *in vivo*.

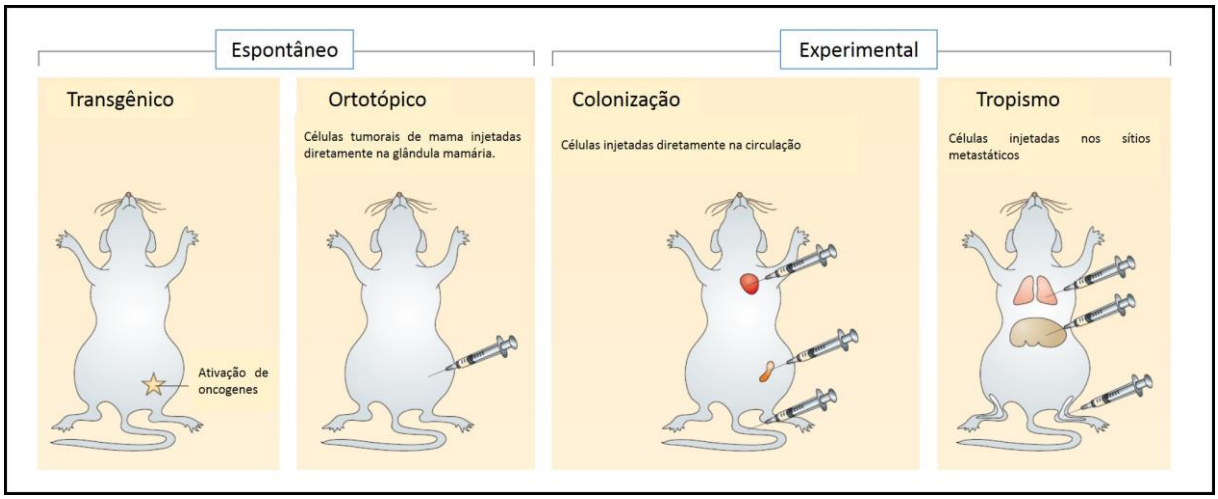

Nesta imagem estão apresentados os modelos de metástase espontâneo divido em transgênico, quando se usa animais modificados geneticamente com ativação de oncogenes, e o modelo ortotópico, quando células tumorais são injetadas no seu tecido de mesma origem. A direita, estão os modelos de metástase experimental, que não possuem a formação do tumor primário em que as células podem ser injetadas diretamente na corrente sanguínea (colonização) migrando para seus sítios metastáticos ou serem injetadas diretamente nos órgãos metastáticos (tropismo). Imagem Modificada de Eckhardt *et al.* (ECKHARDT et al., 2012).

Esses modelos podem variar ainda mais dependendo da linhagem celular utilizada, pois cada linhagem possui características diferentes que as permitem migrar para diferentes órgãos. Isto pode ser visualizado na figura a seguir, onde as linhagens estão indicadas e os círculos indicam os órgãos que estas células tendem a migrar (PEARSON; POULIOT, 2012).

Figura 12 – Esquema das linhagens celulares de câncer de mama com diferentes potenciais metastáticos.

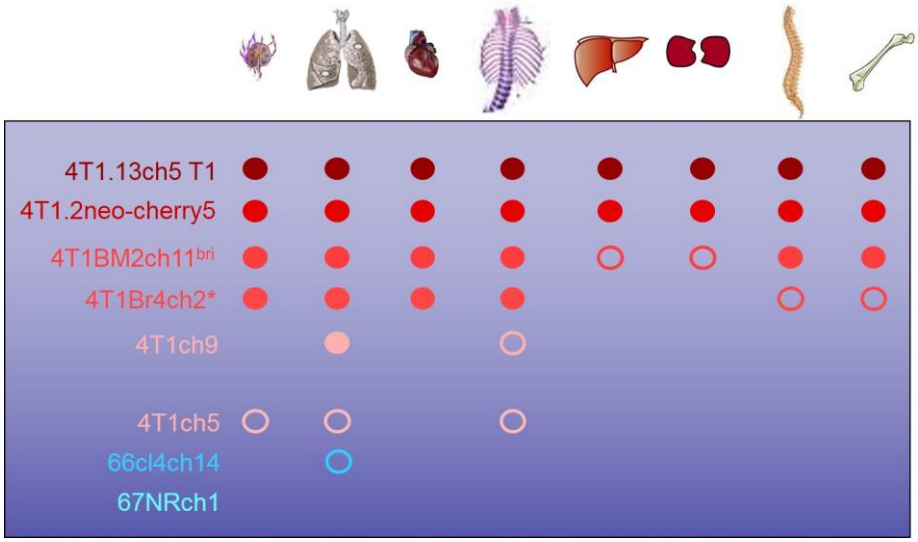

À esquerda estão indicados os nomes das linhagens tumorais de câncer de mama e à direita os possíveis órgãos que estas células podem metastatizar. Na ordem: linfonodos, pulmão, coração, cavidade torácica, fígado, rins, coluna espinal e fêmur. Quanto mais forte a cor nos círculos, maior o poder da linhagem metastatizar para aquele órgão. Imagem gentilmente cedida por Richard Redvers, Laboratório de Metástase – Peter MacCallum – Melbourne - Austrália.

Os modelos utilizados nesse trabalho foram o espontâneo com injeção das células tumorais de mama murino (ortotópico e singênico) no tecido adiposo da quarta mama de camundongas (IMFP- *Intra-mamary Fat Pad*) Balb/c, com e sem cirurgia do tumor primário e tratamento com o produto natural, e o experimental com injeção das células tumorais no ventrículo esquerdo dos animais que em seguida foram tratados com o PN. A linhagem tumoral de mama utilizada foi a 4T1Br4 que tende a ter, além das metástases usuais, como fêmur, coluna espinhal e pulmão, maior índice de metástases cerebrais. Esta linhagem foi isolada a partir da 4T1, uma linhagem usualmente usada em modelos *in vivo* de câncer de mama, a partir de uma metástase cerebral encontrada nos camundongos. O isolamento desta linhagem está explicado na figura abaixo. O modelo de IMFP foi baseado no trabalho de Sloan e colaboradores (SLOAN et al., 2006).

Figura 13 – Seleção da linhagem de células de tumor de mama murino 4T1Br4.

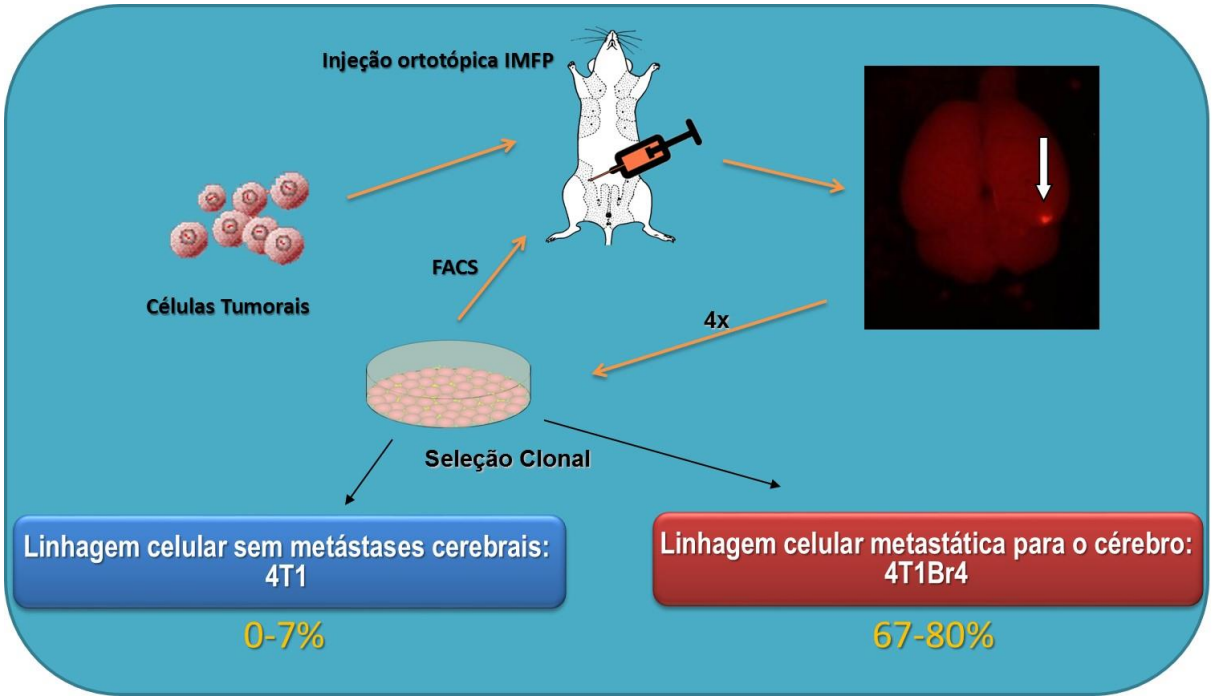

Para isolar a linhagem 4T1Br4, a linhagem 4T1 foi injetada na IMFP. A metástase cerebral foi isolada em cultura e depois selecionada via citometria de fluxo (FACS), pois as células tumorais são marcadas com a fluorescência mCherry, e novamente injetadas na IMFP. Este processo foi repetido 4 vezes até se obter a linhagem 4T1Br4 com uma incidência sete vezes maior de metástase cerebral. Imagem gentilmente cedida por Soo Kim, Laboratório de Metástase – Peter MacCallum – Melbourne – Austrália.

2 JUSTIFICATIVAS

Como dito anteriormente, a maior causa de morte pelo câncer é a metástase (BROOKS et al., 2010; GEIGER; PEEPER, 2009; PERRET; CRÉPIN, 2008). Atualmente a maior parte dos tratamentos para o câncer de mama e de suas metástases apresentam grandes efeitos colaterais, portanto, pesquisas que proporcionem o surgimento de possíveis novos medicamentos, incluindo os provenientes de produtos naturais, são de grande importância (SAFARZADEH; SHOTORBANI; BARADARAN, 2014).

O resveratrol é um composto bem estudado e já se sabe muitas informações sobre sua atividade preventiva e antitumoral *in vitro* e *in vivo* (LIN et al., 2006; SOOK; HA; KIM, 2012). Entretanto, pouco se sabe sobre tais atividades com relação aos gingeróis, principalmente o [10]-gingerol, encontrado em menores quantidades no gengibre.

No laboratório LABEN-UFSCar (Laboratório de Biologia do Envelhecimento) vem sendo estudados diferentes produtos naturais e suas atividades em células tumorais e normais, dentre eles, [6]-, [8]- e [10]-gingerol. Recentemente, este grupo publicou um trabalho comparativo da atividade destes compostos demostrando que dentre eles o [10]-gingerol possui maior potência em células tumorais de câncer de mama (MDA-MB-231) e pouca toxicicidade em células normais (fibroblastos humanos) (SILVA et al., 2012). Em colaboração com o LABEN e o Laboratório de Metástases do Instituto Peter MacCallum iniciamos um novo projeto para estudar a atividade do [10]-gingerol em ensaios *in vitro* e *in vivo* em comparação ao RSVT.

Além disso, esse estudo teve como objetivo estudar uma linhagem celular de câncer de mama TN que forma metástases cerebrais (4T1Br4). Já que este tipo de câncer apresenta maior resistência aos tratamentos usuais, há poucos medicamentos e intervenções possíveis. Alguns produtos naturais são capazes de cruzar a barreira hematoencefálica devido seu tamanho e estrutura química. O RSVT e o [10]-gingerol apresentam estruturas e características químicas similares que nos permite predizer que estes são capazes de atravessar a barreira cerebral, sendo ainda mais interessante o estudo destes compostos.

Portanto, estudos que visam entender os processos envolvidos na progressão tumoral e o estudo de novas moléculas com potencial antitumoral são de grande importância para o desenvolvimento de novos fármacos e justificam o estudo de compostos alternativos que apresentem maior eficácia e menores efeitos colaterais (DORAI; AGGARWAL, 2004).

Com isso, a hipótese desse trabalho é que o [10]-gingerol possui uma atividade antiproliferativa, induz a apoptose e atua na parada do ciclo celular. Além disso, o [10]-gingerol pode inibir o crescimento tumoral e a formação de metástases *in vivo*.

3 OBJETIVOS

OBJETIVO GERAL: Verificar o papel do [10]-gingerol, um produto natural proveniente do gengibre, na progressão tumoral do câncer de mama *in vitro* e em modelo murino.

OBJETIVOS ESPECÍFICOS:

1. Verificar a potência do [10]-gingerol como molécula antitumoral em diferentes linhagens de câncer de mama e seu efeito protetor em linhagens de células normais;
2. Comparar o seu efeito com o resveratrol
3. Determinar a especificidade de receptores celulares pelo [10]-gingerol em uma linhagem de câncer de mama espontaneamente metastática para o cérebro, através de ensaios de adesão e migração celular;
4. Determinar as vias de sinalização que o [10]-gingerol atua em ensaios de apoptose e ciclo celular;
5. Verificar se [10]-gingerol é capaz de inibir o crescimento do tumor primário e a formação de metástases em modelos de metástase de câncer de mama espontâneo e experimental *in vivo*.

4 MATERIAIS E MÉTODOS

4.1 Produtos Naturais: Resveratrol e [10]-gingerol

O [10]-gingerol foi extraído, isolado e fornecido pelo Laboratório de Produtos Naturais da Universidade Federal de São Carlos, no Departamento de Química, liderado pelos Professores Drs. João Batista Fernandes e Paulo Cezar Vieira. O Resveratrol (RSVT) foi adquirido comercialmente pela empresa Sigma-Aldrich para efeito de comparação. O RSVT usado foi o trans-resveratrol que apresentou a melhor atividade contra células tumorais em ensaios *in vitro* e *in vivo*, segundo a literatura revisada (BELLERI et al., 2008). Ambos os produtos naturais foram diluídos em DMSO (Dimetil sulfóxido) e nos ensaios foram adicionados ao meio de cultura apropriado aos mesmos.

As estruturas químicas dos produtos naturais podem ser observadas na Figura 14.

Figura 14 – Estrutura química dos produtos naturais utilizados neste estudo: [10]-gingerol (A) e Trans-resveratrol, RSVT (B).

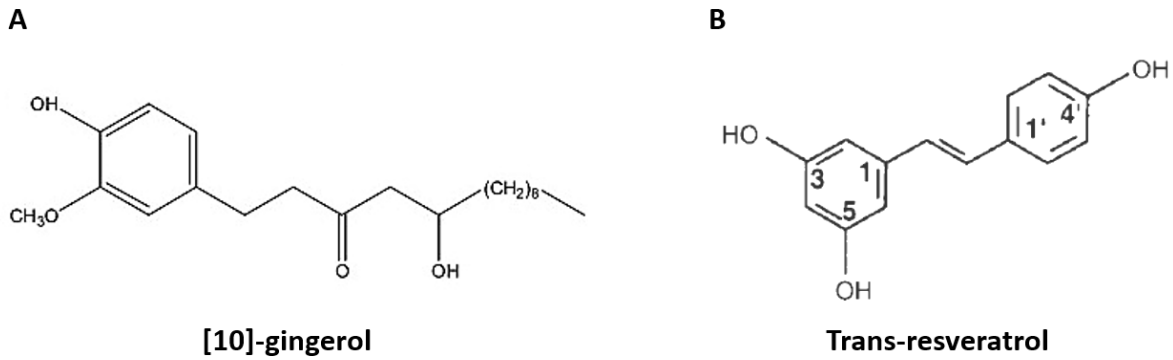

4.2 Linhagens e cultivos celulares

Durante o desenvolvimento deste estudo foram utilizadas diversas linhagens de câncer de mama e de células normais presentes no laboratório de Bioquímica e Biologia Molecular da UFSCar. Parte destas linhagens foram gentilmente cedidas pelo Dr. Normand Pouliot do laboratório de Metástase do Hospital Peter MacCallum, Melbourne – Austrália.

Dentre as linhagens utilizadas estão: 4T1BM2, 4T1BM2 shRNA β3, 4T1Br4, bEnd.3, MDA-MB-231 BrM e MDA-MB-231. As linhagens 4T1BM2, 4T1BM2sh RNAβ3 e 4T1Br4 são derivadas da linhagem 4T1, que foi isolada de um tumor formado espontaneamente em um camundongo Balb/c (ASLAKSON; MILLER, 1992; BLAZAR et al., 1978; HEPPNERY

et al., 1978; MILLER; CARE, 2000). Estas linhagens foram modificadas geneticamente e foram inseridas em seu DNA genômico uma marcação com a fluorescência "mCherry" (CARTER et al., 2015), além disso, possuem diferentes potenciais metastáticos como descrito a seguir.

A as linhagens 4T1BM2 e 4T1BM2 shRNAβ3 (CARTER et al., 2015) tem um maior potencial em formar metástases em ossos (fêmur e coluna espinhal, BM-*Bone Marrow*), além dos outros sítios comuns de metástase da 4T1, como pulmão, fígado e ovários. Estas diferem na expressão da subunidade da integrina β3, em que a linhagem 4T1BM2 expressa altos níveis desse receptor e 4T1BM2 shRNAβ3 não expressa o mesmo.

A linhagem 4T1Br4 forma metástases nos sítios comuns como descrito acima, além disso, apresenta um alto índice de metástases cerebrais (Br-*Brain*).

Para comparamos as atividades dos PNs com células normais foi utilizado a linhagem bEnd.3, que são células endoteliais da microvasculatura cerebral.

Neste trabalho, as linhagens MDA-MB-231 e MDA-MB-231 BrM foram utilizadas para comparamos as atividades dos PNs em células humanas. Estas diferem em seus potenciais metastáticos, em que a linhagem MDA-MB-231 BrM (*Brain Metastasis*) tem maior potencial metastático para o cérebro. Estas duas linhagens foram gentilmente cedidas ao Laboratório de Metástase (Peter MacCallum) pelo pesquisador Dr Joan Massagué.

As linhagens celulares foram cultivadas segundo orientações do ATCC (*American Type Culture Collection*) ou segundo recomendações do laboratório procedente e mantidas em estufa com 5% de CO_2 a 37ºC.Para as linhagens 4T1BM2, 4T1BM2 shRNA β3 e 4T1Br4 foi utilizado meio Alpha MEM (contendo 5% de soro bovino fetal (FBS), 1% de penicilina e estreptomicina, 2,2g $NaHCO_3$, 4g de NaCl, pH 7,2 para 1L). Para as linhagens MDA-MB-231, MDA-MB-231 BrM e bEnd.3 foi utilizado meio DMEM (contendo 10% FBS, 1% penicilina e estreptomicina, pH. 7,4).

4.3 Determinação e Cálculo da IC_{50}

Para calcular o IC_{50} (concentração do composto que inibe o crescimento das linhagens celulares em 50%) foi utilizado o ensaio de proliferação celular. Para isso, $1x10^3$ células foram plaqueadas em placas de 96 poços (linhagens: 4T1BM2, 4T1BM2 shRNA β3, 4T1Br4, bEnd.3, MDA-MB-231 BrM e MDA-MB-231) e incubadas em estufa de 6 a 8h para que as células aderissem aos poços. Decorrido o tempo de incubação os produtos naturais (RSVT e o [10]-gingerol) foram adicionados utilizando-se uma diluição seriada, em meio de cultura

apropriado para cada linhagem, de 200µM até 0, e então as placas foram incubadas por 72h. Depois de três dias de incubação as células foram fixadas com TCA (Ácido Tricloroacético) *overnight* a 4°C. Após uma série de lavagens as placas foram secas e coradas com o corante SRB (0,4% *Sulforodamine B*) por 30min. Decorrido o tempo, as placas foram lavadas e secas para a leitura com Tris 10mM (pH.10,5) no comprimento de onda de 564nm (*Versa Max Microplate Reader*). A determinação do IC_{50} de cada composto foi realizada a partir de uma curva de concentração utilizando o *software* GraphPadPrism 5.0 (SILVA et al., 2012).

4.4 Inibição da adesão celular

Para o ensaio de inibição da adesão, no dia anterior ao experimento, componentes da matriz extracelular como colágeno (10µg por poço de colágeno tipo IV diluído em PBS - *Phosphate-Buffered Saline*) ou vitronectina (5µg/ml) ou laminina 511 foram utilizados como *coating* em placas de 96 poços, *overnight* a 4°C. No dia seguinte os poços foram bloqueados com BSA 1% em PBS, por 2 horas a 37°C. As células tumorais da linhagem 4T1Br4 e MDA-MB-231 BrM foram marcadas com 5µl de calceína/ml células ($1x10^6$ células/ml, calceína 1mg/ml em DMSO – Molecular Probes) incubadas a 37ºC por 30min. O excesso do corante foi removido por lavagem com meio sem soro. As células marcadas ($1x10^5$ células/poço) foram então incubadas com diferentes concentrações dos compostos (10, 50, 100 e 500µM) em meio de cultura sem soro, por 30min no gelo. Decorrido o tempo as células foram depositadas sobre os poços da placa contendo os diferentes compostos da matriz extracelular citados acima e incubadas a 37ºC por 30min. Após uma série de lavagens para remoção das células não aderidas, as células restantes foram lisadas pela adição de SDS a 1% (*Sodium Dodecyl Sulphate)*. Em paralelo, uma curva padrão foi preparada na mesma placa utilizando-se concentrações conhecidas de células marcadas para quantificação do ensaio. A leitura foi realizada em leitor de placa (*Molecular Imager FX – BioRad*) em um comprimento de onda de 530nm (semelhante ao FITC – *Fluorescein Isothiocyanate*) (CARTER et al., 2015).

4.5 Citotoxicidade e Morfologia Celular

Um ensaio de toxicidade é uma forma simples para verificar se os produtos naturais estão atuando nas células de forma tóxica ou não. Para isso, $5x10^4$ células (4T1Br4 e MDA-MB231 BrM) foram plaqueadas e incubadas *overnight.* No dia seguinte, as células foram incubadas com os dois produtos naturais separadamente por diferentes tempos em meio sem

soro (40min, 4h, 8h, 24h). Decorrido o tempo de incubação, as células foram fixadas com tampão formalina 10% e posteriormente, fotos foram obtidas em microscópio invertido (Axiovert - Zeiss) para avaliar a morfologia das células incubadas com os diferentes produtos naturais.

4.6 Ensaios de Migração Celular

4.6.1 Migração Quimiotática

Neste ensaio é verificada a capacidade do produto natural em inibir a migração de forma dependente de um quimioatraente, no caso, o soro fetal bovino (FBS). O FBS foi descrito por ser rico em vitronectina, portanto, este ensaio é capaz de avaliar se o PN poderia inibir a migração através deste componente da MEC (HAYMAN et al., 1985). Para este ensaio, $2x10^5$ células da linhagem 4T1Br4 foram incubadas com diferentes concentrações dos compostos por 30min no gelo (3, 10, 25, 50 e 100µM). Decorrido o tempo, as células foram plaqueadas sobre os insertos de 8µm (*Transwells*- BD) em meio sem soro. Meio contendo 10% soro bovino fetal foi adicionado nos poços inferiores para atuar como quimioatraente das células tumorais.

Depois de 4h de incubação em estufa, as células que não migraram foram removidas com o auxílio de uma haste de algodão e as células que migraram foram fixadas com tampão 10% de formalina; posteriormente seus núcleos foram marcados com DAPI - *4',6-Diamidino-2-Phenylindole, Dihydrochloride* (0,5µg/10mL). Os insertos foram retirados e uma lâmina foi montada com o auxílio de DPX (para montagem de histologia composto de: Distireno, um Plastificante e Xileno - Sigma-Aldrich) entre o inserto e a lâmina/lamínula. Em seguida, as lâminas foram fotografadas em três campos por inserto para quantificar as células que migraram (SLOAN et al., 2006).

4.6.2 Migração Haptotática

Para verificar a especificidades dos compostos por diferentes receptores foi realizado um ensaio de migração celular utilizando componentes da matriz extracelular para verificar quais os possíveis receptores estes compostos poderiam estar se ligando. Para isso, insertos de 8µm foram recobertos com componentes da matriz *overnight* 4°C nas mesmas concentrações utilizadas para o ensaio de inibição da adesão, descrito acima. No dia seguinte, $2x10^5$ células da linhagem 4T1Br4 foram incubadas com diferentes concentrações dos compostos naturais

por 30min no gelo. Decorrido o tempo de incubação as células foram plaqueadas sobre os insertos contendo o *coating* da MEC e foram incubadas em estufa por 3h. Os insertos foram processados e analisados como descrito acima para o ensaio de migração quimiotática (SLOAN et al., 2006).

4.7 Ensaio de proliferação – 5 dias

Para verificar as concentrações que o [10]-gingerol atua na inibição da proliferação, foi realizado um ensaio de proliferação de 5 dias com uma alta e uma baixa concentração de [10]-gingerol, 10 e 50µM, respectivamente Neste ensaio, 500 células da linhagem 4T1Br4 e 2000 células da linhagem MDA-MB-231 BrM, foram plaqueadas por poço em placas de 96 poços overnight em estufa à 37°C. No dia seguinte, as células foram tratadas com o [10]-gingerol nas concentrações de 10 e 50µM por 5 dias. Após 24, 48, 72, 96 e 120h os poços foram lavados com PBS para retirada do produto natural e adicionado uma solução de MTT (3-(4,5-dimethylthiazol-2-yl)-2,5-diphenyltetrazolium bromide, 1mg/mL) por 4h. Decorrido o tempo de incubação, foram adicionados aos poços 150µl de isopropanol e as placas foram incubadas em estufa para dissolver os cristais de formazan. Em seguida, foi realizada a leitura em leitor de placa Dynex (Dynex Revelation 4.02 – software) no comprimento de onda de 540nm.

4.8 Ensaio clonogênico com/ sem radio-sensibilização

Os produtos naturais possuem potentes efeitos citostáticos e citotóxicos, além disso foram descritos como radio-sensitivos em células tumorais. Para comprovar sua eficácia na proliferação/toxicidade e radiosensibilização foi realizado um ensaio clonogênico. Para isso, células em uma baixa densidade da linhagem 4T1Br4 (100 células por poço, em placa de 6 poços) foram plaqueadas e depois de 6h estas foram incubadas com concentrações similares ao encontrado no ensaio de IC_{50}. No dia seguinte, as placas foram irradiadas com diferentes graus de radiação (2, 4 e 6 Gy, radiação por césio) e incubadas por 7 dias em estufa. Posteriormente, as colônias formadas foram coradas com cristal violeta por 30min sobre agitação e as placas secas para posterior análise. As colônias foram contadas manualmente e seus tamanhos analisados com o auxílio do *software* ImageJ (YANG et al., 2012b).

4.9 Ensaio de Condensação nuclear

Para verificar se o [10]-gingerol é capaz de induzir a condensação nuclear, processo que ocorre durante a apoptose celular, $1x10^5$ células/poço da linhagem 4T1Br4 foram plaqueadas sobre lamínulas redondas estéreis em placas de 12 poços por 24h. No dia seguinte, as células foram tratadas com diferentes concentrações de [10]-gingerol (1µM - 100µM) também por 24h. Decorrido o tempo de incubação as células foram fixadas com metanol por 5min e coradas com uma solução de DAPI (5mg/mL diluído em meio sem soro, Invitrogen) por 10min. Em seguida os poços foram lavados com PBS e as lâminas foram montadas para análise qualitativa em microscópio de epifluorescência Olympus Bx50, com os filtros apropriados. O software utilizado para adquirir as imagens foi o CoolSNAP-pro, Image Pro Plus versão 4.1.

4.10 TUNEL

No ensaio conhecido como TUNEL (Terminal deoxynucleotidyl transferase dUTP nick end labeling, *The DeadEnd Colorimetric* TUNEL, Promega) é possível analisar células apoptóticas *in situ* pela coloração do DNA fragmentado destas células. Para isso, $1x10^6$ células da linhagem 4T1Br4 foram plaqueadas sobre lâminas contendo poli-L-Lysina, e posteriormente tratadas com [10]-gingerol por 18h nas concentrações de 10 e 50µM. Decorrido o tempo de incubação, as células foram fixadas em tampão formalina 10% por 25min em temperatura ambiente. Em seguida, as lâminas foram lavadas com PBS por 5min e permeabilizadas com 0,2% Triton X-100 em PBS também por 5min. Logo após, as lâminas foram lavadas com PBS. As lâminas foram coradas conforme protocolo descrito pelo fabricante. Resumidamente, as lâminas foram incubadas com tampão de equilíbrio por 10min; em seguida foi adicionado uma mistura de nucleotídeos biotinilados na reação com a enzima recombinante rTdT (*Terminal Deoxynucleotidyl Transferase*) por 1h, a reação foi cessada através da adição do tampão SSC (contendo NaCl e citrato de sódio) do kit por 15min. Em seguida as lâminas foram lavadas com PBS e a peroxidases endógenas foram bloqueadas pela incubação das lâminas com 0,3% peróxido de hidrogênio e lavadas novamente com PBS. Uma solução de HRP-estreptavidina (*Horseradish peroxidase*-marcada com estreptavidina) foi diluída em PBS (1:500) e adicionada a cada lâmina por 30min a temperatura ambiente. Seu substrato DAB (Iaminobenzidina) foi adicionado após o tempo de incubação até que as lâminas apresentassem um fundo marrom (por volta de 10min).

Por fim, as lâminas foram lavadas várias vezes em água destilada. Então, as lâminas foram preparadas com óleo de imersão (100% glicerol) para análise qualitativa da atividade dos produtos naturais sobre a apoptose das células tumorais. As imagens foram capturadas com auxílio do *software* Motic e de uma câmera (Moticam 1000 – 1,3MP Live Resolution) acoplada ao microscópio (Oleman (N-120)).

4.11 Análise do Ciclo celular

Para analisar a atividade do produto natural no ciclo celular, células tumorais da linhagem 4T1Br4 foram plaqueadas em placas de 6cm ($5x10^5$células/placa) por 24h. Em seguida, as células foram incubadas com o [10]-gingerol nas concentrações de 10 e 50µM por 8 e 24h. Depois do período de incubação, as células foram lavadas com PBS duas vezes, desaderidas e fixadas com etanol 70% gelado por pelo menos 24h. Posteriormente, as células foram lavadas com PBS e incubadas com uma solução de RNAse (0,2mg/mL) por 30min a 37°C. Em seguida, as células foram coradas com uma solução de PI (Iodeto de propídio, 1µg/mL) por 10min, lavadas com PBS e a leitura foi realizada em citomêtro de fluxo (BD Accuri C6). O resultado foi analisado através da quantificação das fases do ciclo celular, conforme indicação do fabricante do citômetro de fluxo (LIN; LIN; TSAY, 2012).

4.12 Atividade das caspases-3 e -7

Para analisar se o [10]-gingerol é capaz de induzir a atividade de caspases, e portanto, da apoptose, células da linhagem 4T1Br4 foram plaqueadas em placas de 6 poços *overnight* (5.10^5 células/poço). No dia seguinte, as células foram tratadas com as concentrações de 10, 25 e 50µM de [10]-gingerol por 8 e 18h de incubação. As células foram lisadas com tampão de lise contendo inibidor de proteases (0,2% de Triton X-100 em 0,2M de Tris-HCl, pH 7.4, inibidor de protease Sigma S2711) e quantificadas com kit de detecção colorimétrica BCA (BCA Protein Assay, Pierce). Para quantificar a atividade das caspases foi utilizado os substratos das caspases-3, -7, (AnaSpec, ANAS 60303). No dia da leitura, foram utilizados 20µl de amostra com 90µl de substrato (contendo 10mM HEPES, 20mM, pH 7,35, contendo NaCl 150mM, KCl 5mM, MgSO4 1mM e MnCl2 1mM; 10% Sacarose; 10mM DTT, Ditiotreitol; e substrato AnaSpec 2µl/mL). As amostras foram plaqueadas em triplicata em placa de 96 poços e incubadas por 30min a temperatura ambiente. A leitura foi realizada em leitor de placa (Hidex Chamaleon™ V) a cada 5min por 2h, nos comprimentos de onda de

460nm de emissão e 365nm de excitação. Para o cálculo da atividade das caspases foi utilizada a seguinte fórmula:

$$Atividade\ de\ caspases = \frac{slope = \Delta/tempo}{[proteína]\ x\ Volume\ da\ Amostra\ (\mu l)}$$

Este experimento foi baseado e modificado dos trabalhos de Gukovskaya *et al.*, Murthy *et al.* e Yusuf *et al.* (GUKOVSKAYA et al., 2002; MURTHY et al., 2010; YUSUF et al., 2002).

4.13 Expressão gênica

4.13.1 Tratamento das células e extração do RNA

A expressão de alguns genes relacionados a apoptose foram analisados com relação a atividade do [10]-gingerol. Para isso, $5x10^5$ células da linhagem 4T1Br4 foram plaqueadas em placas de 6cm por 48h. Após este período, as células foram incubadas com o [10]-gingerol por 6 e 18h. Em seguida, as células foram lavadas duas vezes com PBS estéril e lisadas com reagente Trizol®. O lisado foi armazenado em freezer a -80°C para posterior extração do RNA.

A extração do RNA foi realizada conforme instruções do fabricante. Resumidamente, aos lisados foram adicionados 200µl de clorofórmio e a mistura foi incubada por 15min a temperatura ambiente e em seguida, centrifugada por 15min 12000rpm a 4°C. Após a centrifugação, o sobrenadante foi transferido para um novo tubo ao qual foram adicionados 450µl de isopropanol. Estes tubos foram invertidos 10 vezes para homogeneizar a solução e incubados por 10min a temperatura ambiente. Em seguida, os tubos foram centrifugados 10min a 12000rpm por 10min para formação do *pellet* do RNA. O sobrenadante foi descartado e lavado com 1mL de etanol 70% e centrifugado a 7500rpm a 4°C por 5min. Este processo foi repetido novamente e o *pellet* formado e seco foi ressuspendido em 20µl de água ultra pura. Antes da síntese de cDNA, o RNA foi quantificado e avaliado sua pureza por nanodrop (Thermo Scientific Nano 2000).

4.13.2 Síntese cDNA

Para a síntese do cDNA foram utilizados 1,5µg de RNA num volume final de 8µl. Em seguida, foi adicionada a mistura de dNTPs (concentração final de 10mM), 1µl de oligo dT

(0,5µg/µl) seguido de incubação por 10min a 70°C. Percorrido o tempo, foi adicionado 2µl do tampão 10x da enzima, 1µl da enzima M-MLV *Reverse Trasncriptase* (Sigma M1302) contendo 200 unidades/µl, 1µl de inibidor de RNAse (20 unidades/µl) e 6µl de água ultrapura. Em seguida, a solução foi incubada por 50min a 37°C em banho seco para a síntese do cDNA. Logo após, a reação foi sujeita a uma temperatura de 94°C por 10min para desnaturação da enzima, conforme instruções do fabricante.

4.13.3 Reação de PCR em tempo real e análise

Para análise da expressão gênica de genes associados a apoptose foi utilizado *primers* pré-desenhados e validados da Sigma (KiCqStart®SYBR® Green Primers) com exceção do gene constitutivo RPS27a. Os genes analisados foram: Caspase-3, Caspase-7, Caspase-8, Caspase-9, Bax e Bcl-2 e suas sequências podem ser verificadas na tabela abaixo:

Tabela 1 –Sequências dos primers utilizados e suas concentrações na reação final da PCR em tempo real.

Nome do gene	Sequência (5'-3')	Concentração final do primer na reação de PCR
***Foward Mouse* Caspase-3**	CATAAGAGCACTGGAATGTC	200nM
***Reverse Mouse* Caspase-3**	GCTCCTTTTGCTATGATCTTC	200nM
***Foward Mouse* Caspase-7**	GTAATGGACTGTGTTGGTTG	200nM
***Reverse Mouse* Caspase-7**	CATCTGGTAACATAAGAAGC	200nM
***Foward Mouse* Caspase-8**	CAAGAGAACAAGACAGTGAG	200nM
***Reverse Mouse* Caspase-8**	ACTCAGAGCCTCTTTATCAC	200nM
***Foward Mouse* Caspase-9**	GACCCTTACGGGGAAAACCAT	200nM
***Reverse Mouse* Caspase-9**	AGACAAAGTCCGGCCATCTTC	200nM
***Foward Mouse* Bax**	CCTTTTTGCTACAGGGTTTC	200nM
***Reverse Mouse* Bax**	ATATTGCTGTCCAGTTCATC	200nM
***Foward Mouse* Bcl-2**	ATGACTGAGTACCTGAACC	50nM
***Reverse Mouse* Bcl-2**	ATATAGTTCCACAAAGGCATC	50nM
***Foward Mouse* RPS27a**	GACCCTTACGGGGAAAACCAT	200nM
***Reverse Mouse* RPS27a**	AGACAAAGTCCGGCCATCTTC	200nM

Para a reação de PCR foi utilizado o Sybr Green da Sigma (SYBR®Green JumpStart™Taq ReadyMix) e os componentes da reação estão descritos na tabela abaixo, assim como a reação na Figura 15.

Tabela 2 – Componentes da PCR.

Reação de PCR em tempo real	
Sybr Green	5µl
Primers (Foward + Reverse)	1µl
Água	2,7µl
cDNA (10ng)	1,3µl

Figura 15 – Ciclo da Reação de PCR em tempo real.

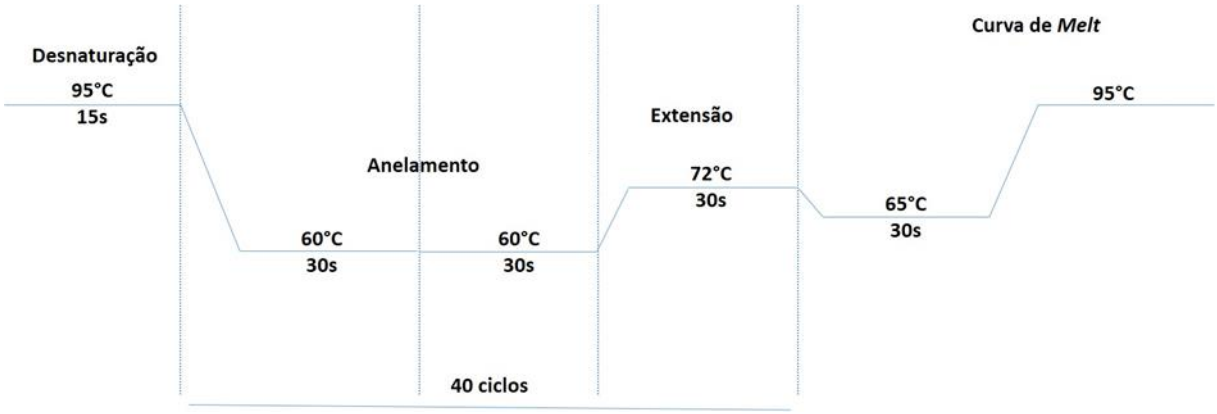

Para as reações foi utilizado termociclador da BioRad (CFX96 BioRad) conforme reação descrito acima, através da análise do Ct das amostras ("*Cycle Threshold*"). Nesta análise, foi realizado o ΔCt (Ct do gene alvo menos o Ct gene constitutivo). Em seguida, foi realizado o cálculo do ΔΔCt (ΔCt das amostras menos a média do ΔCt das amostras controles, nesse caso foi utilizado as amostras sem tratamento do [10]-gingerol). Os dados foram então analisados utilizando a seguinte fórmula: $2^{-\Delta\Delta C_T}$, representando em unidades arbitrárias a expressão gênica dos genes alvos com relação a expressão do gene constitutivo (RPS27a) (LIVAK; SCHMITTGEN, 2001).

4.14 Modelos in vivo de metástase

Ensaios *in vivo* utilizando modelos de formação de metástase espontânea e experimental foram realizados em colaboração com o Dr. Normand Pouliot do Laboratório de Metástase situado no Hospital PeterMacCallum Cancer Centre, Melbourne, Austrália. Além disso, o modelo também foi desenvolvido no laboratório de Bioquímica e Biologia Molecular (Departamento de Ciências Fisiológicas – UFSCar) em colaboração com a Dra Rebeka Tomasin do laboratório de Nutrição e Câncer dirigido pela Profa Dra Maria Cristina Cintra

Gomes Marcondes (UNICAMP) e com o laboratório de Neuroendocrinologia dirigido pela Profa Dra Keico Okino Nonaka.

Os animais utilizados foram camundongos fêmeas Balb/c com idade de 6 a 8 semanas. Estes animais foram adquiridos no Hospital Peter MacCallum e no Biotério da Universidade Estadual de Campinas (UNICAMP), sob autorização do comitê de ética de número (E507, CEUA 3224-1, respectivamente). Os animais foram mantidos em biotério com temperatura controlada de 22°C±2, água e ração *ad libtum*.

4.14.1 Modelo de formação de metástase espontânea IMFP (Intramammary Fat Pad) sem cirurgia do tumor primário

O primeiro modelo utilizado foi o modelo de metástase espontânea singênico ortotópico sem cirurgia, para avaliar as propriedades do [10]-gingerol no crescimento do tumor primário e consequentemente, nas possíveis metástases formadas. Este experimento foi desenvolvido no Laboratório de Metástase, Peter MacCallum – Melbourne/Austrália. Neste modelo $1x10^5$ células/20µL/camundongo da linhagem 4T1Br4 foram injetadas no tecido adiposo da quarta mama de camundongos fêmeas Balb/c (6-8 semanas). A injeção foi realizada com auxílio de uma seringa Hamilton de 50µl em animais anestesiados com isoflurano. Assim que o tumor se tornou palpável (9 dias) os camundongos foram tratados diariamente com [10]-gingerol (5mg/kg diluído em salina), através de injeções intra-peritoniais (IP), invertendo os lados das injeções para evitar lesões devido ao tratamento diário. O grupo controle foi injetado diariamente com o mesmo volume de salina.

Após vinte e sete dias da injeção das células tumorais foi realizada a eutanásia dos animais, o protocolo está esquematizado na Figura 16. Durante todo o período do experimento os camundongos foram monitorados através do peso corporal e seu tumor primário foi mensurado com o uso de um paquímetro digital. Os tumores foram medidos quanto a sua altura e comprimento e estas medidas foram usadas para calcular o volume do tumor e consequentemente, inferir seu peso (volume mm^3= comprimento x comprimento x altura). No dia da eutanásia foram avaliadas as metástases visíveis e foram coletados os fêmures, coluna espinhal e pulmões para análise da RTB (*Relative Tumor Burden*) através de análise do DNA genômico (DNAg). Os órgãos coletados para RTB foram congelados em nitrogênio líquido para posterior extração de DNAg. Os tumores primários, baço, fígado também foram pesados para avaliar de forma indireta indícios de metástases.

Figura 16 - Modelo ortotópico singênico de metástase espontânea sem cirurgia do tumor primário com tratamento diário com [10]-gingerol.

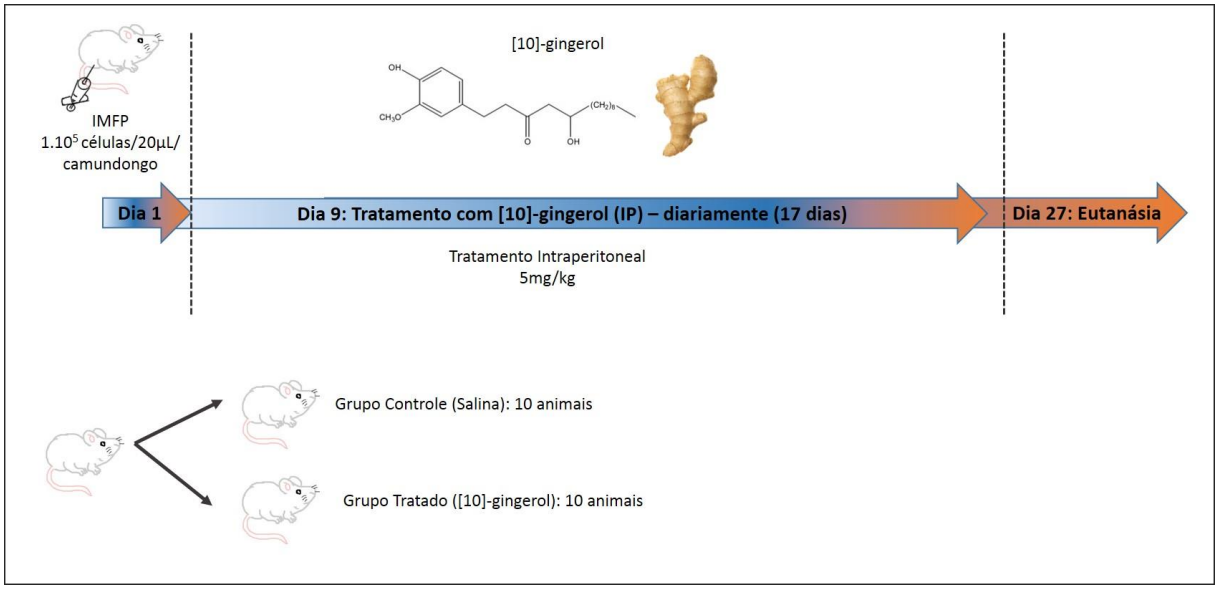

As células tumorais da linhagem4T1Br4 foram injetadas no tecido adiposo da quarta mama de camundongos Balb/c (6-8 semanas) e assim que os tumores se tornaram palpáveis foi realizado o tratamento intraperitoneal diário com 5mg/kg de [10]-gingerol até a eutanásia dos animais. Em seguida, as metástases visíveis foram analisadas e os órgãos (pulmão, fêmur e coluna espinhal) foram usados para análise da *Relative Tumor Burden* (RTB) através de PCR em tempo real.

A RTB foi avaliada após a extração de DNAg utilizando-se a técnica de PCR quantitativo Taqman (Taqman® Fast Universal PCR Master Mix 2x – Applied Biosystens, Life Technologies).

Para a extração do DNAg os órgãos foram homogeneizados em tampão de lise sem SDS (50mM Tris-HCl, 100mM NaCl, 100mM EDTA, pH 7,5) em homogeneizador FastPrep®-24 em tubos (MP *tubes*) contendo *beads* de aço inox e/ou cerâmica (1 *bead* grande e duas pequenas para ossos, e 3 *beads* pequenas para tecidos moles). Foram realizados 3 ciclos de homogeneização de 1min com intervalo de 5min (ciclo 6m/s). Parte do homogeneizado foi digerido em tampão de lise contendo SDS, Proteinase K e RNAse A (50mM Tris-HCl, 100mM NaCl, 100mM EDTA, 1% SDS pH7,5; 2µl/mL de proteinase K e de RNAse A, estoque a 10mg/mL) a 55°C *overnight*. No dia seguinte, foram adicionados 350µl de uma solução super-saturada de NaCl (≥5M), os tubos foram agitados e incubados no gelo por 30min. Em seguida, os tubos foram centrifugados por 10min a 4°C e 16000rpm. O sobrenadante foi transferido para um novo tubo ao qual foi adicionado etanol 100% até a precipitação do DNA. Este DNAg formado foi transferido para um tubo contendo etanol 70% e centrifugado por 5min a 13000rpm. O *pellet* formado foi lavado novamente com 500µl de etanol 70%, em seguida, o sobrenadante foi colhido por inversão do tubo e o restante de etanol foi retirado com auxílio de uma pipeta. O DNA foi seco em fluxo de ar e em seguida

ressuspendido em 200µl de tampão TE (10mM Tris-HCl, 1mM EDTA, pH 8,0). O DNAg foi quantificado em Nanodrop e 40ng foram utilizados na reação de PCR em tempo real.

A RTB para cada animal foi calculada através de PCR em tempo real multiplex usando Taqman®. O DNAg foi sujeito ao PCR multiplex para detectar o Ct (*cycle Threshold*), definido logo acima da linha de base dos níveis de fluorescência para vimentina (presente em todos os tecidos dos animais) e mCherry (presente somente nas células tumorais). Através da comparação dos valores de Ct da vimentina e do mCherry em cada amostra, o ΔCt foi calculado pela subtração do Ct mCherry menos o Ct da Vimentina, em seguida, o valor de ΔCt foi usado na seguinte fórmula RTB = $10.000/2^{\Delta Ct}$. Usando-se essa fórmula os tecidos com valores zero são considerados sem tumor, enquanto que um tecido com valor de 10.000 é composto totalmente por tumor. Estes dados foram analisados conforme descrito por Sloan e colaboradores (SLOAN et al., 2006) para análise da RTB.

Os *primers* e as *probes* utilizadas foram:

Tabela 3 – *Primers* e *probes* utilizados no experimento de PCR em tempo real para determinação do *Relative Tumor Burden* (RTB).

Probe mVim: VIC-CCT TCA TGT TTT GGA TCT CAT CCT GCA GG – TAMRA
Primer mVim Foward: 5’ AGC TGC TAA CTA CCA GGA CAC TAT TG 3’
Primer mVim Reverse: 5’CGA AGG TGA CGA GCC ATC TC 3’
Probe mCherry: 6FAM-CAG CTG CCC GGC GCC TAC A-TAMRA
Primer mCherry Foward: 5' GAC CAC CTA CAA GGC CAA GAA G 3'
Primer mCherry Reverse: 5' AGG TGA TGT CCA ACT TGA TGT TGA 3'

A reação multiplex do PCR foi realizada conforme protocolo já definido no Laboratório de Metástase (Tabela 4) e foram usadas com um protocolo padrão do termociclador (Applied Biosystems, ciclo Fast).

Tabela 4 – Componentes da PCR em tempo real Taqman para os ensaios *in vivo*.

Reação de PCR Taqman	
Reagentes (concentração final)	Volume
Master Mix 2x	5µl
***Primers Foward* + *Reverse* Vimentina (1µM)**	0,5µl
***Probe* Vimentina (1µM)**	0,5µl
***Primers Foward* + *Reverse Cherry* (1µM)**	0,5µl
***Probe Cherry* (1µM)**	0,5µl
Água	1µl
DNAg (40ng)*	2µl

*Para os cérebros foi utilizado 100ng de DNAg.

4.14.2 Modelo de formação de metástase espontânea IMFP (Intramammary Fat Pad) com cirurgia

O segundo modelo utilizado foi o modelo de metástase espontânea singênico ortotópico com cirurgia, para avaliar as propriedades do [10]-gingerol na inibição da formação de metástase, já que o tratamento foi iniciado somente após a cirurgia. Este protocolo tenta mimetizar uma situação normal em mulheres, quando o tumor é detectado e então é realizada a cirurgia para remoção do tumor primário e, em seguida, o tratamento, como a quimioterapia, é iniciado.

Este experimento foi desenvolvido no Laboratório de Bioquímica e Biologia Molecular - Departamento de Ciências Fisiológicas/UFSCar. Neste modelo $1x10^5$ células/20µL/camundongo da linhagem 4T1Br4 foram injetadas no tecido adiposo da quarta mama de camundongos fêmeas Balb/c (6-8 semanas) como descrito no item acima. O tamanho do tumor foi medido com auxílio de um paquímetro digital até que os tumores atingissem o tamanho de ±0,5g. Quando os tumores atingiram o tamanho esperado, foi relizada uma cirurgia para remoção total do tumor primário. Para isso, os camundongos foram anestesiados com ketamina e xilasina (100mg/kg e 16mg/kg, respectivamente), em seguida, foi realizada uma pequena incisão no local e para retirada do tumor primário visível. Os animais foram mantidos aquecidos até que voltassem da anestesia e separados em dois grupos: grupo controle (CTRL, salina) e grupo gingerol (10mg/kg de [10]-gingerol). Na Figura 17 pode-se visualizar o protocolo utilizado.

Figura 17 – Figura representativa do modelo *in vivo* de metástase espontânea com cirurgia do tumor primário.

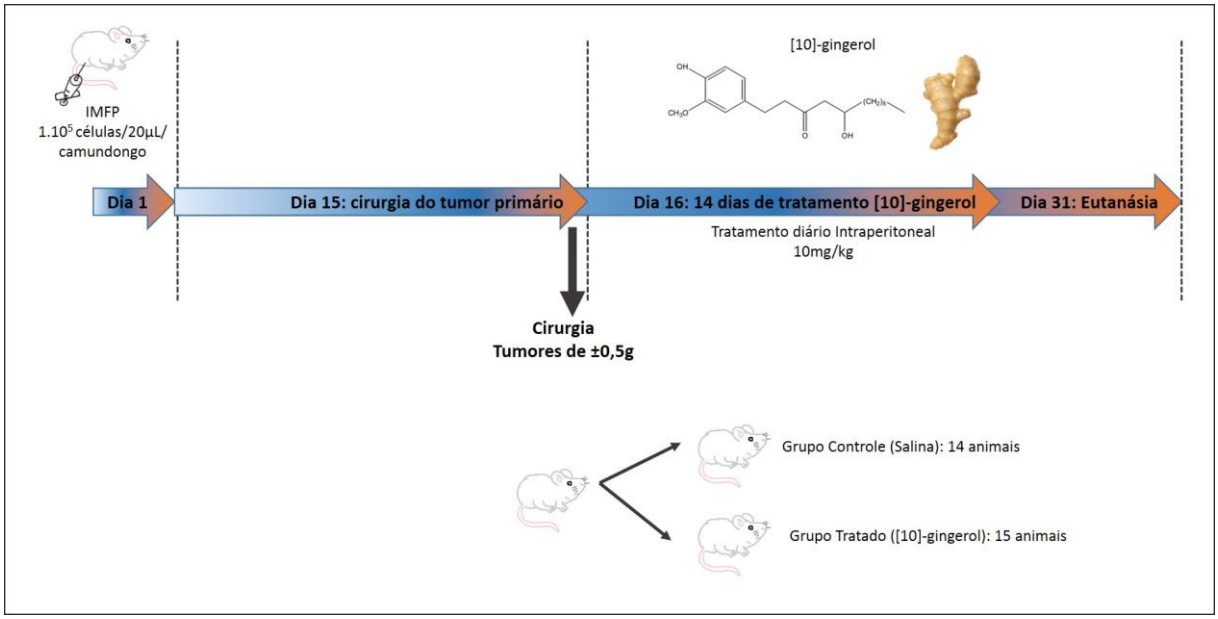

Cerca de $1x10^5$ células/20µl/camundongo foram injetadas no tecido adiposo da quarta mama de camundongos Balb/c. Assim que os tumores alcançaram o tamanho de ±0,5g, o tumor foi retirado. No dia seguinte, o tratamento com 10mg/kg de [10]-gingerol foi iniciado. No dia 31 após a injeção das células tumorais foi realizada a eutanásia dos animais, as metástases visíveis foram mensuradas e os seguintes órgãos foram coletados para análise da *Relative Tumor Burden* (RTB): fêmures, coluna espinhal, pulmão e cérebro.

No dia seguinte da cirurgia, foi inicado o tratamento com o [10]-gingerol na concentração de 10mg/kg intraperitonealmente. O tratamento foi diário até o dia da eutanásia, após 31 dias da cirurgia e totalizando 14 dias de tratamento. Durante o período de experimento após a cirurgia, o peso dos animais foi mensurado para monitorar qualquer tipo de toxicidade e sofrimento dos animais, além de qualquer alteração de comportamento. Após a eutanásia, foram avaliadas as metástases visíveis e os seguintes órgãos foram coletados para análise da RTB: fêmures, coluna espinhal, pulmão e cérebro. Os cérebros foram mantidos em PBS em gelo para análise de metástases pelo aparelho IVIS Spectrum, no Departamento de Biologia Celular e Molecular e Bioagentes Patogênicos – Laboratório de Biologia Celular e Molecular do Câncer, dirigido pela Profa Dra Enilza Maria Espreafico. As células 4T1Br4 foram marcadas com Cherry, portanto, possuíam fluorescência. Logo após as imagens terem sido adquiridas os cérebros foram congelados em nitrogênio líquido para extração do DNAg, como para os outros órgãos e posteriormente análise da RTB, conforme descrito anteriormente.

4.14.3 Modelo de formação de metástase experimental por injeção intracardíaca (IC) e tratamento do [10]-gingerol pós injeção

Um terceiro modelo utilizado foi o de metástase experimental. Neste modelo, o efeito do [10]-gingerol foi analisado somente na inibição da metástase, pois não há formação do tumor primário já que as células tumorais são injetadas diretamente na corrente sanguínea, através do ventrículo esquerdo dos animais. Este experimento foi desenvolvido em colaboração com o Laboratório de Metástase, Peter MacCallum – Melbourne/Austrália.

Para isso, $1x10^5$ células/100µl/camundongo da linhagem 4T1Br4 foram injetadas no ventrículo esquerdo (injeção intracardíaca, IC) com auxílio de uma seringa descartável de 1mL, nos animais já anestesiados com isoflurano. No mesmo dia da injeção foi iniciado o tratamento com o [10]-gingerol (10mg/kg) de forma intraperitoneal diariamente até o dia da eutanásia dos animais, os animais controle foram injetados com o mesmo volume de salina, como indicado na Figura 18.

Figura 18- Protocolo do modelo de metástase experimental.

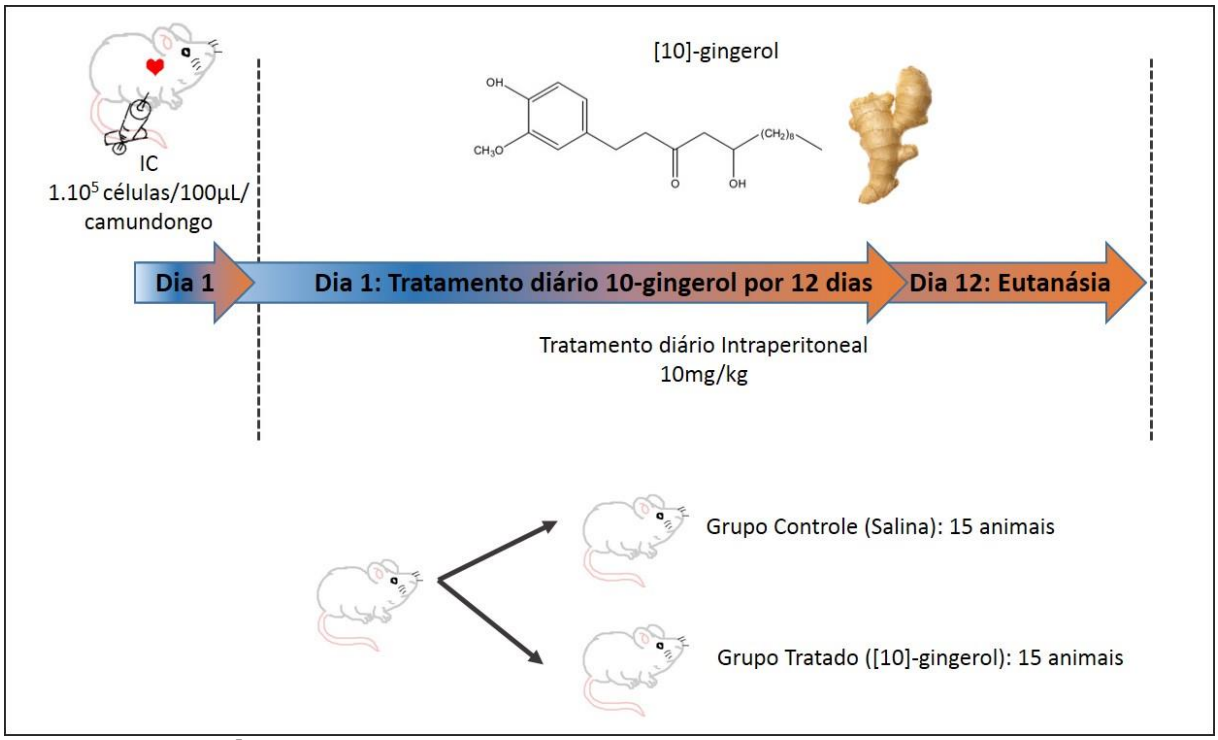

Neste modelo, $1x10^5$ células/100µl/ camundongo foram injetadas no ventrículo esquerdo do coração dos animais. No mesmo dia foi iniciado o tratamento com o [10]-gingerol (10mg]kg) diariamente no peritônio dos animais até o dia da eutanásia, onde foram coletados: fêmures, coluna espinal, pulmão e cérebros para análise da *Relative Tumor Burden* (RTB).

Após 12 dias da injeção IC os animais sofreram eutanásia e os fêmures, coluna espinhal, pulmão e cérebro foram coletados para análise da RTB conforme descrito anteriormente.

4.14.4 *Modelo de formação de metástase experimental com injeção Intracardíaca (IC) com pré-tratamento do [10]-gingerol*

O mesmo ensaio de injeção intracardíaca foi realizado, porém o tratamento com o [10]-gingerol foi iniciado anteriormente à injeção das células tumorais, para verificar se o produto natural possui características preventivas contra a formação de metástase. Este experimento foi desenvolvido em colaboração com o Laboratório de Metástase, Peter MacCallum – Melbourne/Austrália.

Para isso, 3 dias antes da injeção das células tumorais os animais do grupo gingerol foram tratados com 10mg/kg de [10]-gingerol (IP) e o grupo controle com o mesmo volume de salina. No dia da injeção $1x10^5$ células/100µl/camundongo da linhagem 4T1Br4 foram injetadas no ventrículo esquerdo do coração dos animais. O tratamento com o produto natural foi contínuo desde 3 dias antes da injeção, diariamente, até o dia da eutanásia, como indicado na Figura 19.

Figura 19 - Protocolo do modelo de metástase experimental com pré-tratamento com [10]-gingerol.

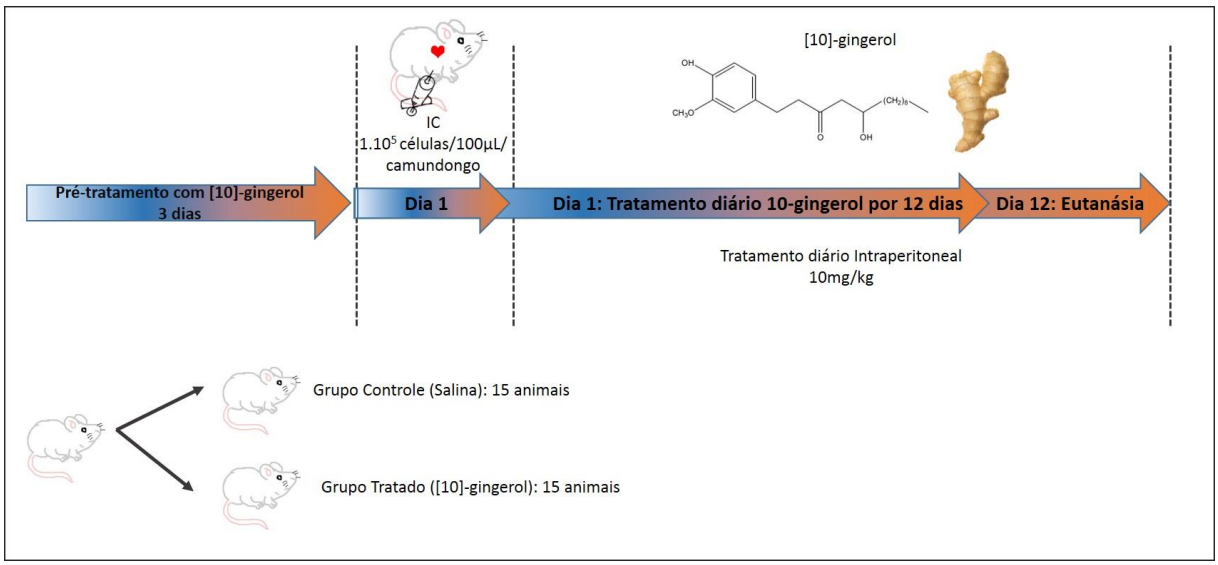

Neste modelo, o tratamento com o produto natural (10mg/kg, IP) foi iniciado 3 dias antes da injeção IC, para injeção: $1x10^5$ células/100µl/ camundongo foram injetadas no ventrículo esquerdo do coração dos animais, o tratamento foi continuado até o dia da eutanásia onde foram coletados os seguintes órgãos: fêmures, coluna espinal e cérebros para análise da *Relative Tumor Burden* (RTB).

A eutanásia foi realizada 12 dias após a injeção IC e os órgãos coletados para RTB foram: fêmures, coluna espinhal, cérebro. Os baços dos animais foram pesados para verificar indícios de metástases.

4.15 Determinação da concentração protéica

A concentração protéica das amostras foi determinada com auxílio do kit *BCA Protein Assay* (Pierce) utilizando a proteína BSA como padrão conforme protocolo do fabricante.

4.16 Análise estatística

Os experimentos *in vitro* foram realizados três vezes em triplicata. Para a análise estatística foi obtida a média e o erro padrão para cada grupo em todos os experimentos. A comparação entre os grupos foi realizada utilizando análise de variância (ONE WAY ou TWO WAY ANOVA), seguido do teste de Tukey, com auxílio do programa GraphPad Prism 5. Para os ensaios *in vivo* o test t de Student foi aplicado.

5 RESULTADOS

5.1 Determinação do IC_{50}

O gráfico na Figura 20 mostra a curva utilizada para o cálculo do IC_{50} do [10]-gingerol nas diferentes linhagens e seus valores estão indicados na tabela da mesma figura.

Figura 20 – Cálculo do IC_{50} nas diferentes linhagens celulares do [10]-gingerol.

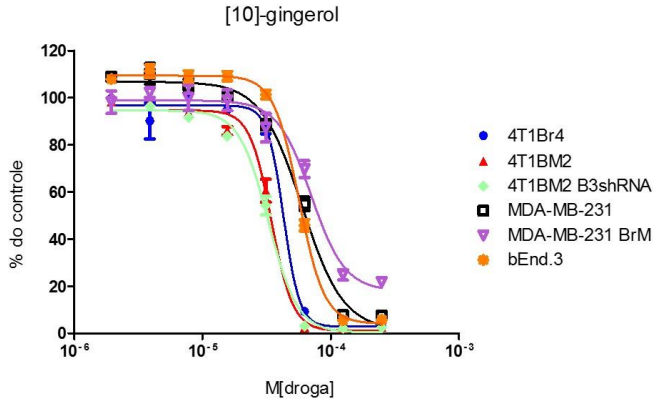

Origem	Linhagem Celular	IC50 (µM)	Desvio Padrão
Camundongo	4T1Br4	40,3	±7,05
Camundongo	4T1BM2	30,0	±4,84
Camundongo	4T1BM2 β3shRNA	30,40	±2,41
Humana	MDA-MB-231	62,90	±2,60
Humana	MDA-MB-231 BrM	65,20	±5,13
Humana	bEnd.3	45,01	±8,45

As linhagens 4T1Br4, 4T1BM2, 4T1BM2 β3shRNA, MDA-MB-231, MDA-MB-231 BrM e bEnd.3 foram incubadas com uma diluição seriada do [10]-gingerol de 200 a 0µM por 72h, decorrido o tempo as células foram fixadas com TCA e coradas com corante SRB, em seguida a leitura foi realizada em leitor de placa no comprimento de onda de 530nm. O Cálculo do IC_{50} foi realizado com auxílio do software GraphPad Prism.

As linhagens humanas apresentam valores de IC_{50} superiores (MDA-MB-231, MDA-MB231 BrM, respectivamente, 62 e 65µM) que os das linhagens de camundongo (4T1Br4, 4T1BM2, 4T1BM2 β3shRNA, respectivamente, 40/29/30µM) para o produto natural [10]-gingerol. Além disso, através do emprego da linhagem não tumoral bEnd.3 (linhagem endotelial de cérebro de camundongo), como controle para acessar a citotoxicidade em células normais, e verificamos que o [10]-gingerol apresenta um IC_{50} ligeiramente maior para as células normais em relação as células tumorais de camundongo, sugerindo uma seletividade por células tumorais (Figura 20).

O resveratrol (RSVT) apresentou valores de IC_{50} menores que os do [10]-gingerol e exibiu a mesma característica verificada no [10]-gingerol, onde as células tumorais humanas apresentaram valores de IC_{50} maiores (MDA-MB-231, MDA-MB231 BrM, respectivamente, 21 e 28µM) que os das linhagens de camundongo, indicando uma resistência maior para as células humanas (4T1Br4, 4T1BM2, 4T1BM2 β3shRNA, respectivamente, 2/5/4µM). Além disso, este produto apresentou uma alta seletividade por células tumorais já que para as

células normais o IC_{50} chegou a ser cerca de 4 vezes maior do que para as células tumorais de camundongo, como indicado na Figura 21.

Figura 21 - Cálculo do IC_{50} nas diferentes linhagens celulares do resveratrol.

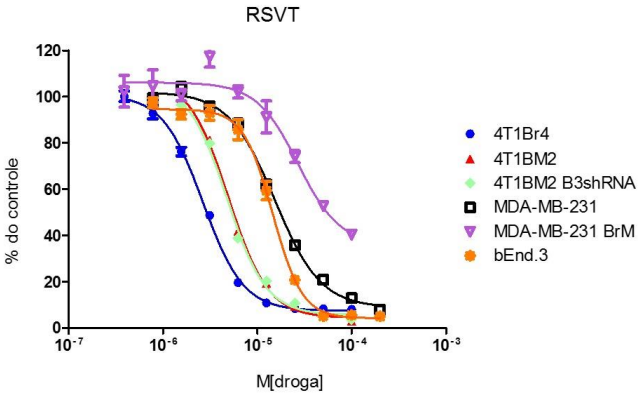

Origem	Linhagem Celular	IC50 (µM)	Desvio Padrão
Camundongo	4T1Br4	2,91	±0,25
Camundongo	4T1BM2	5,00	±1,14
Camundongo	4T1BM2 β3shRNA	4,36	±1,15
Humana	MDA-MB-231	21,19	±7,12
Humana	MDA-MB-231 BrM	28,13	±1,64
Humana	bEnd.3	17,75	±4,52

As linhagens 4T1Br4, 4T1BM2, 4T1BM2 β3shRNA, MDA-MB-231, MDA-MB-231 BrM e bEnd.3 foram incubadas com uma diluição seriada do RSVT de 200 a 0µM por 72h, decorrido o tempo as células foram fixadas com TCA e coradas com corante SRB, em seguida a leitura foi realizada em leitor de placa no comprimento de onda de 530nm. O Cálculo do IC_{50} foi realizado com auxílio do software GraphPad Prism.

5.2 Inibição da adesão celular a diferentes componentes da MEC

Células da linhagem 4T1Br4 quando pré-incubadas com [10]-gingerol nas concentrações de 100 e 500µM não foram capazes de se ligar a vitronectina (VN), portanto, o [10]-gingerol inibe a adesão desta linhagem celular à VN. O [10]-gingerol também inibiu a adesão desta linhagem celular à laminina-511 (LMN-511) nas concentrações de 50, 100 e 500µM. Para o colágeno IV, outro componente da MEC, o [10]-gingerol foi efetivo na inibição da adesão em todas as concentrações testadas (Figura 22 - painéis A, C e E). Estes resultados indicam que não houve seletividade deste composto a nenhum dos componentes da MEC testados. Além disso, os efeitos de inibição da adesão só foram observados em doses acima do IC_{50}, isto pode indicar toxicidade do [10]-gingerol, o mesmo está matando as células e não simplesmente inibindo a adesão das mesmas.

O RSVT inibiu a adesão das células da linhagem 4T1Br4 à VN de forma dependente de concentração. Entretanto, não inibiu a adesão à LMN-511 em nenhuma das concentrações testadas. Além disso, apesar do RSVT ter inibido a adesão desta linhagem ao colágeno IV, esta inibição somente ocorreu nas concentrações de 50 e 100µM, sugerindo uma seletividade

pela vitronectina, e portanto, de seus receptores como a integrina αvβ3 (Figura 22 - painéis B, D e F).

Figura 22 - Ensaio de inibição da adesão na linhagem 4T1Br4 pelo [10]-gingerol e RSVT.

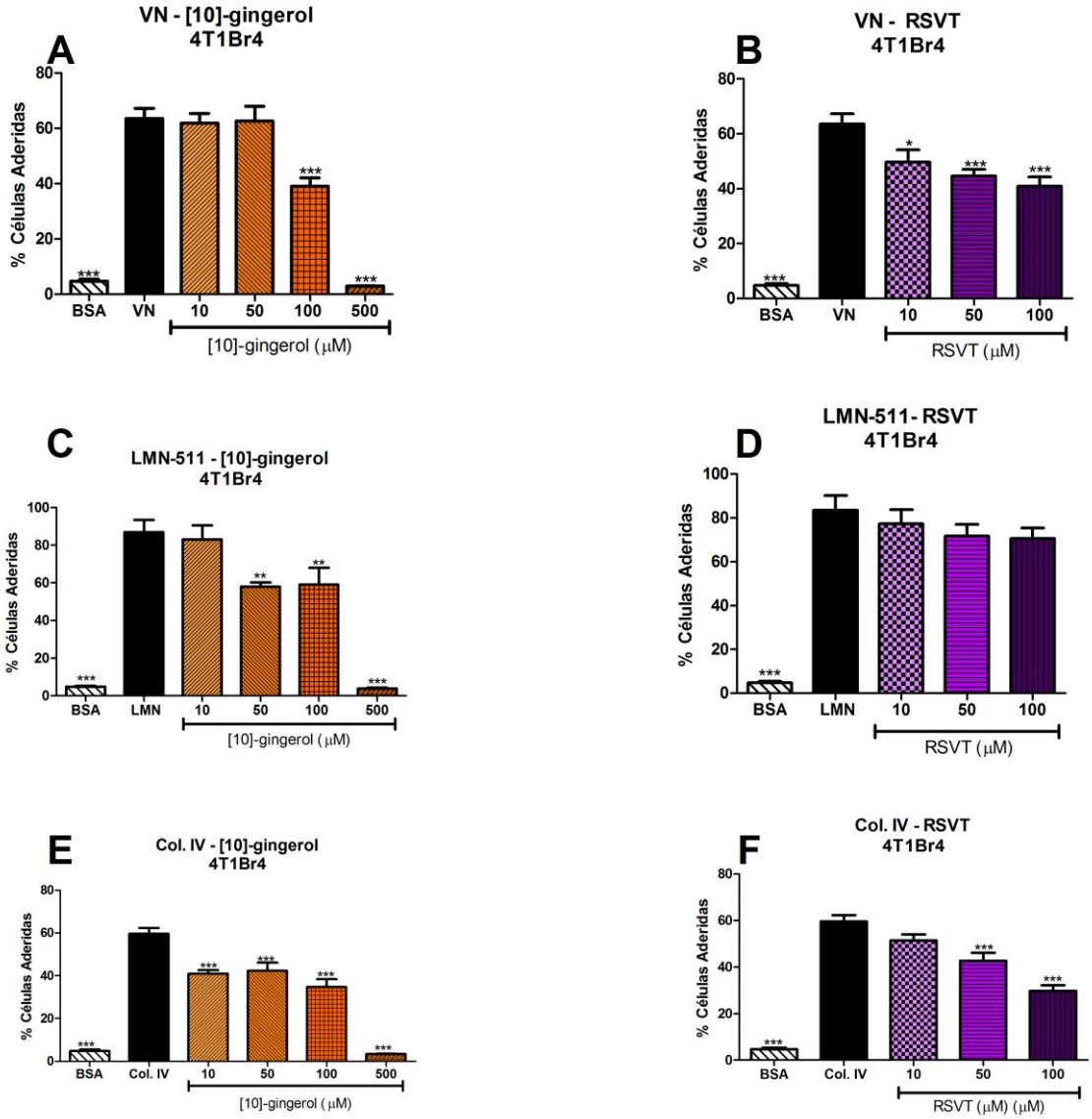

O [10]-gingerol inibiu a adesão das células tumorais à vitronectina, laminina-511 e colágeno IV. O RSVT inibiu a adesão das células tumorais à VN e colágeno IV. As células foram marcadas com calceína e incubadas com as diferentes concentrações dos produtos naturais. Em seguida, foram plaqueadas sobre os diferentes componentes da MEC por 30min. As células não aderidas foram lavadas e as células remanescentes foram lidas em comprimento de onda 530nm. ****p<0,0001.

Com relação a linhagem celular humana MDA-MB-231 o [10]-gingerol inibiu a adesão à VN nas concentrações de 50, 100 e 500µM. Esta inibição da adesão também ocorreu nas concentrações de 100 e 500µM à LMN-511 e somente na maior concentração de 500µM ao colágeno IV. Estes resultados indicam uma possível seletividade do [10]-gingerol para a VN e podem ser visualizados na Figura 23 painéis A, C e E. O RSVT somente inibiu a adesão da linhagem MDA-MB-231 BrM à VN na concentração de 100µM (Figura 23, painel B, D e F), confirmando sua seletividade por receptores a VN.

Neste mesmo ensaio verificamos que o [10]-gingerol, apesar de inibir a adesão das diferentes linhagens celulares testadas aos componentes da MEC, nas concentrações mais elevadas (100 e 500µM), promoveu um alto índice de morte celular, o que poderia influenciar os resultados da inibição da adesão propriamente dita. Visando minimizar este viés experimental, realizamos um ensaio de toxicidade celular para verificar quais concentrações os PNs seriam tóxicos nas condições de experimentos futuros. Este fato não ocorreu para o RSVT, o que sugere que este produto natural possui uma interação com receptores da adesão celular de forma receptor seletiva.

Figura 23 - Ensaio de inibição da adesão na linhagem MDA-MB-231 BrM pelo [10]-gingerol e RSVT.

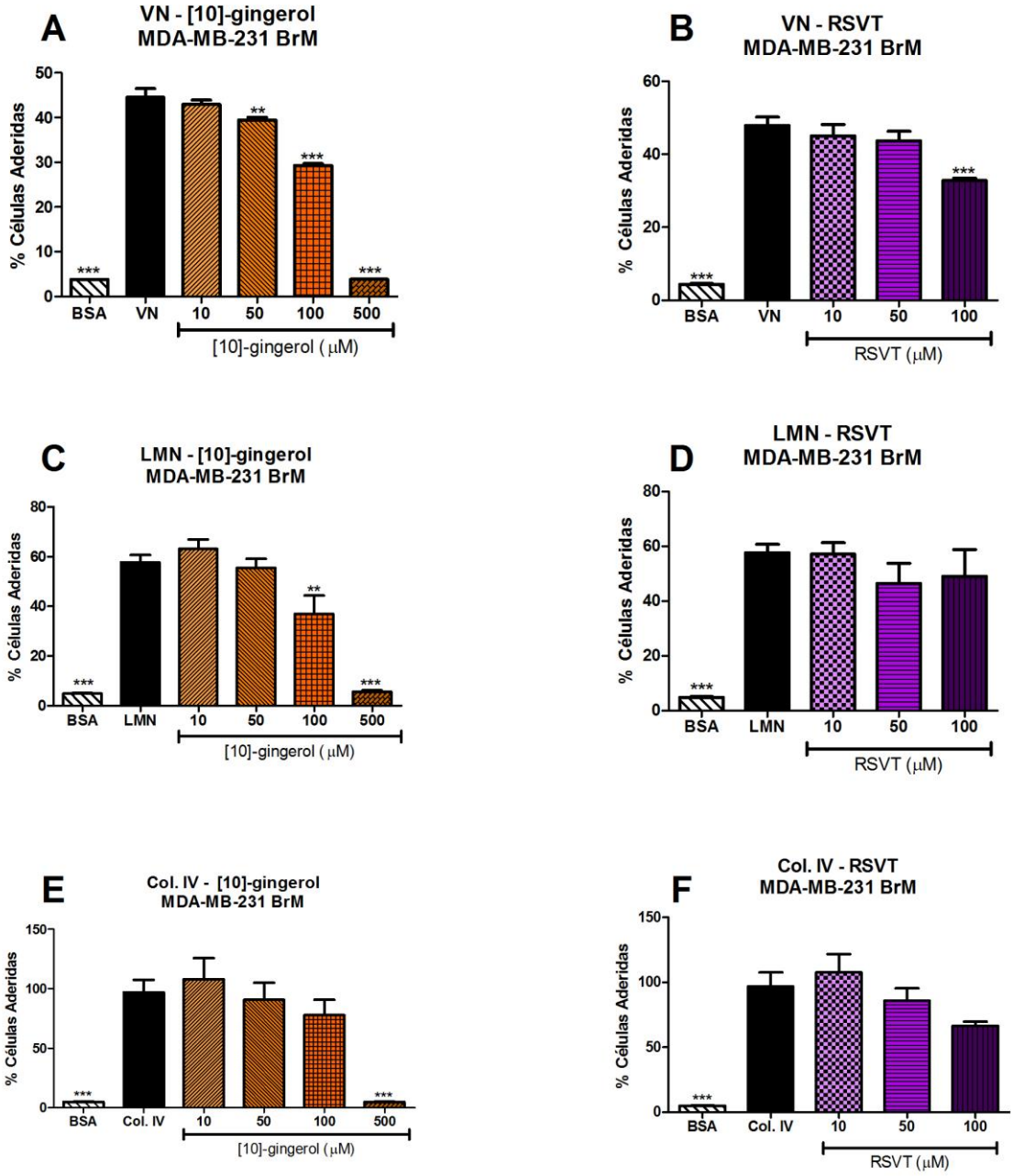

O [10]-gingerol inibiu a adesão das células tumorais à vitronectina, laminina-511 e colágeno IV. O RSVT inibiu a adesão das células tumorais à VN. As células foram marcadas com calceína e incubadas com as diferentes concentrações dos produtos naturais. Em seguida, foram plaqueadas sobre os diferentes componentes da MEC por 30min. As células não aderidas foram lavadas e as células remanescentes foram lidas em comprimento de onda 530nm. ****p<0,0001.

5.3 Toxicidade celular e Morfologia

Este ensaio foi realizado para verificar como e se os produtos naturais, [10]-gingerol e RSVT, estariam atuando sobre as células tumorais e quais as concentrações e tempos esses efeitos ocorreriam.

Tanto para a linhagem 4T1Br4, quanto para a linhagem MDA-MB-231 BrM as concentrações de 100 e 500µM do [10]-gingerol foram capazes de induzir a morte celular nos tempos de 40min e 4h, caracterizado pela redução do número de células, pela alteração da morfologia celular, com o surgimento de células arredondadas em processo de desadesão e formação de vesículas nas células remanescentes na placa (Figura 24 e Figura 25).

Embora as células tratadas com RVST não tenham apresentado indícios de morte celular nas diferentes concentrações e tempos testados para as referidas linhagens, este produto natural atuou na morfologia das células, sobretudo na linhagem MDA-MB-231 BrM, onde fica mais evidente as formações de protrusões celulares, nas concentrações de 50 e 100µM, nos tempos de 8 e 14h, o que reforça a hipótese de que o RSVT interage com receptores celulares (Figura 26 e Figura 27). É interessante notar a diferença da morfologia celular, especialmente na linhagem 4T1Br4, quando incubadas com [10]-gingerol e RSVT. Enquanto as primeiras assumem uma morfologia circular e parecem desaderir da placa nas maiores concentrações e tempos de incubação, as células tratadas com RSVT não apresentam alterações tão marcantes da morfologia celular, o que pode indicar diferentes mecanismos de ação para os produtos naturais testados.

Figura 24 - Toxicidade e Morfologia de células da linhagem 4T1Br4 quando incubadas com o [10]-gingerol.

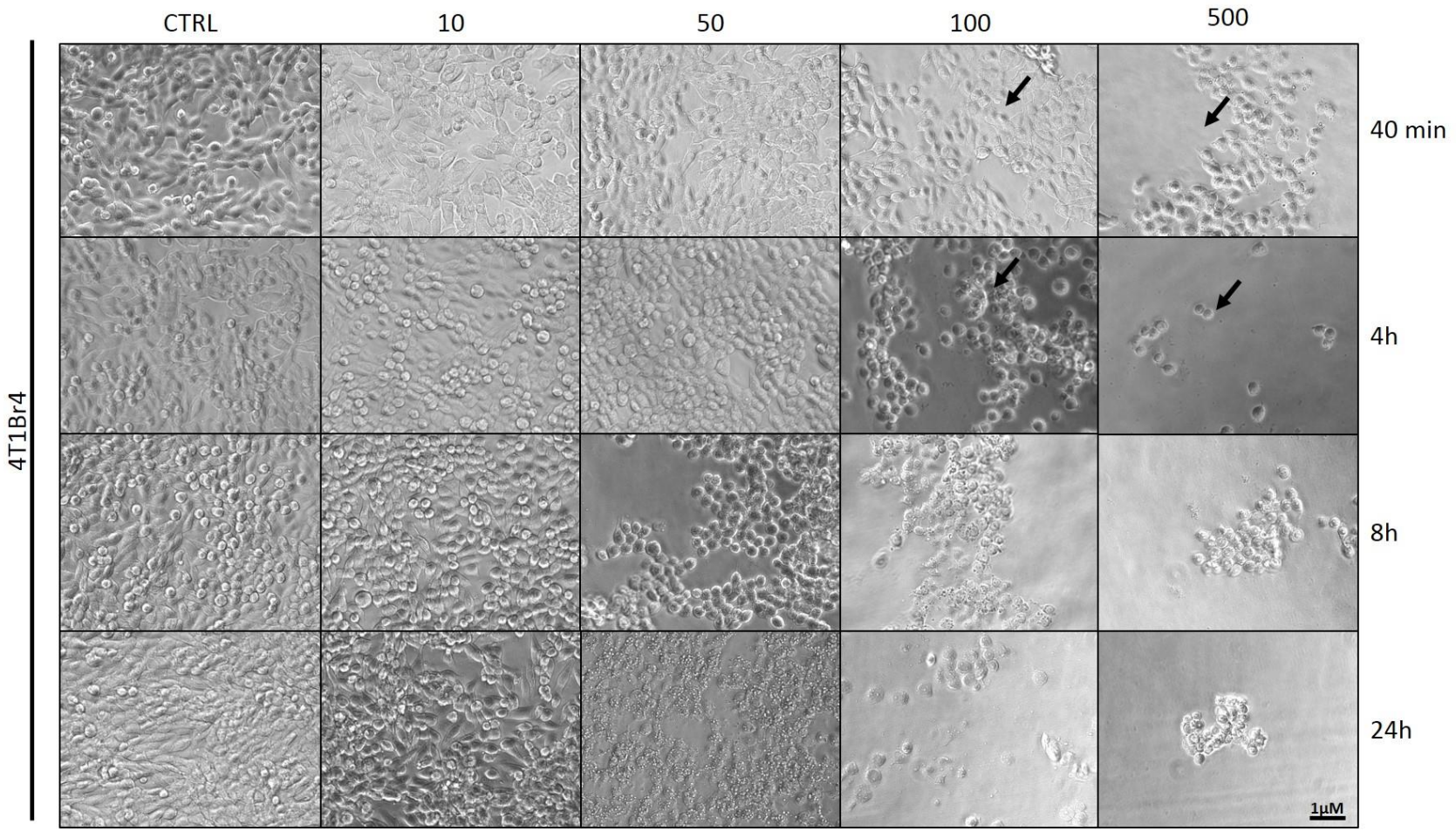

As células foram plaqueadas em placas de 96 poçose incubadas *overnight.* No dia seguinte, foram incubadas com diferentes concentrações e tempos de incubação com o PN. Quando decorrido o tempo de incubação as células foram fixadas com formalina 10% e fotos foram obtidas para análise da morfologia.

Figura 25 - Toxicidade e Morfologia de células da linhagem MDA-MB-231 BrM quando incubadas com o [10]-gingerol.

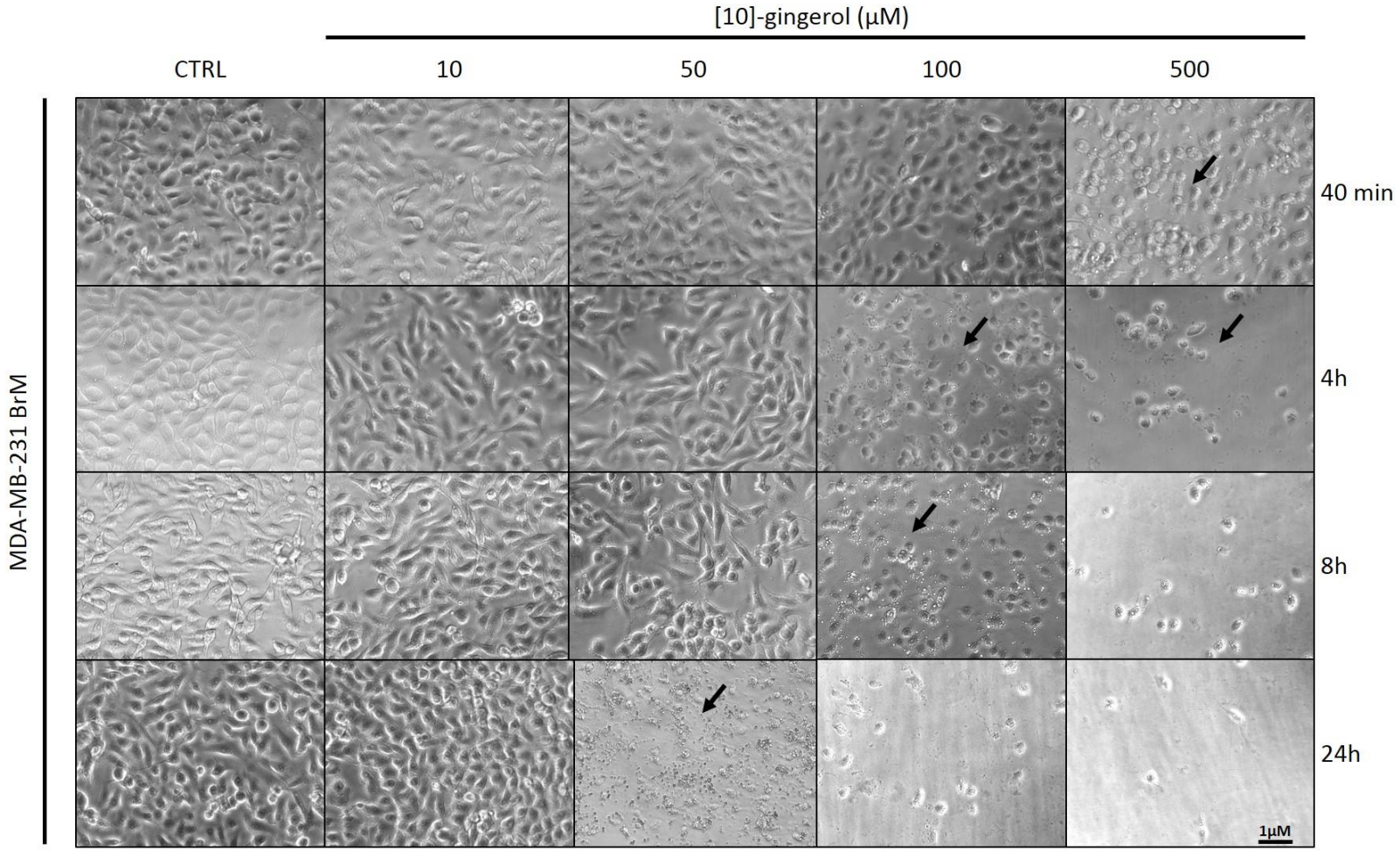

As células foram plaqueadas em placas de 96 poçose incubadas *overnight.* No dia seguinte, foram incubadas com diferentes concentrações e tempos de incubação com o PN. Quando decorrido o tempo de incubação as células foram fixadas com formalina 10% e fotos foram obtidas para análise da morfologia.

Figura 26 - Toxicidade e Morfologia de células da linhagem 4T1Br4 quando incubadas com o RSVT.

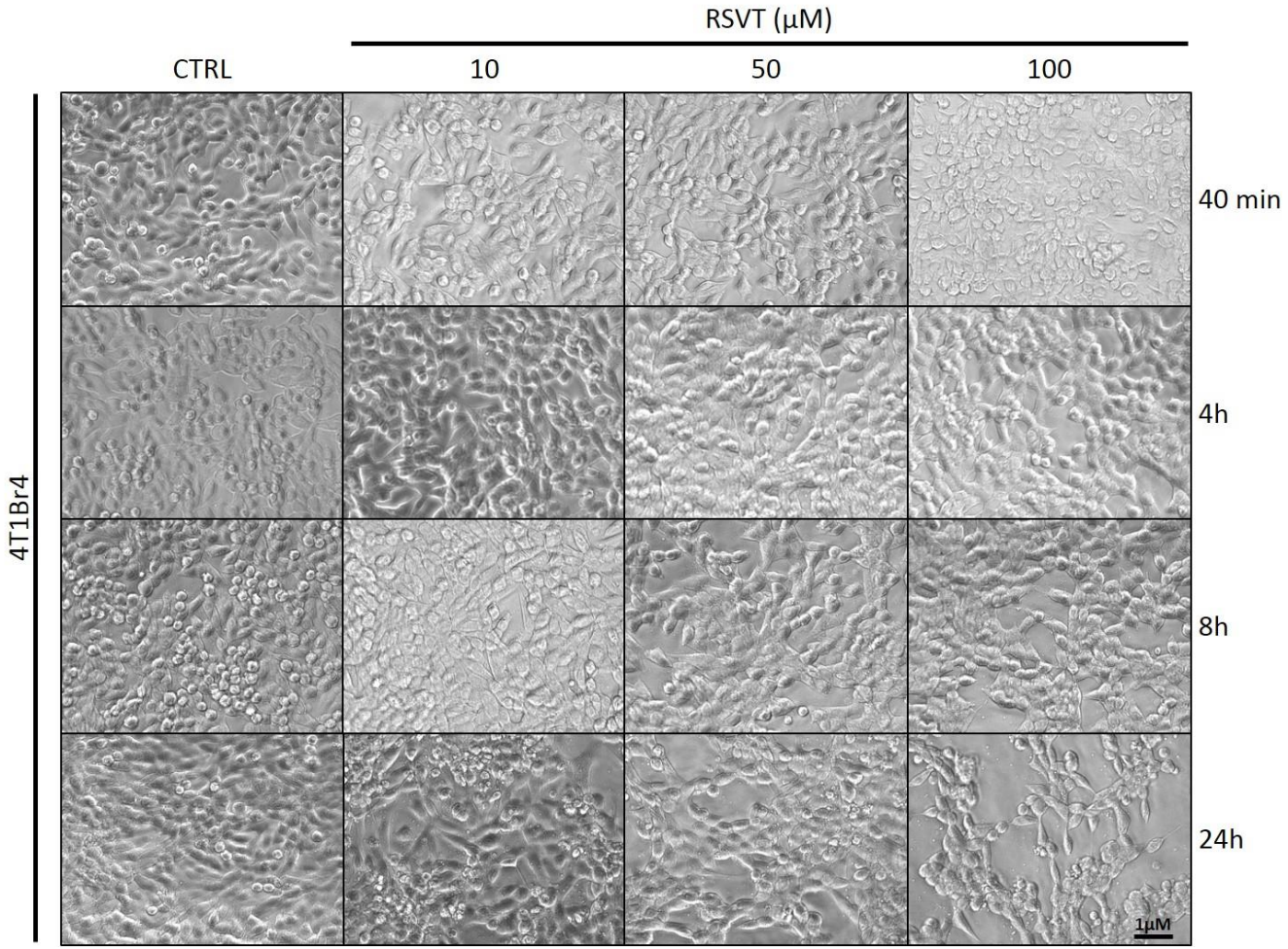

As células foram plaqueadas em placas de 96 poçose incubadas *overnight.* No dia seguinte, foram incubadas com diferentes concentrações e tempos de incubação com o PN. Quando decorrido o tempo de incubação as células foram fixadas com formalina 10% e fotos foram obtidas para análise da morfologia.

Figura 27 - Toxicidade e Morfologia de células da linhagem MDA-MB-231 BrM quando incubadas com o RSVT.

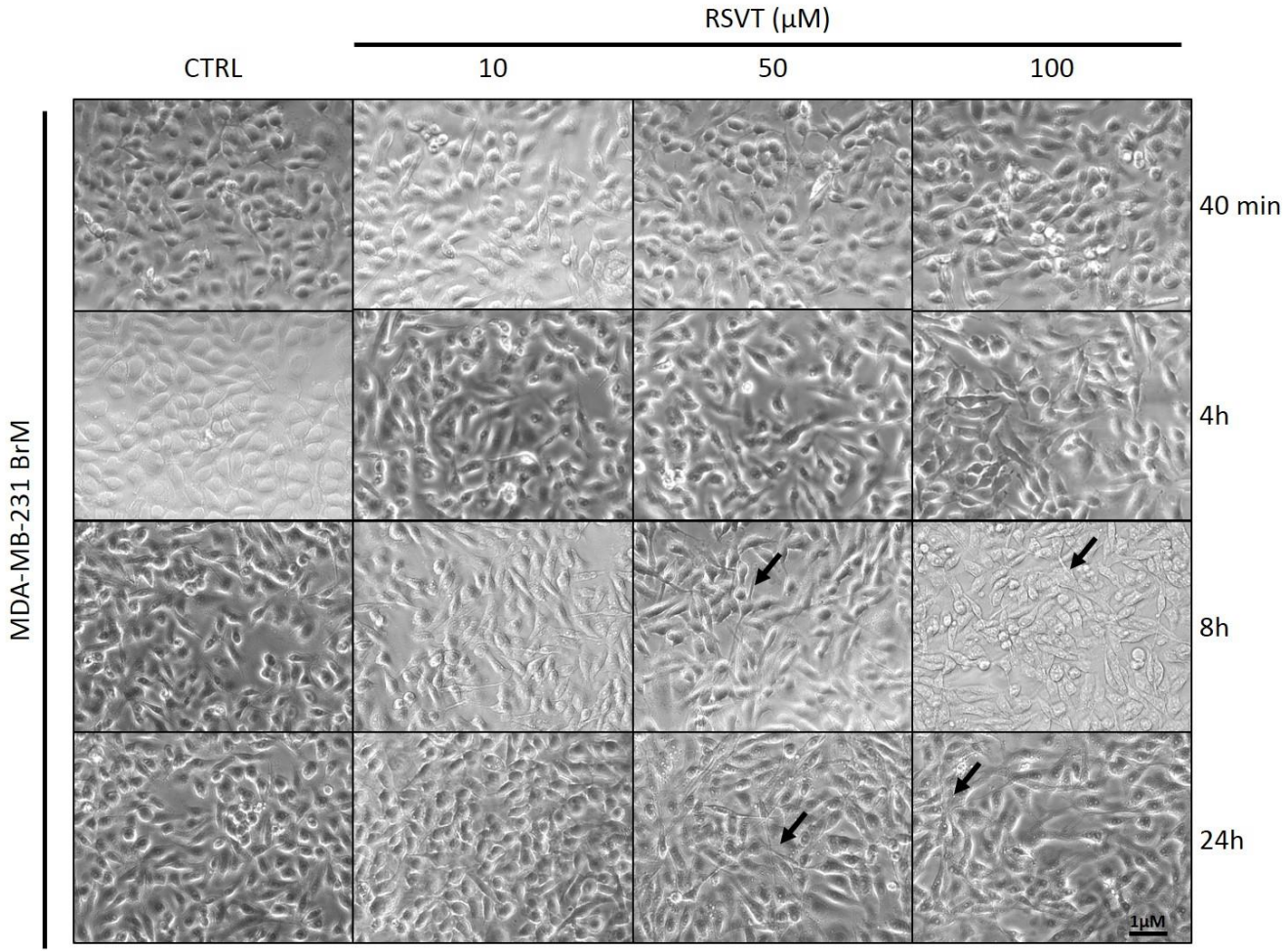

As células foram plaqueadas em placas de 96 poçose incubadas *overnight.* No dia seguinte, foram incubadas com diferentes concentrações e tempos de incubação com o PN. Quando decorrido o tempo de incubação as células foram fixadas com formalina 10% e fotos foram obtidas para análise da morfologia.

5.4 Migração celular

Sabendo-se as concentrações e tempos de incubação tóxicos do [10]-gingerol através do ensaio de citotoxicidade, foi utilizado somente as suas concentrações que não causaram morte celular no tempo de 4h (25 e 50µM) para verificar se o mesmo seria capaz de inibir a migração celular, via receptores de adesão. Assim, verificamos que o [10]-gingerol não inibiu a migração celular da linhagem 4T1Br4 nas concentrações de 25 e 50µM através da vitronectina, laminina-511 e na migração quimiotática utilizando-se soro fetal bovino como quimioatraente (Figura 28 - painéis A, C e E). O soro contém uma alta concentração de vitronectina (HAYMAN et al., 1985), confirmando o ensaio de migração haptotática à vitronectina.

Figura 28 – Ensaio de migração celular hapoptática e quimiotática na linhagem 4T1Br4 na presença de [10]-gingerol e RSVT.

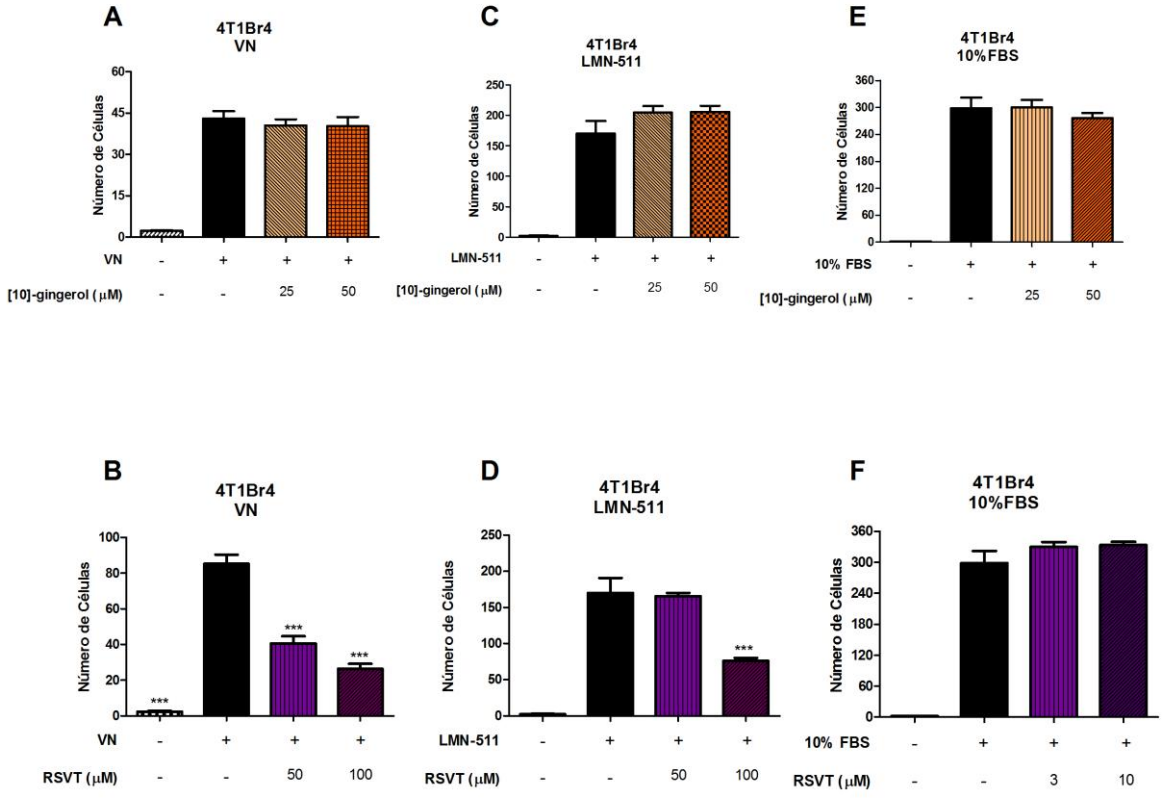

O [10]-gingerol não inibiu a migração à vitronectina, à laminina-511 e ao FBS. O RSVT inibiu a migração à VN e a laminina-511(***p<0,0001).

O RSVT inibiu a migração das células 4T1Br4 através da VN nas concentrações de 50 e 100µM, além disso também inibiu a migração através da LMN-511 na maior concentração,

indicando uma possível seletividade do RSVT pela VN (Figura 28– painéis B, D e F). Apesar do mesmo não ter ocorrido na migração quimiotática, em que o soro presente no poço inferior é rico em vitronectina, isto pode ser devido as concentrações utilizadas do RSVT terem sido menores, 3 e 10µM.

5.5 Ensaio de proliferação celular- 5 dias

A fim de padronizar futuros experimentos, um ensaio de proliferação celular de cinco dias foi realizado, empregando-se as concentrações de 10 e 50µM de [10]-gingerol.

Com isso, foi verificado que na linhagem 4T1Br4, embora a concentração de 10µM não tenha afetado a proliferação celular mesmo pós cinco dias de incubação, a concentração de 50µM, por sua vez, inibiu a proliferação celular a partir do terceiro dia de incubação (Figura 29– painel A). Portanto, o [10]-gingerol atua de maneira dependente da concentração e do tempo: em baixas concentrações não altera a proliferação mesmo quando incubado por longos períodos; porém, em maiores concentrações (50µM) pode inibir a proliferação, até mesmo em tempos menores.

Na linhagem humana, MDA-MB-231 BrM, o [10]-gingerol não inibiu a proliferação, mesmo após cinco dias de incubação nas concentrações mais elevadas, possivelmente por essa concentração de 50µM ser menor que o valor do IC_{50} (65,2 ±5,135µM) para esta linhagem com este produto natural (Figura 29– painel B).

Figura 29 – Ensaio de proliferação de 5 dias na linhagem 4T1Br4 e MDA-MB-231 BrM.

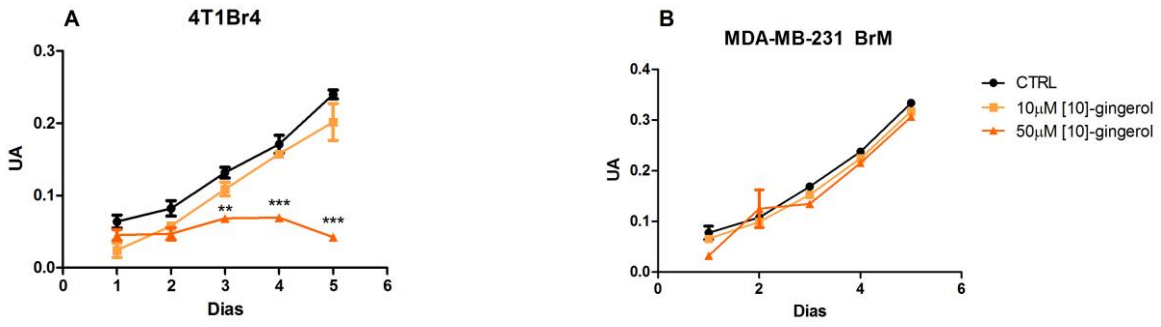

O [10]-gingerol inibiu a proliferação celular na concentração de 50µM na linhagem 4T1Br4 e não inibiu a proliferação na linhagem MDA-MB-231 BrM em nenhuma das concentrações testadas (**p<0,01, ***p<0,0001).

5.6 Ensaio clonogênico

No ensaio clonogênico com o qual foi verificado se o tratamento possui uma atividade citotóxica e/ou citostática sobre as células tumorais o [10]-gingerol reduziu o tamanho das colônias nas concentrações de 10 e 20µM, entretanto não inibiu o número de colônias nas mesmas concentrações, sendo assim, o [10]-gingerol apresentou um efeito citostático (Figura 30, painel A e B). O RSVT, por sua vez, reduziu o tamanho e o número das colônias na concentração de 1,5µM, possuindo um efeito citostático e citotóxico (Figura 30, painel C e D).

Figura 30 – Ensaio clonogênico sem radiação.

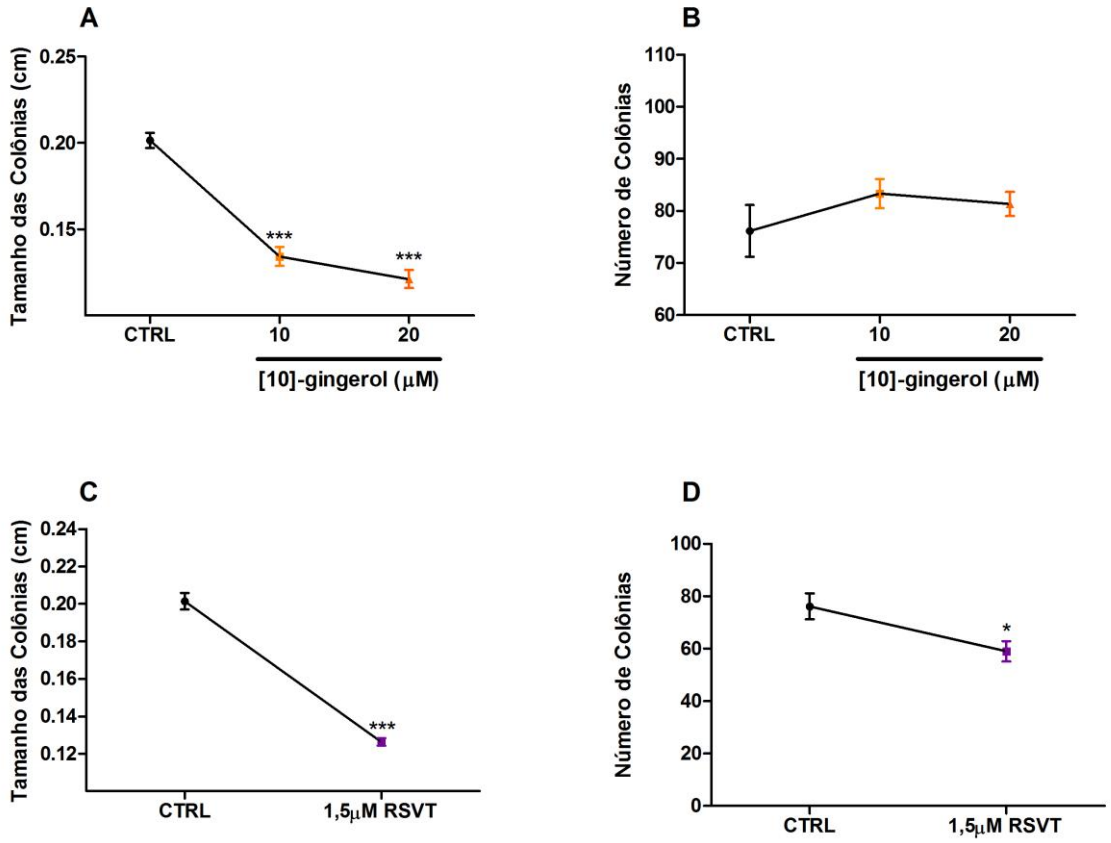

Células da linhagem 4T1Br4 (100 células/poço, placa de 6 poços) foram incubadas com o [10]-gingerol nas concentrações de 10 e 20µM e com o RSVT na concentração de 1,5µM.(A e B) - o [10]-gingerol reduziu o tamanho das colônias mas não alterou o número das colônias. (Ce D) - o RSVT reduziu o tamanho e o número das colônias (*p<0,05, ***p<0,0001).

Ainda através do ensaio clonogênico foi examinado a atividade do produto natural quando combinado à radiação. Os produtos naturais são conhecidos por possuírem uma atividade de radio-sensibilização, ou seja, potencializam o efeito da radiação contra células tumorais. De fato, verificamos que o [10]-gingerol aumentou os efeitos do tratamento por radiação, com um fator de aumento de 1,2 na concentração de 10µM e de 1,4 na concentração de 20µM, evidenciado pela redução do número e do tamanho das colônias na radiação de grau 2, 4 e 6 (Figura 31, painel A e B).

O RSVT teve um fator de aumento da radiação de 1,2 na concentração de 1,5µM reduzindo o número e o tamanho das colônias nas radiações de 2, 4 e 6 (Figura 31, painel C e D).

Figura 31 - Ensaio clonogênico com radiação.

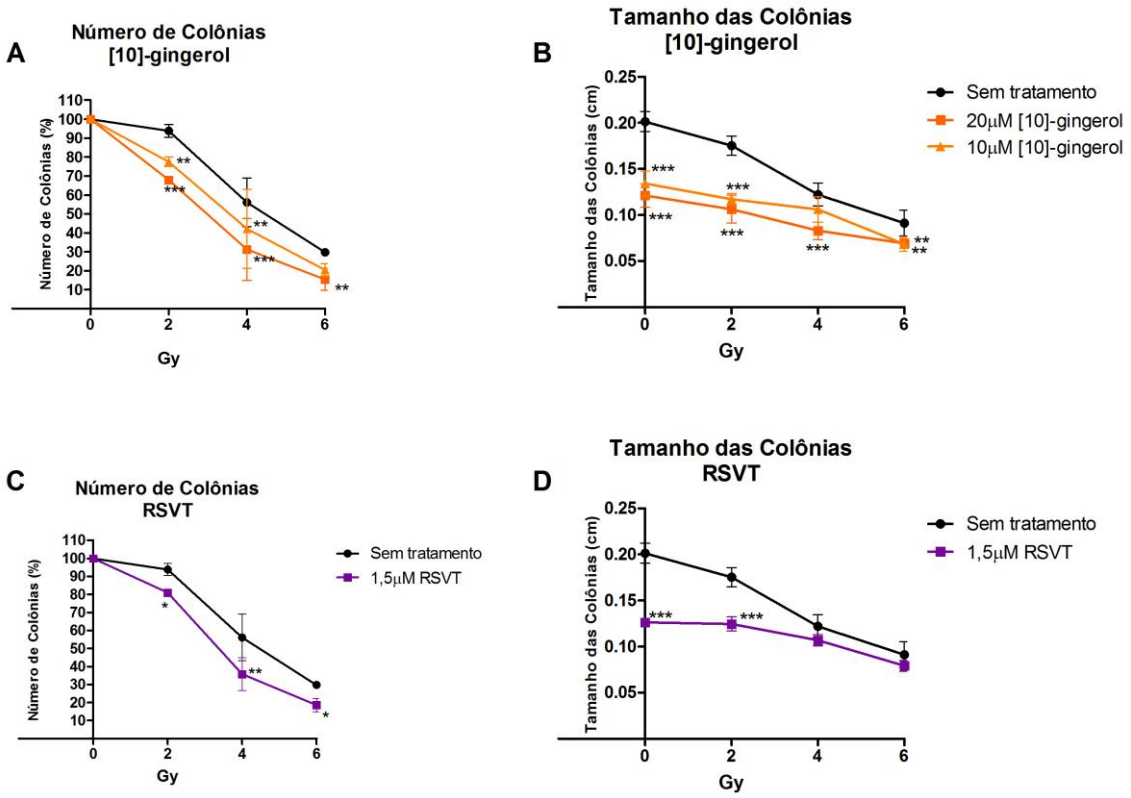

Células da linhagem 4T1Br4 (100 células/poço, placa de 6 poços) foram incubadas com o [10]-gingerol nas concentrações de 10 e 20µM e com o RSVT na concentração de 1,5µM e foram sujeitas a diferentes níveis de radiação (2, 4 e 6 Gy). O [10]-gingerol reduziu o tamanho e número das colônias nas concentrações testadas quando sujeitas a todos os graus de radiação. O RSVT reduziu o tamanho e o número das colônias na concentração testada e nos diferentes níveis de radiação (2, 4 e 6 Gy) (*p<0,05; **p<0,01, ***p<0,0001).

Podemos verificar o efeito citostático do [10]-gingerol na Figura 32 quando a radiação não foi aplicada. Na mesma figura podemos observar o efeito da radiação somado ao produto

natural com aumento do efeito do [10]-gingerol, ocorrendo uma inibição na proliferação e aumento da morte celular.

Figura 32 – Ensaio clonogênico associado a radiação.

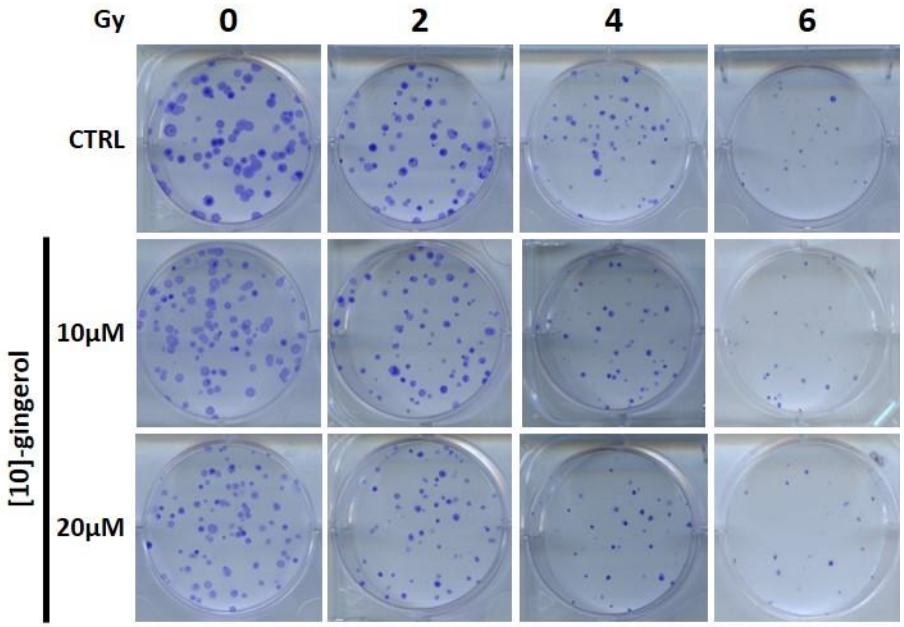

Células da linhagem 4T1Br4 (100 células/poço) foram incubadas nas concentrações de 10 e 20µM do [10]-gingerol e submetidas a diferentes graus de radiação (2, 4, e 6 Gy). O [10]-gingerol possui um efeito citostático quando não sujeito a radiação. Em associação com a radiação o [10]-gingerol apresenta efeito citostático e citotóxico.

Pode-se verificar Na Figura 33 o efeito citostático e citotóxico do RSVT na linhagem 4T1Br4 com e sem aplicação de radiação.

Figura 33 - Ensaio clonogênico associado a radiação.

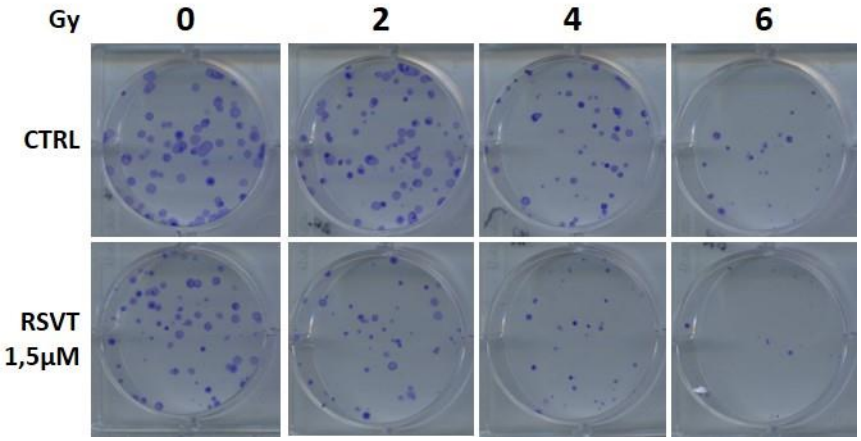

Células da linhagem 4T1Br4 (100 células/poço) foram incubadas na concentração de 1,5µM do RSVT e submetidas a diferentes graus de radiação (2, 4, e 6 Gy). O RSVT possui um efeito citostático e citotóxico na presença e ausência de radiação.

5.7 Ensaio de Condensação nuclear

A condensação nuclear é uma característica típica de células apoptóticas. Células da linhagem 4T1Br4 tratadas com o [10]-gingerol sofreram um aumento da condensação nuclear proporcionalmente dependente ao aumento da concentração do produto natural. Além disso, verificamos uma redução na confluência das células na concentração de 100µM. As setas na Figura 34 indicam células com aumento da condensação nuclear.

Figura 34 - Ensaio de condensação nuclear.

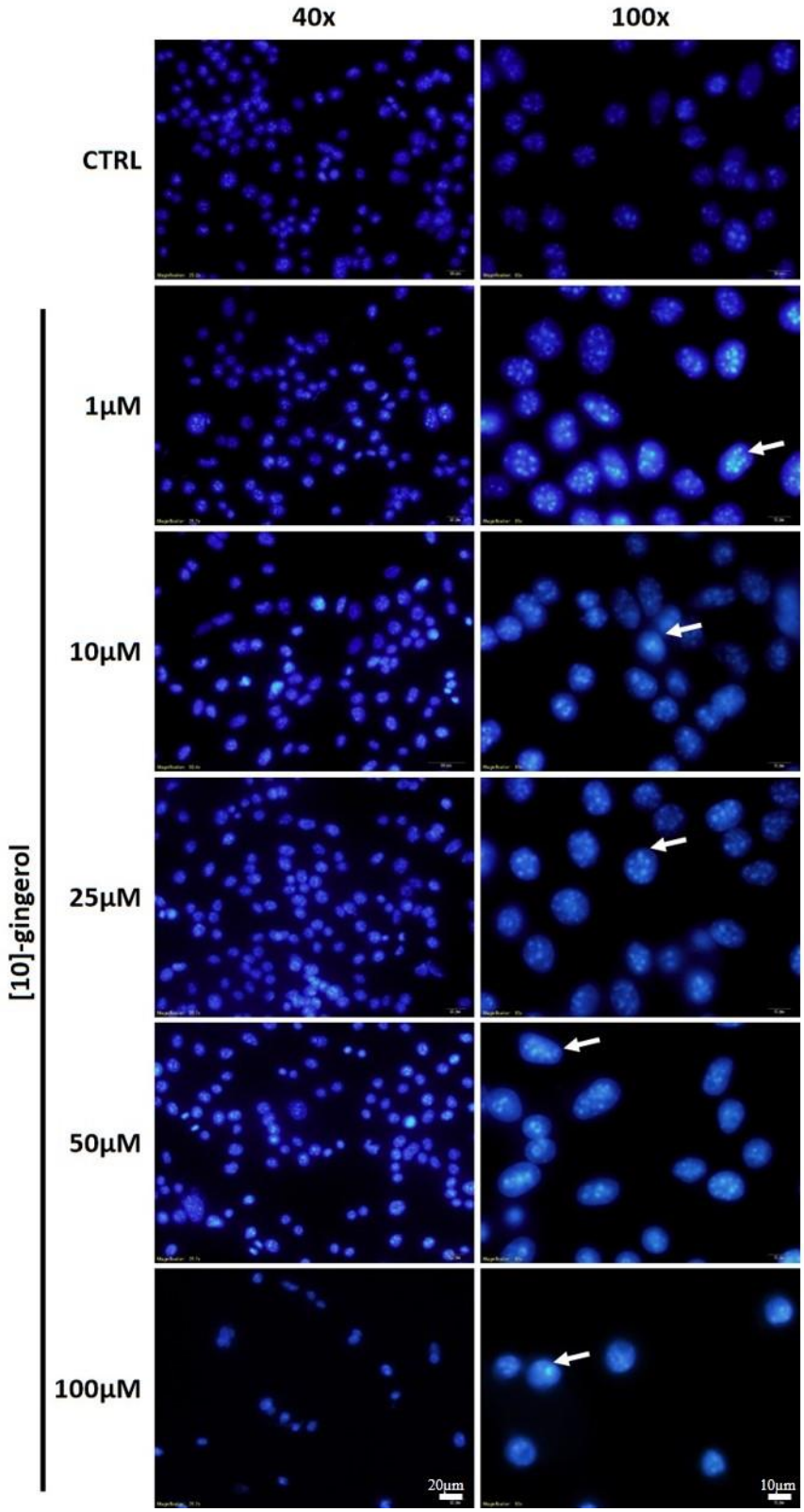

Células da linhagem 4T1Br4 foram incubadas por 24h com o [10]-gingerol e em seguida coradas com DAPI. O [10]-gingerol induziu a condensação nuclear nas concentraçoes de 1, 10, 25, 50 e 100µM como indicado nas setas brancas.

5.8 TUNEL

O ensaio de TUNEL é um método simples de detecção de apoptose a nível celular via detecção colorimétrica de fragmentos degradados de DNA. As células da linhagem 4T1Br4 incubadas por 18h com o [10]-gingerol sofreram apoptose quando expostas às concentrações de 10 e 50µM, estes resultados podem ser observados nas setas da Figura 35

Figura 35 - Ensaio colorimétrico de TUNEL.

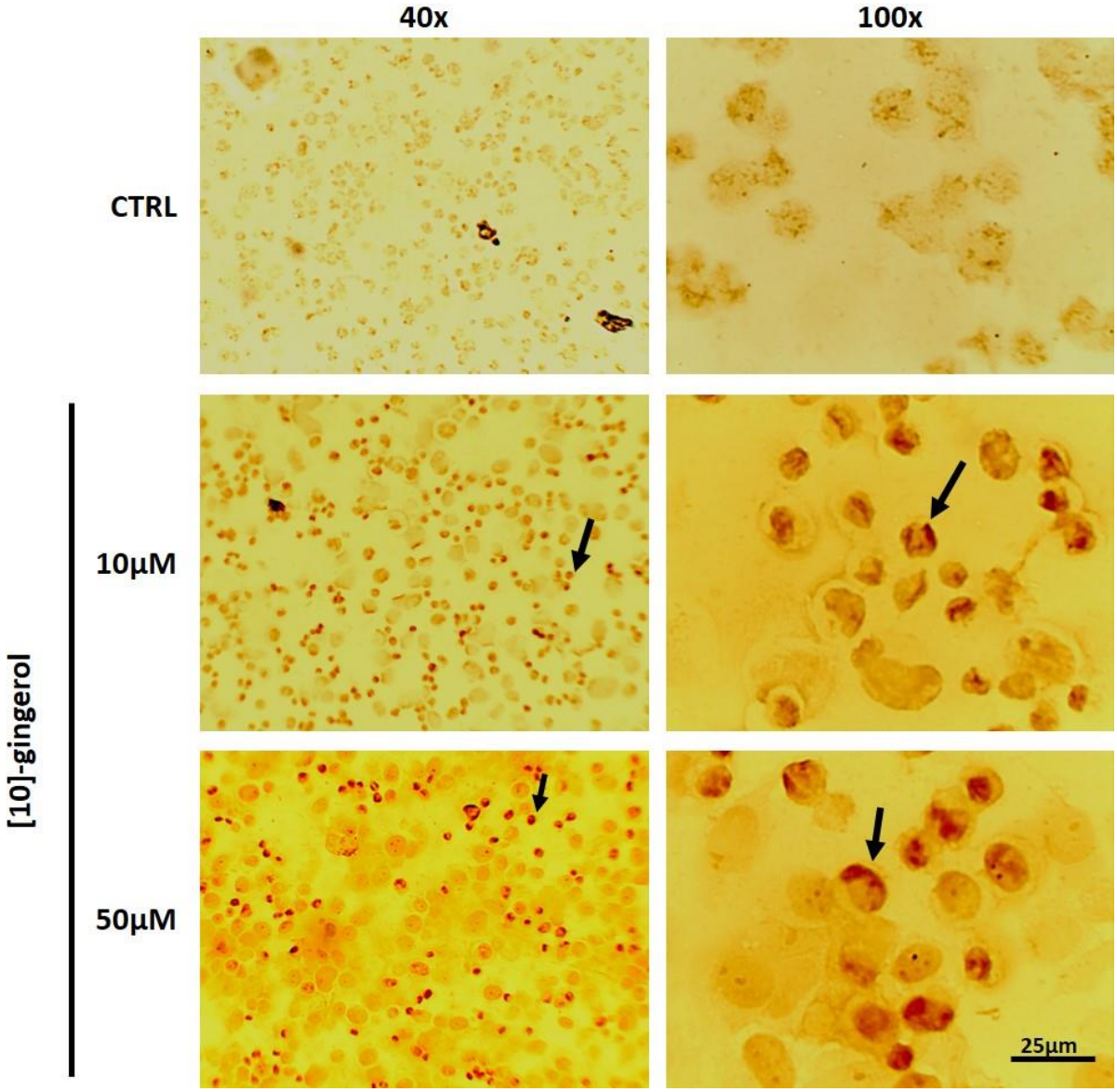

Células da linhagem 4T1Br4 foram incubadas por 18h com o [10]-gingerol nas concentrações de 10 e 50µM. O produto natural induziu a apoptose nas duas concentrações testadas. As setas indicam células em apoptose.

5.9 Análise do Ciclo celular

Células da linhagem 4T1Br4, tratadas por 8h com 50µM do [10]-gingerol, sofreram uma parada no ciclo celular na fase G1, fato evidenciado pelo aumento dessa subpopulação em relação ao controle (Figura 36 – painel A). Considerando-se o período de 24h de incubação, o tratamento com 50µM de [10]-gingerol induziu uma parada no ciclo celular na fase subG1, com o aumento desta subpopulação, fase anterior a G0/G1, como observado com 8h de incubação (Figura 36 – painel B). O tratamento com o [10]-gingerol, na concentração de 10µM, não alterou nenhuma das fases do ciclo celular nos tempos testados.

Figura 36 – Ensaio de ciclo celular.

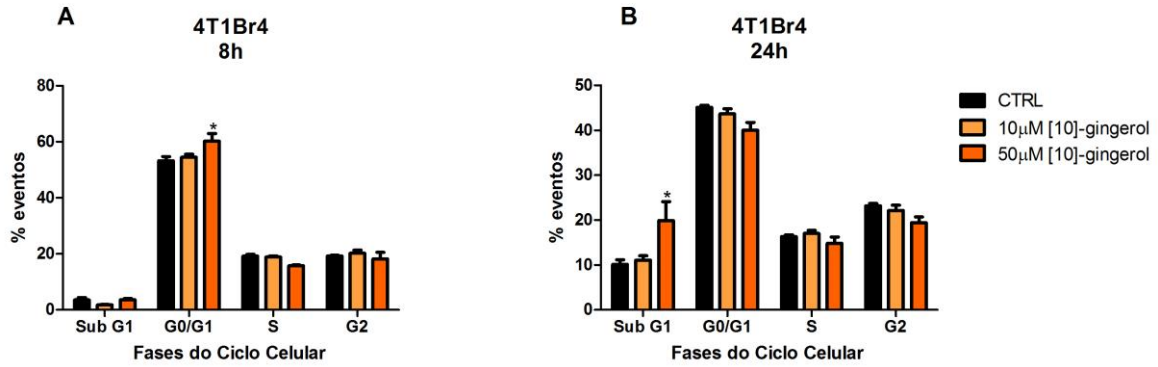

O [10]-gingerol induziu a parada do ciclo celular na fase G0/G1 no tempo de 8h de incubação na concentração de 50µM. Entretanto, no tempo de 24h o [10]-gingerol na mesma concentração induziu a parada da fase sub G0 aumentando esta subpopulação (*p<0,05).

5.10 Atividade de caspases

O ensaio de atividade de caspases verifica a clivagem do peptídeo AMC (7-amino-4-methylcoumarin) pelas caspases, esta clivagem gera uma fluorescência captada no comprimento de onda de emissão de 440-460nm e excitação de 340-350nm. O [10]-gingerol inibiu a atividade das caspases-3 e -7 quando as células de 4T1Br4 foram incubadas por 8h de forma dependente de concentração (10, 25 e 50µM), como observado na Figura 37, painel A. Entretanto, quando as células foram incubadas por 18h com o produto natural houve um aumento da atividade das caspases (Figura 37– painel B).

Figura 37 – Atividade de caspases.

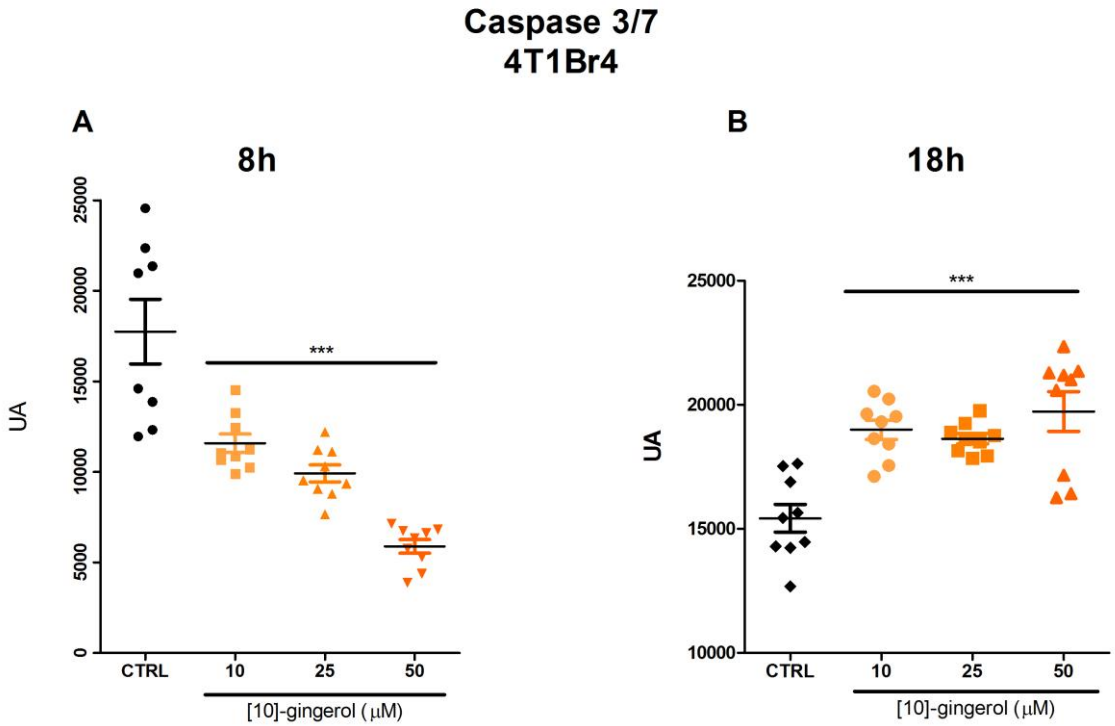

[10]-gingerol reduziu a atividade das caspases-3 e -7 no tempo de 8h de incubação e aumentou a atividade das caspases-3 e -7 no tempo de 18h (***p<0,0001).

5.11 Expressão Gênica

Células da linhagem 4T1Br4 incubadas por 6h com o [10]-gingerol apresentaram um aumento da expressão da caspase-9 na concentração de 100µM e redução na expressão de Bcl-2 nas concentrações de 25, 50 e 100µM. A expressão das caspases-3, -7, -8 e Bax não sofreu alterações nas concentrações testadas no tempo de 6h (Figura 38). Considerando-se o tempo de 18h de incubação, houve redução da expressão das caspases-3 e -7 nas concentrações de 50 e 100µM, bem como redução da expressão gênica da caspase-8 na concentração de 50µM e da caspase-9 na concentração de 100µM. O produto natural aumentou a expressão gênica de Bax (pró-apoptótico) nas concentrações de 50 e 100µM e reduziu a expressão do gene Bcl-2 (anti-apoptótico) em todas as concentrações testadas (1-100µM) como apresentado na Figura 39.

Figura 38 – Expressão de genes relacionados a apoptose em células 4T1Br4 tratadas com [10]-gingerol por 6h.

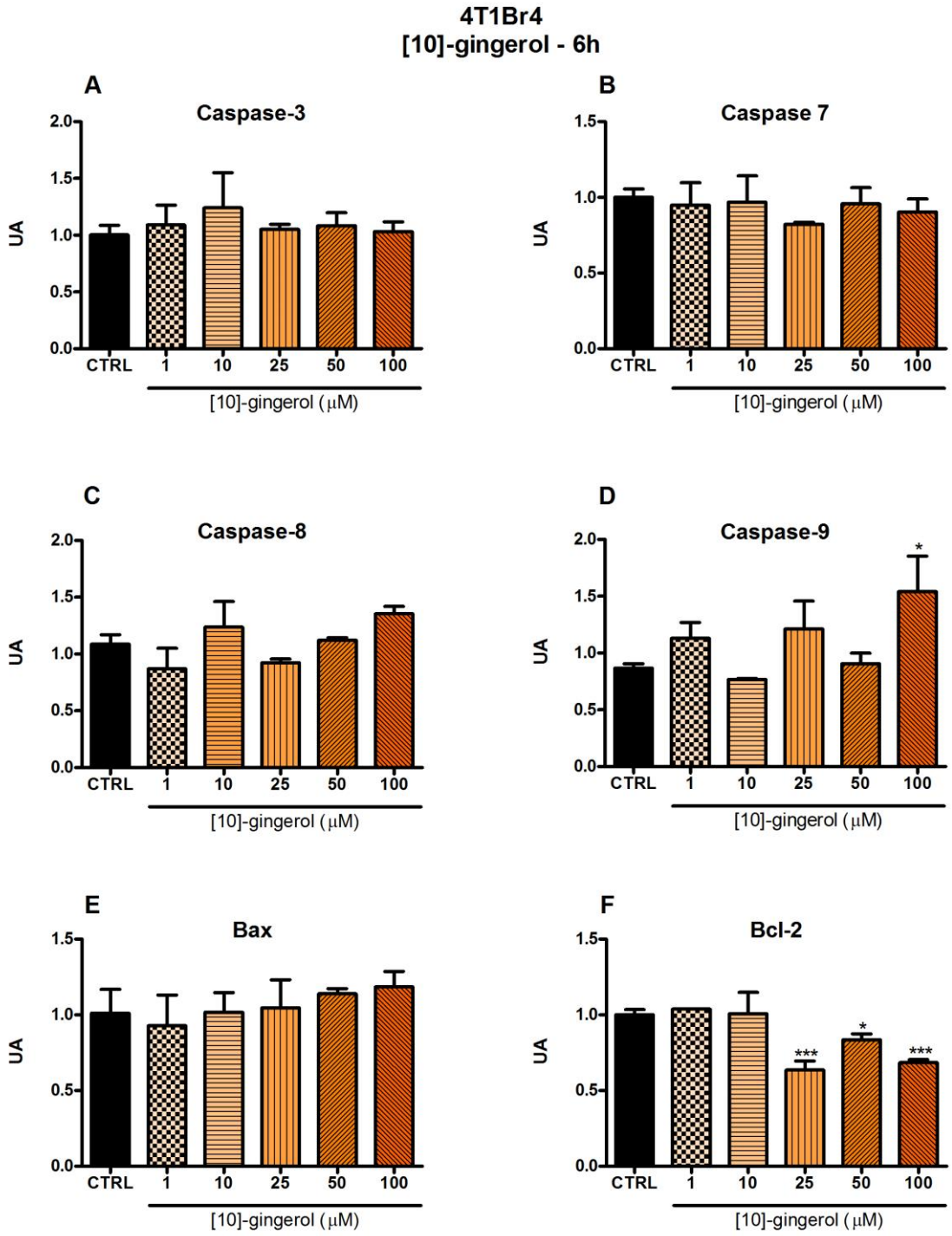

O [10]-gingerol induziu a expressão da caspase-9 e reduziu a expressão de Bcl-2 no tempo de 6h de incubação (*p<0,05;***p<0,0001).

Figura 39 - Expressão de genes relacionados a apoptose em células 4T1Br4 tratadas com [10]-gingerol por 18h.

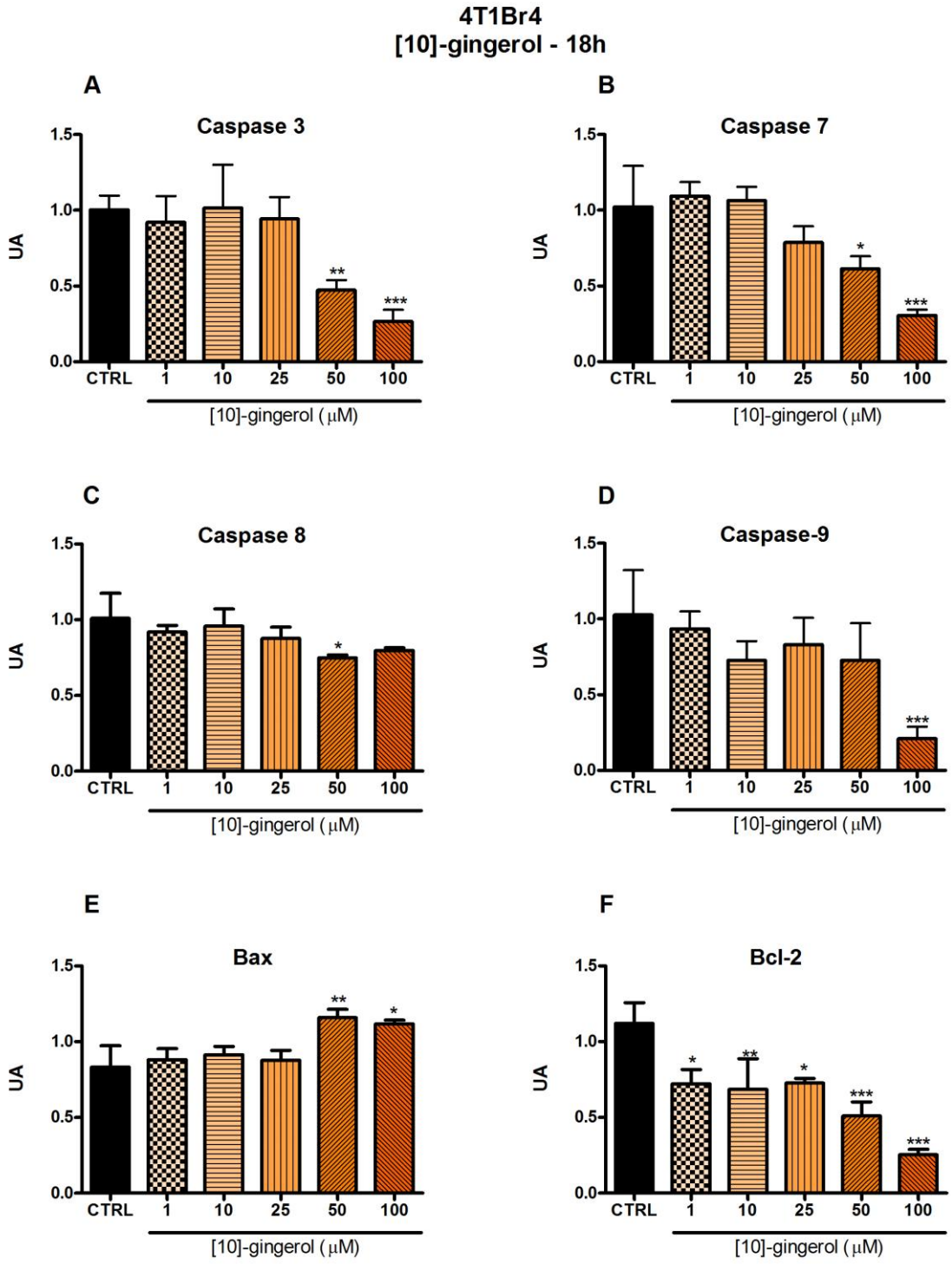

O [10]-gingerol reduziu a expressão das caspases-3/7/8/9 e Bax e reduziu a expressão de Bcl-2 no tempo de 18h de incubação (*p<0,05; **p<0,001; ***p<0,0001).

5.12 Modelo de formação de metástase espontânea IMFP (Intramammary Fat Pad) sem cirurgia do tumor primário

Neste modelo *in vivo*, as células tumorais da linhagem 4T1Br4 foram injetadas no tecido adiposo da quarta mama de camundongos fêmeas (IMFP) e quando os tumores se tornaram palpáveis o tratamento com [10]-gingerol foi iniciado. Neste experimento não houve alteração na massa corporal dos animais tratados quando comparados ao grupo controle (Figura 40– painel A), contudo, o tratamento foi efetivo na redução do tamanho dos tumores primários entre os dias 23 e 25 após a injeção (Figura 40 - painel B). Não houve diferença entre os grupos experimentais com relação ao fígado, indicador de toxicidade, (Figura 40– painel C), em contrapartida, verificamos que o peso do baço, indicador da carga tumoral geral, foi menor no grupo tratado em relação ao controle não tratado (Figura 40– painel D).

Figura 40 – Modelo de formação de metástase espontânea IMFP (*Intramammary Fat Pad*): impactos do tratamento com o [10]-gingerol sobre parâmetros morfométricos.

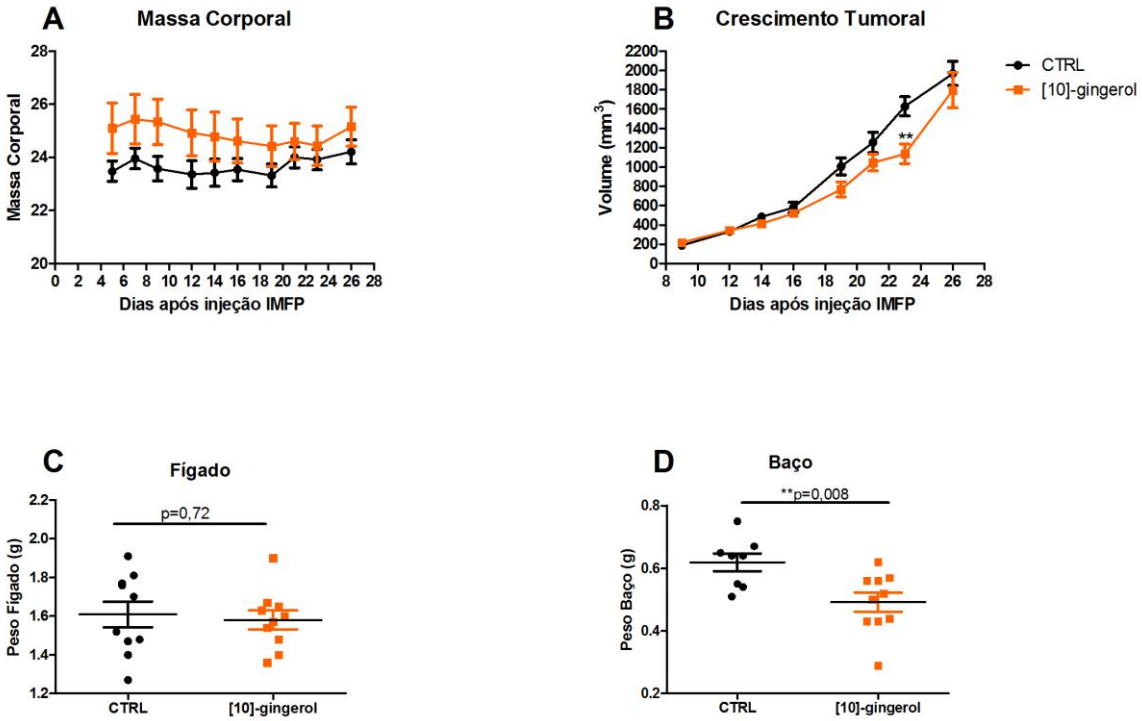

O tratamento com [10]-gingerol reduziu o tamanho dos tumores primários entre os dias 23 e 25 após a injeção e o peso dos baços. Não houve alteração na massa corporal durante o experimento entre os grupos e no peso dos fígados dos animais.

A fim de se verificar a carga tumoral relativa – RTB (**RTB** – ***R**elative **T**umor **B**urden*), indicador de metástases, órgãos como pulmões, coluna vertebral e fêmures dos animais foram

coletados e submetidos à extração de DNAg para a detecção da presença do gene mCherry (exclusivo das células tumorais) e mVimentina (presente em todas as células) nesses órgãos através de PCR multiplex em tempo real.

Através dessa técnica, verificamos que houve redução significativa da RTB nos pulmões (Figura 41 - A) sem alteração da RTB na coluna vertebral, fêmures e ossos (somatória dos valores de RTB da coluna vertebral e fêmures) como indicado na Figura 41, painéis B, C e D.

Figura 41 – Análise da *Relative Tumor Burden* (RTB) no modelo de formação de metástase espontânea IMFP (*Intramammary Fat Pad*) com tratamento do PN.

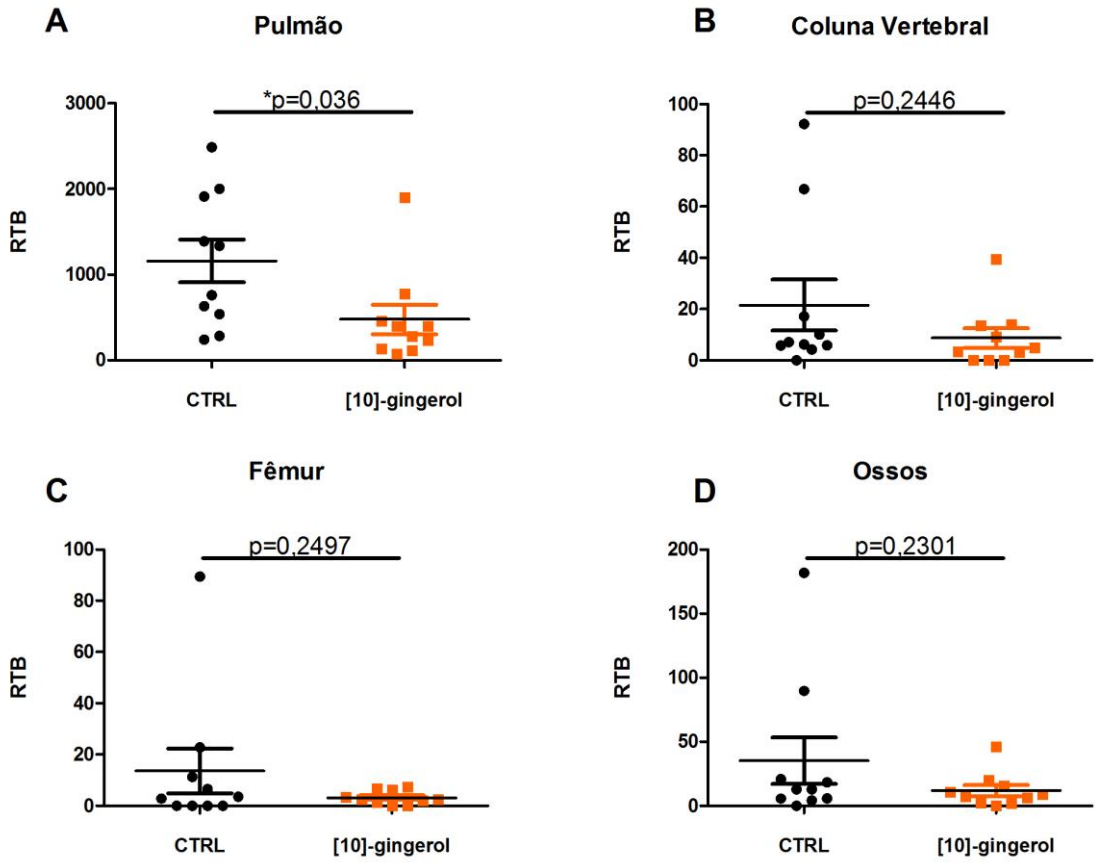

O tratamento com [10]-gingerol reduziu a RTB nos pulmões dos animais tratados e não houve alteração da RTB na coluna vertebral, fêmures e ossos.

As diferenciais mencionadas com relação à carga tumoral, bem como ao peso relativo do baço puderam ser observadas mesmo através de análise visual. Na Figura 42-A podemos observar as metástases pulmonares do grupo controle e proeminente redução destas no grupo tratado com o [10]-gingerol. Na mesma figura, painel B, fica evidente a diferença de tamanho, e consequentemente, do peso dos baços dos animais controle e dos tratados com o produto

natural, evidenciando menor circulação na corrente sanguínea de células tumorais no grupo tratado Figura 42- B.

Neste modelo foi utilizada uma dose de 5mg/kg, e os animais não apresentaram nenhum indício de toxicidade, analisado pelo peso dos fígados, alimentação e movimentação normal dos animais. Portanto, para o próximo modelo foi utilizado uma dose maior de 10mg/kg.

Figura 42 – Imagem representativa das metástases pulmonares e do tamanho dos baços.

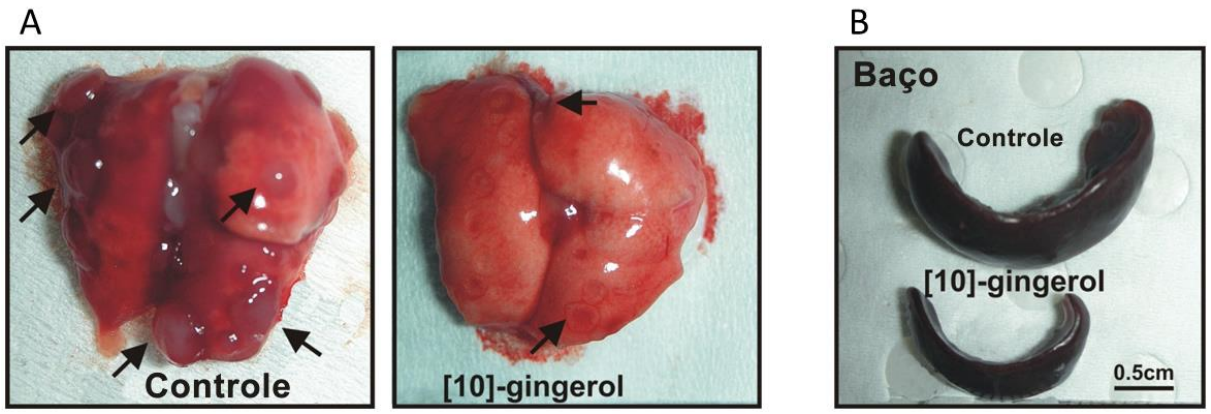

(A) Pulmões do grupo controle e grupo tratado com [10]-gingerol, respectivamente.
(B) Imagem do baço dos animais do grupo controle e do grupo [10]-gingerol.

5.13 Modelo de formação de metástase espontânea IMFP (Intramammary Fat Pad) com cirqugia

Este modelo, onde os tumores primários dos animais foram removidos completamente para que então fosse iniciado o tratamento com o [10]-gingerol, visa mimetizar a situação na qual uma mulher, após o diagnóstico do câncer de mama, é submetida primeiramente à mastectomia e em seguida, a outros tratamentos, tais como a quimioterapia.

Neste experimento, verificou-se que o grupo controle apresentou no decorrer do período experimental, perda de massa corporal, fato não observado no grupo tratado com o [10]-gingerol (10mg/kg), sugerindo uma melhora nas condições gerais dos camundongos tratados com o produto natural (Figura 43A). Também foi verificado que não houve alteração no peso dos baços nos grupos tratados e controle, indicativo de células tumorais circulantes (Figura 43B).

Figura 43 - Modelo de formação de metástase espontânea IMFP (*Intramammary Fat Pad*) seguido de cirurgia: impactos do tratamento com o [10]-gingerol sobre parâmetros morfométricos.

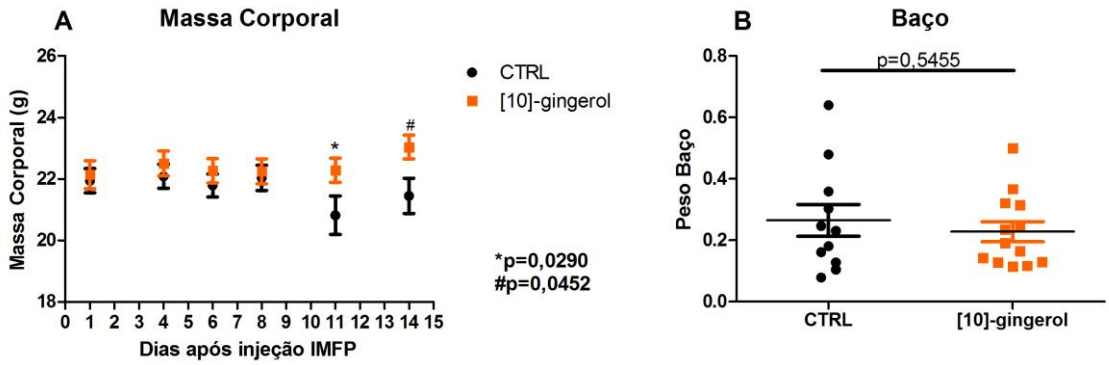

O tratamento com [10]-gingerol inibiu a perda de massa corporal quando comparado ao grupo controle e não houve diferença entre os grupos no peso dos baços dos animais.

Com relação a análise da RTB, o [10]-gingerol reduziu a RTB dos pulmões, fêmures e ossos (Figura 44 A, C e D). Não houve alteração da mesma na coluna vertebral e cérebros (B e E).

Figura 44 - Análise da RTB (*Relative Tumor Burden*) no modelo de formação de metástase espontânea IMFP (*Intramammary Fat Pad*) com tratamento do PN após cirurgia do tumor primário.

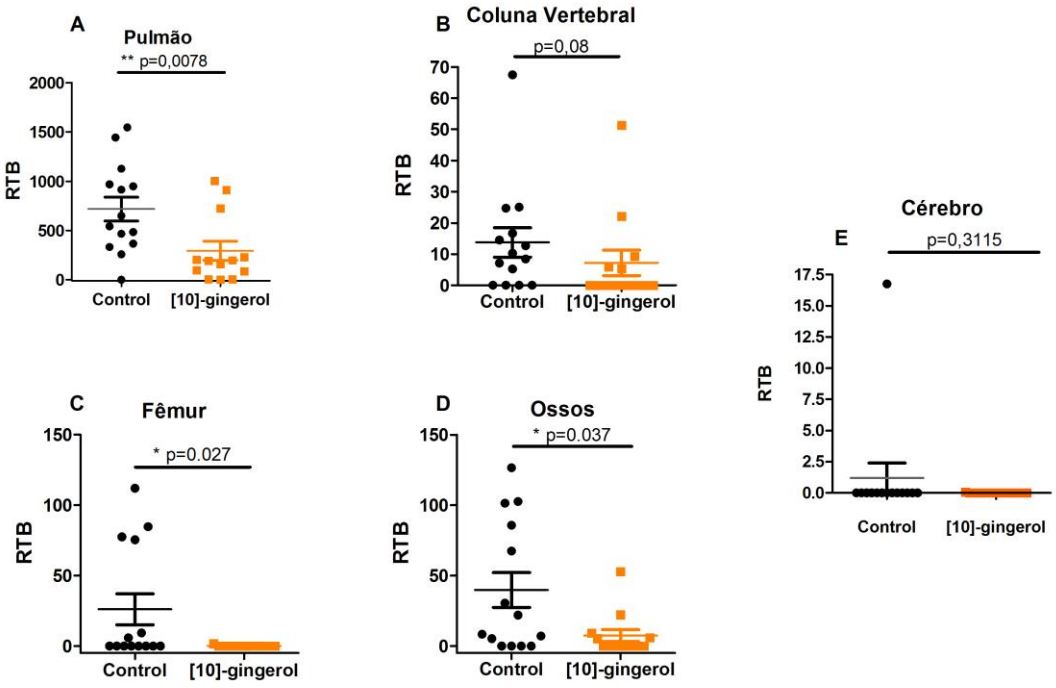

O tratamento com [10]-gingerol reduziu a RTB nos pulmões, fêmures e ossos dos animais tratados e não houve alteração da RTB na coluna vertebral e cérebro.

Embora não tenha sido possível detectar alterações na RTB entre os cérebros dos dois grupos experimentais, através da análise de imagens dos cérebros sob luz fluorescente, verificamos que no grupo controle sete dentre quinze animais apresentaram metástases cerebrais (Figura 45). Os animais #2 e #5 foram analisados separadamente pois apresentaram uma fluorescência menor, portanto, quando retirados os cérebros com alta fluorescência foi possível verificar as metástases cerebrais nestes animais, indicado na mesma figura a direita. Já no grupo tratado com [10]-gingerol, apenas um dentre quinze animais apresentou nódulos metastáticos no cérebro.(Figura 46). Sendo assim, enquanto a incidência de metástases cerebrais no grupo controle foi de 50%, este valor caiu drasticamente no grupo que recebeu o tratamento com [10]-gingerol, atingindo a marca de apenas 6% (Figura 47).

Figura 45 - Imagens fluorescentes dos cérebros do grupo controle.

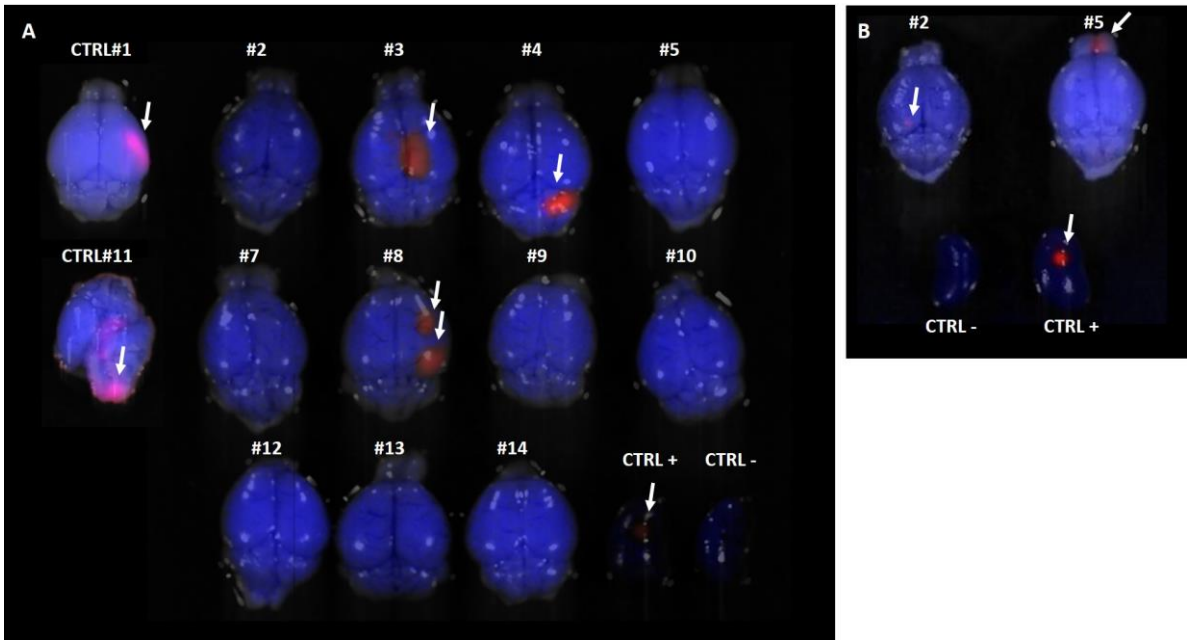

No grupo controle, não tratado com o PN, foram detectadas metástases cerebrais em sete de um total de quatorze animais. As setas apontam os nódulos metastáticos (vermelho), enquanto o tecido normal é apresentado em azul.

Figura 46 - Imagens dos cérebros do grupo tratado com [10]-gingerol.

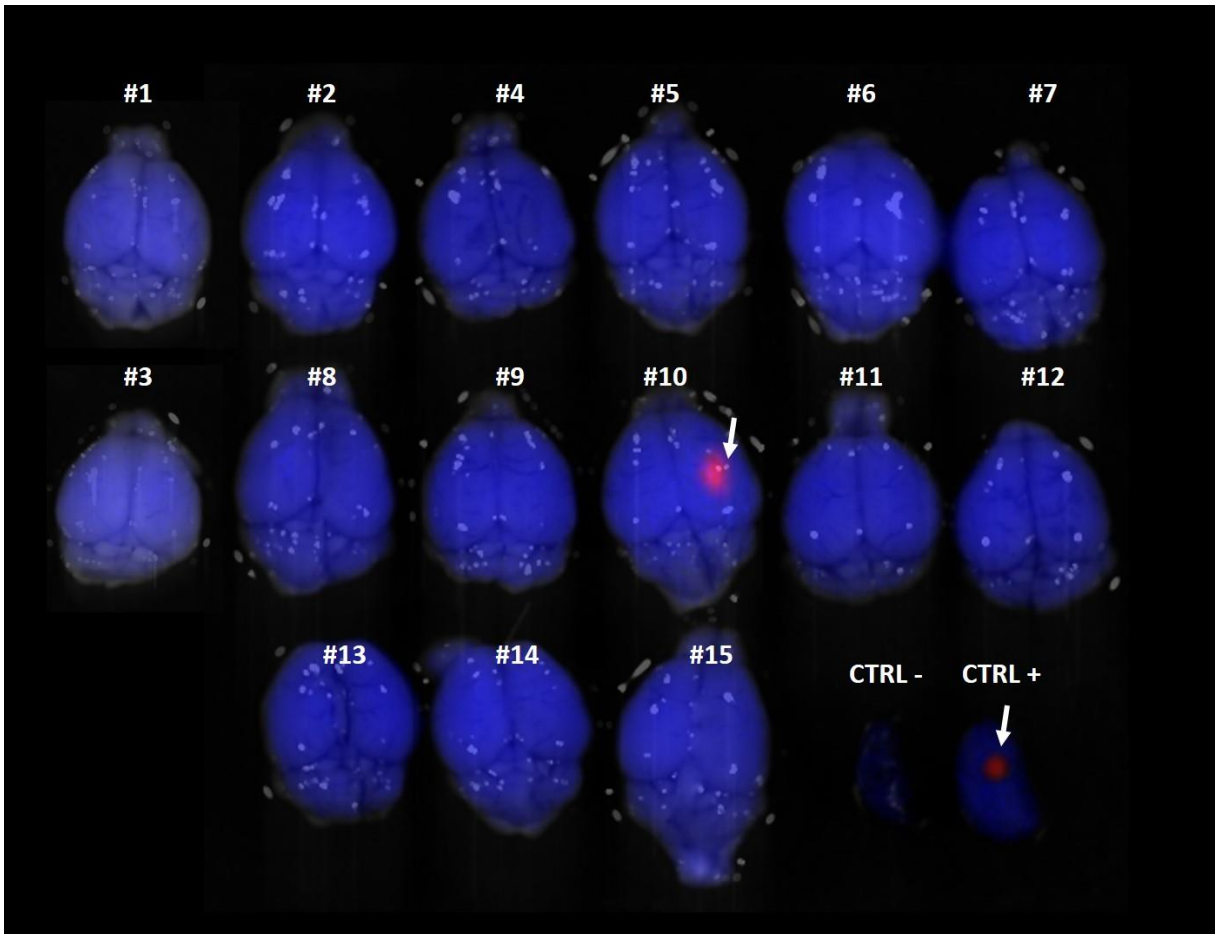

No grupo tratado com o PN foi detectada uma metástase cerebral em um do total de quinze animais. As setas apontam os nódulos metastáticos (vermelhos), enquanto o tecido normal é apresentado em azul. No canto inferior direito: controle positivo.

Figura 47 –Incidência de metástases cerebrais no modelo de metástase espontânea.

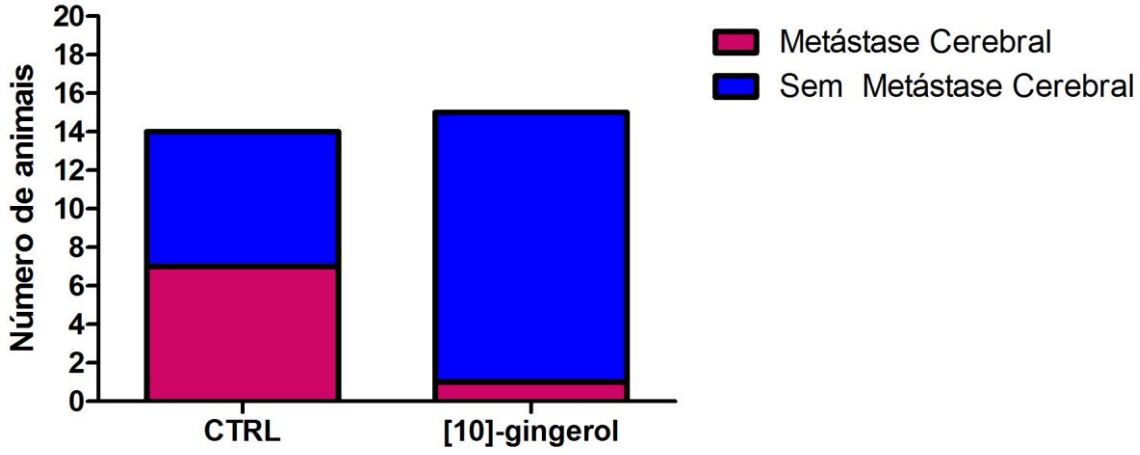

O grupo controle apresentou uma incidência de 50% e o grupo [10]-gingerol apresentou uma incidência de 6% de metástases cerebrais.

5.14 Modelo de formação de metástase experimental, injeção intracardíaca (IC) com tratamento do [10]-gingerol pós injeção

O modelo de injeção IC é utilizado para o estudo das fases mais tardias do processo metastático, uma vez que simula a presença das células tumorais na circulação sanguínea diretamente, sem a formação do tumor primário. Esta abordagem permite assim verificar se o tratamento usado realmente inibe o estabelecimento de metástases clinicamente detectáveis. Os resultados demonstraram que neste modelo o [10]-gingerol reduziu a RTB nos fêmures e nos ossos. Não houve alteração na massa corpórea, RTB da coluna espinhal, pulmões e cérebro (Figura 48).

Figura 48 – Modelo de metástase experimental com tratamento do [10]-gingerol após a injeção intracardíaca (IC).

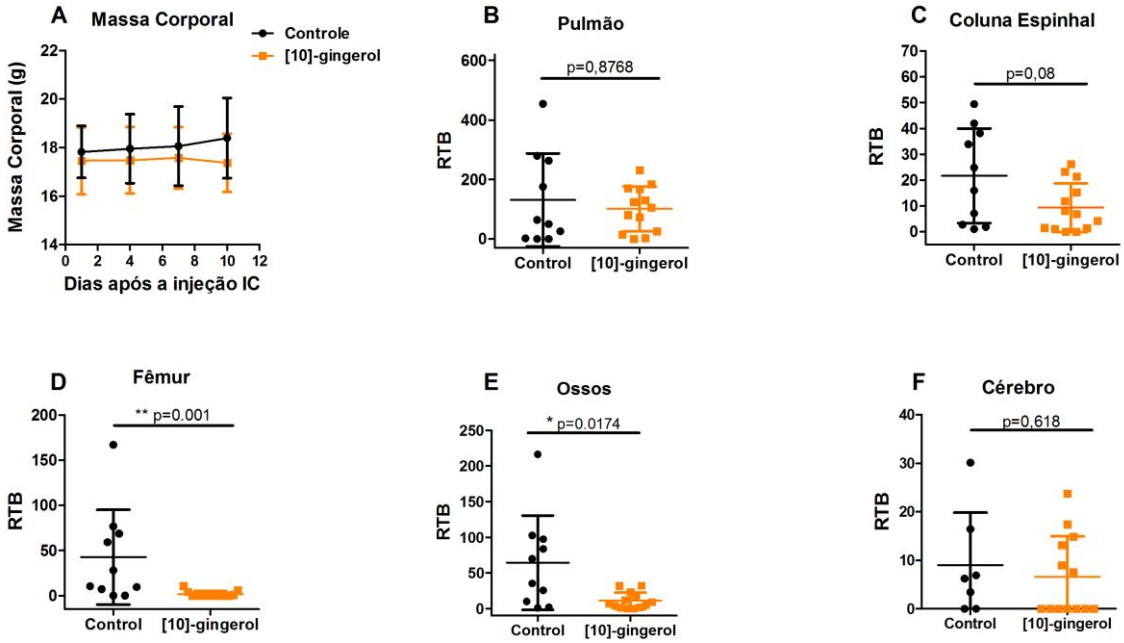

O tratamento com [10]-gingerol reduziu a RTB (Relative Tumor Burden) dos fêmures e ossos.

5.15 Modelo de formação de metástase experimental com injeção Intracardíaca (IC) com pré-tratamento do [10]-gingerol

Os produtos naturais são conhecidos por prevenirem a formação de tumores e de metástases. Sendo assim, realizamos um pré-tratamento de 3 dias nos animais com o [10]-gingerol antes da injeção IC, seguindo-se o tratamento também após a injeção IC. Neste

modelo não houve alteração da massa corpórea, assim como, não houve redução da RTB em nenhum dos órgãos coletados, como podemos verificar na Figura 49.

Figura 49 - Modelo de metástase experimental com tratamento do [10]-gingerol antes e após a injeção IC.

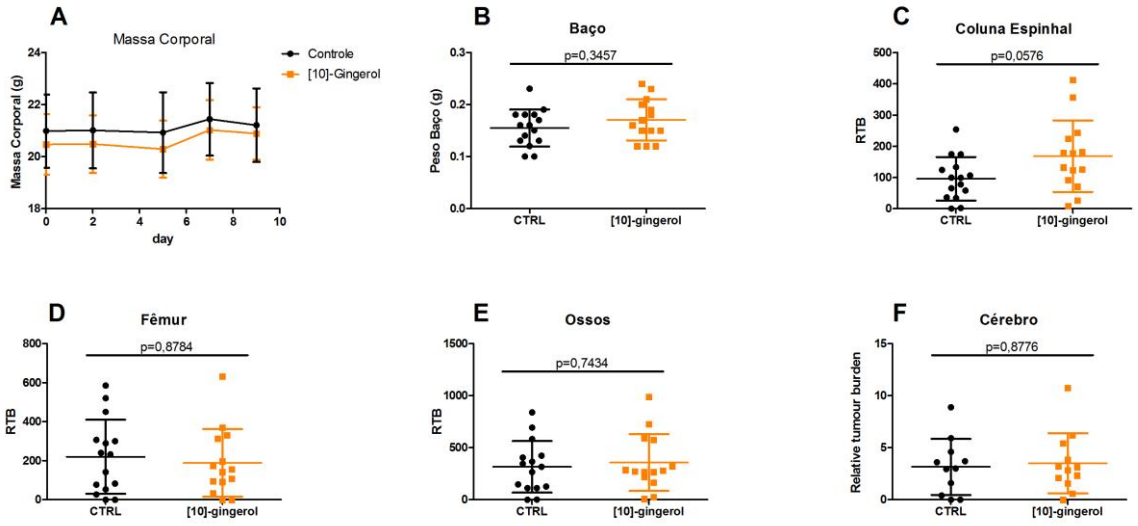

O tratamento com [10]-gingerol não alterou a massa corporal e não reduziu a RTB (*Relative Tumor Burden*) dos órgãos analisados.

6 DISCUSSÃO

Atualmente os tratamentos para o câncer e metástases como a radioterapia e a quimioterapia ainda apresentam diversos efeitos colaterais. Portanto, torna-se importante o estudo de novos medicamentos, principalmente provenientes da flora e fauna, sabendo-se que grande parte dos medicamentos utilizados são produzidos a partir de elementos naturais (SAFARZADEH; SHOTORBANI; BARADARAN, 2014). Este trabalho demonstrou os efeitos indutores do [10]-gingerol *in vitro* nas vias de apoptose, ciclo celular, radiosensibilização, e uma provável forma de ação de inibição de metástase em modelos *in vivo* de câncer de mama em metástase óssea, pulmonar e cerebral.

Nos experimentos *in vitro*, para efeito de comparação, foi utilizado o resveratrol (RSVT), um produto natural cujo uso para a prevenção e tratamento do câncer já está extremamente descrito e melhor estabelecido na literatura. Neste estudo, foi empregado o *trans*-resveratrol, pois foi demonstrado por Belleri e colaboradores (BELLERI et al., 2008), que este isomêro apresenta atividade inibitória em ensaios de proliferação, adesão e angiogênese, diferente da isoforma *cis* muito menos ativa.

O *trans*-resveratrol foi descrito como um ligante da integrina β3 (BELLERI et al., 2008; LIN et al., 2006), portanto, foram utilizadas duas linhagens: 4T1BM2, que expressa altos níveis da integrina αvβ3 e a 4T1BM2 shRNAβ3, que foi silenciada para a subunidade β3. Estas duas linhagens foram utilizadas para compararmos as atividades dos dois produtos naturais (PNS) na proliferação celular e sua possível ligação a este receptor. Verificou-se que não houve diferença nos IC_{50} nas duas linhagens para ambos os PNs, indicando que para desempenhar os efeitos sobre a proliferação celular não há diferença na ligação desta integrina com estes PNs.

Neste trabalho foi verificado que o [10]-gingerol inibiu a proliferação celular de todas as linhagens de câncer de mama estudadas, com diferentes IC_{50}. Este produto apresentou valores de IC_{50} maiores nas linhagens humanas do que nas linhagens de camundongo, o mesmo padrão de IC_{50} foi observado quando utilizamos o produto natural resveratrol no ensaio de proliferação. Ainda no ensaio de proliferação celular aonde foi determinado o IC_{50}, foi observado uma certa seletividade dos PNs por células tumorais em relação à linhagem normal utilizada, a bEnd.3, célula endotelial da microvasculatura cerebral de camundongos. Esta seletividade foi ainda mais visível quando as células tumorais foram incubadas com o RSVT. Já foi descrito que o resveratrol é um agente seletivo. Podhorecka e colaboradores descreveram que o RSVT induziu a apoptose na população de células tumorais de leucemia

crônica linfoide mas não teve o mesmo efeito em células normais, células sanguíneas periféricas e medula óssea, demonstrando a seletividade deste PN por células tumorais (PODHORECKA et al., 2011). Por sua vez, anteriormente nosso grupo demonstrou que o [10]-gingerol possui um IC_{50} de 12,1 ±0,3µM na linhagem tumoral MDA-MB-231 e não foi o possível o cálculo do IC_{50} na linhagem normal (fibroblastos humanos) já que a concentração inicial que estas células começaram a ter algum efeito de morte foi em 500µM (SILVA et al., 2012).

No presente trabalho, verificou-se que o [10]-gingerol inibiu a adesão aos diferentes componentes da MEC somente nas maiores concentrações, indicando que não houve uma seletividade deste produto natural por nenhum dos compostos da MEC testados. Curiosamente, os efeitos inibitórios do [10]-gingerol ocorreram somente em concentrações mais altas quando comparadas ao trabalho de Lee e colaboradores (LEE et al., 2008) no qual, para a linhagem MDA-MB-231, o [6]-gingerol inibiu a adesão em 16% com relação ao controle na concentração de 10µM. As discrepâncias entre os resultados por nós obtidos para o [10]-gingerol, em relação aos resultados descritos pela literatura para o [6]-gingerol podem ser devidas ao fato de que durante o ensaio de adesão celular, possivelmente, não houve real inibição da adesão pelo produto natural em si, mas sim, indução da morte celular; além disso, as linhagens foram adquiridas de diferentes fontes pode influenciar os resultados dos testes.

Quanto ao outro produto natural testado, o RSVT, foi descrito na literatura por inibir a adesão de células endoteliais GM7373 à vitronectina sem afetar a adesão à fibronectina e à laminina (BELLERI et al., 2008), sugerindo seletividade por receptores de vitronectina, tais como a integrina αvβ3. Contrariamente, Lee e colaboradores (2012) (SOOK; HA; KIM, 2012) descreveram que o RSVT inibiu a adesão à fibronectina na linhagem tumoral de mama 4T1. Considerando o resultado do presente trabalho, foi observado que o RSVT apresentou seletividade para vitronectina nas linhagens tumorais de mama analisadas, indicando novamente que há uma diferença de interação destes produtos naturais com os diferentes componentes da MEC, ou seja, há um comportamento linhagem-dependente.

Devido aos resultados obtidos nos ensaios de adesão, onde as células entravam em processo de morte celular prejudicando a interpretação dos dados, foi realizado um ensaio de citotoxicidade e avaliação morfológica nas condições dos ensaios *in vitro*, para assim estabelecer as concentrações que poderiam ter alguma atividade nos ensaios sem induzir alguma morte celular. Neste ensaio de toxicidade, foi verificado que o [10]-gingerol induziu características apoptóticas nas duas linhagens testadas, murina e humana, como desadesão, encolhimento celular e formação de vesículas nas concentrações de 100 e 500µM

prontamente em 40min de incubação. Este efeito foi mais evidente nas células de camundongo já que seu IC_{50} tem um valor duas vezes menor que para a linhagem tumoral humana. Para o RSVT, verificou-se que este possui um efeito na morte celular somente na maior concentração testada em 24h, evidenciando pelo menor número de células na placa. Em intervalos de tempos mais curtos, o RSVT provocou mais mudanças morfológicas, tais como o aumento das protrusões celulares nas duas linhagens tumorais, sobretudo na linhagem humana, MDA-MB-213 BrM. Chakraborty e colaboradores, observaram que o [6]-gingerol induziu mudanças morfológicas características da apoptose na concentração de 400µM conforme o aumento do tempo de incubação (1 a 8h) na linhagem HeLa, carcinoma cervical humano (CHAKRABORTY et al., 2012). Radhakrishnan e colaboradores demonstraram que na linhagem SW-480 de câncer de cólon o [6]-gingerol também induziu alterações morfológicas, como formação de vesículas, nas concentrações de 50, 100 e 200µM com um tempo de incubação de 72h (RADHAKRISHNAN et al., 2014). Assim, os resultados obtidos nesse trabalho e na literatura indicam que estes produtos naturais, principalmente os gingeróis atuam nas células tumorais via indução da morte celular.

Para o restante dos experimentos decidiu-se usar somente a linhagem 4T1Br4 para posterior uso em experimentos *in vivo*. O ensaio de migração haptotática com o [10]-gingerol e o RSVT foi realizado para verificar se estes PNs possuem algum tipo de especificidade à receptores de adesão usando concentrações não tóxicas às células. Com isso, foi verificado que o [10]-gingerol não inibiu a migração à vitronectina e à laminina-511 em nenhuma das concentrações testadas. Em contrapartida, o RSVT apresentou novamente uma seletividade para vitronectina, e portanto, para seu receptor clássico a integrina αvβ3. O [10]-gingerol também não foi capaz de inibir a migração quimiotática ao FBS. Esperava-se que o RVST inibiria a migração ao FBS, porém, isso não ocorreu, provavelmente devido as concentrações utilizadas serem menores do que as usadas anteriormente nos ensaios de adesão celular e até mesmo no ensaio de migração haptotática. O [6]-gingerol foi descrito por inibir a migração das células MDA-MB-231 ao FBS nas concentrações de 2,5-10µM e inibir a migração através do ensaio de *wound healing* nas mesmas concentrações (LEE et al., 2008). Entretanto, outros autores relataram que não obtiveram inibição da migração pelo [6]-gingerol em células endoteliais HUVEC (KIM et al., 2005) e em células células hepatocarcinoma (WENG et al., 2010).

Os produtos naturais são conhecidos radiosensibilizadores por aumentarem o efeito da radiação quando células tumorais são tratadas em conjunto com radiação (NAMBIAR; RAJAMANI; SINGH, 2011). Neste trabalho foi verificado que o [10]-gingerol reduziu o

tamanho das colônias formadas no ensaio clonogênico, mas não alterou o número de colônias, o que caracteriza um efeito citostático e não citotóxico. Entretanto, quando as células foram tratadas com radiação, deram origem à colônias menores e em menor número, tendo ocorrido então um efeito citostático e citotóxico nestas condições, evidenciando a ação radio-sensibilizadora do [10]-gingerol. Liu e colaboradores mostraram que o extrato do gengibre com a radiação aumentou o efeito antiproliferativo em células de câncer endometrial (LIU et al., 2012). Entretanto, em células HepG2 quando prétratadas com [6]-gingerol por apenas 1h (5μM) e depois sujeitas a radiação, o PN promoveu uma proteção às células, aumentando a porcentagem de células viáveis, sugerindo um efeito protetor contra toxicidade por radiação (CHUNG; UDDIN; KIM, 2013). Estes resultados indicam que esse efeito é tempo-dependente para o [10]-gingerol. Neste trabalho, o RSVT reduziu o tamanho e número de colônias tanto na presença quanto na ausência da radiação, comprovando seu efeito radio-sensibilizador, citotóxico e citostático. O RSVT foi descrito por Fang e colaboradores por potencializar o efeito da radiação em células de câncer de próstata, PC3, reduzindo o número de colônias de forma concentração-dependente (FANG; DEMARCO; NICHOLL, 2012).

A partir dos resultados acima e da literatura relacionada ao [10]-gingerol iniciaram-se experimentos para avaliar a atuação desta molécula na morte celular, e por quais vias seria efetuado seu mecanismo de ação (paradas no ciclo celular, indução apoptose etc). Para tanto, um primeiro experimento realizado visou avaliar a condensação nuclear através da marcação dos núcleos com DAPI. Neste experimento foi verificado que houve um aumento da condensação da cromatina de forma concentração-dependente quando as células 4T1Br4 foram tratadas com [10]-gingerol. Corroborando com estes resultados, dados da literatura demonstraram que o mesmo ocorreu quando células HepG2 foram tratadas com [6]-gingerol nas concentrações de 50 a 200μM, por 24h (YANG et al., 2012a). Ainda, um trabalho recente demonstrou que o [10]-gingerol induziu a formação de corpos apoptóticos, encolhimento celular e condensação na cromatina de células de câncer de cólon HCT116 (RYU; CHUNG, 2014).

A fim de confirmar a hipótese de que o [10]-gingerol atua predominantemente via mecanismo de morte celular foi realizado um ensaio TUNEL, que verifica a fragmentação de DNA, e portanto, apoptose. Neste experimento o [10]-gingerol induziu a morte celular nas concentrações de 10 e 50μM após 18h de incubação. No trabalho de Chakraborty, o [6]-gingerol induziu apoptose pelo ensaio de TUNEL nas células HeLa de forma dependente de concentração (CHAKRABORTY et al., 2012). O mesmo foi encontrado em células HepG2,

nas quais o [6]-gingerol promoveu a apoptose nas concentrações de 50, 100 e 200µM (YANG et al., 2012a). Estes estudos corroboram com os dados deste trabalho.

Diversos produtos naturais foram descritos como indutores de paradas no ciclo celular de células tumorais, principalmente por interferir na formação de microtúbulos, degradação de DNA, alterar a expressão das ciclinas, entre outros (CRAGG; NEWMAN, 2005). O [10]-gingerol induziu a parada do ciclo nas células 4T1Br4 na fase G0/G1 no tempo de 8h e posteriormente induziu a parada na fase sub G0 após 24h de incubação. O surgimento do pico sub G0 é um indicador de apoptose (SHUKLA et al., 2007). Um trabalho recente também demostrou que o [10]-gingerol nas concentrações de 10-50µM aumentou a população sub G1 de células HCT116 de câncer de cólon após 24h de incubação, característico de células que estão sofrendo apoptose (RYU; CHUNG, 2014).

Para a confirmação da indução da apoptose pelo [10]-gingerol verificou-se a atividade das caspases-3 e -7. Neste ensaio foi observado que o [10]-gingerol reduz atividade destas caspases no tempo de 8h, porém, no tempo de 18h há um aumento da atividade das mesmas, sugerindo que em tempos menores o [10]-gingerol não seria capaz de induzir a morte celular pela via dependente de caspases e que esta resposta é dependente de tempo. No trabalho de Ishiguro e colaboradores, o [6]-gingerol (50µg/mL) só ativou as caspases-3 e -7 nas células HGC (células gástricas tumorais) quando induzidas com TRAIL no tempo de 6h (ISHIGURO et al., 2007). Já em células de carcinoma colorretal (COLO 205), o 6-shogaol ativou as caspases-3, -8 e -9 de forma concentração-dependente após 12h de tratamento, ativando as vias intrínsecas e extrínsecas da apoptose (PAN et al., 2008).

A apoptose pode ser desencadeada por duas diferentes vias, a intrínseca e a extrínseca (FULDA, 2014a, 2014b). Para verificar qual a via ativada pelo [10]-gingerol, foi realizada a análise da expressão de genes associados a apoptose. Os resultados obtidos sugerem que o [10]-gingerol atua na apoptose via intrínseca pelo aumento da caspase-9, redução de Bcl-2 e aumento de Bax. Não foi encontrado na literatura trabalhos que demonstram os efeitos do [10]-gingerol na expressão de genes relacionados à apoptose e poucos trabalhos demostraram a alteração da expressão gênica pelo [6]-gingerol através do uso da técnica de PCR. Somente o trabalho de Chakraborty e colaboradores, utilizou a técnica de RT-PCR (*Reverse transcription*-PCR) e observou que o [6]-gingerol aumentou a expressão gênica de Bax e citocromo c, e diminuiu a expressão de Bcl-2, comprovando suas propriedades apoptóticas (CHAKRABORTY et al., 2012). Utilizando a mesma técnica, Nigam e colaboradores verificaram que 48h de tratamento com o [6]-gingerol, diminuiu a expressão de Bcl-2 e

aumentou a expressão de Bax, caspase-3 e 9, enfatizando o provável efeito desses gingeróis na via apoptótica intrínseca (NIGAM et al., 2009).

Sabendo-se da atividade antitumoral do [10]-gingerol *in vitro* via apoptose, inibição da proliferação celular e parada no ciclo celular da linhagem 4T1Br4, neste trabalho foi verificado o resultado da combinação destes efeitos *in vivo* em modelos espontâneos e experimentais metastáticos de câncer de mama. Inicialmente, foi observado o efeito deste produto natural no modelo espontâneo de metástase e no crescimento do tumor primário. Neste modelo, foi verificado que o [10]-gingerol (5mg/kg) inibiu o crescimento do tumor primário, reduziu o tamanho dos baços (indicativo de células tumorais circulantes) e inibiu a formação de metástases pulmonares de forma significativa. Em um modelo semelhante, mas com ressecção do tumor primário, o qual visava analisar se o PN teria uma atividade antimetastática, sem atuar no tumor primário, foi verificado que o [10]-gingerol (10mg/kg) inibiu a formação de metástases pulmonares, ósseas e até mesmo de metástases cerebrais. Além disso, este PN mostrou ter baixa toxicidade pois os animais tratados mantiveram condição física geral igual ou superior aos animais não tratados, tanto em relação ao comportamento, quanto à massa corpórea. Este trabalho é inédito ao utilizar o [10]-gingerol em modelos de formação de metástase *in vivo*, porém mais análises devem ser realizadas para confirmar seus efeitos antitumorais e sua baixa toxicidade. Singh e colaboradores, utilizaram o mesmo modelo com células da linhagem 4T1 no tecido adiposo da quarta mama e posteriormente trataram os animais com a curcumina. Neste experimento, os autores observaram que o tratamento oral com curcumina (50mg/animal +0,48mg óleo de pimenta preta) inibiu o crescimento do tumor primário e também do número de metástases nos animais, resultando portanto, em efeitos similares ao [10]-gingerol utilizado neste trabalho (SINGH et al., 2013).

Estes resultados indicam a atividade do [10]-gingerol na inibição do crescimento do tumor primário, nas fases inicias do processo metastático, que vão desde a degradação da matriz extracelular ao intravasamento, bem como os processos mais tardios necessários para o estabelecimento e formação de metástases clinicamente detectáveis a partir de células tumorais que atingiram a circulação sanguínea.

A fim de confirmar e esclarecer o papel do [10]-gingerol na inibição de metástases, foi realizado um modelo de metástase experimental em que as células 4T1Br4 foram injetadas no ventrículo esquerdo do coração dos animais. Neste experimento o tratamento com o [10]-gingerol inibiu a formação de metástases ósseas, reafirmando seu potencial uso como agente antimetastático. É interessante salientar que o tipo de abordagem dos modelos de metástase

experimental avaliam apenas os processos mais tardios da cascata metastática, e sendo assim, através da combinação dos resultados obtidos nos experimentos de modelo de metástase espontânea e modelo de metástase experimental, pode-se sugerir que o [10]-gingerol atua tanto inibindo o crescimento do tumor primário, bem como ao longo de todo o processo metastático.

Estudos verificaram que o [6]-gingerol possui atividade antimetastática. No trabalho de Kim e colaboradores, células da linhagem B16F10 foram injetadas na veia caudal de camundongos C57BL/6, que foram posteriormente tratados com [6]-gingerol a cada dois dias (5mg/Kg - IP), resultando em inibição significativa na formação de colônias metastáticas no pulmão desses animais (KIM et al., 2005). Em um modelo semelhante, células da linhagem 4T1 foram injetadas na veia caudal de camundongos Balb/c que foram tratados oralmente com 200mg/kg de resveratrol (diariamente) diluído em etanol, os autores verificaram que o tratamento com o RSVT reduziu significativamente o número de colônias nos pulmões (SOOK; HA; KIM, 2012). A somatória destes resultados indica o grande potencial do uso de produtos naturais como agentes antitumorais e antimetastáticos no combate ao câncer.

Por outro lado, neste trabalho foi observado que o pré-tratamento de animais com o [10]-gingerol que foram posteriormente injetados com células tumorais no modelo experimental de metástase com injeção intracardíaca, prosseguindo o tratamento com o PN, não promoveu a inibição da formação de metástases pulmonares, óssea e cerebrais.

Diante dos resultados obtidos neste trabalho pode-se concluir que os produtos naturais analisados, sejam provenientes do gengibre e de outras fontes naturais, como a uva, podem ter grande utilidade na busca por moléculas com potencial antimetastático e com baixos efeitos colaterais ao hospedeiro. Deve-se enfatizar que estes compostos são utilizados há milhares de anos e com grande efetividade na cultura popular. Isto é um indício de que determinados produtos naturais têm potencial medicinal, o que é confirmado pelo fato de que, dentre os medicamentos no mercado entre os anos de 1981 e 2008, 63% são relacionados a produtos naturais (MARTIN-CORDERO et al., 2012b). Mais estudos para a compreensão de como o [10]-gingerol atua a nível molecular na inibição de metástases devem ser realizados para uma futura aplicação clínica. Modificações na estrutura das moléculas estudadas bem como a combinação com nanopartículas também são estratégias que merecem ser avaliadas de forma a vislumbrar futuras aplicações na clínica.

7 CONCLUSÕES

Neste projeto, verificamos que:

- ✓ o [10]-gingerol e o RSVT possuem efeitos antiproliferativos sobre diferentes linhagens tumorais de mama;
- ✓ o [10]-gingerol induz a apoptose;
- ✓ o [10]-gingerol e o RSVT apresentam efeitos de radiosensibilização;
- ✓ o [10]-gingerol inibe o crescimento do tumor primário e de suas metástases em modelos de metástase espontâneos e experimentais.

Portanto, o [10]-gingerol apresenta-se como um promissor agente terapêutico para o câncer de mama. Faz-se necessário a realização de outros estudos para verificar quais vias e mecanismos de ação estão envolvidos na atuação do [10]-gingerol como um agente antitumoral e antimetastático, além de verificar a baixa toxicidade do mesmo. O resumo desses efeitos está apresentado na figura a seguir:

Figura 50 – Resumo da atuação do [10]-gingerol *in vitro* e *in vivo.*

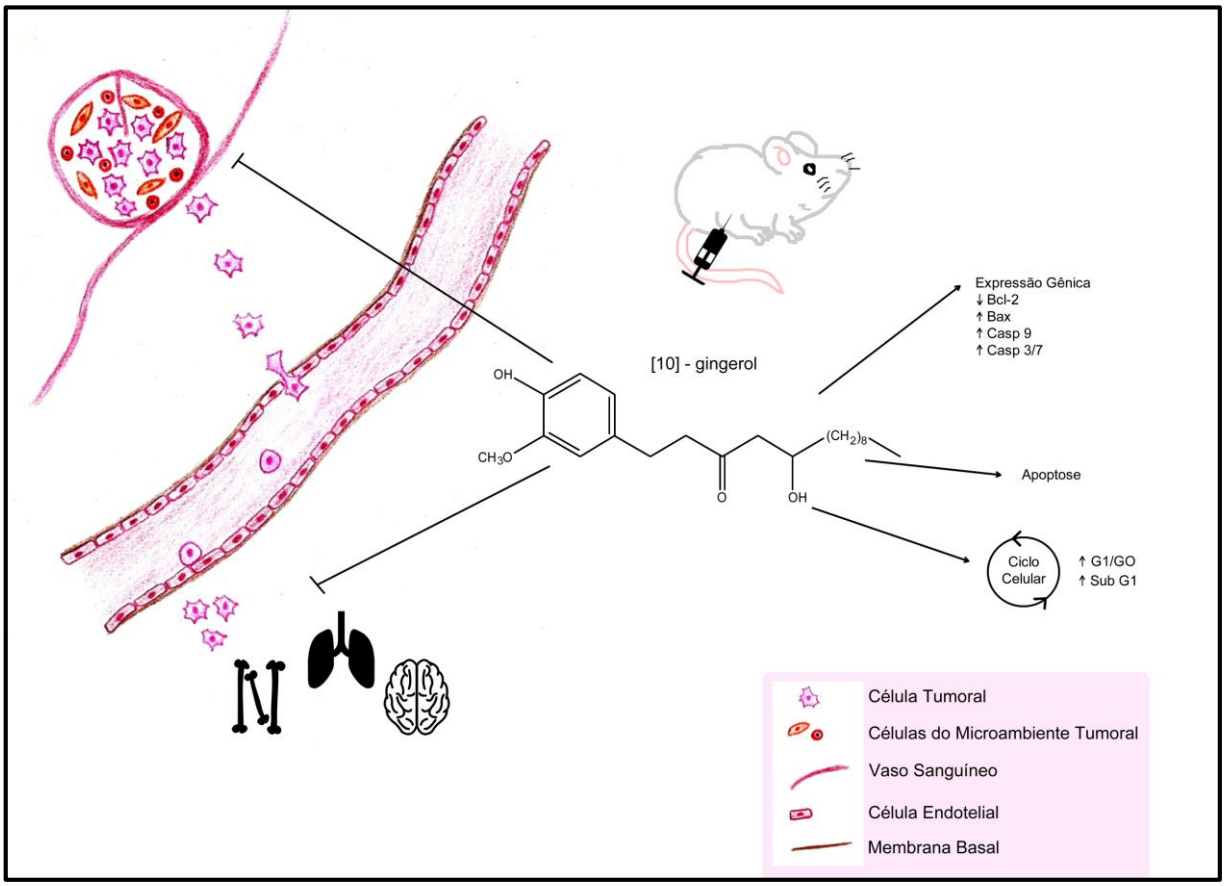

O [10]-gingerol induziu a expressão gênica de Bax, caspases-9/3/7, reduziu a expressão de Bcl-2, induziu a apoptose via diferentes ensaios *in vitro*, induziu a parada do ciclo celular nas fases G0/G1 e sub G1. Além disso, o PN inibiu o crescimento do tumor primário e a formação de metástases ósseas, pulmonares e cerebrais em modelos de metástase experimentais e espontâneos *in vivo.*

8 PERSPECTIVAS FUTURAS

Em vista dos resultados obtidos neste projeto, outras análises podem ser realizadas para um melhor entendimento dos mecanismos de ação do [10]-gingerol na inibição tumoral e metastática. Como:

- Expressão de proteínas relacionadas a apoptose como a survivina, citocromo c, PARP, caspases-3/6/7/8/9, ciclinas, Bcl-2, Bad, Bax para definitivamente comprovar a atuação do [10]-gingerol através da via intrínseca da apoptose;

- Fragmentação de DNA, apoptose (por citometria de fluxo com uso de anexina V e PI) e expressão de MMPs;

- Experimentos *in vivo*, com uso oral do [10]-gingerol em modelos singênicos ortotópicos e também em modelos xenográficos, para uma observação mais ampla de sua atuação em modelos distintos;

- Alteração da estrutura molecular do [10]-gingerol, por exemplo, formulação com nanopartículas ou inserção de ligantes que possam aumentar sua captação pelas células tumorais;

9 REFERÊNCIAS BIBLIOGRÁFICAS

ALIZADEH, A. M.; SHIRI, S.; FARSINEJAD, S. **Metastasis review: from bench to bedside**. [s.l: s.n.].

AMĂLINEI, C. et al. Matrix metalloproteinases involvement in pathologic conditions. **Romanian journal of morphology and embryology = Revue roumaine de morphologie et embryologie**, v. 51, n. 2, p. 215–28, jan. 2010.

AMERICAN CANCER SOCIETY. Cancer Facts & Figures. **Cancer Facts and Figures**, 2014.

ASLAKSON, C. J.; MILLER, F. R. Selective Events in the Metastatic Process Defined by Analysis of the Sequential Dissemination of Subpopulations of a Mouse Mammary Tumor1. **Cancer Research**, p. 1399–1405, 1992.

BEASLEY, K. D.; TOMS, S. A. The molecular pathobiology of metastasis to the brain: A review. **Neurosurgery Clinics of North America**, v. 22, n. 1, p. 7–14, 2011.

BELLERI, M. et al. alphavbeta3 Integrin-dependent antiangiogenic activity of resveratrol stereoisomers. **Molecular cancer therapeutics**, v. 7, p. 3761–3770, 2008.

BERRIER, A. L.; YAMADA, K. M. Cell – Matrix Adhesion. **Journal of Cellular Physiology**, n. June, p. 565–573, 2007.

BLAZAR, A. et al. Heterogeneity of Tumor Cells from a Single Mouse Mammary Tumor1. **Cancer Research**, v. 38, n. October, p. 3174–3181, 1978.

BONNANS, C.; CHOU, J.; WERB, Z. Remodelling the extracellular matrix in development and disease. **Nature Reviews Molecular Cell Biology**, v. 15, n. 12, p. 786–801, 2014.

BROOKS, S. A et al. Molecular interactions in cancer cell metastasis. **Acta histochemica**, v. 112, n. 1, p. 3–25, jan. 2010.

CARTER, R. Z. et al. Tumour but not stromal expression of B3 integrin is essential , and is required early , for spontaneous dissemination of bone-metastatic breast cancer. **Journal of Pathology**, 2015.

CHAKRABORTY, D. et al. [6]-Gingerol induces caspase 3 dependent apoptosis and autophagy in cancer cells: Drug-DNA interaction and expression of certain signal genes in HeLa cells. **European Journal of Pharmacology**, v. 694, n. 1-3, p. 20–29, 2012.

CHATTERJEE, S. J.; MCCAFFREY, L. Emerging role of cell polarity proteins in breast

cancer progression and metastasis. **Breast cancer (Dove Medical Press)**, v. 6, p. 15–27, 2014.

CHRISTOFFERSON, D. E.; YUAN, J. Necroptosis as an alternative form of programmed cell death. **Current Opinion in Cell Biology**, p. 263–268, 2010.

CHUNG, D.; UDDIN, S. M. N.; KIM, J. K. [6] -Gingerol Attenuates Radiation-induced Cytotoxicity and Oxidative Stress in HepG2 Cells. **Korean J. Environ. Biol.**, v. 31, n. 4, p. 376–382, 2013.

COUPLAND, L. A.; PARISH, C. R. Platelets, selectins, and the control of tumor metastasis. **Seminars in Oncology**, v. 41, p. 422–434, 2014.

CRAGG, G. M.; NEWMAN, D. J. Plants as a source of anti-cancer agents. **Journal of Ethnopharmacology**, v. 100, p. 72–79, 2005.

CRISCITIELLO, C. et al. Understanding the biology of triple-negative breast cancer. **Annals of Oncology**, v. 23, n. Supplement 6, 2012.

DESGROSELLIER, J. S.; CHERESH, D. A. Integrins in cancer: biological implications and therapeutic opportunities. **Nature reviews. Cancer**, v. 10, n. 1, p. 9–22, jan. 2010.

DIAZ-MORALLI, S. et al. Targeting cell cycle regulation in cancer therapy. **Pharmacology & therapeutics**, v. 138, n. 2, p. 255–71, 2013.

DORAI, T.; AGGARWAL, B. B. Role of chemopreventive agents in cancer therapy. **Cancer Letters**, v. 215, p. 129–140, 2004.

ECKHARDT, B. L. et al. Genomic Analysis of a Spontaneous Model of Breast Cancer Metastasis to Bone Reveals a Role for the Extracellular Matrix. **Molecular Cancer Research**, v. 8144, p. 1–13, 2005.

ECKHARDT, B. L. et al. Strategies for the discovery and development of therapies for metastatic breast cancer. **Nature Reviews Drug Discovery**, v. 11, n. 6, p. 479–497, 2012.

ELMORE, S. Apoptosis: a review of programmed cell death. **Toxicologic pathology**, v. 35, p. 495–516, 2007.

ENGEBRAATEN, O.; VOLLAN, H. K. M.; BØRRESEN-DALE, A.-L. Triple-negative breast cancer and the need for new therapeutic targets. **The American journal of pathology**, v. 183, n. 4, p. 1064–74, 2013.

FANG, Y.; DEMARCO, V. G.; NICHOLL, M. B. Resveratrol enhances radiation sensitivity in prostate cancer by inhibiting cell proliferation and promoting cell senescence and

apoptosis. **Cancer Science**, v. 103, n. 6, p. 1090–1098, 2012.

FOLKMAN, J. Angiogenesis and apoptosis. **Seminars in cancer biology**, v. 13, n. 2, p. 159–67, abr. 2003.

FRANTZ, C.; STEWART, K. M.; WEAVER, V. M. The extracellular matrix at a glance. **Journal of cell science**, v. 123, n. Pt 24, p. 4195–200, 15 dez. 2010.

FRIEDL, P.; BRÖCKER, E. B. The biology of cell locomotion within three-dimensional extracellular matrix. **Cellular and molecular life sciences : CMLS**, v. 57, n. 1, p. 41–64, 20 jan. 2000.

FULDA, S. Targeting apoptosis for anticancer therapy. **Seminars in Cancer Biology**, 2014a.

FULDA, S. Molecular pathways: Targeting inhibitor of apoptosis proteins in cancer-from molecular mechanism to therapeutic application. **Clinical Cancer Research**, v. 20, p. 289–295, 2014b.

GALLUZZI, L.; KROEMER, G.; VILLEJUIF, F.-. Previews Necroptosis : A Specialized Pathway of Programmed Necrosis. **Cell**, p. 2007–2009, 2008.

GEIGER, T. R.; PEEPER, D. S. Metastasis mechanisms. **Biochimica et biophysica acta**, v. 1796, n. 2, p. 293–308, dez. 2009.

GIALELI, C.; THEOCHARIS, A. D.; KARAMANOS, N. K. Roles of matrix metalloproteinases in cancer progression and their pharmacological targeting. **The FEBS journal**, v. 278, n. 1, p. 16–27, jan. 2011.

GUKOVSKAYA, A. S. et al. Mechanisms of Signal Transduction : Cholecystokinin induces caspase activation and mitochondrial dysfunction in pancreatic acinar cells : Roles in cell injury processes of pancreatitis Michelle Mouria. **The Journal of biological Chemistry**, 2002.

HANAHAN, D.; WEINBERG, R. A. Hallmarks of cancer: The next generation. **Cell**, v. 144, n. 5, p. 646–674, 2011.

HANIADKA, R. et al. (Ginger) as an Anti-Emetic in Cancer Chemotherapy: A Review. **The Journal of Alternative and Complementary Medicine**, v. 18, n. 5, p. 440–444, 2012.

HASSAN, M. et al. Apoptosis and molecular targeting therapy in cancer. **BioMed Research International**, v. 2014, 2014.

HAYMAN, E. G. et al. Vitronectin--a major cell attachment-promoting protein in fetal bovine serum. **Experimental cell research**, v. 160, p. 245–258, 1985.

HEPPNERY, G. H. et al. Heterogeneity in Drug Sensitivity among Tumor Cell Subpopulations Single Mammary Tumor1. **Cancer research**, v. 38, n. November, p. 3758–3763, 1978.

HOOD, J. D.; CHERESH, D. A. Role of integrins in cell invasion and migration. **Nature reviews. Cancer**, v. 2, n. 2, p. 91–100, fev. 2002.

HU, X.; XUAN, Y. Bypassing cancer drug resistance by activating multiple death pathways - A proposal from the study of circumventing cancer drug resistance by induction of necroptosis. **Cancer Letters**, v. 259, p. 127–137, 2008.

HYNES, R. O.; NABA, A. Overview of the Matrisome — An Inventory of Extracellular Matrix Constituents and Functions. **Cold Spring Harbor Perspectives in Biology**, p. 1–16, 2012.

IBRAHIM, A. S. et al. Gingerol-derivatives: emerging new therapy against human drug-resistant MCF-7. **Tumor Biology**, 2014.

INCA. **Estimativa Incidência de câncer no Brasil - 2014**. [s.l: s.n.].

ISHIGURO, K. et al. Ginger ingredients reduce viability of gastric cancer cells via distinct mechanisms. **Biochemical and Biophysical Research Communications**, v. 362, p. 218–223, 2007.

JOYCE, J. A; POLLARD, J. W. Microenvironmental regulation of metastasis. **Nature reviews. Cancer**, v. 9, n. 4, p. 239–52, abr. 2009.

KAPP, T. G. et al. Integrin modulators: a patent review. **Expert opinion on therapeutic patents**, v. 23, p. 1273–95, 2013.

KESSENBROCK, K.; PLAKS, V.; WERB, Z. Matrix metalloproteinases: regulators of the tumor microenvironment. **Cell**, v. 141, n. 1, p. 52–67, 2 abr. 2010.

KIM, E. C. et al. [6]-Gingerol, a pungent ingredient of ginger, inhibits angiogenesis in vitro and in vivo. **Biochemical and Biophysical Research Communications**, v. 335, p. 300–308, 2005.

KUBOTA, Y. Tumor angiogenesis and anti-angiogenic therapy. **The Keio Journal of Medicine**, v. 61, p. 47–56, 2012.

LAPENNA, S.; GIORDANO, A. Cell cycle kinases as therapeutic targets for cancer. **Nature reviews. Drug discovery**, v. 8, n. juLy, p. 547–566, 2009.

LEE, H. S. et al. [6]-Gingerol inhibits metastasis of MDA-MB-231 human breast cancer cells.

The Journal of nutritional biochemistry, v. 19, n. 5, p. 313–9, maio 2008.

LEE, S.-H.; CEKANOVA, M.; BAEK, S. J. Multiple mechanisms are involved in 6-gingerol-induced cell growth arrest and apoptosis in human colorectal cancer cells. **Molecular carcinogenesis**, v. 47, n. April 2007, p. 197–208, 2008.

LIN, C. BIN; LIN, C. C.; TSAY, G. J. 6-gingerol inhibits growth of colon cancer cell LoVo via induction of G2/M arrest. **Evidence-based Complementary and Alternative Medicine**, v. 2012, 2012.

LIN, H. Y. et al. Integrin alphaVbeta3 contains a receptor site for resveratrol. **The FASEB journal : official publication of the Federation of American Societies for Experimental Biology**, v. 20, p. 1742–1744, 2006.

LIU, Y. et al. Terpenoids from Zingiber officinale (Ginger) Induce Apoptosis in Endometrial Cancer Cells through the Activation of p53. **PLoS ONE**, v. 7, n. 12, 2012.

LIVAK, K. J.; SCHMITTGEN, T. D. Analysis of Relative Gene Expression Data Using Real-Time Quantitative PCR and the 2 ⁻ ⁻ C T Method. **Methods**, v. 408, p. 402–408, 2001.

LIVES, T. AACR Cancer Progress Report 2012. **Clinical Cancer Research**, 2012.

MALUMBRES, M.; BARBACID, M. Cell cycle, CDKs and cancer: a changing paradigm. **Nature reviews. Cancer**, v. 9, n. mArCH, p. 153–166, 2009.

MARTIN-CORDERO, C. et al. Pro-Oxidant Natural Products as Anticancer Agents. **Natural Products in Chemical Biology, First Edition. Edited by Natanya Civjan**, v. 13, p. 1006–1028, 2012a.

MARTIN-CORDERO, C. et al. **Pro-Oxidant Natural Products as Anticancer AgentsCurrent Drug Targets**, 2012b.

MENDOZA, M.; KHANNA, C. Revisiting the seed and soil in cancer metastasis. **The international journal of biochemistry & cell biology**, v. 41, n. 7, p. 1452–62, jul. 2009.

MILLER, F.; CARE, A. Mouse 4T1 Breast Tumor Model. **Tumor Immunology**, p. 1–16, 2000.

MURTHY, A. et al. Ectodomain shedding of EGFR ligands and TNFR1 dictates hepatocyte apoptosis during fulminant hepatitis in mice. **The Journal of clinical investigation**, v. 120, n. 8, 2010.

NAMBIAR, D.; RAJAMANI, P.; SINGH, R. P. Effects of phytochemicals on ionization

radiation-mediated carcinogenesis and cancer therapy. **Mutation Research - Reviews in Mutation Research**, v. 728, n. 3, p. 139–157, 2011.

NEWMAN, D. J.; CRAGG, G. M.; SNADER, K. M. Natural Products as Sources of New Drugs over the Period 1981-2002. **J. Nat. prof.**, v. 70, p. 461–477, 2007.

NIGAM, N. et al. [6]-Gingerol induces reactive oxygen species regulated mitochondrial cell death pathway in human epidermoid carcinoma A431 cells. **Chemico-Biological Interactions**, v. 181, p. 77–84, 2009.

NIIKURA, N. et al. Brain Metastases in Breast Cancer. v. 44, n. October, p. 1133–1140, 2014.

PAN, M. H. et al. 6-Shogaol induces apoptosis in human colorectal carcinoma cells via ROS production, caspase activation, and GADD 153 expression. **Molecular Nutrition and Food Research**, v. 52, p. 527–537, 2008.

PEARSON, H. B.; POULIOT, N. Modeling metastasis in vivo. **Metastatic Cancer: Integrated Organ System and Biological Approach**, v. 26, p. 513–523, 2012.

PEINADO, H.; LAVOTSHKIN, S.; LYDEN, D. The secreted factors responsible for pre-metastatic niche formation: old sayings and new thoughts. **Seminars in cancer biology**, v. 21, n. 2, p. 139–46, abr. 2011.

PERRET, G. Y.; CRÉPIN, M. New pharmacological strategies against metastatic spread. **Fundamental & clinical pharmacology**, v. 22, n. 5, p. 465–92, out. 2008.

PODHORECKA, M. et al. Resveratrol increases rate of apoptosis caused by purine analogues in malignant lymphocytes of chronic lymphocytic leukemia. **Annals of Hematology**, v. 90, p. 173–183, 2011.

POLLARD, J. W. et al. Charting a course to a distant site. **Nature Reviews**, p. 60614, 2009.

PRAKASH, O. et al. Anticancer Potential of Plants and Natural Products: A Review. **American Journal of Pharmacological Sciences**, v. 1, n. 6, p. 104–115, 2013.

RADHAKRISHNAN, E. K. et al. Prevents PMA-Induced Proliferation in Colon Cancer Cells by Inhibiting MAPK / AP-1 Signaling. **PloS one**, v. 9, n. 8, 2014.

RAKHA, E. A.; CHAN, S. Metastatic Triple-negative Breast Cancer. **Clinical Oncology**, v. 23, n. 9, p. 587–600, 2011.

RYU, M. J.; CHUNG, H. S. [10]-Gingerol induces mitochondrial apoptosis through activation ofMAPK pathway in HCT116 human colon cancer cells. **In vitro Cell. Dev. Biol.**,

2014.

SAFARZADEH, E.; SHOTORBANI, S. S.; BARADARAN, B. Herbal Medicine as Inducers of Apoptosis in Cancer Treatment. **Advanced Pharmaceutical Bulletin**, v. 4, n. Suppl 1, p. 421–427, 2014.

SAYERS, T. J. Targeting the extrinsic apoptosis signaling pathway for cancer therapy. **Cancer Immunology, Immunotherapy**, v. 60, p. 1173–1180, 2011.

SCULLY, O. J. et al. Breast cancer metastasis. **Cancer genomics & proteomics**, v. 9, p. 311–20, 2012.

SHASTRY, M.; YARDLEY, D. A. Updates in the treatment of basal/triple-negative breast cancer. **Current opinion in obstetrics & gynecology**, v. 25, p. 40–8, 2013.

SHUKLA, Y. et al. In vitro and in vivo modulation of testosterone mediated alterations in apoptosis related proteins by [6]-gingerol. **Molecular Nutrition and Food Research**, v. 51, p. 1492–1502, 2007.

SHUKLA, Y.; SINGH, M. **Cancer preventive properties of ginger: A brief reviewFood and Chemical Toxicology**, 2007.

SILVA, J. A. DA et al. Purification and differential biological effects of ginger-derived substances on normal and tumor cell lines. **Journal of Chromatography B: Analytical Technologies in the Biomedical and Life Sciences**, v. 903, p. 157–162, 2012.

SINGH, M. et al. Curcumin improves the therapeutic efficacy of Listeriaat-Mage-b vaccine in correlation with improved T-cell responses in blood of a triple-negative breast cancer model 4T1. **Cancer Medicine**, v. 2, p. 571–582, 2013.

SLOAN, E. K. et al. Tumor-specific expression of alphavbeta3 integrin promotes spontaneous metastasis of breast cancer to bone. **Breast cancer research : BCR**, v. 8, n. 2, p. R20, 2006.

SOOK, L. H.; HA, A. W.; KIM, W. K. Effect of resveratrol on growth of 4T1 breast cancer cells in vitro and in vivo. **Biochemical and biophysical research communications**, v. 6, n. 4, p. 294–300, 2012.

TAKADA, Y.; YE, X.; SIMON, S. The integrins. **Genome biology**, v. 8, n. 5, p. 215, jan. 2007.

TANZER, M. L. Current concepts of extracellular matrix. **Journal of orthopaedic science : official journal of the Japanese Orthopaedic Association**, v. 11, n. 3, p. 326–31, maio 2006.

VERMEULEN, K.; VAN BOCKSTAELE, D. R.; BERNEMAN, Z. N. The cell cycle: A review of regulation, deregulation and therapeutic targets in cancer. **Cell Proliferation**, v. 36, p. 131–149, 2003.

VICI, P. et al. Triple positive breast cancer : A distinct subtype ? **CANCER TREATMENT REVIEWS**, 2014.

WENG, C. J. et al. Anti-invasion effects of 6-shogaol and 6-gingerol, two active components in ginger, on human hepatocarcinoma cells. **Molecular Nutrition and Food Research**, v. 54, p. 1618–1627, 2010.

WENG, C. J.; YEN, G. C. **Chemopreventive effects of dietary phytochemicals against cancer invasion and metastasis: Phenolic acids, monophenol, polyphenol, and their derivativesCancer Treatment Reviews**, 2012.

WOLF, K.; FRIEDL, P. Molecular mechanisms of cancer cell invasion and plasticity. **The British journal of dermatology**, v. 154 Suppl , p. 11–5, maio 2006.

YANG, G. et al. 6-gingerol induces apoptosis through lysosomal-mitochondrial axis in human hepatoma G2 cells. **Phytotherapy Research**, v. 26, n. November 2011, p. 1667–1673, 2012a.

YANG, Y. P. et al. Resveratrol suppresses tumorigenicity and enhances radiosensitivity in primary glioblastoma tumor initiating cells by inhibiting the STAT3 axis. **Journal of Cellular Physiology**, v. 227, n. 325, p. 976–993, 2012b.

YILMAZ, M.; CHRISTOFORI, G.; LEHEMBRE, F. Distinct mechanisms of tumor invasion and metastasis. **Trends in molecular medicine**, v. 13, n. 12, p. 535–41, dez. 2007.

YUSUF, K. et al. Trophoblast Differentiation Modulates the Activity of Caspases in Primary Cultures of Term Human Trophoblasts. **Pediatric Research**, v. 52, n. 3, p. 411–415, 2002.

ANEXOS

18/09/2015 860150213452 15:17 NPWB

0000221505517669

Protocolo

BR 10 2015 024093 7

Número

Código QR

INSTITUTO NACIONAL DA PROPRIEDADE INDUSTRIAL
Diretoria de Patentes
Sistema e-Patentes/Depósito

	Tipo de Documento:		Página:
DIRPA e-PATENTES	Recibo de Peticionamento Eletrônico	DIRPA	1 / 2

Título do Documento:	Código:	Versão:
Recibo	RECIBO	01
DIRPA-FQ001 - Depósito de Pedido de Patente ou de Certificado de Adição	Modo: Produção	

O Instituto Nacional da Propriedade Industrial informa:

Este é um documento acusando o recebimento de sua petição conforme especificado abaixo:

Dados do INPI:

Número de processo:	BR 10 2015 024093 7
Número da GRU principal:	00.000.2.2.15.0551766.9 (serviço 200)
Número do protocolo:	860150213452
Data do protocolo:	18 de Setembro de 2015, 15:17 (BRT)
Número de referência do envio:	139157

Dados do requerente ou interessado:

Tipo de formulário enviado:	DIRPA-FQ001 v.006
Referência interna:	2014/028
Primeiro requerente ou interessado:	Fundação Universidade Federal de São Carlos
CNPJ do primeiro requerente ou interessado:	45.358.058/0001-40
Número de requerentes ou interessados:	2
Título do pedido:	COMPOSIÇÃO FARMACÊUTICA COMPREENDENDO [10]-GINGEROL E USO COMO MOLÉCULA ANTITUMORAL E ANTIMETASTÁTICA

Arquivos enviados:

Arquivo enviado	Documento representado pelo arquivo	Número de páginas
[package-data.xml]	Arquivo com informações do pacote em XML	---
[brf101-request.xml]	Formulário de depósito de pedido de patente ou de certificado de adição em XML	---
[application-body.xml]	Arquivo com dados do corpo do conteúdo patentário em XML	---
[brf101-request.pdf]	Formulário de depósito de pedido de patente ou de certificado de adição em PDF	
DOCUMENTO.pdf *[DOCUMENTO.pdf]*	Arquivo com conteúdo técnico-patentário da petição *- Reivindicações em formato eletrônico PDF* *página 1*	1
minuta gingerol_-_relatorio descritivo.pdf *[DOCUMENTO-1.pdf]*	Arquivo com conteúdo técnico-patentário da petição *- Relatório descritivo em formato eletrônico PDF* *páginas 1 a 31*	31
minuta gingerol_-_resumo.pdf *[DOCUMENTO-2.pdf]*	Arquivo com conteúdo técnico-patentário da petição *- Resumo em formato eletrônico PDF* *página 1*	1
minuta gingerol_-_relatorio descritivo.txt *[RELATDESCTXT.txt]*	Relatório descritivo em formato eletrônico texto	---
minuta gingerol_-_reinvidicacoes.txt *[REIVINDTXT.txt]*	Reivindicações em formato eletrônico texto	---
minuta gingerol_-_resumo.txt *[RESUMOTXT.txt]*	Resumo em formato eletrônico texto	---
GRU - 200 - COMPROVANTE.pdf *[GRU-1.pdf]*	Guia de Recolhimento da União (GRU) paga com comprovante de pagamento em formato eletrônico PDF *[Código de serviço: 200, Número: 00.000.2.2.15.0551766.9, Nome do sacado: Fundação Universidade Federal de São Carlos]*	2
Procuração - UFSCar.pdf *[INDEXADO-1.pdf]*	Procuração em formato eletrônico PDF	1
Procuração UNICAMP.pdf *[INDEXADO-2.pdf]*	Procuração em formato eletrônico PDF	1

Arquivo enviado	Documento representado pelo arquivo	Número de páginas
Amanda Blanque Becceneri.pdf *[INDEXADO-3.pdf]*	Documento de cessão ou autorização do inventor em formato eletrônico PDF	1
Ana Carolina Baptista Moreno Martin.pdf *[INDEXADO-4.pdf]*	Documento de cessão ou autorização do inventor em formato eletrônico PDF	1
Heloisa Sobreiro Selistre-de-Araujo.pdf *[INDEXADO-5.pdf]*	Documento de cessão ou autorização do inventor em formato eletrônico PDF	1
James Almada da Silva.pdf *[INDEXADO-6.pdf]*	Documento de cessão ou autorização do inventor em formato eletrônico PDF	1
João Batista Fernandes.pdf *[INDEXADO-7.pdf]*	Documento de cessão ou autorização do inventor em formato eletrônico PDF	1
Márcia Regina Cominetti.pdf *[INDEXADO-8.pdf]*	Documento de cessão ou autorização do inventor em formato eletrônico PDF	1
Maria Cristina Cintra Gomes Marcondes.pdf *[INDEXADO-9.pdf]*	Documento de cessão ou autorização do inventor em formato eletrônico PDF	1
Normand Pouliot.pdf *[INDEXADO-10.pdf]*	Documento de cessão ou autorização do inventor em formato eletrônico PDF	1
Paulo Cezar Vieira.pdf *[INDEXADO-11.pdf]*	Documento de cessão ou autorização do inventor em formato eletrônico PDF	1
Rebeka Tomasin.pdf *[INDEXADO-12.pdf]*	Documento de cessão ou autorização do inventor em formato eletrônico PDF	1
SUBSTABELECIMENTO Ok.pdf *[OUTROS-1.pdf]*	Documentos de qualquer outra natureza em formato eletrônico PDF	1
Angelina Maria Fuzer.pdf *[INDEXADO-13.pdf]*	Documento de cessão ou autorização do inventor em formato eletrônico PDF	1

Dados sobre o envio:

Responsável pelo envio:	Patricia Villar Martins:16b7424ddfd300a28278ba5ae8dccf48
Assinatura (Requerente, Interessado ou Procurador):	MARCELO FERRO GARZON:21855538873,OU=Autenticado por Ass. dos Advogados de Sao Paulo,OU=(EM BRANCO),OU=RFB e-CPF A3,OU=Secretaria da Receita Federal do Brasil - RFB,O=ICP-Brasil,C=BR
Método de envio:	Eletrônico pela Internet
Código de segurança:	06:67:E5:AE:4D:19:81:95:57:25:32:B1:41:5F:FC:04:E9:57:48:CE

Cell Adhesion & Migration
Publication details, including instructions for authors and subscription information:
http://www.tandfonline.com/loi/kcam20

Recombinant disintegrin domain of human ADAM9 inhibits migration and invasion of DU145 prostate tumor cells

Ana Carolina Baptista Moreno Martin[a], Ana Carolina Ferreira Cardoso[a], Heloisa Sobreiro Selistre-de-Araujo[a] & Márcia Regina Cominetti[b]

[a] Departamento de Ciências Fisiológicas; Universidade Federal de São Carlos; São Carlos, Brazil

[b] Departamento de Gerontologia; Universidade Federal de São Carlos; São Carlos, Brazil

Published online: 25 Jul 2015.

RESEARCH PAPER

Cell Adhesion & Migration 9:4, 1–7; August 2015; © 2015 Taylor and Francis Group, LLC

Recombinant disintegrin domain of human ADAM9 inhibits migration and invasion of DU145 prostate tumor cells

Ana Carolina Baptista Moreno Martin[1], Ana Carolina Ferreira Cardoso[1], Heloisa Sobreiro Selistre-de-Araujo[1], and Márcia Regina Cominetti[2,*]

[1]Departamento de Ciências Fisiológicas; Universidade Federal de São Carlos; São Carlos, Brazil; [2]Departamento de Gerontologia; Universidade Federal de São Carlos; São Carlos, Brazil

Keywords: ADAM, cell adhesion, disintegrin, integrin, invasion, metastasis, prostate cancer

One of the most important features of malignant cells is their capacity to invade adjacent tissues and metastasize to distant organs. This process involves the creation, by tumor and stroma cells, of a specific microenvironment, suitable for proliferation, migration and invasion of tumor cells. The ADAM family of proteins has been involved in these processes. This work aimed to investigate the role of the recombinant disintegrin domain of the human ADAM9 (rADAM9D) on the adhesive and mobility properties of DU145 prostate tumor cells. rADAM9D was able to support DU145 cell adhesion, inhibit the migration of DU145 cells, as well as the invasion of this cell line through matrigel *in vitro*. Overall this work demonstrates that rADAM9D induces specific cellular migratory properties when compared with different constructs having additional domains, specially those of metalloproteinase and cysteine-rich domains. Furthermore, we showed that rADAM9D was able to inhibit cell adhesion, migration and invasion mainly through interacting with α6β1 in DU145 tumor cell line. These results may contribute to the development of new therapeutic strategies for prostate cancer.

Introduction

Prostate cancer is the second leading cause of death by cancer in men. It has become the most common cancer in men in the Western world, with approximately 40,000 new cases yearly in the UK. In Europe and North America, more than 500,000 cases are diagnosed per year. The disease incidence varies worldwide, being more common in Western countries compared to East Asian and developing countries. The disease incidence has increased in the past 2 decades, probably due the improvements in early detection and/or treatment, and also an increased public awareness.[11] Because of the high prostate cancer incidence, the development of new therapeutic tools should be created to combat this disease.

The ADAM (A Disintegrin And Metalloproteinase) family of proteins comprises a group of multifunctional proteins that play important roles in many biological processes, such as cell fusion, cell adhesion, proteolysis, and in some diseases as well, including cancer.[2,3] These type I transmembrane proteins are characterized by the presence of a prodomain, an N-terminal metallopeptidase domain, a disintegrin domain, a cysteine-rich domain, an EGF-like domain, a transmembrane region, and a cytoplasmic tail with signaling properties.[4]

Among the 30 described members of the ADAM family, ADAM9 or Meltrin-γ, is a widely expressed, non-RGD-containing protein that has been shown to bind to the α6β1 integrin on fibroblasts,[5] αvβ5 on myeloma cells[6] as well as osteoblasts.[7] Furthermore, the disintegrin domain of ADAM9 was demonstrated to bind directly to α6β4 and α2β1 integrins on the surface of colon carcinoma cells.[8] After binding to these integrins, the disintegrin domain of ADAM9 is able to promote different cell signaling responses, such as an increase in IL-6 production via the p38MAPK and cPLA2 pathways.[7] Recombinant disintegrin domain of ADAM9 (rADAM9D) was demonstrated to bind to MDA-MB-231 tumor breast cells through β1, α3, αvβ3, αvβ5 and α2 integrins and also to inhibit the adhesion of this cell line and platelets to collagen type I under dynamic flow conditions.[9]

The adhesive properties of the different ADAMs domains are still a matter of controversy. Whereas some works attribute adhesive properties to the disintegrin domain,[5,7-9] others indicate the cysteine-rich domain as having adhesive functions.[10, 11] Recent data from different model systems suggest that ADAM9 is involved in tumor formation/progression. In many types of human cancers ADAM9, as well as other specific ADAMs, are up-regulated.[12-18]

In the present work we demonstrated the pro- and anti-adhesive properties of the rADAM9D on DU145 prostate cancer cells. rADAM9D was able to promote adhesion of DU145 cells, therefore acting as an adhesion molecule, similarly to other

*Correspondence to: Márcia Regina Cominetti; Email: mcominetti@ufscar.br
Submitted: 09/02/2014; Revised: 10/24/2014; Accepted: 11/24/2014
http://dx.doi.org/10.4161/19336918.2014.994917

molecules such as collagens, laminin and fibronectin. Furthermore, rADAM9D inhibited the adhesion of DU145 cells to laminin-coated wells, but not to collagen type I. The adhesion of rADAM9D to DU145 cells can occur through β1, α6, αvβ5 and αvβ3, since the incubation with anti-integrin blocker antibodies directed against these integrins, inhibited cell adhesion to rADAM9D. rADAM9D was also able to inhibit DU145 cell migration and invasion through matrigel. Overall, this study may contribute to the development of new therapeutic strategies for prostate cancer.

Results

rADAM9D promotes DU145 cell adhesion

rADAM9D was able to promote adhesion of DU145 cell line, similarly to different extracellular matrix proteins (collagen type I and IV, laminin and fibronectin), therefore supporting cell adhesion as an extracellular matrix protein, probably by interacting with DU145 integrins. There was no difference among quantities (5, 10 or 50 μg) of rADAM9 plated on the wells to promote the adhesion of DU145 cells (**Fig. 1**).

ADAM9D interacts with DU145 prostate tumor cells through β1, α6, αvβ5 and αvβ3

Since rADAM9D supported DU145 cell adhesion we verified which integrins in this prostate cancer cell line would be specific for this disintegrin. For that, we incubated DU145 cells with different anti-integrin blocking antibodies before plate on an rADAM9D (10 μg) coating. The antibodies against β1, α6, αvβ5 and αvβ3, inhibited DU145 cell adhesion to rADAM9D (**Fig. 2A**), confirming that this recombinant protein could bind to these integrins on the surface of DU145 cells. On the other hand, antibodies against α2 and α4 integrins chains did not inhibit the adhesion of DU145 cells to rADAM9D (**Fig. 2A**). To confirm this result, rADAM9D (1 μM) was previously incubated with DU145 cells and the mixture was then incubated with anti-integrin antibodies. Subsequently, cells were analyzed by flow cytometry (**Fig. 2B**) and the results obtained confirmed that rADAM9D inhibits the binding of anti-β1, anti-α6, anti-αvβ5 and anti-αvβ3 antibodies to DU145 cells, probably because rADAM9D binds to these integrins on these cell line, preventing previous binding of cited antibodies. The inhibition of anti-α6 antibody promoted by rADAM9D was lower compared to the other antibodies using cytometry analysis (**Fig. 2B**). rADAM9D did not promote inhibition of the binding of anti-α2 and α-4 antibodies to DU145 cells. Integrin profile in DU145 cell line was measured by flow cytometry, using the antibodies mentioned above. This cell line presented higher levels of α2 and β1, moderate levels of α6, αvβ3 and αvβ5, and low levels of α4 integrin subunit (**Fig. 2C**).

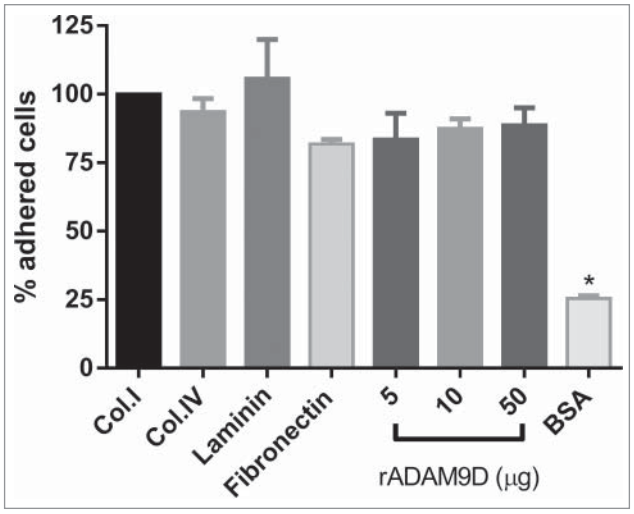

Figure 1. rADAM9D promotes DU145 cell adhesion. Collagen type I (Col.I), collagen type IV (Col.IV), laminin, fibronectin (10 μg) (positive controls) or different quantities of ADAM9D (5, 10 and 50μg) were immobilized in the wells of a 96-well plate in adhesion buffer at 4°C. After blocking with 1% BSA (negative control), CMFDA-labeled DU145 cells (1×10^5 cells/well) were seeded in the wells. The plates were incubated at 37 °C for 30 min, washed, lysed and read for the release of fluorescence. BSA was used as negative control for cell adhesion. The results were obtained from 3 independent experiments in triplicate. The means that are significantly different from those of cells growing on collagen using ANOVA followed by post hoc Dunnett's test were shown by *($P \leq 0.001$). The results were normalized by the collagen type I values in each experiment. The error bars show the SE of three samples with less deviation from the mean.

rADAM9D inhibits the adhesion of DU145 cells to laminin but not to collagen type I

Since rADAM9D seemed to bind specifically α6β1 integrin on DU145 prostate cancer cell line, we further investigate whether this rADAM9 domain would inhibit tumor cell adhesion to laminin, a known α6β1 integrin ligand. Therefore, we tested the capacity of rADAM9D to inhibit the adhesion of DU145 cells to laminin and collagen type I, which has no specificity for α6β1 integrin. For that, DU145 cells were previously incubated with different rADAM9D concentrations and then plated on laminin or collagen type I-coated wells. Results indicate that incubation of rADAM9D with DU145 cells inhibited their adhesion to laminin (**Fig. 3A**) but not to collagen type I-coated wells (**Fig. 3B**). In other words, the blocking of receptors on DU145 cells promoted by rADAM9D was specific to inhibit the adhesion of this cell line to laminin but not to collagen type I. rADAM9D at concentrations of 2000nM were also tested for the inhibition of DU145 cells to collagen type I, but there was no inhibition (data not shown).

rADAM9D inhibits invasion and migration of DU145 cells

rADAM9D was tested to its ability to inhibit DU145 cell invasion and migration. rADAM9D, at concentrations ranging from 100 to 1000 nM, was able to significantly inhibit DU145 cell invasion (**Fig. 4**). In a wound healing migration assay, rADAM9D significantly inhibited DU145 cell migration at 100, 500, 1000 and 2000nM (**Fig. 5A and B**). The effects were more striking after 24 hours of wound repopulation.

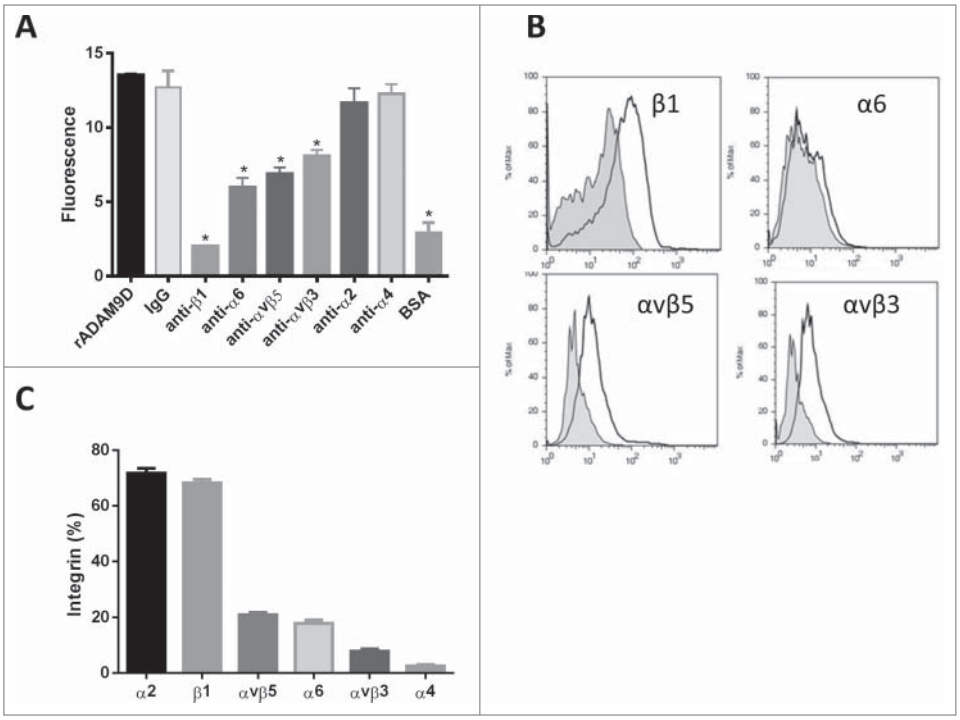

Figure 2. rADAM9D binds to DU145 through β1, α6, αvβ5 and αvβ3 integrins as demonstrated by an antibody competition assay (**A**) and by flow cytometry analysis (**B**). The integrin content of DU145 cell line was assessed by flow cytometry (**C**). (**A**) For antibody competition assay CMFDA-labeled cells were incubated with different anti-integrin antibodies (β1, α6, αvβ5, αvβ3, α2 and α4, at 10 μg/ml) and IgG control (10 μg/ml) before being plated on rADAM9D-coated (10 μg) wells. DU145 directly plated on rADAM9D or IgG-coated wells, without previous incubation with any antibody was used as positive control and BSA was used as negative control. (**B**) The integrin content of DU145 cells was determined by flow cytometry. Cells (1×10^5) were incubated for 40 min at 4°C with the specific antibodies cited earlier or control IgG. Cells were washed and incubated with secondary antibody labeled with FITC, at same conditions described before, washed and fixed with FACs buffer contaning 1% phormaldehyde overnight at 4°C. C. To verify the interaction with integrins, rADAM9D (1 μM) was previously incubated (30 min at room temperature) with DU145 cells, before the addition of antibodies. Cells were analyzed in FACSCanto. The results were obtained from 3 independent experiments in triplicate. The error bars show the SE of three samples with less deviation from the mean. The means that are significantly different from rADAM9D and IgG-coated wells using ANOVA followed of post hoc Dunnett's test were shown by *($P \leq 0.001$).

Discussion

The progression of malignant tumors results from invasion of the primary tumor to a secondary site, causing metastasis in a multi-step process. These steps can be summarized as follows: cell detachment from the primary tumor, migration and invasion into the ECM, intravasation into a blood or lymphatic vessel, survival within the vasculature, adherence of these tumor cells in the endothelium, extravasation, and formation of secondary tumors.[19-21] Therefore, metastasis necessitates disruption of cellular interactions with the tumor microenvironment, increased migratory and invasion capacity and the ability to overcome the pro-apoptotic signals provided by diminished intercellular and cell-ECM interactions mainly through integrin receptors.[22]

Several members of the integrin family, including α1β1, α2β1, α3β1, α6β1, α7β1 and α6β4 heterodimers serve as laminin receptors on a variety of normal and tumor cell types[23] and DU145 prostate cell line was reported to have abundant content of integrin β1, along with α1, α2, α3, α5 and α6 integrin subunits.[24,25] In this work, we have demonstrated that DU145 tumor cell line contains high amounts of α2β1, moderate amounts of αvβ5 and α6 and low quantities of αvβ3 and α4 integrins. Additionally, we showed that the recombinant disintegrin domain of ADAM9 (rADAM9D) was able to inhibit the adhesion of DU145 prostate cancer cells to laminin, mainly by binding to α6β1 integrin receptor, therefore rADAM9D may act at the beginning of metastatic cascade, disrupting the binding of prostate cells to the ECM laminin component. Furthermore, rADAM9D was able to inhibit DU145 cell invasion and migration of this tumor cell line.

It was demonstrated in the literature that ADAM9 transcripts are alternatively spliced to express a transmembrane protein (ADAM9-L) and a secreted variant (ADAM9-S) with opposite functions in breast cancer cells and that the balance between these isoforms is an important determinant in manifestation of aggressive migratory phenotypes associated with breast cancer progression. According to the authors, ADAM9-S is an enhancer, whereas ADAM9-L is a suppressor of cell migration.[26] Mazzocca and colleagues[8] have demonstrated the presence of these alternatively spliced variants of ADAM9. In hepatic stellate cells, it was demonstrated that ADAM9-S induced a highly invasive phenotype and promotes tumor cell invasion. Moreover, they demonstrated that ADAM9-S binds directly to α6β4 and α2β1 integrins on the surface of colon carcinoma cells through the disintegrin domain.[8] Our results are not in accordance with these data since we have demonstrated that rADAM9D is an inhibitor of invasion and migration in prostate tumor cells. ADAM9-S is a construct composed by a signal sequence, a prodomain, a metalloproteinase domain and by disintegrin and cysteine-rich domains. In our work, however, only the disintegrin domain of ADAM9 was recombinantly produced in a bacterial system and this difference in protein structure may explain the differential biological activities of both molecules. Additionally, it is important to point out that the adhesion properties of the isolated rADAM9D domain are not sufficient to explain the molecular interactions and functional significance of the entire protein in a cellular and *in vivo* system. Moreover, the native disintegrin domain of ADAM9 has a N-glycosylation site,[27] which

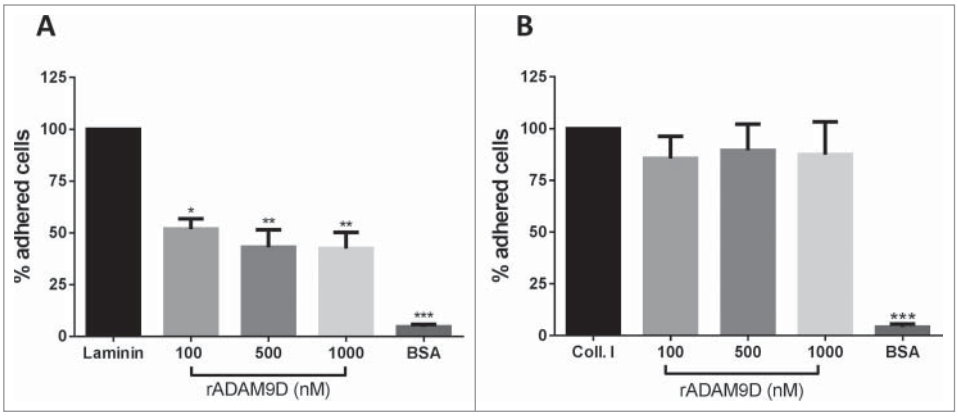

Figure 3. rADAM9D inhibits the adhesion of DU145 to laminin but not to collagen type I. Ninety six-well plates were coated with laminin (**A**) or collagen type I (**B**) (10 μg/well) in adhesion buffer or 0.1% acetic acid, respectively, overnight at 4°C. After blocking with 1% BSA, CMFDA-labeled cells (1×10^5 cells/well) were incubated with different concentrations (100, 500, 1000nM) of rADAM9D and seeded in the wells. The plates were incubated at 37°C for additional 30 min. After washing, remaining cells were lysed, and the plate was read for the release of fluorescence. The results were obtained from 3 independent experiments and in triplicate. The results for rADAM9D were normalized by the collagen or laminin values in each experiment. The error bars show the SE of three samples with less deviation from the mean. The means for all rADAM9 concentrations were significantly different from the laminin using ANOVA followed by post hoc Dunnett's test: *($P \leq 0.05$), **($P \leq 0.01$) and ***($P \leq 0.001$).

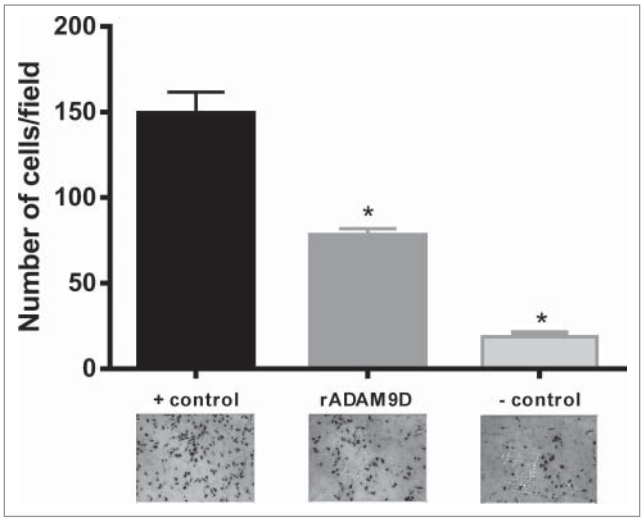

Figure 4. rADAM9D inhibits the invasion of DU145 cells through matrigel. DU145 cells (1.25×10^5 cells/ml) were seeded on the inserts (12 well-plate) of the invasion chamber in the presence or absence of rADAM9D (1 μM). Complete medium was used as a chemoattractant at the lower chamber. Plates were incubated for 22 h at 37°C and 5% CO_2. Non-invading cells were removed with a cotton swab from the upper surface of the membrane and invading cells were fixed and 10 random fields from microscope slides were photographed and cells were counted using Image J software. Positive control (+ control) was made in the presence of chemoattractant (10% FBS) at the lower chamber and negative control (− control) was FBS free medium at the lower chamber. The results were obtained from 3 independent experiments in triplicate. The error bars show the SE of three samples with less deviation from the mean. The means that are significantly different from the positive control using ANOVA followed by post hoc Dunnett's test: *($P \leq 0.001$).

undoubtedly influences its adhesion properties. In this work, however, rADAM9D does not have the presence of this N-glycosylation, since bacterial systems to produce recombinant proteins are not able to perform such types of post-translational modifications. Furthermore, Takeda and co-workers,[11] resolving the crystal structure of VAP-1, a homolog of mammalian ADAMs, demonstrated that the binding area of the disintegrin domain in a C-type conformation is not accessible for protein binding and a Hyper-Variable Region (HVR) of the cysteine-rich domain may instead be involved in substrate interaction. Therefore, alone the disintegrin domain may only contribute, when in native conformation, but not mediate cell adhesion in physiological conditions.

On the other hand, Zigrino and coworkers[10] prepared a construct only with disintegrin and cysteine-rich domains of ADAM9 and reported that this protein functions as a cell adhesion molecule. These authors also demonstrated that the recombinant ADAM9 disintegrin-cysteine-rich domains specifically interact with the β1 integrin subunit on keratinocytes. However, engagement of integrin receptors by the ADAM9 disintegrin-cysteine-rich domains resulted in ERK phosphorylation and increased MMP9 synthesis. Additionally, keratinocytes adhering to the immobilized disintegrin and cysteine-rich domains showed increased motility, which was partially due to the induction of MMP9 secretion in this cell line.[10] In our work, instead, rADAM9D inhibited DU145 cell migration and invasion, again demonstrating the influence of different protein constructs on its functional activity.

This is the first time that the effects of a recombinant domain of an human ADAM are demonstrated on adhesion, migration and invasion of prostate tumor cells. Taken together, our results demonstrate that recombinant ADAM9D has specific migratory properties when compared with different constructs having additional domains, specially those of metalloproteinase and cysteine-rich domains. Furthermore, we showed that rADAM9D was able to inhibit cell adhesion, migration and invasion mainly through interacting with α6β1 in DU145 tumor cell line.

Conclusion

The potential of the rADAM9D as an anti-adhesive molecule can be explored as tool to combat metastasis and cancer progression and for the design of selective inhibitors against the adhesion and extravasation of cancer cells. Other studies, using animal models, should be conducted to confirm this hypothesis.

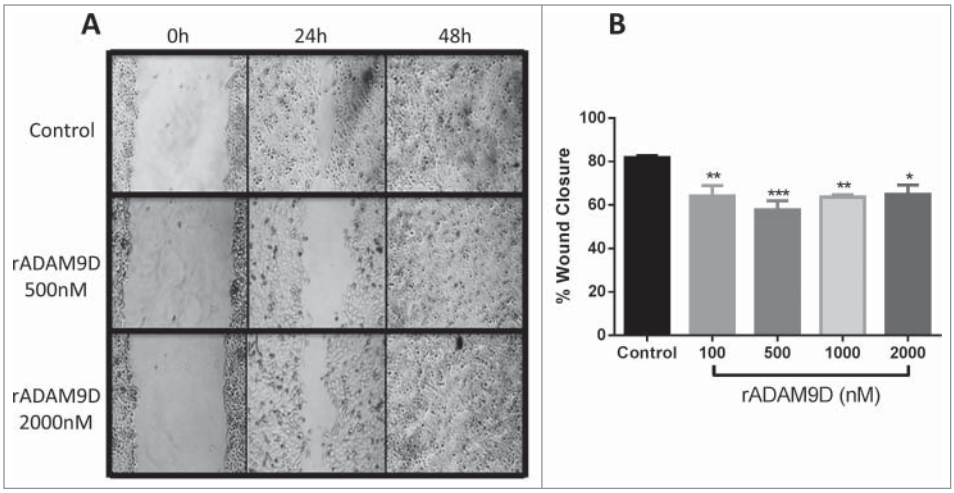

Figure 5. rADAM9D inhibits the migration of DU145 cells in a wound healing assay. (**A**) Cells (1×10^5 cells/ml) were plated in 24-wells plates and incubated properly until the culture reached 100% of confluence. Afterwards, a straight scratch was made with a pipette tip and cells were washed with culture medium to remove unbound cells and debris. Cells were incubated with ADAM9D (100, 500, 1000 and 2000 nM) for 24 h and 48 h. Only pictures from rADAMD9 500 and 2000 nM are represented. Central field was photographed at 0h, 24 h and 48 h (when cells close the scratch completely). (**B**) Closure area of migrating cells was measure using ImageJ software, and it was calculated the percentage of wound closure, comparing time zero and 24 hour. Results are expressed as percent of wound closure relative to control (untreated) cells. The results were obtained from 3 independent experiments in triplicate. The error bars show the SE of three samples with less deviation from the mean. The means that are significantly different from the control using ANOVA followed by post hoc Dunnett's test: *($P \leq 0.05$), **($P \leq 0.01$) and ***($P \leq 0.001$).

Material and Methods

Recombinant ADAM9 disintegrin domain (rADAM9D)

Expression and purification of the recombinant disintegrin domain of ADAM9 (rADAM9D) was performed as previously described.[9] Briefly, total RNA from a VMM12 human melanoma cell line was reverse transcribed and resulting cDNA was used for amplification of the disintegrin domain of human ADAM9 (ADAM9D) (GenBank accession no. NM003816). For ADAM9D expression it was used the pGEX-4T-1 vector which is classically used to produce GST fusion proteins. After the transformation of *Escherichia coli* DH5-α cells, the ampicillin-resistant recombinant plasmids were selected for restriction analysis. The confirmed recombinant plasmids (pADAM9D) were used to transform the *E. coli* AD494(DE3) expression strain. Cultures of *E. coli* AD494(DE3)pADAM9D were induced for expression by addition of 0.5 mM isopropyl thio-β-D-galactopyranoside (IPTG). Four hours after induction, cells were harvested by centrifugation (7000 rpm, 15 min, 4°C) and cell pellet was suspended in PBS buffer (140 mM NaCl, 2.7 mM KCl, 10 mM Na_2HPO_4, 1.8 mM KH_2PO_4, pH 7.3) and lysed by sonication (5 times, 4°C, 1 min interval). ADAM9D was released from the fusion protein (GST) by thrombin cleavage. Thrombin was eliminated from samples containing ADAM9D by purification in a Benzamidine-Sepharose 4B column (GE Healthcare). Fractions were analyzed by SDS-PAGE with Coomassie brilliant blue staining and rADAM9D concentration was determined by BCA protein assay (Pierce).

Antibodies

For flow cytometry and competition assays the monoclonal blockers antibodies used against human α2 (MAB 1233), α6 (MAB13501), β1 (MAB17781) and αvβ5 (MAB2528) integrins, were obtained from R&D Systems (R&D Systems Inc.., Minneapolis, MN, USA). Antibodies against αvβ3 integrin (MAB1976) were from Chemicon, and antibodies to the α4 integrin subunit (I6528) were from Sigma-Aldrich. Control IgG was from Dako. Secondary antibody goat anti-mouse IgG-FITC (Fluorescein isothiocyanate, sc-2010), used for flow cytometry, were purchased from Santa Cruz Biotechnology.

Cell line and culture

DU145 human prostate tumor cell line was obtained from ATCC and maintained at 37°C in 5% CO_2 in RPMI culture medium (Cultilab) containing 10% FBS, penicillin (100 UI/ml), streptomycin (100 μg/ml) and L-glutamine (2mM). Cell cultures and experiments were conducted in a humidified environment with 5% CO_2 at 37°C.

Cell adhesion and antibody competition

Cell adhesion and inhibition of cell adhesion were performed as described before.[9] Briefly, collagen type I, collagen type IV, laminin, fibronectin (10 μg), rADAM9D (5, 10 and 50 μg) or 1% BSA were immobilized overnight at 4°C in 96 well plate. Wells were blocked with 1% BSA in adhesion buffer (HEPES 20mM, pH 7,35; containing NaCl 150 mM, KCl 5 mM, $MgSO_4$ 1 mM and $MnCl_2$ 1 mM) for 2 h. DU145 cells were labeled with 12.5 μM CMFDA (37°C for 30 min) and then 1×10^5 cells/well were plated and maintained for 30min at 37°C. Wells were washed and the remaining cells were lysed using 0.5% Triton X-100. Fluorescence was read in a fluorimeter Spectra-Max Gemini XS (Molecular Devices, Sunnyvale, CA, USA) with 485nm excitation and 530nm emission filters. For inhibition of adhesion assay, cells were labeled and measured as described above, except that the cells were pre-incubated with rADAM9D in different concentrations (100, 500, 1000 nM) and then plated on 10 μg of collagen type I (Sigma-Aldrich) in acetic acid (0.1%) or on 10 μg of laminin (Sigma-Aldrich) in adhesion buffer. For antibody competition assays CMFDA-labeled cells were incubated with different anti-integrin

antibodies (αvβ3, αvβ5, β1, α2, α4, α6 at 10 μg/ml) and IgG control (10 μg/ml) before being plated on rADAM9D-coated wells.

Flow cytometry analysis

DU145 cells were submitted to flow cytometry analysis to verify their integrin cell profile. Cells (1×10^5cells/ml) were incubated for 40 min at 4°C with specific antibodies against αvβ3, αvβ5, β1, α2, α4, α6 and control IgG. Cells were washed and incubated with secondary antibody labeled with FITC, at same conditions described before, washed and fixed with FACs buffer contaning 1% phormaldehyde overnight at 4°C. To verify the interaction with integrins, rADAM9D (1 μM) was previously incubated
(30 min at room temperature) with DU145 cells, before the addition of antibodies. Cells were analyzed in FACSCanto (BD Biosciences).

Invasion

Invasion assays were performed with DU145 prostate cancer cells incubated with rADAM9D using the BioCoat Matrigel Invasion Chambers (BD Biosciences). Briefly, DU145 cells (1.25×10^5 cells/ml) were seeded on the inserts (12 well-plate) of the invasion chamber in the presence or absence of rADAM9D (1 μM). Complete medium was used as a chemoattractant at the lower chamber. Plates were incubated for 22 h at 37°C and 5% CO_2. Non-invading cells were removed with a cotton swab from the upper surface of the membrane and invading cells were fixed using 100% methanol and stained with 1% toluidine blue in 1% borax. Ten random fields from microscope slides were photographed and cells were counted using Image J software. Positive control was made in the presence of chemoattractant (10% FBS) at the lower chamber and negative control was FBS free medium at the lower chamber.

Wound healing

Cells (1×10^5 cells/ml) were plated in 24-wells plates and incubated properly until the culture reached 100% of confluence. Afterwards, a straight scratch was made with a pipette tip and cells were washed with culture medium to remove unbound cells and debris. Cells were incubated with rADAM9D (100, 500, 1000 and 2000 nM) for 24 h and 48 h. Central field was photographed at 0 h, 24 h and 48 h (when cells close the scratch completely). Closure area of migrating cells was measure using ImageJ software, and it was calculated the percentage of wound closure, comparing time zero and 24 hours later, using a formula from Yue et al.,[28] showing the difference between 0 h and 24 h:

$$\%\ of\ wound\ closure = \frac{(A_{t=0h} - A_{t=\Delta h})}{(A_{t=0h})} \times (100)$$

Statistical analysis

All experiments were repeated 3 times in triplicate and the mean and standard deviation were calculated. Comparisons were made using one-way analysis (ANOVA) and when samples presented significance, Dunnet's post hoc analysis was applied to verify difference between groups.

Disclosure of Potential Conflicts of Interest

No potential conflicts of interest were disclosed.

Funding

The authors are grateful for the financial support of FAPESP (Fundação de Amparo à Pesquisa do Estado de São Paulo, #2004/06986-6). Martin ACBM had a scholarship sponsored by CNPq (National Council of Research, #130539/2009-0).

References

1. Maximum androgen blockade in advanced prostate cancer: an overview of the randomised trials. Prostate Cancer Trialists' Collaborative Group. Lancet 2000; 355:1491-8; PMID:10801170; http://dx.doi.org/10.1016/S0140-6736(00)02163-2
2. Stone AL, Kroeger M, Sang QX. Structure-function analysis of the ADAM family of disintegrin-like and metalloproteinase-containing proteins (review). J Protein Chem 1999; 18:447-65; PMID:10449042; http://dx.doi.org/10.1023/A:1020692710029
3. Klein T, Bischoff R. Active metalloproteases of the A Disintegrin and Metalloprotease (ADAM) family: biological function and structure. J Proteome Res 2011; 10:17-33; PMID:20849079; http://dx.doi.org/10.1021/pr100556z
4. Blobel CP. ADAMs: key components in EGFR signalling and development. Nat Rev Mol Cell Biol 2005; 6:32-43; PMID:15688065; http://dx.doi.org/10.1038/nrm1548
5. Nath D, Slocombe PM, Webster A, Stephens PE, Docherty AJ, Murphy G. Meltrin gamma(ADAM-9) mediates cellular adhesion through alpha(6)beta(1) integrin, leading to a marked induction of fibroblast cell motility. J Cell Sci 2000; 113 (Pt 12):2319-28; PMID:10825303
6. Zhou M, Graham R, Russell G, Croucher PI. MDC-9 (ADAM-9/Meltrin gamma) functions as an adhesion molecule by binding the alpha(v)beta(5) integrin. Biochem Biophys Res Commun 2001; 280:574-80; PMID:11162558; http://dx.doi.org/10.1006/bbrc.2000.4155
7. Karadag A, Zhou M, Croucher PI. ADAM-9 (MDC-9/meltrin-gamma), a member of the a disintegrin and metalloproteinase family, regulates myeloma-cell-induced interleukin-6 production in osteoblasts by direct interaction with the alpha(v)beta5 integrin. Blood 2006; 107:3271-8; PMID:16373656; http://dx.doi.org/10.1182/blood-2005-09-3830
8. Mazzocca A, Coppari R, De Franco R, Cho JY, Libermann TA, Pinzani M, et al. A secreted form of ADAM9 promotes carcinoma invasion through tumor-stromal interactions. Cancer Res 2005; 65:4728-38; PMID:15930291; http://dx.doi.org/10.1158/0008-5472.CAN-04-4449
9. Cominetti MR, Martin AC, Ribeiro JU, Djaafri I, Fauvel-Lafeve F, Crepin M, et al. Inhibition of platelets and tumor cell adhesion by the disintegrin domain of human ADAM9 to collagen I under dynamic flow conditions. Biochimie 2009; 91:1045-52; PMID:19505527; http://dx.doi.org/10.1016/j.biochi.2009.05.012
10. Zigrino P, Steiger J, Fox JW, Loffek S, Schild A, Nischt R, et al. Role of ADAM-9 disintegrin-cysteine-rich domains in human keratinocyte migration. JBiol Chem 2007; 282:30785-93; PMID:17704059; http://dx.doi.org/10.1074/jbc.M701658200
11. Takeda S, Igarashi T, Mori H, Araki S. Crystal structures of VAP1 reveal ADAMs' MDC domain architecture and its unique C-shaped scaffold. EMBO J 2006; 25:2388-96; PMID:16688218; http://dx.doi.org/10.1038/sj.emboj.7601131
12. Fritzsche FR, Jung M, Tolle A, Wild P, Hartmann A, Wassermann K, et al. ADAM9 expression is a significant and independent prognostic marker of PSA relapse in prostate cancer. Euro Urol 2008; 54:1097-106; PMID:18061337; http://dx.doi.org/10.1016/j.eururo.2007.11.034
13. Carl-McGrath S, Lendeckel U, Ebert M, Roessner A, Rocken C. The disintegrin-metalloproteinases ADAM9, ADAM12, and ADAM15 are upregulated in gastric cancer. Int JOncol 2005; 26:17-24; PMID:15586220
14. Peduto L, Reuter VE, Shaffer DR, Scher HI, Blobel CP. Critical function for ADAM9 in mouse prostate cancer. Cancer research 2005; 65:9312-9; PMID:16230393; http://dx.doi.org/10.1158/0008-5472.CAN-05-1063
15. Li J, Ji Z, Qiao C, Qi Y, Shi W. Overexpression of ADAM9 Promotes Colon Cancer Cells Invasion. J Invest Surg 2013; 26; PMID:23514059; http://dx.doi.org/10.3109/08941939.2012.728682
16. Josson S, Anderson CS, Sung SY, Johnstone PA, Kubo H, Hsieh CL, et al. Inhibition of ADAM9 expression induces epithelial phenotypic alterations and sensitizes human prostate cancer cells to radiation and

chemotherapy. Prostate 2011; 71:232-40; PMID:20672324; http://dx.doi.org/10.1002/pros.21237
17. Peduto L. ADAM9 as a potential target molecule in cancer. Curr Pharm Des 2009; 15:2282-7; PMID:19601830; http://dx.doi.org/10.2174/138161209788682415
18. Zhang J, Chen N, Qi J, Zhou B, Qiu X. HDGF and ADAM9 are novel molecular staging biomarkers, prognostic biomarkers and predictive biomarkers for adjuvant chemotherapy in surgically resected stage I non-small cell lung cancer. JCancer ResClin Oncol 2014; 140:1441-9; PMID:24770635; http://dx.doi.org/10.1007/s00432-014-1687-2
19. Hood JD, Cheresh DA. Role of integrins in cell invasion and migration. Nat Rev Cancer 2002; 2:91-100; PMID:12635172; http://dx.doi.org/10.1038/nrc727
20. Pontier SM, Muller WJ. Integrins in breast cancer dormancy. APMIS 2008; 116:677-84; PMID:18834411; http://dx.doi.org/10.1111/j.1600-0463.2008.01026.x
21. Van den Eynden GG, Majeed AW, Illemann M, Vermeulen PB, Bird NC, Hoyer-Hansen G, et al. The multifaceted role of the microenvironment in liver metastasis: biology and clinical implications. Cancer Res 2013; 73:2031-43; PMID:23536564; http://dx.doi.org/10.1158/0008-5472.CAN-12-3931
22. Sakamoto S, Kyprianou N. Targeting anoikis resistance in prostate cancer metastasis. Mol Aspects Med 2010; 31:205-14; PMID:20153362; http://dx.doi.org/10.1016/j.mam.2010.02.001
23. Belkin AM, Stepp MA. Integrins as receptors for laminins. Microsc Res Techniq 2000; 51:280-301; PMID:NOT_FOUND; http://dx.doi.org/10.1002/1097-0029(20001101)51:3%3c280::AID-JEMT7%3e3.0.CO;2-O
24. Skogseth H, Holt RU, Larsson E, Halgunset J. Tyrosine kinase inhibitors alter adhesivity of prostatic cancer cells to extracellular matrix components. APMIS 2006; 114:225-33; PMID:16643189; http://dx.doi.org/10.1111/j.1600-0463.2006.apm_365.x
25. Witkowski CM, Rabinovitz I, Nagle RB, Affinito KS, Cress AE. Characterization of integrin subunits, cellular adhesion and tumorgenicity of four human prostate cell lines. J Cancer Res Clin Oncol 1993; 119:637-44; PMID:7688749; http://dx.doi.org/10.1007/BF01215981
26. Fry JL, Toker A. Secreted and membrane-bound isoforms of protease ADAM9 have opposing effects on breast cancer cell migration. Cancer Res 2010; 70:8187-98; PMID:20736367; http://dx.doi.org/10.1158/0008-5472.CAN-09-4231
27. Roghani M, Becherer JD, Moss ML, Atherton RE, Erdjument-Bromage H, Arribas J, et al. Metalloprotease-disintegrin MDC9: intracellular maturation and catalytic activity. J Biol Chem 1999; 274:3531-40; PMID:9920899; http://dx.doi.org/10.1074/jbc.274.6.3531
28. Yue PY, Leung EP, Mak NK, Wong RN. A simplified method for quantifying cell migration/wound healing in 96-well plates. J Biomol Screen 2010; 15:427-33; PMID:20208035; http://dx.doi.org/10.1177/1087057110361772

JLB

Article

ADAM9 disintegrin domain activates human neutrophils through an autocrine circuit involving integrins and CXCR2

Rafael S. Amendola, Ana Carolina B. M. Martin,† Heloísa S. Selistre-de-Araújo,† Heitor A. Paula-Neto,*,[1] Roberta Saldanha-Gama,* and Christina Barja-Fidalgo*,[2]*

*Laboratório de Farmacologia Celular e Molecular, Departamento de Biologia Celular, Instituto de Biologia Roberto Alcantara Gomes, Universidade do Estado do Rio de Janeiro, Rio de Janeiro, Brazil; and †Laboratório de Bioquímica e Biologia Molecular, Departamento de Ciências Fisiológicas, Universidade Federal de São Carlos, São Carlos, Brazil

RECEIVED SEPTEMBER 29, 2014; REVISED FEBRUARY 4, 2015; ACCEPTED FEBRUARY 18, 2015. DOI: 10.1189/jlb.3A0914-455R

ABSTRACT

ADAM9 is a member of the ADAM family whose expression positively correlates with tumor progression. Besides the metalloprotease activity, ADAM9D interacts with different integrins, modulating cell-adhesion events. Previous studies pointed to an important role for neutrophils in tumor development, as the inhibition of neutrophil migration or depletion of this immune cell impairs tumor growth. However, our understanding of the molecular mechanisms involved in this process, as well as the main key players acting on neutrophils, is very limited. Here, we investigated the possible modulatory effects of ADAM9D on human neutrophil functions. Our results show that ADAM9D promotes neutrophil activation and chemotaxis in a process that depends on the engagement of $\alpha_v\beta_3$ and $\alpha_9\beta_1$ integrins and on the activation of PI3K/Akt and MAPK signaling pathway. ADAM9D impairs migration of neutrophils toward fMLP, LTB_4, and IL-8 as classic chemoattractants. This effect is blocked by PTX, a G(i)PCR inhibitor. Furthermore, CXCR2 antagonists RPTX and SB225002 also impaired neutrophil chemotaxis in response to ADAM9D, suggesting a hierarchical cross-talk of integrins with CXCR2. Our results indicate that ADAM9D activates neutrophil functions and may be implicated in the inflammatory events associated with cancer and other disorders. *J. Leukoc. Biol.* 97: 951–962; 2015.

Introduction

During inflammation, neutrophils are the first cells to leave the circulation and infiltrate the inflamed tissue. Within tissues, neutrophils are activated, contributing to pathogen clearance [1], although they may also contribute to aggravating tissue injury [2]. Therefore, the infiltration and activation of these immune cells within tissues must be tightly regulated to optimize defense and minimize collateral damage. Neutrophil migration to the inflamed tissue is a process highly dependent on cell–cell and cell–matrix adhesion events [3, 4]. Integrins are key adhesion receptors in neutrophils, able to modulate their functions and survival [5].

It is well established that integrins recognize multiple endogenous ligands, such as extracellular matrix proteins [6, 7] and adhesion receptors [5, 8]. Furthermore, several ADAMs have been reported to interact with integrins that are expressed by different cell types [9–12]

ADAM is a family of proteins involved in various physiologic and pathologic processes. ADAM family members have a well-conserved structure with 8 domains, among which are a protease and an integrin-binding (disintegrin) domain [13]. The ADAM metalloprotease domain acts as a sheddase and has been reported to modulate a series of biologic processes by cleaving transmembrane proteins, which then can act as soluble ligands and regulate cellular signaling [14–16]. In inflammatory events, for example, ADAM17 can cleave TNF-α to limit its proinflammatory effects [15]. Moreover, ADAM family members can bind to specific integrins through the disintegrin domain and regulate many aspects of cell–cell and cell–matrix interactions [9–12]. In accordance, it was recently demonstrated that ADAM10 expressed on leukocytes is essential for their migration to inflamed tissues [17].

ADAM9 is a member of the ADAM family whose expression has been detected in different cells types, including fibroblast [18], activated VSMCs [12], monocytes [19], activated macrophages [20], and many tumor cells [21–25]. In addition, Roychaudhuri

Abbreviations: ADAM9 = a disintegrin and metalloproteinase 9, ADAM9D = disintegrin domain of human a disintegrin and metalloproteinase 9, BCA = bicinchoninic acid, BLT = leukotriene B_4R, G(i)PCR = G(i)-protein-coupled receptor, GPCR = G-protein-coupled receptor, LDH = lactate dehydrogenase, LTB_4 = leukotriene B_4, NET = neutrophil extracellular trap, p = phosphorylation, PI = propidium iodide, PTX = pertussis toxin, PVDF = polyvinylidene difluoride, RGD = Arg-Gly-Asp, ROS = reactive oxygen species, RPTX = repertaxin, VSMC = vascular smooth cell

The online version of this paper, found at www.jleukbio.org, includes supplemental information.

1. Current affiliation: Universidade Federal do Rio de Janeiro, Rio de Janeiro, RJ, Brazil.

2. Correspondence: Laboratório de Farmacologia Celular e Molecular, IBRAG, Universidade do Estado do Rio de Janeiro, Av. 28 de Setembro, 87 fds, Vila Isabel, Rio de Janeiro, RJ, Brazil. E-mail: barja-fidalgo@uerj.br

et al. [26] reported that besides expressing ADAM9 on the membrane surface, activated neutrophils can also express soluble ADAM9 in a manner similar to that observed in tumor cells [25]. However, the potential involvement of ADAM9 in physiologic and pathologic processes remains poorly known. Most of what we currently know about ADAM9 is related to tumor development and progression. Indeed, increased ADAM9 expression correlates positively with tumor malignancy and metastatic potential [21–25]. Additionally, ADAM9 and its secreted soluble isoform seem to be crucial for cancer cells to disseminate [25, 27]. Through its metalloprotease activity, ADAM9 participates in the degradation of matrix components, allowing the migration of tumor cells [21–26].

Besides the metalloprotease activity, ADAM9 has a disintegrin domain, which is highly homologous to many snake-venom disintegrins [28]. This domain allows the interaction between ADAM9 and integrins, granting the ability to ADAM9 to modulate, positively or negatively, cell adhesion events [18, 29, 30]. In accordance, ADAM9D has been shown to interact with $\alpha_6\beta_1$ [10], $\alpha_6\beta_4$ [27], $\alpha_v\beta_5$ [29], and $\alpha_9\beta_1$ [30] integrins, depending on the cell type.

Previous studies have shown that when neutrophils are depleted, or their migration is blocked, tumor growth is impaired [31, 32], indicating an important role for these cells in tumor development [31–33]. However, our understanding of the molecular mechanisms involved in this process, as well as the main key players acting on the neutrophils, is limited. Therefore, we investigated whether ADAM9, a molecule that is overexpressed in many types of cancers, would be able to modulate neutrophil chemotactic response and activation. Our results offer new insights on the dynamic of interaction between tumor cells and neutrophils and indicate that ADAM9 has an important participation in this interaction.

MATERIALS AND METHODS

Reagents

Percoll was from GE Healthcare (Buckinghamshire, United Kingdom), RPMI culture medium was from Gibco (Carlsbad, CA, USA), and polycarbonate chemotaxis membranes with 5 μm pores were from Neuro Probe (Gaithersburg, MD, USA). All antibodies used were purchased from Santa Cruz Biotechnology (Santa Cruz, CA, USA). Selective inhibitors for PI3K (wortmannin and LY294002) and p38 (SB203580) and the CXCR2 selective antagonist (SB225002) were obtained from Calbiochem (Darmstadt, Germany). DAPI ProLong was obtained from Invitrogen (Carlsbad, CA, USA). RPTX and PTX were kindly provided by Drs. Erik Svensjoand and Claudio Canetti (Instituto de Biofísica Carlos Chagas Filho/ Universidade Federal do Rio de Janeiro). PVDF membranes and analytical-grade Western blot reagents were purchased from GE Healthcare. The ECL development kit was obtained from Pierce Biotechnology (Rockford, IL, USA).

ADAM9D cloning, expression, and isolation

ADAM9D was cloned and purified as described previously [30]. A sequence of ADAM9D, corresponding to the nucleotides 1318–1588 (GenBank Accession No. NM003816), was cloned in a pGEX-4T-1 vector and used to transform the *Escherichia coli* AD494(DE3) expression strain. ADAM9D was purified from cell extracts, and resulting fractions were analyzed by SDS-PAGE with Coomassie brilliant blue staining. ADAM9D concentration was determined by BCA protein assay, and protein yield was determined to be ~2.5 mg/L culture.

Neutrophil isolation

Blood was collected from healthy human volunteers (Protocol Number UERJ 2786/2010; Ethics Committee, Hospital Pedro Ernesto, Universidade do Estado do Rio de Janeiro). Blood was transferred immediately to EDTA-containing tubes. Neutrophils were isolated by use of a 4-step Percoll gradient as described [34]. Neutrophil purity and viability were always >97% and >99%, respectively, as accessed by differential counts and trypan dye exclusion.

Neutrophil treatment

In experiments involving integrin blockade, freshly isolated cells were preincubated with different neutralizing antibodies at 10 μg/ml for 5 min. In the set of experiments that use pharmacological inhibitors, the neutrophils were treated as follows: the PI3K inhibitors, LY294002 (10 μM) and wortmannin (100 nM), the p38 inhibitor SB203580 (10 μM), or the CXCR2 allosteric inhibitor RPTX (1 mM) were all added 15 min before the assays; the CXCR2 selective inhibitor SB225002 (1 mM) and PTX (100 ng/ml) were added 30 min before the assays. After all treatments, cells were washed and resuspended in RPMI medium before use in experiments.

In vitro neutrophil chemotaxis

Neutrophil chemotaxis was evaluated by use of a 48-well Boyden chamber (Neuro Probe) with 5 μm pore-sized polyvinylpyrrolidone-free polycarbonate membranes, as described [34]. In brief, chemoattractants (28 μl) were placed in the bottom chamber, and 50 μl of the neutrophil suspension (10^6 cells/ml) was added to the top chamber. The chambers were then incubated for 1 h at 37°C with 5% CO_2, after which membranes were removed, fixed, and stained with the Diff-Quik staining kit (Laborclin, Pinhais, Parana, Brazil). The number of neutrophils that migrated to the lower side of the filter was counted in at least 5 random fields (1000× magnification). The results are representative of at least 3 independent experiments performed in triplicate for each sample and are expressed as mean ± SD of the number of neutrophils/field. Chemoattractants used were fMLP (100 nM), LTB_4 (100 nM), IL-8 (30 nM), or ADAM9D (0.1–1000 nM). Migration to medium alone (random migration) was used as a negative control.

Apoptosis detection

Annexin V-FITC binding assay. Apoptosis was evaluated by estimation of phosphatidylserine membrane exposure by use of Annexin-V binding, as described [35]. In brief, fresh neutrophils (control group) or neutrophils incubated or not with ADAM9D (100 nM) for 20 h at 37°C in a 5% CO_2 atmosphere were washed with binding buffer (10 mM HEPES, 150 mM NaCl, 5 mM KCl, 1 mM $MgCl_2$, and 1.8 mM $CaCl_2$, pH 7.4) and resuspended in 100 μl binding buffer containing FITC-conjugated Annexin V (1:500 dilution). After 20 min of incubation at room temperature in the dark, 400 μl binding buffer was added, and the samples were analyzed immediately in BD Accuri C6 flow cytometer (BD Biosciences, San Jose, CA, USA).

Morphology. Neutrophils were stimulated or not with ADAM9D (100 nM) for 20 h at 37°C in a 5% CO_2 incubator. Cells were cytocentrifuged, stained with Diff-Quik, and counted under high magnification to determine the proportion of cells showing apoptotic morphology. Cells were considered apoptotic when displaying pyknotic nuclei and cell volume shrinkage. At least 300 cells were counted/slide.

Caspase activity. Caspase activity was evaluated by use of the NucView 488 Caspase-3 Assay Kit, following the manufacturer's instructions. In brief, neutrophils (2×10^5 cells/ml in 200 μl RPMI) were stimulated or not with ADAM9D (100 nM) for 20 h at 37°C in a 5% CO_2. Cells were then incubated with 5 μM NucView substrate for 30 min at room temperature and protected from light. After incubation with substrate, 300 μl RPMI was added to each group, and the cells were analyzed immediately on a BD Accuri C6 flow cytometer (BD Biosciences). Freshly isolated neutrophils were used as controls.

ROS production assay

Neutrophils (10^5 cells/well in a final volume of 200 μl) were resuspended in HBSS and placed in a white 96-well plate. Cells were loaded with luminol (500 μM) and stimulated or not with ADAM9D (100 nM) or PMA (30 nM), a known NADPH oxidase activator. Nonstimulated cells were used as controls, and neutrophils stimulated with PMA were used as positive control. Chemiluminescence was measured in each well for 15 min (luminol assay) by use of an EnVision Multilabel Plate Reader (PerkinElmer, Waltham, MA, USA).

In vitro NET assay

The cells were allowed to attach to poly-L-lysine-coated slides at 37°C for 20 min. The attached neutrophils were stimulated with ADAM9D or LPS (positive control) at 37°C for 60 min. After stimulation, neutrophils were fixed, permeabilized, and blocked for immunofluorescence staining. Cells were incubated with goat antineutrophil elastase (1:300; Santa Cruz Biotechnology), followed by secondary antibody coupled with Alexa Fluor 488 (1:400; Invitrogen). DNA was stained by use of DAPI ProLong (Invitrogen) and examined under fluorescence microscopy (1000×).

LDH activity

LDH activity was measured by use of a kinetic UV commercial kit (Bioclin, Minas Gerais, Brazil), according to the manufacturer's instructions. Supernatants of neutrophils incubated in the presence or absence of the CXCR2 inhibitor SB225002 were used. Supernatant from neutrophils lysed with 0.1% Triton X-100 in PBS was used as positive control.

Neutrophil adhesion assay

Neutrophil adhesion assay was carried out as described previously [36]. In brief, ELISA plates were coated overnight at 4°C with 100 μl/well of a 10 μg/ml solution of rADAM9D in bicarbonate buffer (pH 9.4). Unspecific binding sites were then blocked with a 1% BSA solution in PBS for 30 min at 37°C. After extensive wash with PBS–0.1% BSA, cells (10^4 neutrophils/well in 100 μl PBS–0.1% BSA) were added to wells and incubated for 15 min at 37°C in the presence of blocking antibodies. Wells were then washed with PBS–0.1% BSA, and adherent neutrophils were quantified by myeloperoxidase assay. Neutrophil numbers in each well were estimated based on the readings of a standard curve made with human neutrophils.

Western blotting analysis

Neutrophils (5×10^6 cells), stimulated with ADAM9D (100 nM), were resuspended in 100 μl lysis buffer (10 mM Hepes, 5 mM EDTA, 250 mM sucrose, 1 mM orthovanadate, pH 7.4). Lysates were boiled for 3 min, sonicated, and boiled for another 3 min. Samples of 3 μl were diluted 1:10 and used for protein quantification by the BCA method. Lysates were mixed with 20 μl sample buffer, boiled for 3 min, and stored at 20°C until use. Protein samples of 25 μg were separated on 10% SDS-PAGE and transferred to PVDF membranes. Akt, pAkt, Erk-2, pErk, p38, pp38, and caspase-3 were detected by use of specific primary antibodies at 1:1,000 dilution, followed by appropriate HRP-conjugated secondary antibodies (1:10,000). Immunoreactive bands were visualized by ECL. Images were acquired and then analyzed with ImageJ software.

Real-time PCR

Total RNA was isolated by use of RNeasy Mini Kit (Qiagen, Hamburg, Germany). cDNA was generated by use of a random primer and RT (Superscript II; Life Technologies), according to the manufacturer's instructions. Quantitative real-time PCR was performed in a Rotor-Gene Q by use of a SYBR-Green fluorescence quantification system (Qiagen) to quantify amplicons. The standard PCR conditions were 95°C for 5 min and then 35 cycles at 95°C (5 s) and 60°C (10 s), followed by the standard denaturation curve. IL-8 primers (Hs_IL8_1_SG, QT00000322) were used to amplify human IL-8. Actin primers (Hs_ACTB_2_SG, QT01680476) were used to validate the cDNA in each reaction.

CXCR2 membrane expression

Neutrophils were treated with ADAM9D (100 nM) or IL-8 (30 nM) at the indicated times and fixed immediately with ice-cold 1% paraformaldehyde in PBS. After extensive washing in FACS buffer (2% BSA, 5% FCS, 0.1% sodium azide in PBS), cells were resuspended in 50 μl FACS buffer and incubated with FITC-labeled mouse IgG1 anti-human CXCR2 (1:50) for 60 min at 4°C. Cells were then washed in FACS buffer and analyzed by use of a BD Accuri C6 flow cytometer (BD Biosciences).

Statistical analysis

All results are presented as means ± SD, derived from at least 3 independent experiments. Data were analyzed with help of GraphPad Prism 5.0 for Windows. Statistical significance was tested by use of ANOVA, followed by Bonferroni post-test. Differences with $P < 0.05$ were considered statistically significant.

RESULTS

ADAM9D induces human neutrophil activation

To understand better the role of ADAM9D on human neutrophils, we investigated the effects of ADAM9D by testing some classic parameters of neutrophil activation. Firstly, the ability of neutrophils to migrate in response to increasing doses of ADAM9D was evaluated. Neutrophil chemotaxis was enhanced with increasing concentrations of ADAM9D and peaked at 100 nM when it reached similar levels to those obtained with an optimal concentration of fMLP, a well-known neutrophil chemotactic. At a higher concentration (1000 nM), a lower number of cells migrated. This behavior resulted in a bell-shaped curve, characteristic of classic chemoattractants (**Fig. 1A**).

We then evaluated the effects of ADAM9D on spontaneous neutrophil apoptosis. Twenty hours after adding ADAM9D to the suspension of neutrophils, 50–60% of cells were Annexin V negative (viable cells) compared with 20–30% of control cells (Fig. 1B). Importantly, we did not observe significant changes in a PI-positive neutrophil population, indicating that ADAM9D specifically affects spontaneous apoptosis (Fig. 1B). Similar results were observed by counting the number of neutrophils presenting morphologic features characteristic of apoptosis (Fig. 1C). Furthermore, we observed that ADAM9D was able to reduce procaspase-3 cleavage (Fig. 1D) and decrease caspase-3 activity (Fig. 1E) in neutrophils. Altogether, these results demonstrate an antiapoptotic effect of ADAM9D on human neutrophils.

The ability of ADAM9D to induce ROS production in human neutrophils was also investigated. In the presence of ADAM9D, as detected by luminol assay, human neutrophils produced large amounts of ROS compared with media alone (Fig. 1F). The dynamics of ROS generation that we observed (slow increase with delayed peak at 45 min) was similar to the adhesion- and integrin-dependent, cytochalasin-sensitive response reported originally by Nathan [37]. An adhesion-like effect, mediated by the binding of ADAM9D to integrins, was ruled out by disrupting cytoskeleton with cytochalasin D and observing no effect on ROS production triggered by ADAM9D (data not shown), suggesting that this peptide may act as a direct agonist of ROS generation.

Finally, we evaluated whether ADAM9D could promote NET formation. As seen in Fig. 1G, the disintegrin domain induced NET formation similarly to the group of cells treated with LPS,

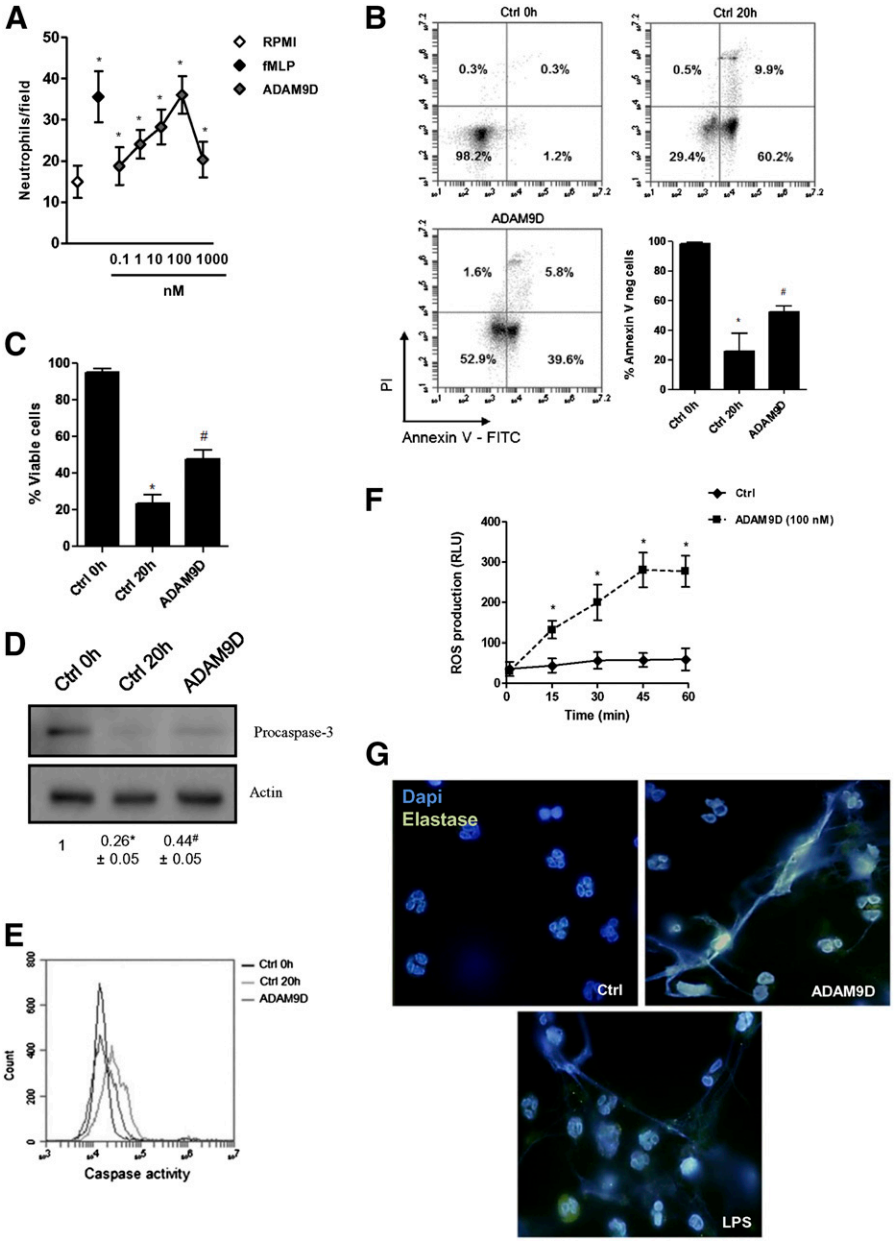

Figure 1. Effects of ADAM9D on human neutrophil activation. (A) Neutrophil chemotaxis in response to ADAM9D (0.1 nM–1 μM) or fMLP (10^{-7} M). Data represent the means ± SD of the number of neutrophils/1000× field of view counted under optical microscopy. *$P < 0.05$ compared with neutrophils migrating in the absence of stimulus. Apoptosis of neutrophils incubated or not with ADAM9D (100 nM) was evaluated by Annexin V and PI staining (B) or by morphologic criteria (C). Cells presenting pyknotic nuclei and cytoplasm shrinkage were considered apoptotic.*$P < 0.05$ relative to 0 h controls; #$P < 0.05$ relative to 20 h. (D) Western blot analysis of procaspase-3 content in freshly isolated neutrophils (Ctrl 0 h) or neutrophils incubated for 20 h in the absence (Ctrl 20 h) or presence of 100 nM ADAM9D. Image is derived from 1 representative Western blot, and numbers bellow images represent means ± SD of procaspase-3 expression relative to 0 h control. *$P < 0.05$ relative to 0 h control; #$P < 0.05$ relative to 20 h control in the absence of ADAM9D. (E) Caspase-3 activity as evaluated by FACS by use of a caspase-3 activity fluorescent probe. Histogram is 1 representative image derived from 3 independent experiments with similar results. (F) ROS generation on neutrophils stimulated or not with ADAM9D. Values are expressed in relative luminescence unit at different time-points. *$P < 0.05$ compared with unstimulated cells. RLU, Relative light unit(s). (G) Analysis of NET release in unstimulated cells (Ctrl) and cells stimulated with ADAM9D (100 nM) or LPS (100 ng/ml). Elastase is visualized as green fluorescence (Alexa Fluor 488) and chromatin as blue (DAPI) ×1000. All data are derived from at least 3 independent experiments, with neutrophils from 1 different donor in each experiment, with $n = 3$ for each experiment.

our positive control. To rule out the effect of LPS contamination on our ADAM9D preparations, we performed the apoptosis and NET assays in the presence of polymyxin B (25 μg/ml). No significant differences were observed between polymyxin B and control groups (Supplemental Fig. 1A and B), suggesting that the observed effects were attributable to ADAM9D. Together, these data indicate that ADAM9D activates human neutrophils.

Chemotactic effect of ADAM9D is mediated by $\alpha_9\beta_1$ and $\alpha_v\beta_3$ integrins

ADAM9D has been reported to interact with specific members of the integrin family that are expressed by human neutrophils [30, 38]. To investigate the engagement of integrin in the chemotactic effect of ADAM9D, neutrophils were incubated with specific antibodies recognizing different β-integrin subunits. Blockade of β_1 or β_3 integrin subunits (**Fig. 2A** and **B**) impaired the migration of human neutrophils toward ADAM9D. Interestingly, antibody against the β_2 subunit did not affect chemotaxis (Fig. 2C).

Neutrophil activation has been shown for other $\alpha_v\beta_3$-binding disintegrins [34]. Furthermore, the engagement of $\alpha_9\beta_1$, another putative receptor for ADAM9D, has been shown previously to activate different neutrophil functions [35]. Therefore, we investigated whether the migratory effect of ADAM9D on human neutrophils would involve its interaction with those integrins. In cells preincubated with blocking antibodies to α_v and $\alpha_9\beta_1$ integrins, neutrophil migration was inhibited in response to ADAM9D (Fig. 2D and E). Importantly, incubation of neutrophils with all anti-integrin antibodies used did not interfere with the chemotactic effect of IL-8, revealing the specificity of ADAM9D. To confirm that the blocking antibodies that we used

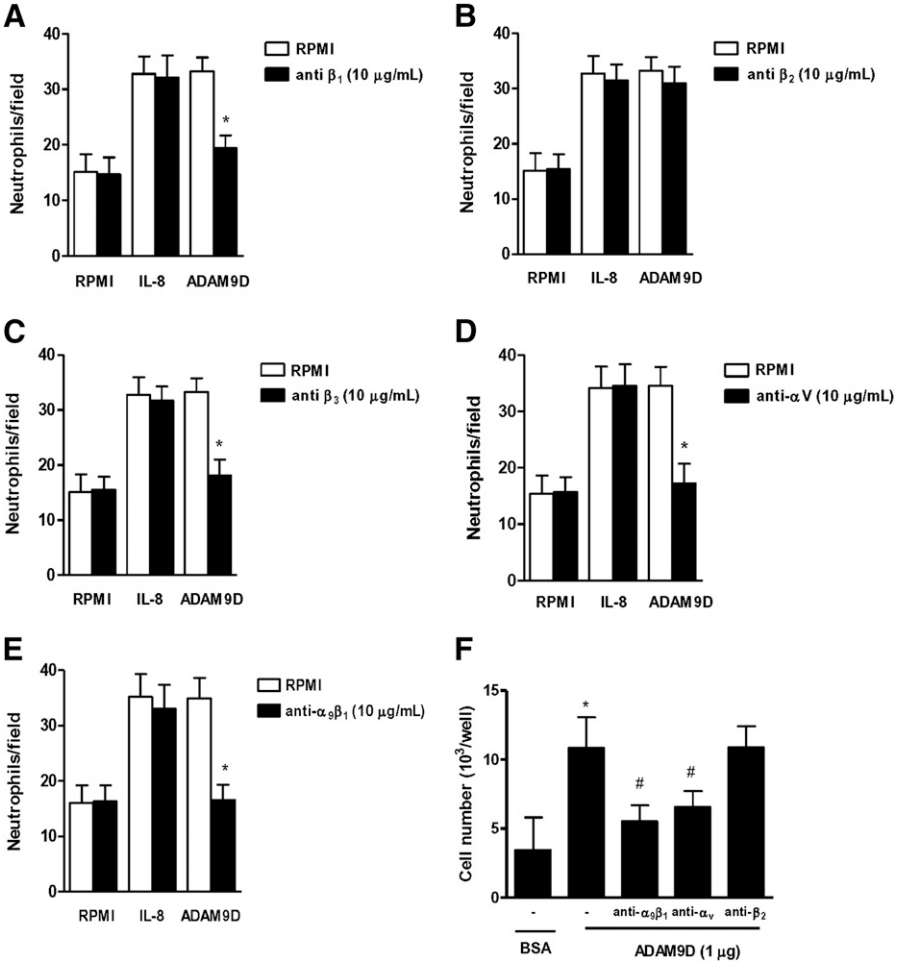

Figure 2. Involvement of $\alpha_9\beta_1$- and $\alpha_V\beta_3$-integrins on human neutrophil migration induced by ADAM9D. Neutrophils were incubated for 5 min with neutralizing antibodies to β_1 (A), β_2 (B), β_3 (C), or α_v (D) integrin subunits or to $\alpha_9\beta_1$ integrin (E). Cells were then assayed for chemotaxis in response to IL-8 (30 nM) or ADAM9D (100 nM). Data represent mean ± SD of the number of neutrophils/1000× field of view counted under optical microscopy. Data are derived from 3 independent experiments. $^*P < 0.05$ compared with cells migrating in response to ADAM9D in the absence of antibodies. (F) Neutrophil adhesion to ADAM9D-coated plates in the presence of anti-$\alpha_9\beta_1$, -α_v, or -β_2 blocking antibodies. Data are means ± SD of the estimated number of adherent neutrophils/well. Wells coated with BSA were used as negative controls. $^*P < 0.05$ relative to BSA-coated wells; $\#P < 0.05$ relative to neutrophils adhering to ADAM9D-coated wells in the absence of antibody. All data are derived from at least 3 independent experiments, with neutrophils from 1 different donor in each experiment, with $n = 3$ for each experiment.

were able to interfere specifically with ADAM9D binding to neutrophils, we carried out an in vitro adhesion assay. We evaluated the ability of neutrophils to adhere onto ADAM9D-coated plates in the presence of α_v and $\alpha_9\beta_1$ integrins blocking antibodies. As shown in Fig. 2F, both blocking antibodies significantly inhibited neutrophil adhesion to ADAM9D. Together, the data suggest that ADAM9D induces neutrophil chemotaxis by engaging $\alpha_9\beta_1$ and $\alpha_v\beta_3$ integrins.

ADAM9D activates intracellular signaling in human neutrophils

PI3K/Akt and p38 MAPK are 2 major signaling pathways involved in neutrophil chemotaxis [39, 40]. Integrin activation has been shown to trigger PI3K/Akt and MAPK pathways, modulating neutrophil migration and apoptosis [35, 37–40]. **Figure 3A** shows that neutrophils stimulated with ADAM9D presented increased pAkt, at levels similar to those triggered by IL-8, a known PI3K/Akt activator in neutrophils.

Stimulation of neutrophils with ADAM9D also increased pErk-2 (Fig. 3B) at levels comparable with those observed after Erk-2 stimulation with fMLP. On the other hand, differently than the effect of fMLP, ADAM9D did not affect pp38 MAPK in neutrophils (Fig. 3C).

To investigate whether PI3K/Akt signaling would be involved with the chemotactic response of neutrophils, a chemotaxis assay was performed in the presence of LY294002 (Fig. 3D) or wortmannin (Fig. 3E), 2 known inhibitors of the PI3K/Akt pathway. Pharmacological inhibition of PI3K through LY294002 or wortmannin resulted in a complete suppression of a neutrophil chemotactic response to ADAM9D.

To rule out a possible role of p38 activation on neutrophil migration, as induced by ADAM9D, pharmacological inhibition of p38 MAPK by SB203580, a p38 MAPK inhibitor, did not affect neutrophil chemotaxis (Fig. 3F), whereas it completely blocked chemotaxis to fMLP, a known chemoattractant that induces p38 [40].

PI3K/Akt and Erk signaling pathways have been widely demonstrated to promote cell survival. Moreover, our group has shown previously that these signaling pathways contribute to the increase in neutrophil lifespan triggered by snake-venom disintegrins [35, 41]. Therefore, we sought to investigate whether the activation of PI3K/Akt and Erk signaling pathways could account for the antiapoptotic effect of ADAM9D. Indeed, pretreatment of neutrophils with the PI3K inhibitor LY294002 or Erk-2 inhibitor PD98059, similarly blocked the antiapoptotic effect of ADAM9D (**Fig. 4A and B**). Interestingly, we observed that Erk-2 activation induced by ADAM9D seems to depend on

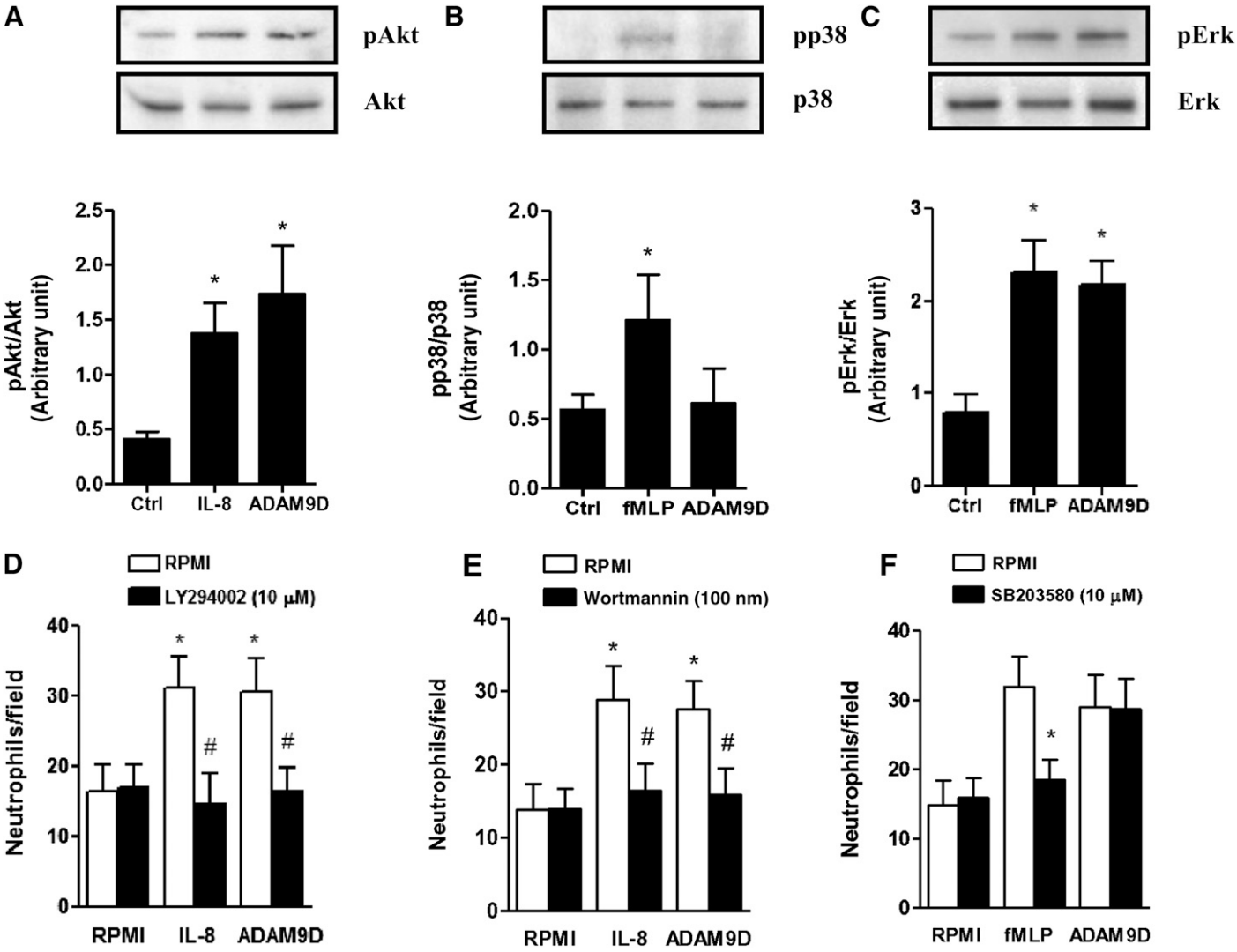

Figure 3. ADAM9D induces neutrophil chemotaxis through PI3K/Akt. Neutrophils were stimulated or not with IL-8 (30 nM), fMLP (10^{-7} M), or ADAM9D (100 nM) for 5 min and lysed. Activation of Akt (A), p38 (B), and Erk-2 (C) was analyzed by Western blot. The graphs show mean ± SD from 4 independent experiments. *$P < 0.05$ compared with control. Neutrophils were preincubated with LY294002 (D), wortmannin (E), or SB203580 (F) and then assayed for chemotaxis toward IL-8 (30 nM), fMLP (10^{-7} M), or ADAM9D (100 nM). Data represent mean ± SD of the number of neutrophils/1000× field of view counted under optical microscopy. Data are derived from 4 independent experiments.*$P < 0.05$ compared with negative control (cells migrating toward medium alone); #$P < 0.05$ compared with neutrophils without inhibitors.

PI3K/Akt, as pretreatment of neutrophils with LY294002 inhibited pErk-2 (data not shown). Taken together, these data suggest that ADAM9D activates PI3K/Akt and Erk signaling pathways that both contribute to stimulate neutrophil migration and to promote their survival.

ADAM9D impairs neutrophil migration to other chemoattractants

To evaluate a possible influence of ADAM9D on the chemotactic effect of known inflammatory mediators able to induce neutrophil migration, cells were stimulated with ADAM9D (100 nM) for 5 min and then allowed to migrate toward IL-8 (30 nM), LTB_4 (100 nM), fMLP (100 nM), or ADAM9D. In the presence of ADAM9D, the response of neutrophils to these chemoattractants and to ADAM9D itself was inhibited significantly (**Fig. 5A–D**). It is well recognized that LPS is able to blunt neutrophil responses to various chemoattractants. To exclude the interference of LPS contamination in our chemotaxis assays, we performed these experiments in the presence of polymyxin B. Once more, we did not observe significant differences between polymyxin B and control groups (Supplemental Fig. 1C).

Interestingly, when cells were in the presence of chemoattractants and stimulated to migrate in response to ADAM9D, migratory response was also inhibited (Fig. 5E–G). This suggests that classic chemoattractants could interfere directly with the neutrophil chemotactic response to ADAM9D.

Chemotactic effect of ADAM9D on human neutrophils depends on CXCR2 activation

Neutrophils express different chemoattractant receptors [42, 43] that can communicate with one another [44]. This cross-talk

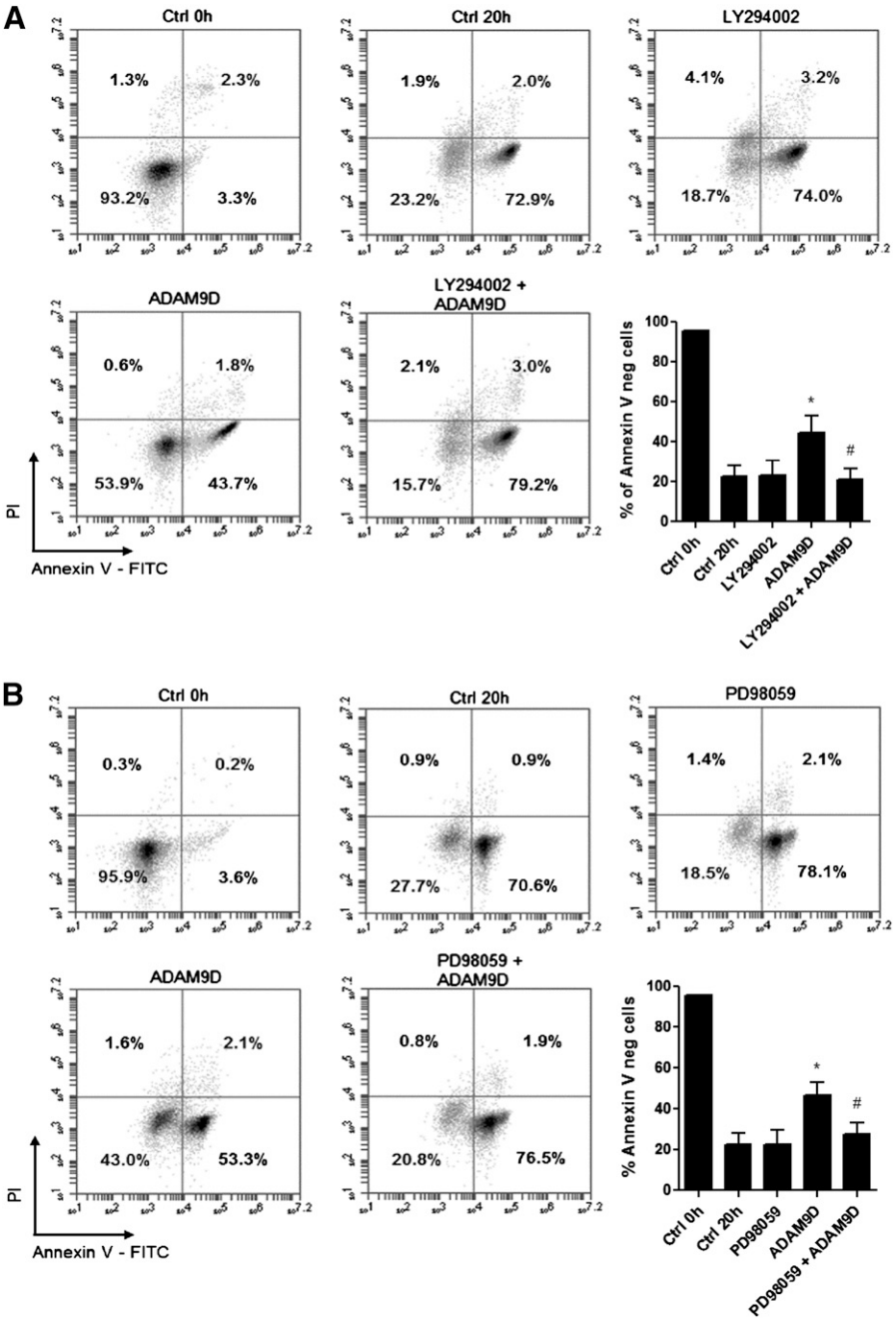

Figure 4. ADAM9D inhibits neutrophil spontaneous apoptosis through PI3K/Akt and Erk-2 signaling. Neutrophils were preincubated with LY294002 (A) or PD98059 (B) and then incubated for 20 h at 37°C in the presence or absence of ADAM9D (100 nM). Apoptosis was then evaluated by Annexin V and PI staining. Freshly isolated neutrophils were used as controls (0 h control). $*P < 0.05$ relative to 0 h controls; $\#P < 0.05$ relative to cells incubated for 20 h.

usually involves the activation of G(i)PCR, which triggers signaling pathways that are essential for cell mobilization and receptor desensitization [44]. To investigate a possible modulation of the ADAM9D chemotactic effect by GPCR, cells were preincubated with PTX, an inhibitor of the Gi protein. The inhibition of the Gi protein impaired neutrophil chemotaxis induced by IL-8 and ADAM9D (**Fig. 6A**). To evaluate the contribution of known chemotactic GPCRs, neutrophils were incubated with 2 different antagonists of CXCR2: RPTX and SB225002. As shown in Figs. 6B and C, both antagonists inhibited neutrophil chemotaxis toward ADAM9D. In contrast, CP105696, a selective BLT1 inhibitor, did not affect neutrophil chemotaxis in response to ADAM9D (Fig. 6D).

Consistent with these data, treatment of neutrophils with the CXCR2 inhibitor SB225002 impaired ADAM9D-induced pAkt (Fig. 6E), reinforcing the participation of CXCR2 on ADAM9D effects on neutrophils. It is important to note that SB225002 was not toxic to cells, as LDH activity in the supernatant of neutrophils incubated with this CXCR2 inhibitor was negligible and similar to those observed for the control group (Fig. 6F).

Finally, with the consideration of the effects of ADAM9D on neutrophils and its dependence on CXCR2 activation, we investigated whether ADAM9D could modulate the IL-8 transcription and CXCR2 membrane expression. In fact, the disintegrin domain was able to increase the levels of IL-8 mRNA significantly (**Fig. 7A**). Curiously, we observed that incubation of

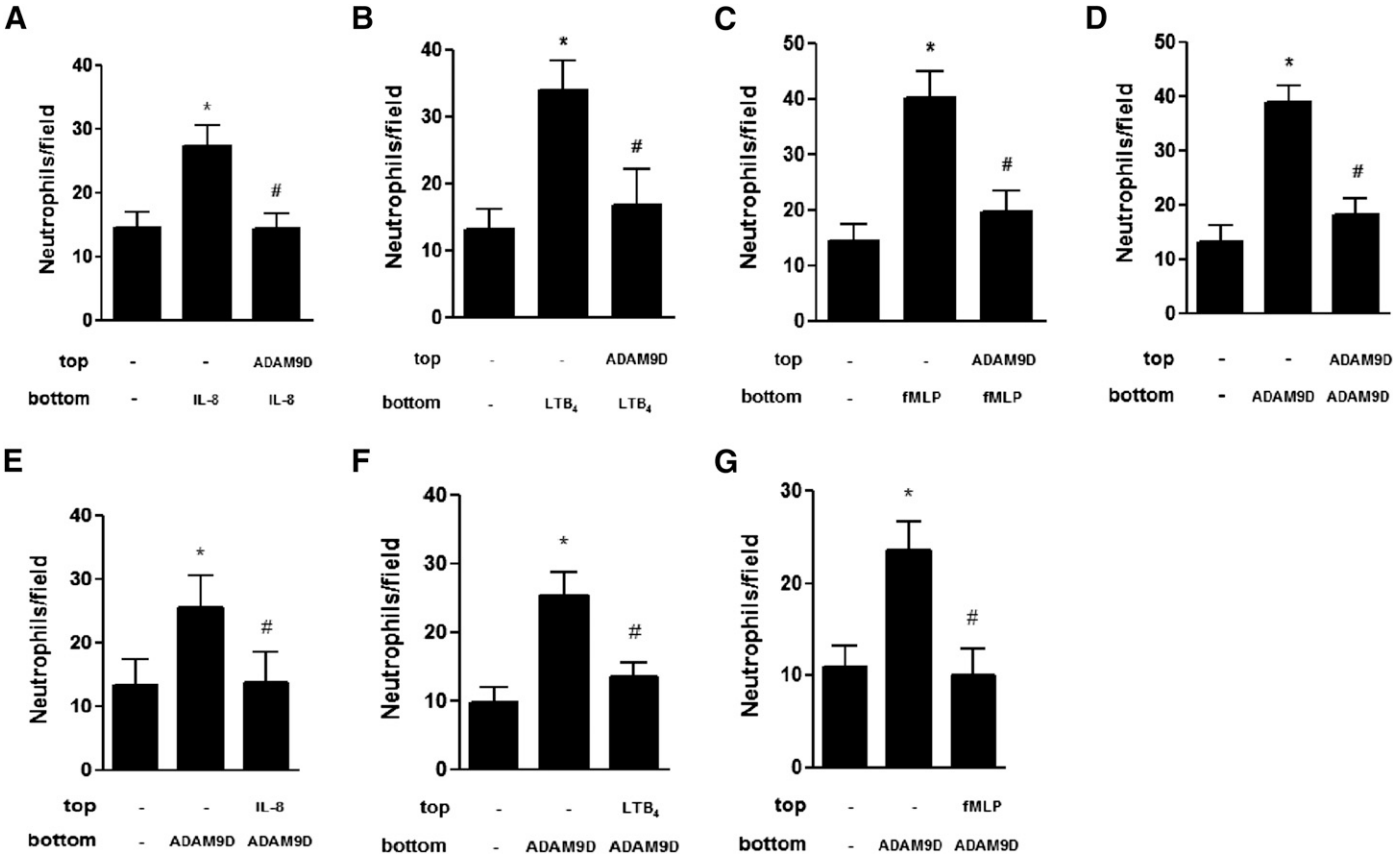

Figure 5. ADAM9D interferes with neutrophil chemotaxis toward other chemoattractants. Neutrophils were preincubated with ADAM9D (100 nM) and then assayed for chemotaxis in response to IL-8 (30 nM; A), LTB_4 (100 nM; B), fMLP (10^{-7} M; C), or ADAM9D itself (100 nM; D). Inversely, neutrophils were preincubated with the same chemoattractants at those same concentrations (IL-8, E; LTB_4, F; or fMLP, G) and assayed for chemotaxis in response to ADAM9D. In the graphs, *x*-axis labels refer to the stimuli used to induce chemotaxis (that were added to the lower of the wells; bottom) and the stimuli used for preincubation (that were present in the upper part of the wells together with neutrophils; top). Data represent mean ± SD of the number of neutrophils/1000× field of view counted under optical microscopy. Data are derived from 3 independent experiments. $*P < 0.05$ compared with negative control; $\#P < 0.05$ relative to unstimulated neutrophils migrating toward the stimulus (positive controls).

neutrophils with ADAM9D did not result in a decrease in CXCR2 membrane expression after 60 or 180 min (Fig. 7B).

DISCUSSION

The present study provides in vitro evidence that ADAM9D can modulate human neutrophil migration by interacting with $\alpha_9\beta_1$ and $\alpha_v\beta_3$ integrins. Moreover, ADAM9D can act as a neutrophil chemoattractant that functions indirectly through the activation of CXCR2 and the PI3K signaling pathway.

Neutrophil activation and migration are key events that depend on cell–cell and cell–matrix interactions occurring during the inflammatory process [45]. We describe herein that ADAM9D can interact with integrins on human neutrophils, activating these cells and inducing chemotaxis, ROS production, NET formation, and delay of neutrophil spontaneous apoptosis. The capacity of other disintegrins to interact with specific integrins on neutrophils and modulate different cell functions has been reported previously by our group [34, 35]. The chemotactic effect of ADAM9D strongly depends on its ability to interact with $\alpha_v\beta_3$ or $\alpha_9\beta_1$ integrins, as this chemotactic effect was inhibited completely by specific neutralizing antibodies. In support of this view, isolated snake venom RGD and non-RGD disintegrins that selectively bind to these integrins were shown to activate neutrophils, induce chemotaxis, and prolong cell survival [34, 35, 46]. Additionally, ADAM9D triggers integrin-associated signaling pathways PI3K/Akt and MAPK, which are canonical pathways involved in neutrophil migration and survival, a behavior previously observed in other disintegrins [34, 35, 46]. The contribution of the PI3K/Akt pathway for cell migration is well demonstrated in studies in vivo with p110γ-deficient mice, which leads to reduced neutrophil chemotaxis [39]. In addition, PI3K is a known prosurvival pathway in neutrophils that can modulate ROS production through the activation of protein kinase C [47]. PI3K/Akt activation in neutrophils, which has already been seen for other disintegrins, can lead to a subsequent phosphorylation of the Erk pathway [35, 41, 45]. Our group showed previously that activation of Erk1/2 is involved in the antiapoptotic effect of $\alpha_9\beta_1$ ligands on neutrophils [35]. Altogether, these findings suggest that ADAM9D is an integrin ligand able to activate integrin-associated signaling and trigger neutrophil functions.

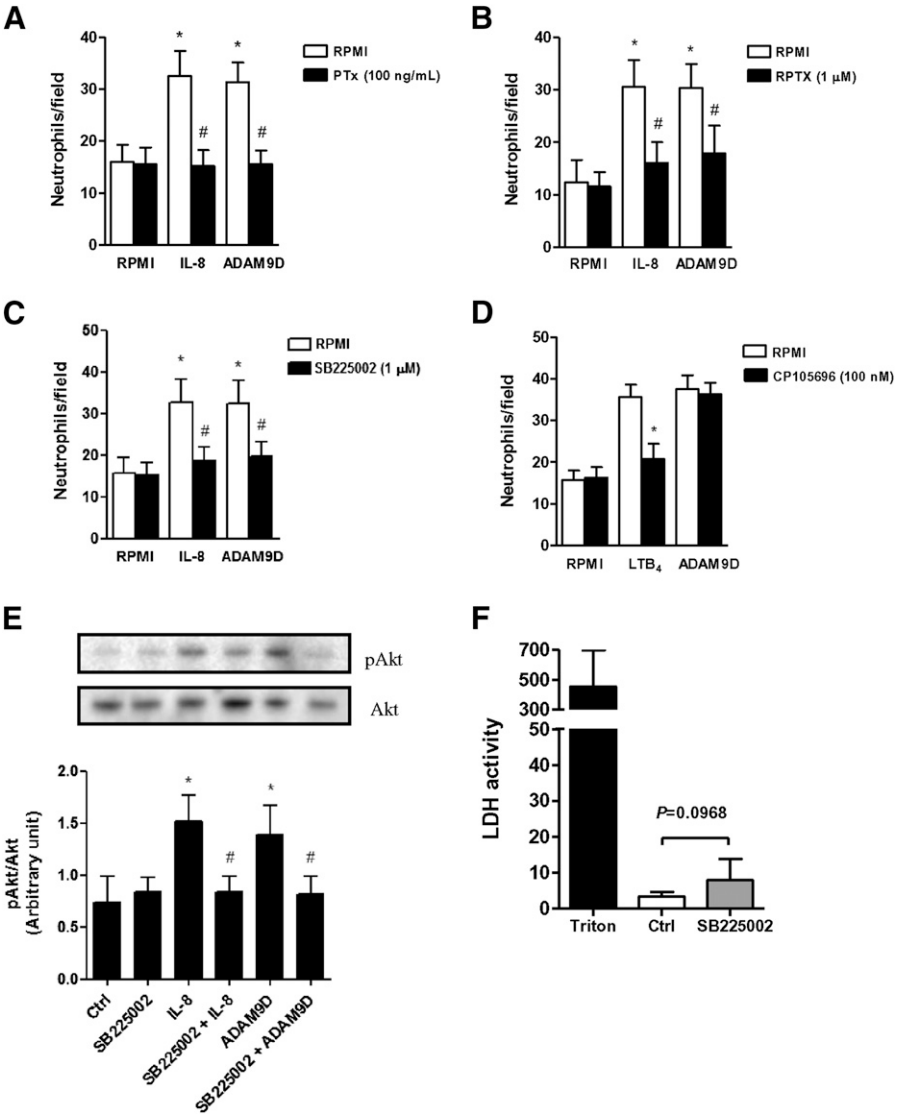

Figure 6. ADAM9D-induced neutrophil chemotaxis requires CXCR2. Neutrophils were preincubated with (A) PTX, (B) RPTX, (C) SB225002, or (D) CP105696 before assaying chemotaxis toward ADAM9D (100 nM; A–D), IL-8 (30 nM; A–C), or LTB_4 (100 nM; D). Data represent mean ± SD of the number of neutrophils/1000× field of view counted under optical microscopy. Data are derived from 3 independent experiments. $*P < 0.05$ compared with negative control; $\#P < 0.05$ relative to neutrophils incubated without inhibitors. (E) Western blot analysis of pAkt in neutrophils preincubated or not with SB225002 (1 μM) and stimulated with ADAM9D (100 nM) or IL-8 (30 nM) for 1 h. Images are derived from 1 representative experiment. The graph shows mean ± SD from 3 independent experiments. $*P < 0.05$ compared with unstimulated neutrophils; $\#P < 0.05$ relative to incubated neutrophils with IL-8 or ADAM9D alone. (F) LDH activity in the supernatant of neutrophils, incubated or not with SB225002. Neutrophils lysed in PBS-Triton were used as positive controls. Data are derived from 3 independent experiments.

Our results also show that once stimulated with ADAM9D, neutrophils are unable to migrate in response to other chemoattractants or to ADAM9D itself. The opposite was also true, as stimulation with IL-8, LTB_4 or fMLP also impaired neutrophil migration toward ADAM9D, indicating a possible heterologous desensitization [48]. A model for neutrophil migration based on a hierarchy among chemoattractants was proposed previously [49]. In this model, the so-called intermediary chemoattractants (such as IL-8 and LTB_4) signal through PI3K, and this signal would be over-ridden by p38 activation triggered by end chemoattractants (such as fMLP and C5a) [47]. Here, we show that neutrophil migration mediated by ADAM9D requires PI3K activation but not pp38. Based on this hierarchy model, ADAM9D (a molecule that signals through PI3K) would not be expected to impair neutrophil chemotaxis toward end chemoattractants, such as fMLP. However, we show that the molecule can also activate other signaling pathways, such as Erk-2, which has been shown to also be involved with cell migration and survival [34, 35, 41, 45]. Thus, the ability of ADAM9D to impair neutrophil chemotaxis may be an outcome of Erk-2 activation. This hypothesis is corroborated by other data depicting Erk-2 activation as a final stop signal to neutrophil migration [50, 51] and supports the hierarchy model in light of our results. Moreover, we show that Erk activation triggered by ADAM9 depends on the PI3K/Akt pathway signaling, as LY294002 (a PI3K/Akt pharmacological inhibitor) inhibited pErk-2 (data not shown).

An interesting feature of ADAM9D effects on human neutrophils was the engagement of G(i)PCR activation, more specifically, CXCR2, modulating disintegrin-induced cell chemotaxis. We show that treatment of neutrophils with PTX (a pan-inhibitor of the Gi protein) or with CXCR2 inhibitors impaired chemotactic responses toward ADAM9D, indicating that the disintegrin effect might be modulated through coactivation of CXCRs. This cross-talk of integrin with a chemotactic receptor seems to be specific for CXCR2, as treatment with an inhibitor of BLT1 had no effect on neutrophil migration. Moreover, inhibition of CXCR2 impairs ADAM9D-induced pAkt, suggesting that PI3K/Akt pathway activation, which is essential for neutrophil chemotaxis, is downstream to the cross-talk of integrin and CXCR2. Recently, our group showed that the effect triggered by

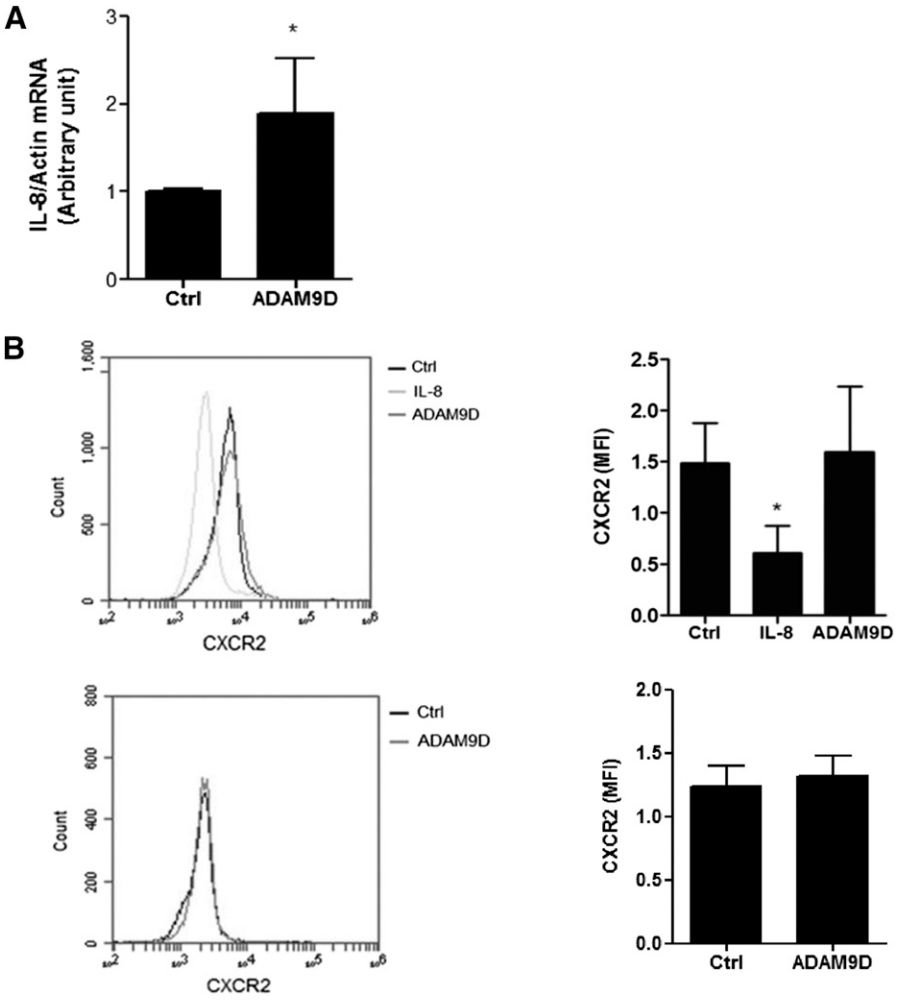

Figure 7. Effects of ADAM9D on IL-8 gene transcription and CXCR2 expression on neutrophils. (A) Neutrophils were incubated or not with ADAM9D (100 nM) for 4 h, and then total mRNA was harvested for analysis of IL-8 mRNA expression by quantitative RT-PCR. Results were normalized by use of actin as a housekeeping gene. Graph represents IL-8 mRNA transcription relative to control. (B) CXCR2 membrane expression in neutrophils, as accessed by FACS analysis in cells stimulated with ADAM9D (100 nM) or IL-8 (30 nM) for 60 min (upper) or 180 min (lower). Histograms are derived from 1 representative experiment, where control cells (black lines), as well as cells stimulated with IL-8 (light gray lines) or ADAM9D (dark gray lines), are represented. Graphs present data from 4 independent experiments and indicate means ± SD of CXCR2 mean fluorescence intensity (MFI). $*P < 0.05$ compared with control cells.

LTB_4 (which exerts its actions through the interactions with BLT1 and BLT2) on VSMC migration depends on the integrin-signaling activation [52]. Additionally, Pruessmeyer et al. [17] show that ADAM10 expressed in human neutrophils and monocytes is required for migration of these immune cells in response to chemotactic stimulus. The presence of such trans-activation mechanisms reinforces our hypothesis of a signaling pathway, where ADAM9D activates human neutrophils through an autocrine circuit involving integrins and CXCR2. On the other hand, even though we observed that ADAM9D is able to induce the synthesis of IL-8 mRNA, we did not observe changes in the expression of CXCR2 on the neutrophil membrane. However, protein synthesis in eukaryotes is a lengthy process that may require >1 h to occur, which could explain the inability of the disintegrin domain to induce receptor internalization in our model. Our results indicate that the engagement of ADAM9D with integrins leads to the activation of CXCR2 through an inside-out signaling axis.

It has been shown that increased expression of ADAM9 positively correlates with tumor development. In accordance, high levels of ADAM9 protein were observed in different tumor types, such as breast [25], prostate [22], lung [21], kidney [24], and melanoma [23]. However, whether there is increased expression of the peptide ADAM9D in tumors remains to be evaluated. Moreover, the mechanisms by which this peptide could be produced inside the tumor microenvironment can only be speculated and may involve shedding of the membrane-bound ADAM9 expressed by tumor cells or the proteolytic cleavage of soluble ADAM9 by proteases secreted by infiltrating leukocytes. The expression or availability of ADAM9D in tumors and how this correlates with clinical outcome in cancer patients should be addressed in future studies.

The ability of tumor cells to produce an immunosuppressive microenvironment that contributes to their growth has been demonstrated [53–55]. In this sense, there is emerging evidence for a role of neutrophils in cancer-associated inflammation [31, 33, 55]. Tumor-infiltrating neutrophils have been reported to modulate the tumor microenvironment to promote cancer progression by stimulating cell migration and invasion and by presenting a proangiogenic activity [31, 33, 55]. Furthermore, it has been shown that the tumor can predispose neutrophils to produce NETs [56], which in turn, sequester circulating tumor cells to new sites, leading to metastasis [57]. Therefore, based on our results, it is tempting to speculate that tumor cells use ADAM9 to interact with neutrophils and modulate their activity to promote tumor development. In this model, ADAM9 secreted by transformed cancer cells would promote neutrophil infiltration into tumor mass. Moreover, ADAM9 would inhibit

neutrophil responses to activating signals, such as IL-8 and formylated peptides. This blunted response would prevent classic neutrophil activation and bias their activation toward an alternative, tumor-promoting phenotype. Future studies should address this hypothesis more closely and investigate, for example, whether ADAM9 expression positively correlates with neutrophil infiltration into tumors.

In a recent report, Roychaudhuri and colleagues [26] showed that neutrophils secrete ADAM9 and that this ADAM9 is able to bind to the neutrophil but only when at high concentrations (2 μM). However, in contrast to our study, they showed that metalloprotease and ADAM9D are dispensable for in vivo neutrophil recruitment to the lung [26]. It is important to note though that neutrophils use different adhesive mechanisms in different tissues. In the liver, for example, selectin engagement and rolling do not occur, and the integrins used for adhesion differ whether neutrophil adhesion is triggered by infection or sterile injury [58]. Therefore, it is possible that the relative contribution of ADAM9 varies with the adhesive mechanisms used by neutrophils, being more relevant in some tissues than others. The adhesive mechanisms used by neutrophils to infiltrate tumors are not well described, and it may be that ADAM9 contributes more significantly to this process than to neutrophil infiltration in lungs.

To our knowledge, our study is the first to report that ADAM9D binds to neutrophil integrins and signals through a cross-talk with CXCRs to activate these cells to migrate. Additionally, ADAM9D can impair neutrophil responses to other chemoattractants in a process that may have profound clinical and therapeutic implications.

AUTHORSHIP

R.S.A. and C.B.-F. designed the research. R.S.A. performed experiments (neutrophil isolation, treatment, chemotaxis, apoptosis, ROS generation, NET formation, Western blotting, CXCR2 expression), analyzed data, and was the primary author of the manuscript. A.C.B.M.M. and H.S.S.-d.-A. were instrumental in providing the ADAM9D. R.S.-G. performed the IL-8 mRNA transcription and adhesion assay and interpreted data. H.A.P.-N. made significant contributions to design of the study and wrote the manuscript. All authors provided important and intellectual input into the research and contributed to discussion of the results, followed by writing and reviewing the manuscript.

ACKNOWLEDGMENTS

This work was supported by Fundação de Amparo à Pesquisa do Estado do Rio de Janeiro (FAPERJ), Coordenação de Aperfeiçoamento de Pessoal de Nível Superior (CAPES), and Conselho Nacional de Desenvolvimento Científico e Tecnológico (CNPq). The authors thank Genilson Rodrigues, RenataTureta, and Gabrielle Estevão for technical support.

DISCLOSURES

The authors declare no conflicts of interest.

REFERENCES

1. Nauseef, W. M., Borregaard, N. (2014) Neutrophils at work. *Nat. Immunol.* **15,** 602–611.
2. Bardoel, B. W., Kenny, E. F., Sollberger, G., Zychlinsky, A. (2014) The balancing act of neutrophils. *Cell Host Microbe* **15,** 526–536.
3. Smith, C. W., Rothlein, R., Hughes, B. J., Mariscalco, M. M., Rudloff, H. E., Schmalstieg, F. C., Anderson, D. C. (1988) Recognition of an endothelial determinant for CD 18-dependent human neutrophil adherence and transendothelial migration. *J. Clin. Invest.* **82,** 1746–1756.
4. Gonzalez, A. L., El-Bjeirami, W., West, J. L., McIntire, L. V., Smith, C. W. (2007) Transendothelial migration enhances integrin-dependent human neutrophil chemokinesis. *J. Leukoc. Biol.* **81,** 686–695.
5. Ley, K., Laudanna, C., Cybulsky, M. I., Nourshargh, S. (2007) Getting to the site of inflammation: the leukocyte adhesion cascade updated. *Nat. Rev. Immunol.* **7,** 678–689.
6. Berton, G., Yan, S. R., Fumagalli, L., Lowell, C. A. (1996) Neutrophil activation by adhesion: mechanisms and pathophysiological implications. *Int. J. Clin. Lab. Res.* **26,** 160–177.
7. Streuli, C. H. (2009) Integrins and cell-fate determination. *J. Cell Sci.* **122,** 171–177.
8. Lawrence, M. B., Springer, T. A. (1991) Leukocytes roll on a selectin at physiologic flow rates: distinction from and prerequisite for adhesion through integrins. *Cell* **65,** 859–873.
9. Nath, D., Slocombe, P. M., Webster, A., Stephens, P. E., Docherty, A. J. P., Murphy, G. (2000) Meltrin γ(ADAM-9) mediates cellular adhesion through α(6)β(1)integrin, leading to a marked induction of fibroblast cell motility. *J. Cell Sci.* **113,** 2319–2328.
10. Eto, K., Huet, C., Tarui, T., Kupriyanov, S., Liu, H. Z., Puzon-McLaughlin, W., Zhang, X. P., Sheppard, D., Engvall, E., Takada, Y. (2002) Functional classification of ADAMs based on a conserved motif for binding to integrin alpha 9beta 1: implications for sperm-egg binding and other cell interactions. *J. Biol. Chem.* **277,** 17804–17810.
11. Bridges, L. C., Hanson, K. R., Tani, P. H., Mather, T., Bowditch, R. D. (2003) Integrin alpha4beta1-dependent adhesion to ADAM 28 (MDC-L) requires an extended surface of the disintegrin domain. *Biochemistry* **42,** 3734–3741.
12. Sun, C., Wu, M. H., Guo, M., Day, M. L., Lee, E. S., Yuan, S. Y. (2010) ADAM15 regulates endothelial permeability and neutrophil migration via Src/ERK1/2 signalling. *Cardiovasc. Res.* **87,** 348–355.
13. Duffy, M. J., McKiernan, E., O'Donovan, N., McGowan, P. M. (2009) The role of ADAMs in disease pathophysiology. *Clin. Chim. Acta* **403,** 31–36.
14. Sahin, U., Weskamp, G., Kelly, K., Zhou, H. M., Higashiyama, S., Peschon, J., Hartmann, D., Saftig, P., Blobel, C. P. (2004) Distinct roles for ADAM10 and ADAM17 in ectodomain shedding of six EGFR ligands. *J. Cell Biol.* **164,** 769–779.
15. Bell, J. H., Herrera, A. H., Li, Y., Walcheck, B. (2007) Role of ADAM17 in the ectodomain shedding of TNF-α and its receptors by neutrophils and macrophages. *J. Leukoc. Biol.* **82,** 173–176.
16. Möller-Hackbarth, K., Dewitz, C., Schweigert, O., Trad, A., Garbers, C., Rose-John, S., Scheller, J. (2013) A disintegrin and metalloprotease (ADAM) 10 and ADAM17 are major sheddases of T cell immunoglobulin and mucin domain 3 (Tim-3). *J. Biol. Chem.* **288,** 34529–34544.
17. Pruessmeyer, J., Hess, F. M., Alert, H., Groth, E., Pasqualon, T., Schwarz, N., Nyamoya, S., Kollert, J., van der Vorst, E., Donners, M., Martin, C., Uhlig, S., Saftig, P., Dreymueller, D., Ludwig, A. (2014) Leukocytes require ADAM10 but not ADAM17 for their migration and inflammatory recruitment into the alveolar space. *Blood* **123,** 4077–4088.
18. Zigrino, P., Nischt, R., Mauch, C. (2011) The disintegrin-like and cysteine-rich domains of ADAM-9 mediate interactions between melanoma cells and fibroblasts. *J. Biol. Chem.* **286,** 6801–6807.
19. Namba, K., Nishio, M., Mori, K., Miyamoto, N., Tsurudome, M., Ito, M., Kawano, M., Uchida, A., Ito, Y. (2001) Involvement of ADAM9 in multinucleated giant cell formation of blood monocytes. *Cell. Immunol.* **213,** 104–113.
20. Oksala, N., Levula, M., Airla, N., Pelto-Huikko, M., Ortiz, R. M., Järvinen, O., Salenius, J. P., Ozsait, B., Komurcu-Bayrak, E., Erginel-Unaltuna, N., Huovila, A. P., Kytömäki, L., Soini, J. T., Kähönen, M., Karhunen, P. J., Laaksonen, R., Lehtimäki, T. (2009) ADAM-9, ADAM-15, and ADAM-17 are upregulated in macrophages in advanced human atherosclerotic plaques in aorta and carotid and femoral arteries—Tampere vascular study. *Ann. Med.* **41,** 279–290.
21. Shintani, Y., Higashiyama, S., Ohta, M., Hirabayashi, H., Yamamoto, S., Yoshimasu, T., Matsuda, H., Matsuura, N. (2004) Overexpression of ADAM9 in non-small cell lung cancer correlates with brain metastasis. *Cancer Res.* **64,** 4190–4196.
22. Peduto, L., Reuter, V. E., Shaffer, D. R., Scher, H. I., Blobel, C. P. (2005) Critical function for ADAM9 in mouse prostate cancer. *Cancer Res.* **65,** 9312–9319.
23. Zigrino, P., Mauch, C., Fox, J. W., Nischt, R. (2005) Adam-9 expression and regulation in human skin melanoma and melanoma cell lines. *Int. J. Cancer* **116,** 853–859.

24. Fritzsche, F. R., Wassermann, K., Jung, M., Tölle, A., Kristiansen, I., Lein, M., Johannsen, M., Dietel, M., Jung, K., Kristiansen, G. (2008) ADAM9 is highly expressed in renal cell cancer and is associated with tumour progression. *BMC Cancer* **8,** 179.
25. Fry, J. L., Toker, A. (2010) Secreted and membrane-bound isoforms of protease ADAM9 have opposing effects on breast cancer cell migration. *Cancer Res.* **70,** 8187–8198.
26. Roychaudhuri, R., Hergrueter, A. H., Polverino, F., Laucho-Contreras, M. E., Gupta, K., Borregaard, N., Owen, C. A. (2014) ADAM9 is a novel product of polymorphonuclear neutrophils: regulation of expression and contributions to extracellular matrix protein degradation during acute lung injury. *J. Immunol.* **193,** 2469–2482.
27. Mazzocca, A., Coppari, R., De Franco, R., Cho, J. Y., Libermann, T. A., Pinzani, M., Toker, A. (2005) A secreted form of ADAM9 promotes carcinoma invasion through tumor-stromal interactions. *Cancer Res.* **65,** 4728–4738.
28. Jia, L. G., Shimokawa, K., Bjarnason, J. B., Fox, J. W. (1996) Snake venom metalloproteinases: structure, function and relationship to the ADAMs family of proteins. *Toxicon* **34,** 1269–1276.
29. Karadag, A., Zhou, M., Croucher, P. I. (2006) ADAM-9 (MDC-9/meltrin-gamma), a member of the a disintegrin and metalloproteinase family, regulates myeloma-cell-induced interleukin-6 production in osteoblasts by direct interaction with the alpha(v)beta5 integrin. *Blood* **107,** 3271–3278.
30. Cominetti, M. R., Martin, A. C., Ribeiro, J. U., Djaafri, I., Fauvel-Lafève, F., Crépin, M., Selistre-de-Araujo, H. S. (2009) Inhibition of platelets and tumor cell adhesion by the disintegrin domain of human ADAM9 to collagen I under dynamic flow conditions. *Biochimie* **91,** 1045–1052.
31. Jamieson, T., Clarke, M., Steele, C. W., Samuel, M. S., Neumann, J., Jung, A., Huels, D., Olson, M. F., Das, S., Nibbs, R. J., Sansom, O. J. (2012) Inhibition of CXCR2 profoundly suppresses inflammation-driven and spontaneous tumorigenesis. *J. Clin. Invest.* **122,** 3127–3144.
32. Gong, L., Cumpian, A. M., Caetano, M. S., Ochoa, C. E., De la Garza, M. M., Lapid, D. J., Mirabolfathinejad, S. G., Dickey, B. F., Zhou, Q., Moghaddam, S. J. (2013) Promoting effect of neutrophils on lung tumorigenesis is mediated by CXCR2 and neutrophil elastase. *Mol. Cancer* **12,** 154.
33. Jablonska, J., Wu, C. F., Andzinski, L., Leschner, S., Weiss, S. (2014) CXCR2-mediated tumor-associated neutrophil recruitment is regulated by IFN-β. *Int. J. Cancer* **134,** 1346–1358.
34. Coelho, A. L., De Freitas, M. S., Mariano-Oliveira, A., Oliveira-Carvalho, A. L., Zingali, R. B., Barja-Fidalgo, C. (2001) Interaction of disintegrins with human neutrophils induces cytoskeleton reorganization, focal adhesion kinase activation, and extracellular-regulated kinase-2 nuclear translocation, interfering with the chemotactic function. *FASEB J.* **15,** 1643–1645.
35. Saldanha-Gama, R. F., Moraes, J. A., Mariano-Oliveira, A., Coelho, A. L., Walsh, E. M., Marcinkiewicz, C., Barja-Fidalgo, C. (2010) alpha(9)beta(1) Integrin engagement inhibits neutrophil spontaneous apoptosis: involvement of Bcl-2 family members. *Biochim. Biophys. Acta* **1803,** 848–857.
36. Marcinkiewicz, C., Rosenthal, L. A., Mosser, D. M., Kunicki, T. J., Niewiarowski, S. (1996) Immunological characterization of eristostatin and echistatin binding sites on alpha IIb beta 3 and alpha V beta 3 integrins. *Biochem. J.* **317,** 817–825.
37. Nathan, C. F. (1987) Neutrophil activation on biological surfaces. Massive secretion of hydrogen peroxide in response to products of macrophages and lymphocytes. *J. Clin. Invest.* **80,** 1550–1560.
38. Mahimkar, R. M., Visaya, O., Pollock, A. S., Lovett, D. H. (2005) The disintegrin domain of ADAM9: a ligand for multiple beta1 renal integrins. *Biochem. J.* **385,** 461–468.
39. Hirsch, E., Katanaev, V. L., Garlanda, C., Azzolino, O., Pirola, L., Silengo, L., Sozzani, S., Mantovani, A., Altruda, F., Wymann, M. P. (2000) Central role for G protein-coupled phosphoinositide 3-kinase gamma in inflammation. *Science* **287,** 1049–1053.
40. Heit, B., Liu, L., Colarusso, P., Puri, K. D., Kubes, P. (2008) PI3K accelerates, but is not required for, neutrophil chemotaxis to fMLP. *J. Cell Sci.* **121,** 205–214.
41. Coelho, A. L., De Freitas, M. S., Mariano-Oliveira, A., Rapozo, D. C., Pinto, L. F., Niewiarowski, S., Zingali, R. B., Marcinkiewicz, C., Barja-Fidalgo, C. (2004) RGD- and MLD-disintegrins, jarastatin and EC3, activate integrin-mediated signaling modulating the human neutrophils chemotaxis, apoptosis and IL-8 gene expression. *Exp. Cell Res.* **292,** 371–384.
42. Paula-Neto, H. A., Alves-Filho, J. C., Souto, F. O., Spiller, F., Amêndola, R. S., Freitas, A., Cunha, F. Q., Barja-Fidalgo, C. (2011) Inhibition of guanylyl cyclase restores neutrophil migration and maintains bactericidal activity increasing survival in sepsis. *Shock* **35,** 17–27.
43. Walther, A., Riehemann, K., Gerke, V. (2000) A novel ligand of the formyl peptide receptor: annexin I regulates neutrophil extravasation by interacting with the FPR. *Mol. Cell* **5,** 831–840.
44. Cotton, M., Claing, A. (2009) G Protein-coupled receptors stimulation and the control of cell migration. *Cell. Signal.* **21,** 1045–1053.
45. Zarbock, A., Ley, K. (2008) Mechanisms and consequences of neutrophil interaction with the endothelium. *Am. J. Pathol.* **172,** 1–7.
46. Mariano-Oliveira, A., Coelho, A. L., Terruggi, C. H., Selistre-de-Araújo, H. S., Barja-Fidalgo, C., De Freitas, M. S. (2003) Alternagin-C, a nonRGD-disintegrin, induces neutrophil migration via integrin signaling. *Eur. J. Biochem.* **270,** 4799–4808.
47. Arruda, M. A., Barcellos-de-Souza, P., Sampaio, A. L., Rossi, A. G., Graça-Souza, A. V., Barja-Fidalgo, C. (2006) NADPH oxidase-derived ROS: key modulators of heme-induced mitochondrial stability in human neutrophils. *Exp. Cell Res.* **312,** 3939–3948.
48. Stanton, K. J., Frewin, M. B., Gudewicz, P. W. (1999) Heterologous desensitization of IL-8-mediated chemotaxis in human neutrophils by a cell-binding fragment of fibronectin. *J. Leukoc. Biol.* **65,** 515–522.
49. Heit, B., Tavener, S., Raharjo, E., Kubes, P. (2002) An intracellular signaling hierarchy determines direction of migration in opposing chemotactic gradients. *J. Cell Biol.* **159,** 91–102.
50. Hu, Q., Klippel, A., Muslin, A. J., Fantl, W. J., Williams, L. T. (1995) Ras-dependent induction of cellular responses by constitutively active phosphatidylinositol-3 kinase. *Science* **268,** 100–102.
51. Liu, X., Ma, B., Malik, A. B., Tang, H., Yang, T., Sun, B., Wang, G., Minshall, R. D., Li, Y., Zhao, Y., Ye, R. D., Xu, J. (2012) Bidirectional regulation of neutrophil migration by mitogen-activated protein kinases. *Nat. Immunol.* **13,** 457–464.
52. Moraes, J., Assreuy, J., Canetti, C., Barja-Fidalgo, C. (2010) Leukotriene B4 mediates vascular smooth muscle cell migration through αvβ3 integrin transactivation. *Atherosclerosis* **212,** 406–413.
53. Halliday, G. M., Le, S. (2001) Transforming growth factor-beta produced by progressor tumors inhibits, while IL-10 produced by regressor tumors enhances, Langerhans cell migration from skin. *Int. Immunol.* **13,** 1147–1154.
54. Bekeredjian-Ding, I., Schäfer, M., Hartmann, E., Pries, R., Parcina, M., Schneider, P., Giese, T., Endres, S., Wollenberg, B., Hartmann, G. (2009) Tumour-derived prostaglandin E and transforming growth factor-beta synergize to inhibit plasmacytoid dendritic cell-derived interferon-alpha. *Immunology* **128,** 439–450.
55. Fridlender, Z. G., Sun, J., Kim, S., Kapoor, V., Cheng, G., Ling, L., Worthen, G. S., Albelda, S. M. (2009) Polarization of tumor-associated neutrophil phenotype by TGF-beta: "N1" versus "N2" TAN. *Cancer Cell* **16,** 183–194.
56. Demers, M., Krause, D. S., Schatzberg, D., Martinod, K., Voorhees, J. R., Fuchs, T. A., Scadden, D. T., Wagner, D. D. (2012) Cancers predispose neutrophils to release extracellular DNA traps that contribute to cancer-associated thrombosis. *Proc. Natl. Acad. Sci. USA* **109,** 13076–13081.
57. Cools-Lartigue, J., Spicer, J., McDonald, B., Gowing, S., Chow, S., Giannias, B., Bourdeau, F., Kubes, P., Ferri, L. (2013) Neutrophil extracellular traps sequester circulating tumor cells and promote metastasis. *J. Clin. Invest.* **123,** 3446–3458.
58. Jenne, C. N., Kubes, P. (2013) Immune surveillance by the liver. *Nat. Immunol.* **14,** 996–1006.

KEY WORDS:
signal transduction · granulocyte · chemotaxis · apoptosis · IL-8

Journal of Pathology
J Pathol 2015
Published online in Wiley Online Library
(wileyonlinelibrary.com) DOI: 10.1002/path.4490

ORIGINAL PAPER

Tumour but not stromal expression of β3 integrin is essential, and is required early, for spontaneous dissemination of bone-metastatic breast cancer

Rachel Zoe Carter,[1#] Kelli Cristina Micocci,[2#] Anthony Natoli,[1] Richard Paul Redvers,[1] Sophie Paquet-Fifield,[3] Ana Carolina Baptista Moreno Martin,[2] Delphine Denoyer,[1] Xiawei Ling,[1] Soo-Hyun Kim,[1,4] Rebeka Tomasin,[6] Heloisa Selistre-de-Araújo,[2] Robin Lesley Anderson[1,4,5‡] and Normand Pouliot[1,4,5‡,*]

[1] *Metastasis Research Laboratory, Peter MacCallum Cancer Centre, Melbourne, Australia*
[2] *Department of Physiological Sciences, Federal University of São Carlos, Brazil*
[3] *Endothelial Regulation Laboratory, Peter MacCallum Cancer Centre, Melbourne, Australia*
[4] *Department of Pathology, University of Melbourne, Australia*
[5] *Sir Peter MacCallum Department of Oncology, University of Melbourne, Australia*
[6] *Laboratory of Nutrition and Cancer, Department of Functional and Structural Biology, Institute of Biology, State University of Campinas, São Paulo, Brazil*

**Correspondence to: Normand Pouliot, Peter MacCallum Cancer Centre, Locked Bag 1, A'Beckett Street, Melbourne, Victoria 8006, Australia. e-mail: normand.pouliot@petermac.org*

‡Co-senior authors
#These authors contributed equally to this study.

Abstract

Although many preclinical studies have implicated β3 integrin receptors (αvβ3 and αIIbβ3) in cancer progression, β3 inhibitors have shown only modest efficacy in patients with advanced solid tumours. The limited efficacy of β3 inhibitors in patients could arise from our incomplete understanding of the precise function of β3 integrin and, consequently, inappropriate clinical application. Data from animal studies are conflicting and indicate heterogeneity with respect to the relative contributions of β3-expressing tumour and stromal cell populations in different cancers. Here we aimed to clarify the function and relative contributions to metastasis of tumour versus stromal β3 integrin in clinically relevant models of spontaneous breast cancer metastasis, with particular emphasis on bone metastasis. We show that stable down-regulation of tumour β3 integrin dramatically impairs spontaneous (but not experimental) metastasis to bone and lung without affecting primary tumour growth in the mammary gland. Unexpectedly, and in contrast to subcutaneous tumours, orthotopic tumour vascularity, growth and spontaneous metastasis were not altered in mice null for β3 integrin. Tumour β3 integrin promoted migration, protease expression and trans-endothelial migration *in vitro* and increased vascular dissemination *in vivo*, but was not necessary for bone colonization in experimental metastasis assays. We conclude that tumour, rather than stromal, β3 expression is essential and is required early for efficient spontaneous breast cancer metastasis to bone and soft tissues. Accordingly, differential gene expression analysis in cohorts of breast cancer patients showed a strong association between high β3 expression, early metastasis and shorter disease-free survival in patients with oestrogen receptor-negative tumours. We propose that β3 inhibitors may be more efficacious if used in a neoadjuvant setting, rather than after metastases are established.

Keywords: breast cancer; β3 integrin; bone metastasis; syngeneic mouse model; vitronectin; DisBa-01

Received 23 July 2014; Revised 9 November 2014; Accepted 25 November 2014

No conflicts of interest were declared.

Introduction

β3 integrins (αvβ3 and αIIbβ3) mediate cellular adhesion to extracellular matrix (ECM) substrates, including vitronectin, bone sialoprotein, osteopontin and fibrinogen, and are attractive therapeutic targets for metastatic cancers [1]. Studies employing αv or β3 inhibitors demonstrate that αvβ3 integrin regulates multiple cellular responses required for metastasis, including cell survival, migration, invasion through the ECM and angiogenesis [2]. However, while high β3 integrin expression is reported in several cancer types [3–8], its prognostic significance is still unclear. Tumour expression of αvβ3 integrin correlates inversely with invasive and metastatic behaviours in some melanoma and ovarian cancer lines [9,10] and is associated with better survival in ovarian cancer patients [10]. Enhanced αvβ3 levels in bone metastases compared to matched

primary breast tumours have been reported in some [4,11], but not all [5], studies.

Preclinical studies evaluating the function of αvβ3 in breast cancer bone metastasis have been limited by lack of robust and clinically relevant animal models. High levels of αvβ3 in a bone metastatic subline of human MDA-MB-231 breast tumour cells (BO2) [12], or exogenous expression of β3 integrin in parental cells [5], correlate with increased adhesion to cortical bone and an increased number of osteolytic lesions in mice compared to parental cells, following tail vein injection. We showed previously that exogenous expression of β3 integrin in weakly metastatic 66 cl4 mammary carcinoma cells, that otherwise do not express αvβ3 or spread to bone from the mammary gland, is sufficient to promote their spontaneous metastasis to bone without altering orthotopic tumour growth in immunocompetent mice [13]. While the above studies employing β3 over-expression showed that tumour αvβ3 integrin can 'contribute' to bone metastasis, whether expression of αvβ3 is 'essential' for spontaneous bone metastasis has yet to be demonstrated. Clinically, this distinction is important, since the effectiveness of therapies targeting tumour αvβ3 and their impact on bone metastasis and patient survival will be dictated by the dependency of tumours on αvβ3 integrin for successful metastasis. To our knowledge, the efficacy of αvβ3 integrin antagonists specifically against bone metastases has not been evaluated in patients.

Discrepancies also exist with regard to the precise contribution of β3 integrin expressed on stromal lineages to tumour growth and metastasis [14–20]. MMTV-c-neu transgenic mice null for either β3 or β3 and β5 integrins show no apparent changes in mammary tumour growth and vascularization compared to normal MMTV-c-neu mice [20]. This contrasts with the anti-tumour/anti-angiogenic effects of αv or β3 inhibitors against subcutaneous melanoma and breast tumours [21–23] and with the enhanced growth and angiogenesis of transplanted melanoma, lung and colon tumours in β3-null mice [16,19]. Moreover, while experimental melanoma metastasis to bone is decreased in β3-null compared to wild-type mice [17], loss of β3 integrin has no impact on the spontaneous metastasis of mammary tumours to lung in MMTV-c-neu mice null for β3 [20]. Importantly, since none of these models metastasize spontaneously to bone, the role of stromal β3 integrin in spontaneous metastasis to bone remains unknown. Collectively, these observations, derived from various animal models of metastasis, indicate that regulation of tumour growth, vascularization and metastasis by tumour and stromal β3 integrin is likely to vary between tumour types and sites of tumour growth. These differences may account for the limited efficacy of integrin inhibitors in advanced cancer patients with solid tumours [2,24–34]. Accordingly, improvement in the efficacy of β3 integrin inhibitors in patients with metastatic cancer may require a reappraisal of the precise contribution of β3-type receptors to the growth and metastasis of each tumour type.

Here, using clinically relevant mouse models of breast cancer metastasis to bone [35–37], a combination of *in vitro* assays, gene knockdown and β3-null mice, we demonstrate that β3 integrin in tumour cells, but not in stromal cells, is essential for spontaneous breast cancer metastasis and is required early for vascular dissemination to bone and other tissues. These findings have important implications for the design of therapies targeting β3 integrin in breast cancer patients.

Materials and methods

Cell culture

66 cl4 mammary carcinoma cells stably expressing β3 integrin (66cl4pBabeβ3^{high}) and control empty pBabe-puro retroviral vector (66cl4pBabe) were described previously [13]. Bone-metastatic 4 T1.2 with hygromycin resistance and 4 T1BM2 with mCherry expression were derived from 4 T1 cells [35–38]. All lines were maintained for up to 4 weeks in α-minimal essential medium (αMEM)/5% fetal calf serum (FCS)/1% penicillin–streptomycin at 37 °C, 5% CO_2. bEnd.3 murine microvascular endothelial cells, provided by Dr R Hallman (Jubileum Institute, Sweden), were cultured as described [13].

Knockdown of β3 integrin

Two oligonucleotides targeting β_3 integrin (NM-016780: sh1, AAGGATGATCTGTCCACGATC; and sh2, AGCAAACAACCCGCTGTATAA, start position 2387) were inserted into pRetroSuper (sh1) or pLMP (sh2) retroviral vectors, using standard methodology [35]. A non-targeting sequence (AGTACTGCTTACGATACGG) was used as control. Viral supernatants from transfection of PT67 packaging cells were used to infect 4 T1.2 (sh1 hairpin) and 4 T1BM2 (sh2 hairpin) cells. Cells expressing low levels of β3 integrin were isolated by flow cytometry, expanded in culture and frozen. Changes in integrin receptor expression were analysed by standard flow cytometry [13,39]. The primary antibodies used are described in Supplementary materials and methods (see supplementary material).

In vitro assays

Proliferation, adhesion and migration assays [13,35,36,39], zymography [40] and immunoblotting [41] are described in Supplementary materials and methods (see supplementary material). For trans-endothelial migration, bEnd.3 cells (1×10^5) were seeded in triplicate Transwell inserts and incubated at 37 °C for 24 h to form a monolayer. Adherent cells were washed with phosphate-buffered saline (PBS) and calcein-labelled tumour cells (2×10^5) were added to the insert in 200 µl serum-free αMEM/glutamine (2 mM)/bovine serum albumin (BSA; 0.05%)/sodium pyruvate (1 mM) and antibiotics. Medium containing 10% FCS was added to

the bottom chambers as a chemoattractant. After 48 h of incubation at 37 °C, migrated tumour cells on the underside [green (calcein) cytoplasm and red (propidium iodide) nucleus] (three random × 20 fields) were photographed on an Olympus BX-61 microscope and counted using Metamorph (Molecular Devices).

Tumour growth and metastasis

Procedures involving mice were completed in accordance with National Health and Medical Research Council ethics guidelines and approved by the Peter MacCallum Animal Ethics Committee. Wild-type female Balb/c mice were purchased from the Walter and Eliza Hall Institute (Australia). β3-null mice [42] were backcrossed to a Balb/c background (10 generations).

For spontaneous metastasis assays, 8–10 week-old mice were inoculated with 10^5 cells into the fourth mammary fat pad. Tumour growth was measured using electronic calipers [13,35] and the mice were harvested as a group on day 30, or earlier if showing signs of distress due to metastatic disease. Analysis of tumour microvascular density [43] is described in Supplementary materials and methods (see supplementary material). Lungs, femurs and spines were snap-frozen in liquid nitrogen before processing for relative tumour burden (RTB) quantitation by real-time qPCR of the tumour-expressed reporter gene, as described previously [13,35,40]. For experimental bone metastasis assays, 5×10^4 (4 T1.2 and 4 T1BM2 cells) or 1×10^5 (66 cl4) cells/100 µl PBS were injected into the left cardiac ventricle [44]. These mice were harvested as a group on day 15, or earlier if showing signs of distress. Specific primers and probes are detailed in Supplementary materials and methods (see supplementary material). When comparing metastatic burden from two tumour lines, RTB values were adjusted for reporter gene copy number, calculated from the level in genomic DNA in cultured cells.

Statistical analysis

Data were analysed using Prism 5.01 for Windows. For *in vitro* assays comparing multiple groups, a one-way ANOVA Tukey's multiple comparisons test was completed. Proliferation assays were evaluated by two-way ANOVA with Bonferroni post-test. For *in vivo* assays, Fisher's exact test was used for metastatic incidence and a Mann–Whitney test was completed for metastatic burden analysis. $p \leq 0.05$ was considered significant.

Results

Knockdown of β3 integrin in bone metastatic tumour cells

Exogenous expression of β3 in weakly lung-metastatic 66 cl4 cells contributes to their spontaneous metastasis from the mammary gland to bone [13]. However, this approach does not reveal an essential requirement for bone metastasis, a critical consideration for anti-metastatic therapy. To address this, β3 integrin expression was reduced by stable expression of RNA interference vectors encoding separate hairpins in 4 T1.2 (sh1) and 4 T1BM2 (sh2) cells. These models were chosen for their clinical relevance, with both expressing αvβ3 integrin and, unlike xenograft models, metastasizing spontaneously to bone, with high incidence from mammary tumours in immunocompetent mice [36,37].

β3 expression was substantially reduced in 4 T1BM2-β3lo compared to 4 T1BM2-ctrl and parental 4 T1BM2 cells and accompanied by down-regulation of αv integrin at the cell surface (Figure 1A, B; see also supplementary material, Figure S1A). Suppression of β3 transcript levels in 4 T1BM2-β3lo cells was confirmed by qRT–PCR (Figure 1C). Despite reduced surface levels of αv integrin, α*v* mRNA expression was not decreased (Figure 1D). Moreover, western blot analysis of whole-cell lysates showed that total αv protein levels in 4 T1BM2-ctrl and 4 T1BM2-β3lo cells were similar to parental cells (87% and 85% of parental cells, respectively) and not significantly different from each other when normalized to tubulin (Figure 1E). Thus, surface localization, rather than expression of αv integrin, is impaired by suppression of β3 integrin. Sustained, coordinated down-regulation of surface β3 and αv integrins was also observed using a different β3-targeting shRNA in 4 T1.2 bone-metastatic cells (see supplementary material, Figure S1B). The overall expression pattern of other integrins was comparable between 4 T1BM2 and 4 T1.2 parental lines (see supplementary material, Figure S2A, B), with the exception that α2 was expressed at low levels in 4 T1.2 but not in 4 T1BM2 cells. The expression of α2, α3, α5, α6, β1, β4, β5 and β6 integrin subunits was not significantly altered in 4 T1BM2-β3lo cells compared to 4 T1BM2-ctrl cells, whereas 4 T1.2 cells showed a small increase in α6 and β4 subunits following β3 down-regulation.

Suppression of β3 integrin inhibits spontaneous metastasis to bone and soft tissues without altering primary tumour growth

Adhesion of all lines to uncoated plastic (30 min) was negligible, irrespective of β3 integrin levels (Figure 2A; see also supplementary material, Figure S3A). As expected, adhesion of 4 T1BM2-β3lo and 4 T1.2-β3lo cells to vitronectin, the classical αvβ3 integrin ligand, was decreased (45–60% inhibition) compared to cells expressing a non-targeting shRNA. Adhesion to laminin (LM)-511 was unaffected by β3 suppression. Similarly, haptotactic migration towards vitronectin, but not LM-511, was significantly inhibited by β3 suppression (Figure 2B; see also supplementary material, Figure S3B), indicating that reduced adhesion and migration of cells with low β3 expression are substrate-specific. Proliferation of 4 T1BM2 and 4 T1.2 cells was unaffected by β3 integrin down-regulation (Figure 2C; see also supplementary material, Figure S3C).

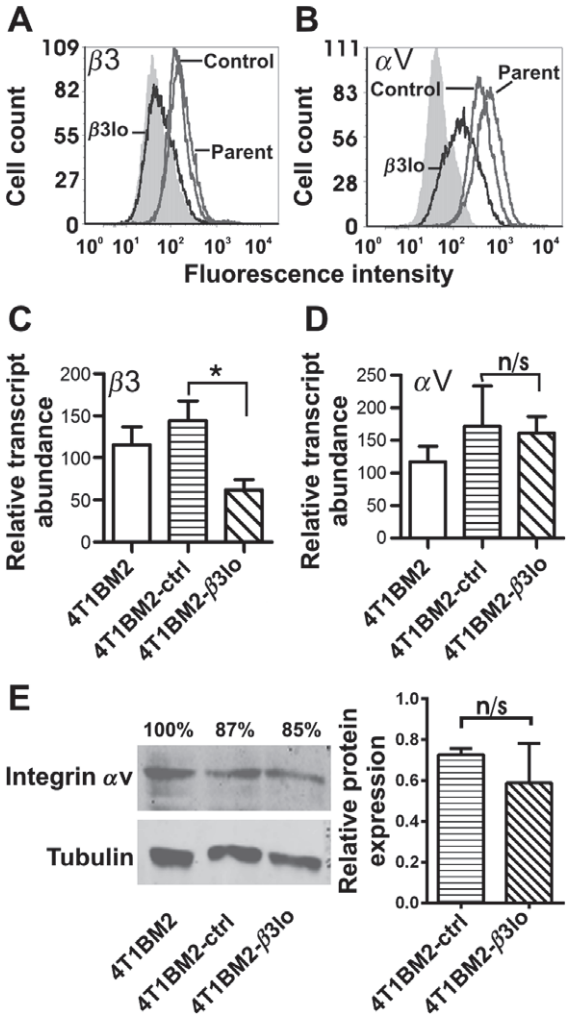

Figure 1. Stable suppression of β3 integrin expression induces coordinated down-regulation of αv integrin subunits at the cell surface. Parental 4T1BM2 cells (Parent) and cells expressing a non-targeting (Control) or a β3-targeting shRNA (β3lo) were analysed for the expression of β3 (A) and αv (B) integrins by standard flow cytometry; solid grey, isotype control antibody. β3 (C) and αv (D) mRNA transcripts were analysed by qRT–PCR; graph shows mean transcript abundance relative to *GAPDH* ± SEM of nine independent replicates; $*p < 0.05$; one-way ANOVA, Tukey's multiple comparisons test. (E) Representative western blot analysis of total integrin αv and tubulin (loading control) detected in whole-cell lysates (left) and quantitation of triplicate samples of 4T1BM2-ctrl versus 4T1BM2-β3lo (right) by densitometry; n/s, not significant; $p = 0.700$

In vivo, 4T1BM2-ctrl and 4T1BM2-β3lo tumours grew at the same rate (Figure 2D, E). However, visual examination of mice at harvest and quantitation of metastatic burden, using a sensitive quantitative PCR (qPCR)-based assay [35], revealed a dramatic effect of β3 down-regulation on spontaneous metastasis. Semi-quantitative measurement (presence or absence) of metastasis indicated a significantly lower incidence of mice developing bone but not lung metastases in the 4T1BM2-β3lo group (Figure 2F). However, visual inspection of lungs at harvest showed fewer and smaller metastatic nodules in mice bearing 4T1BM2-β3lo tumours, indicating a lower overall lung metastatic burden (Figure 2F, right panels). These observations were confirmed and quantitated by qPCR, with 4T1BM2-β3lo metastatic burden in lung, femur, spine and bone (combined femur and spine) (Figure 2G–J) decreased significantly compared to 4T1BM2-ctrl bearing mice ($p < 0.01$ in all organs). Suppression of β3 integrin similarly reduced metastatic burden in lung, femur, spine and bone but not tumour growth in the 4T1.2 model (see supplementary material, Figure S3D–G). These results demonstrate conclusively that expression of β3 in mammary tumour cells is required for efficient spontaneous metastasis to multiple organs.

Loss of stromal β3 integrin expression does not alter orthotopic primary tumour growth or metastasis

Conflicting results exist regarding the contribution of stromal cell populations expressing β3 integrin to primary tumour growth [16,19–21] and metastasis [17,20]. Importantly, no study has investigated the role of stromal β3 integrin in spontaneous breast cancer metastasis to bone. Therefore, we compared the orthotopic growth and metastatic dissemination of 4T1BM2 (Figure 3) or 4T1.2 tumours (see supplementary material, Figure S4) in β3-null versus wild-type littermates. We found no difference in primary tumour growth (Figure 3A; see also supplementary material, Figure S4A), final tumour weight (Figure 3B; see also supplementary material, Figure S4B) or metastatic burden in lung, femur, spine or bone (combined femur and spine; Figure 3C–F; see also supplementary material, Figure S4C–F, respectively) between integrin β3-null and wild-type mice.

The lack of effect of stromal β3 deletion on primary tumour growth contrasts with enhanced subcutaneous growth and vascularization of melanoma, colon and lung carcinomas in β3-null mice [16,19] and could be due to differences in tumour type or to the site of tumour growth. To address this, we compared the growth of 4T1BM2 cells inoculated in the mammary fat pad or subcutaneously in wild-type and β3-null mice. Orthotopic 4T1BM2 tumours grew at the same rate in wild-type and β3-null mice (Figure 3G–I). Importantly, while subcutaneous growth of 4T1BM2 tumours in wild-type or β3-null mice was visibly slower than in the orthotopic site (cf Figure 3G, J), it was significantly enhanced in β3-null mice compared to wild-type littermates (Figure 3J–L). Moreover, quantitation of microvascular density revealed no difference in orthotopic tumours growing in wild-type and β3-null mice (Figure 3M) but a significant increase in microvascular density in subcutaneous tumours growing in β3-null compared to wild-type mice (Figure 3N). Collectively, these results indicate that, unlike subcutaneous tumours, orthotopic growth and vascularization of mammary tumours are not affected by stromal β3 integrin deletion.

Tumour β3 integrin is required early to promote metastasis to bone

To assess the stage at which tumour β3 is required for metastasis to bone, we bypassed the formation of

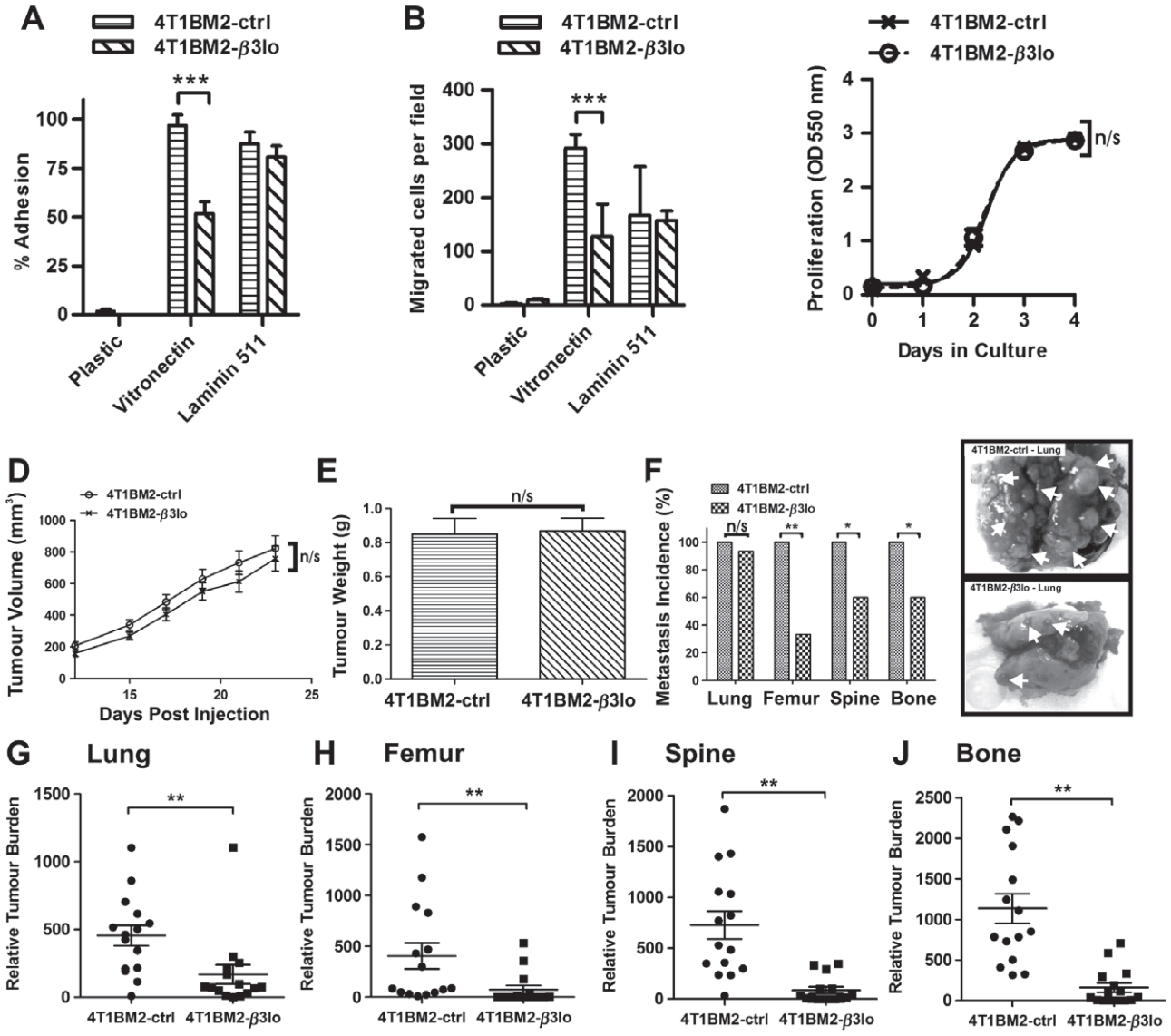

Figure 2. Down-regulation of αvβ3 integrin impairs vitronectin-mediated adhesion and migration and inhibits 4T1BM2 spontaneous metastasis to bone and lung. (A) Short-term adhesion (30 min) was measured in uncoated (plastic) or vitronectin- or LM-511-coated 96-well plates, as indicated. Data show % total cell input ± SD of representative experiments ($n = 3$), each completed in triplicate; $^{***}p < 0.001$; one-way ANOVA, Tukey's multiple comparisons test. (B) Haptotactic migration towards vitronectin or LM-511 was measured in Transwell chambers after 4 h at 37°C in the absence of serum; data show mean number of migrated cells ± SEM of nine replicate images (three random fields of view/Transwell membrane × three membranes; $^{***}p < 0.001$, one-way ANOVA, Tukey's multiple comparisons test). (C) Proliferation was measured in 96-well plates in the presence of 5% serum and quantitated every 24 h, using a sulphorhodamine B colorimetric assay; data are presented as mean ± SEM of six replicate wells/condition and are representative of three independent experiments; n/s, not significant; $p = 0.634$). (D) 4T1BM2-ctrl and 4T1BM2-β3lo orthotopic tumour growth was monitored thrice weekly by caliper measurements ($p = 0.254$; two-way ANOVA). (E) Tumour weight at harvest (day 26, $p = 0.782$, Mann–Whitney test): data in (D, E) show mean ± SD of 15 mice/group. (F) The incidence of mice developing metastases in lung, femur, spine or bone (combined femur + spine) was assessed by visual inspection and confirmed by qPCR detection of a marker gene (*mCherry*) relative to *vimentin*. Organs with a qPCR amplification signal above background compared to a naïve mouse were considered positive (n/s in lung, $p = 1.00$, $^{*}p < 0.05$, $^{**}p < 0.01$; Fisher's exact test): (right panels) representative images of lungs from 4T1BM2-ctrl and 4T1BM2-β3lo tumour-bearing mice; arrows, metastases. Metastatic burden in lung (G), femur (H), spine (I) and combined bone score (J) was determined by genomic qPCR detection of *mCherry* DNA relative to *vimentin* DNA; data show one point for each mouse ($n = 15$/group) and mean burdens (horizontal bar) ± SEM ($^{**}p < 0.01$; Mann–Whitney test)

primary tumours by inoculating 4T1BM2 cells directly into the left cardiac ventricle of wild-type mice. In contrast to the strong reduction in spontaneous bone metastasis, suppression of tumour β3 integrin did not reduce experimental metastasis to femur, spine or bone (femur and spine combined) (Figure 4A–C). We also compared the bone metastatic ability of 66cl4β3^{high} cells that over-express β3 integrin and metastasize spontaneously to bone to that of non-expressing 66cl4pBabe cells that do not spread spontaneously to bone from the mammary gland [13]. Surprisingly, extensive metastasis to femur, spine or both (Figure 4D–F) was observed, regardless of β3 expression. Thus, tumour β3 integrin is not essential for homing, survival and colonization of bone.

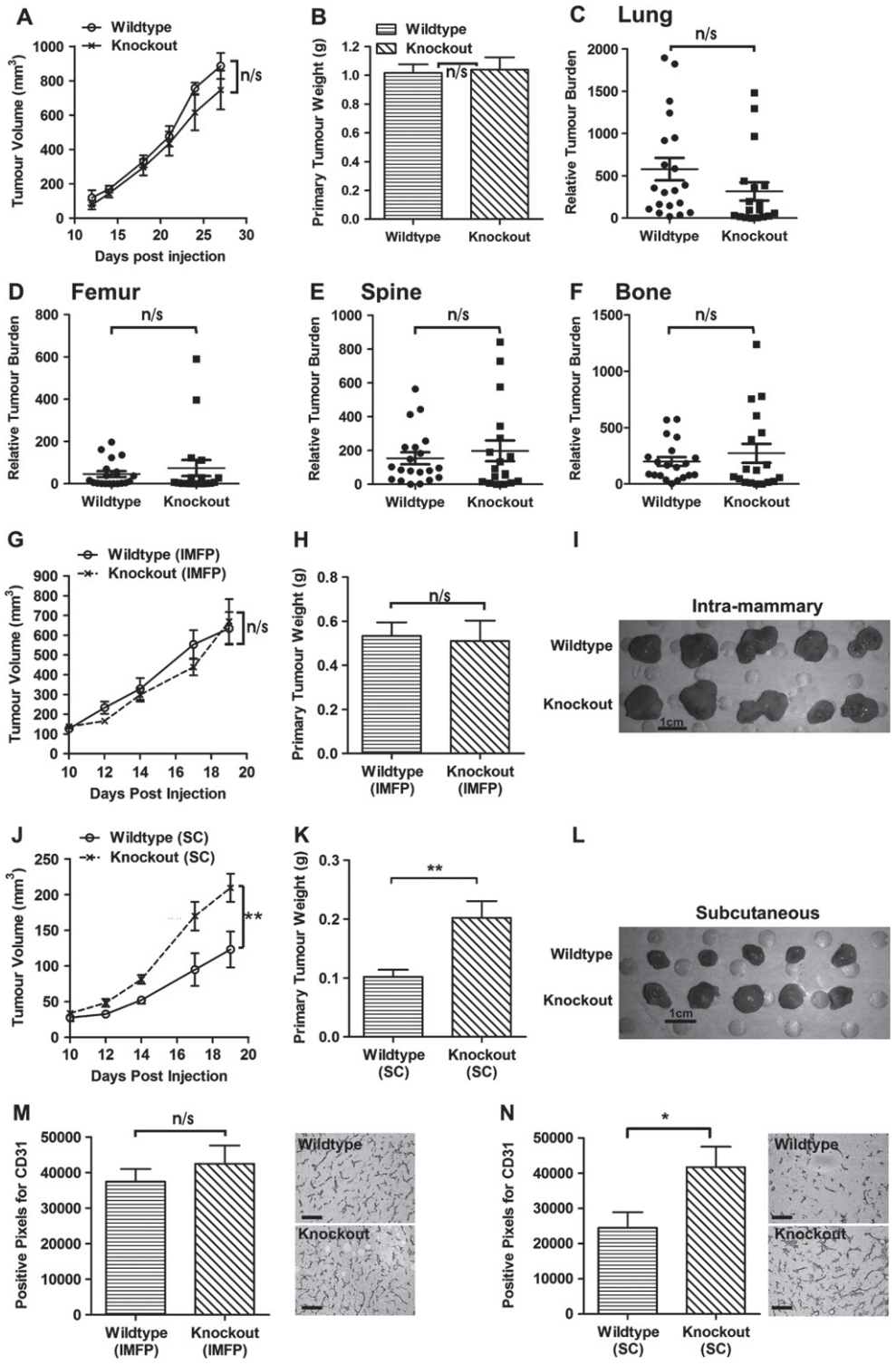

Figure 3. Stromal deletion of β3 integrin does not alter 4T1BM2 orthotopic tumour growth and spontaneous metastasis, but enhances subcutaneous tumour growth and vascularization; parental 4T1BM2 cells (1×10^5) were inoculated orthotopically into wild-type ($n = 20$) or littermate β3 knockout ($n = 18$) syngeneic Balb/c mice. Tumour growth rate (A), tumour weight at harvest (day 27) (B) and metastatic burden in lung (C), femur (D), spine (E) and bone (F) were measured as described in the legend to Figure 2. Data show one point for each mouse and mean burdens (horizontal bar) ± SEM; no statistical differences (n/s) in tumour growth rate ($p = 0.848$; two-way ANOVA), tumour end weight ($p = 0.895$; Mann–Whitney test) or metastatic burden between WT and KO mice were observed in lung ($p = 0.056$), femur ($p = 0.578$), spine ($p = 0.793$) or bone ($p = 0.530$); Mann–Whitney test. Parental 4T1BM2 cells (1×10^5) were inoculated orthotopically (IMFP; G–I) or subcutaneously (SC; J–L) into wild-type or β3 knockout mice (five mice/group) as indicated. (G, J) Tumour growth was monitored over 19 days and differences in growth rate analysed by two-way ANOVA, Bonferroni post-test (n/s, not significant; $p = 0.590$; $^{**}p < 0.01$). (H, K) Tumour weight at harvest (Mann–Whitney test; n/s, $p = 0.854$, $^{**}p < 0.01$). Data in (G, H, J, K) show mean ± SD of five replicates/group. (I, L) Images showing size comparison between orthotopic (I) or subcutaneous (L) tumours growing in wild-type and β3 knockout mice; scale bar = 1 cm. Microvascular density in orthotopic (M) and subcutaneous (N) tumours was analysed by IHC detection of CD31; data show mean pixels ± SEM from 15 replicates (three fields/section ± five sections/tumour; $n = 5$ mice/group; n/s, $p = 0.444$, $^{*}p < 0.05$, Mann–Whitney test). Representative CD31 stainings in wild-type and β3 knockout mice are shown in the right panels. Scale bar = 100 μm

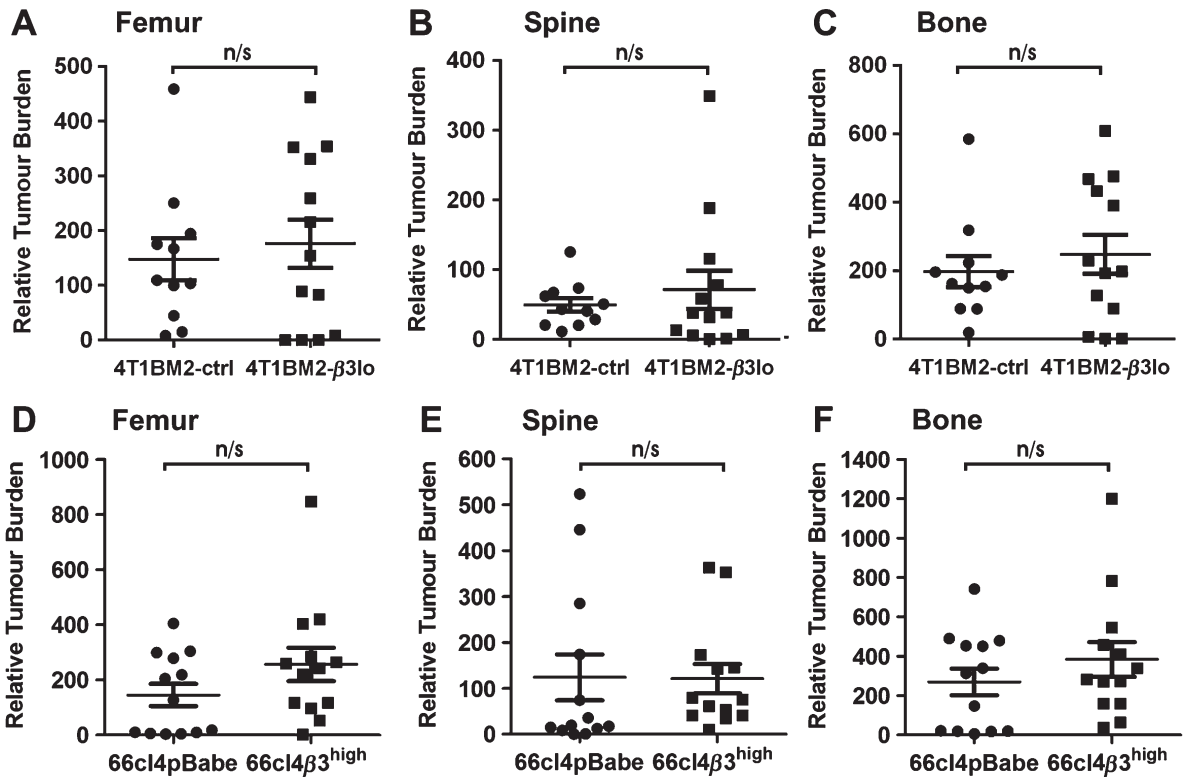

Figure 4. Experimental bone metastasis is not affected by changes in tumour β3 integrin expression. Balb/c mice were inoculated into the left ventricle of the heart with 4T1BM2-ctrl versus 4T1BM2-β3lo cells (5×10^4/mouse, $n = 11$ and 13 mice/group, respectively) (A–C) or 66cl4pBabe versus 66cl4β3^{high} cells (10^5/mouse, $n = 13$ mice/group) (D–F). The mice were sacrificed after 14 days and metastatic burden in femurs (A, D), spine (B, E) or bone (C, F) analysed by genomic qPCR detection of *mCherry* or the puromycin resistance gene relative to *vimentin*; data show one point for each mouse and mean burdens (horizontal bar) ± SEM. No statistical differences (n/s) in metastatic burden were found between 4T1BM2-ctrl and 4T1BM2-β3lo femur ($p = 0.368$), spine ($p = 0.495$) or bone ($p = 0.511$) and between 66cl4pBabe and 66cl4β3high femur ($p = 0.140$), spine ($p = 0.964$) or bone ($p = 0.315$) (Mann–Whitney test)

Next, we compared the ability of 4T1BM2-ctrl and 4T1BM2-β3lo or 4T1.2-ctrl and 4T1.2-β3lo cells to migrate towards a gradient of serum, a rich source of soluble vitronectin [45]. Integrin β3 suppression impaired migration towards serum by approximately 50% ($p < 0.001$; see supplementary material, Figure S5A, B). To further confirm that serum chemotaxis was specifically dependent on β3 integrin, we used DisBa-01, a potent snake venom-derived disintegrin that targets αvβ3 integrin [46]. DisBa-01 dose-dependently inhibited haptotatic migration of 4T1BM2 towards vitronectin, but not towards collagen-IV, demonstrating its specificity towards αvβ3 integrin substrates (see supplementary material, Figure S5C). Importantly, chemotactic migration towards serum was also inhibited by DisBa-01 in a dose-dependent manner (see supplementary material, Figure S5D).

4T1-derived tumour lines secrete abundant MMP9, which contributes to their migration and invasion [13,36]. We found that 4T1BM2-β3lo and 4T1.2-β3lo cells secrete significantly less MMP9 than control cells (see supplementary material, Figure 6A, B). Moreover, migration across a monolayer of endothelial cells was enhanced significantly by elevated β3 expression in 66cl4 cells (Figure 5A) and was inhibited by suppression of β3 integrin in 4T1BM2 cells (Figure 5B). Reduced chemotaxis, protease secretion and trans-endothelial migration following β3 down-regulation would be expected to prevent or delay tumour cell migration and intravasation. Indeed, qPCR signal for the *mCherry* tumour marker in blood on day 26 was near or below the limit of detection in the majority of 4T1BM2-β3lo tumour-bearing mice (mean value = 1.132) compared to control mice (mean value = 16.22; $p = 0.01$) (Figure 5C).

In a second series of experiments, blood was collected by cardiac puncture when tumours were small (~0.5 cm^3) and viable tumour cells scored by colony formation *in vitro*. Tumour weights were similar in both groups ($p = 0.944$; Figure 5D) and, while macro-metastases were not visible in either group at this early stage, qPCR quantitation revealed a higher lung ($p = 0.05$) and spine ($p = 0.012$) tumour burden in control mice (Figure 5E). Importantly, only blood from 4T1BM2-ctrl-bearing mice gave rise to colonies ($p = 0.0006$; Figure 5F), confirming that down-regulation of tumour β3 significantly impairs the ability 4T1BM2-β3lo cells to enter the vasculature.

Since αvβ3 integrin controls an early step required for metastatic dissemination to multiple sites, high β3 expression in breast cancer patients would be expected to be associated with poor clinical outcome. To assess clinical relevance, we first ran a differential expression analysis for integrin β3 in Oncomine 4.4.4.3 [47],

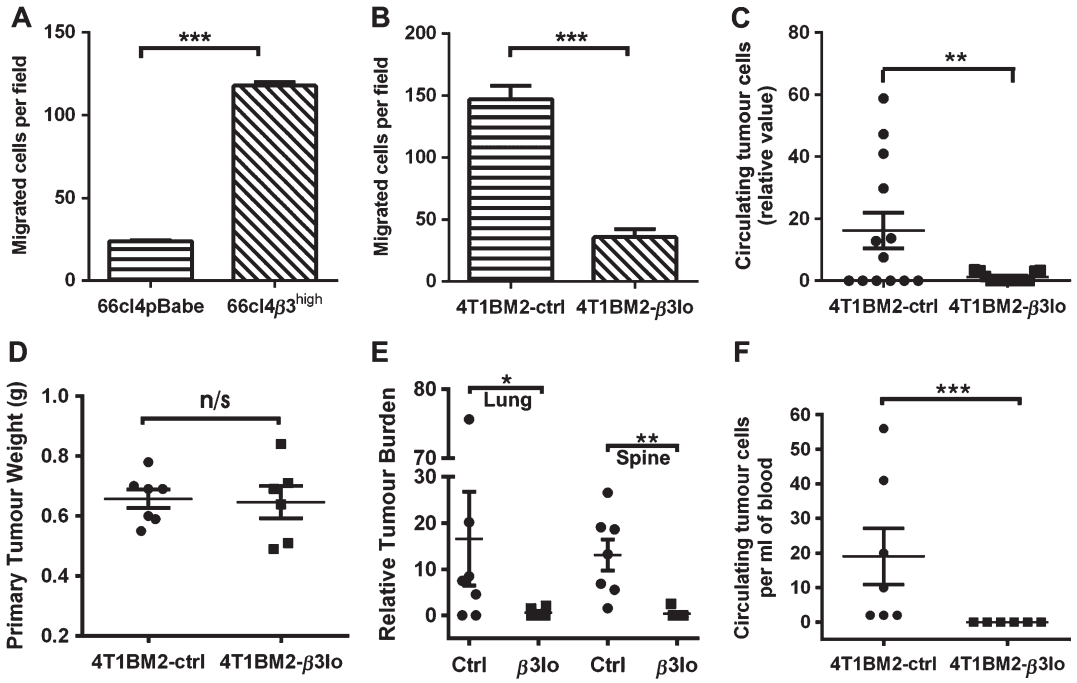

Figure 5. Integrin αvβ3 promotes trans-endothelial migration and intravasation of tumour cells. (A) β3 integrin over-expression enhances trans-endothelial migration *in vitro*. (B) β3 integrin suppression inhibits trans-endothelial migration *in vitro*. Migration of tumour cells (1×10^5 cells/well) through a monolayer of bEnd.3 endothelial cells was measured after 48 h. Data in (A, B) show mean number of migrated cells ± SD of nine replicate images (three random fields of view/Transwell membrane × three membranes) from a representative experiment ($n = 3$; $^{***}p < 0.001$, Mann–Whitney test). (C) β3 Integrin suppression inhibits intravasation *in vivo*: 4T1BM2-ctrl and 4T1BM2-β3lo tumour cells (1×10^5) were inoculated orthotopically into syngeneic Balb/c mice and blood collected by cardiac puncture after 26 days; relative number of circulating tumour cells was quantitated by genomic qPCR detection of *mCherry* gene relative to *vimentin*; data show one point for each mouse and mean (horizontal bar) ± SEM ($n = 13$ mice/group; $^{**}p = 0.01$; Mann–Whitney test). (D–F) β3 Integrin suppression delays vascular dissemination: mice were inoculated with 4T1BM2-ctrl ($n = 7$) and 4T1BM2-β3lo cells ($n = 6$), as above; blood was collected by cardiac puncture when mammary tumours reached ~0.5cm^3 and viable circulating tumour cells scored by colony formation in culture (0.5 ml/dish). (D) Tumour weight at harvest. (E) Metastatic burden in lung and spine was determined by genomic qPCR. (F) Colony formation assay: the number of colonies after 10 days (> 50 cells) was counted and the data expressed as the number of circulating tumour cells/ml blood. Data in (D–F) show one point/mouse and mean values (horizontal bar) ± SEM (n/s, not significant; $p = 0.944$, $^{*}p < 0.05$, $^{**}p < 0.01$, $^{***}p < 0.001$; Mann–Whitney test)

focusing on clinical outcome in breast cancer patients (fold-change ≥ 1.5; $p \leq 0.05$). In all, 10/13 analyses indicated that high β3 was associated with metastasis and recurrence (see supplementary material, Figure S7A, B). The prognostic value of β3 integrin expression was further investigated in molecular subtypes of breast cancer, using the BreastMark prognostic biomarker analysis tool [48]. High β3 integrin expression was correlated with shorter disease-free survival in patients with oestrogen receptor-negative (ER^-) tumours (Figure 6A, B) or with lymph node metastasis (LN^+; Figure 6E, F). No significant association was found between β3 expression and progesterone receptor (PR) status (Figure 6C, D), high tumour grade (Gr3; Figure 6G) or HER2 status (data not shown; $HER2^+$, $p = 0.121$; $HER2^-$, $p = 0.282$). Multivariate analyses showed that high β3 expression is significantly associated with reduced survival in ER^-/PR^- (Figure 6H), ER^-/LN^+ (Figure 6I) and $ER^-/LN^+/Gr3^+$ tumours (Figure 6J). These observations in human breast tissues are consistent with the lack of ER and PR in 4T1BM2 primary tumours and the aggressive nature of this mouse model of metastasis (see supplementary material, Figure S7C).

Discussion

The diversity of experimental approaches, animal models and tumour types used to investigate the contribution of β3 integrin to tumour growth and metastasis has made it difficult to reconcile some of the discrepancies between earlier studies. Unlike xenograft models, the 4T1BM2 and 4T1.2 models used herein have the unique ability to metastasize spontaneously and aggressively in immunocompetent mice [35–37]. Our data demonstrate conclusively that tumour-associated αvβ3 integrin is essential for efficient spontaneous metastasis to bone and lung, but not for growth in the mammary gland. Integrin αvβ3 mediates tumour cell attachment to several bone-derived ECM proteins, and is thought to be a critical for homing and colonization of bone [13,49,50]. Unexpectedly, we found that β3 down-regulation in 4T1BM2 and 4T1.2 decreased spontaneous, but not experimental, bone metastasis. Moreover, exogenous expression of β3 in 66cl4β3^{high} cells, which promotes spontaneous metastasis to bone [13], did not enhance experimental bone metastatic burden compared to control cells. Clearly, 66cl4 cells do not require αvβ3 to

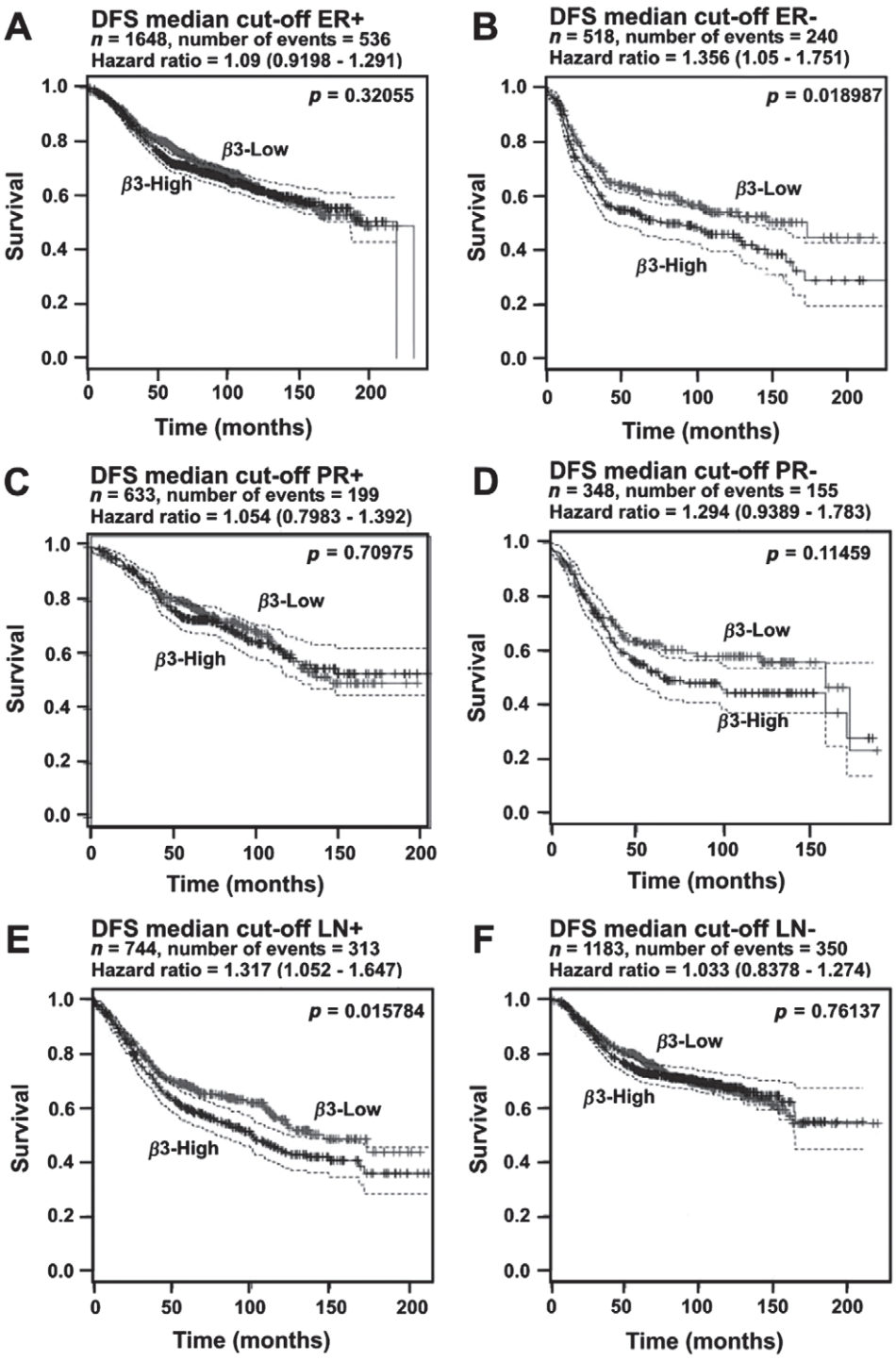

Figure 6. Association between β3 integrin expression and disease-free survival (DFS). The association between β3 expression and DFS in human breast tumour samples was interrogated in public databases, using the BreastMark prognostic biomarker analysis tool [48]. $\beta3^{high}$ and $\beta3^{low}$ (median cut-off) are shown in black and grey, respectively; dotted lines show confidence intervals. (A) Oestrogen receptor-positive (ER^+) tumours. (B) Oestrogen receptor-negative (ER^-) tumours. (C) Progesterone receptor-positive (PR^+) tumours. (D) Progesterone receptor-negative (PR^-) tumours. (E) Lymph node-positive (LN^+) tumours. (F) Lymph node-negative (LN^-) tumours. (G) Grade 3 (Gr3) tumours. (H) Oestrogen receptor-negative/progesterone receptor-negative (ER^-/PR^-) tumours. (I) Oestrogen receptor-negative/lymph node-positive (ER^-/LN^+) tumours. (J) Oestrogen receptor-negative/lymph node-positive/grade 3 (ER^-/LN^+/Gr3) tumours

home and colonize bone, since they formed experimental bone metastases in 100% of animals (see Figure 4), even though they do not express this receptor [13]. These observations indicate that tumour αvβ3 is essential primarily during the early, rather than late, steps of breast cancer metastasis.

Suppression of tumour β3 reduced MMP9 secretion, serum chemotaxis and trans-endothelial migration. These responses are expected to contribute to the early dissemination of αvβ3-expressing breast tumours *in vivo* through interactions with its ligands, a conclusion further supported by decreased circulating tumour cells

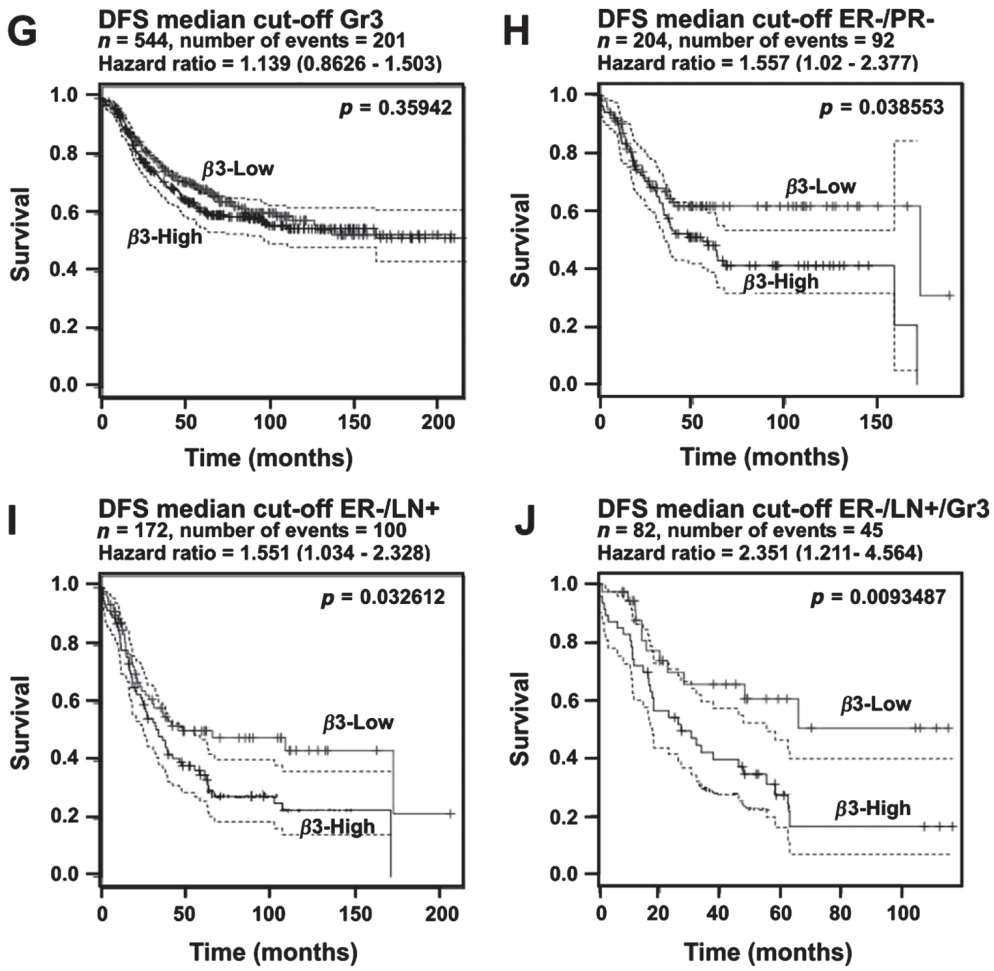

Figure 6. Continued

observed in 4T1BM2-β3lo tumour-bearing mice. Consistent with this, the expression of the αvβ3 ligand, vitronectin, is elevated in small vessel walls surrounding cancer cells in patients with early stage breast cancer, and the concentration of vitronectin in serum is elevated in advanced breast cancer patients [51]. We therefore conclude that the most critical role of tumour αvβ3 is to facilitate the early escape and intravasation of breast tumours, resulting in enhanced vascular dissemination and subsequent metastasis to multiple organs. The clinical relevance of our findings in mouse models is strongly supported by the correlation observed between high β3 expression, metastatic disease and poor clinical outcome in ER-negative breast cancer patients.

Our data appear to be at odds with earlier reports showing increased experimental bone metastasis in β3-over-expressing MDA-MB-231 variants [5,12]. However, it should be noted that, while mice inoculated with these cells showed increased number of osteolytic lesions, the overall incidence of mice developing experimental bone metastases was, in agreement with our study, high in both control and β3-over-expressing groups. Tumour αvβ3 integrin does not directly stimulate metastatic growth in bone, but promotes the recruitment of active osteoclasts in proximity to metastatic lesions [5,13]. Degradation of the bone matrix and the subsequent release of growth factors could provide a growth stimulus for breast tumour cells in bone. Consistent with this, β3 inhibitors reduce the formation of osteolytic lesions more potently when used as pretreatment [18], or as long-term daily treatments [5], at concentrations that also inhibit osteoclast activity. The extent to which αvβ3-expressing osteoclasts contribute to bone colonization is likely to vary between tumours. MDA-MB-231 cells are aggressively osteolytic compared to 4T1 or 66cl4 cells, and presumably their growth in bone may be more dependent on the release of bone-derived growth factors. Collectively, data from the above studies and ours indicate that, while there is heterogeneity amongst tumour lines in their dependency on osteoclasts to colonize bone, tumour αvβ3 is not essential for bone metastases to develop.

Most surprising was the lack of effect of stromal β3 ablation on tumour growth, vascularization and spontaneous metastasis, given the numerous studies that have implicated endothelial cells or platelets in these processes [16,19,52–54]. Studies employing subcutaneous tumour transplantation models reported enhanced tumour growth and vascularization following stromal β3 deletion [16,19]. While we could replicate these observations in mammary tumour cells implanted into

the subcutis, stromal deletion of β3 integrin did not alter tumour growth in the mammary gland. These observations indicate that stromal β3 regulates tumour growth and angiogenesis in a tissue-specific manner, and argue against a critical role for endothelial β3 in promoting the orthotopic growth and angiogenesis of breast tumours. Our data support those reported in the MMTV-c-neu/$\beta3^{-/-}$ transgenic model of breast cancer metastasis [20] and resolve the apparent conflicts with earlier tumour transplantation studies employing β3-null mice [55].

Most studies supporting the role of platelet αIIbβ3 in metastasis have made use of *in vitro* surrogate assays or *in vivo* experimental metastasis models, in which tumour cells are injected directly into the vasculature [5,12,52,53,56]. In one study, pharmacological inhibition of platelet αIIbβ3 significantly reduced experimental melanoma metastasis to bone, which was attributed to disruption of tumour cell-induced platelet aggregation [17]. Conceivably, injection of a large bolus of cells could enhance experimental metastasis by promoting excessive tumour cell clumping and/or exaggerating tumour-induced platelet aggregation, processes known to promote embolic arrest of tumour cells [53,57,58]. Interestingly, the well-documented correlation between the ability of tumour cells to induce platelet aggregation and metastatic potential has not been observed consistently in breast cancer metastasis models [59]. To minimize tumour cell clumping and non-specific tumour–platelet interactions in our experimental metastasis assays, the number of cells injected (5×10^4–1×10^5) was significantly lower than that employed in most xenograft studies [5,12]. We do not interpret our results as evidence that tumour–platelet interactions are not required for spontaneous metastasis of breast tumours. Rather, we propose that platelet αIIbβ3 function is not essential for efficient breast cancer metastasis to bone and lung. Indeed, liposome-encapsulated Cilostazol, a platelet aggregation inhibitor, reduces spontaneous metastasis of 4T1 tumours to lung by 50% [60]. However, the effects of Cilostazol on bone metastasis and of αIIbβ3 integrin inhibition on spontaneous metastasis were not investigated in this study.

Current experimental and clinical evidence indicates that not all tumour types (or anatomical sites) could benefit from therapies employing αvβ3 integrin antagonists such as cilengitide [25,61]. Our study demonstrates for the first time that tumour rather than stromal β3 integrin is a critical determinant of metastatic potential in breast cancer and is essential for efficient spontaneous metastasis to multiple sites, including bone. Regulation of early steps of metastasis to multiple organs by tumour β3 integrin is consistent with the association between high β3 expression and poor clinical outcome in ER-negative breast cancer patients. Our findings have important implications for the design of anti-metastatic therapies targeting β3 integrin in breast cancer, and could explain in part the limited therapeutic response observed in clinical trials testing β3 inhibitors in patients with advanced metastatic disease [26–30]. We propose that to achieve optimal efficacy in breast cancer patients, β3 inhibitors should be used in a neo-adjuvant setting to target early steps of metastatic progression, rather than after metastases are established.

Acknowledgements

We thank Dr SL Teitelbaum for providing β3 integrin-null mice and Ms Rachel Walker for assistance with subcutaneous injections. We acknowledge the kind donation of pLMP retroviral vector by Dr Ross Dickins (WEHI, Australia). This work was supported by the National Health and Medical Research Council (Project Grant No. 509131, to NP) and the National Breast Cancer Foundation (a postgraduate scholarship to RZC and a fellowship to RLA).

Author contributions

NP and RLA conceived and managed the study and wrote the manuscript; experimental work was carried out by NP, RZC, KCM, AN, SP-F, ACBMM, DD, XL, S-HK and RT; HAS provided purified DisBa-01 and expert guidance; and RPR completed the prognostic analyses. All authors revised and approved the final manuscript.

Abbreviations

ECM, extracellular matrix; ER, oestrogen receptor; LM, laminin; MMTV, mouse mammary tumour virus; PR, progesterone receptor.

References

1. Switala-Jelen K, Dabrowska K, Opolski A, *et al.* The biological functions of β3 integrins. *Folia Biol* 2004; **50:** 143–152.
2. Desgrosellier JS, Cheresh DA. Integrins in cancer: biological implications and therapeutic opportunities. *Nat Rev Cancer* 2010; **10:** 9–22.
3. Albelda SM, Mette SA, Elder DE, *et al.* Integrin distribution in malignant melanoma: association of the β3 subunit with tumor progression. *Cancer Res* 1990; **50:** 6757–6764.
4. Liapis H, Flath A, Kitazawa S. Integrin αvβ3 expression by bone-residing breast cancer metastases. *Diagn Mol Pathol B* 1996; **5:** 127–135.
5. Zhao Y, Bachelier R, Treilleux I, *et al.* Tumor αvβ3 integrin is a therapeutic target for breast cancer bone metastases. *Cancer Res* 2007; **67:** 5821–5830.
6. Cooper CR, Chay CH, Pienta KJ. The role of αvβ3 in prostate cancer progression. *Neoplasia* 2002; **4:** 191–194.
7. Gruber G, Hess J, Stiefel C, *et al.* Correlation between the tumoral expression of β3-integrin and outcome in cervical cancer patients who had undergone radiotherapy. *Br J Cancer* 2005; **92:** 41–46.
8. Vonlaufen A, Wiedle G, Borisch B, *et al.* Integrin αvβ3 expression in colon carcinoma correlates with survival. *Mod Pathol* 2001; **14:** 1126–1132.

9. Danen EH, Jansen KF, Van Kraats AA, *et al.* αv-integrins in human melanoma: gain of αvβ3 and loss of αvβ5 are related to tumor progression *in situ* but not to metastatic capacity of cell lines in nude mice. *Int J Cancer* 1995; **61:** 491–496.
10. Kaur S, Kenny HA, Jagadeeswaran S, *et al.* β3-Integrin expression on tumor cells inhibits tumor progression, reduces metastasis, and is associated with a favorable prognosis in patients with ovarian cancer. *Am J Pathol* 2009; **175:** 2184–2196.
11. Kitazawa S, Maeda S. Development of skeletal metastases. *Clin Orthop Rel Res* 1995; **312**: 45–50.
12. Pecheur I, Peyruchaud O, Serre CM, *et al.* Integrin αvβ3 expression confers on tumor cells a greater propensity to metastasize to bone. *FASEB J* 2002; **16:** 1266–1268.
13. Sloan EK, Pouliot N, Stanley KL, *et al.* Tumor-specific expression of αvβ3 integrin promotes spontaneous metastasis of breast cancer to bone. *Breast Cancer Re* 2006; **8:** R20.
14. Brooks PC, Clark RA, Cheresh DA. Requirement of vascular integrin αvβ3 for angiogenesis. *Science* 1994; **264:** 569–571.
15. Brooks PC, Montgomery AM, Rosenfeld M, *et al.* Integrin αvβ3 antagonists promote tumor regression by inducing apoptosis of angiogenic blood vessels. *Cell* 1994; **79:** 1157–1164.
16. Reynolds LE, Wyder L, Lively JC, *et al.* Enhanced pathological angiogenesis in mice lacking β3 integrin or β3 and β5 integrins. *Nat Med* 2002; **8:** 27–34.
17. Bakewell SJ, Nestor P, Prasad S, *et al.* Platelet and osteoclast β3 integrins are critical for bone metastasis. *Proc Natl Acad Sci USA* 2003; **100:** 14205–14210.
18. Harms JF, Welch DR, Samant RS, *et al.* A small molecule antagonist of the αvβ3 integrin suppresses MDA-MB-435 skeletal metastasis. *Clin Exp Metast* 2004; **21:** 119–128.
19. Taverna D, Moher H, Crowley D, *et al.* Increased primary tumor growth in mice null for β3- or β3/β5-integrins or selectins. *Proc Natl Acad Sci USA* 2004; **101:** 763–768.
20. Taverna D, Crowley D, Connolly M, *et al.* A direct test of potential roles for β3 and β5 integrins in growth and metastasis of murine mammary carcinomas. *Cancer Res* 2005; **65:** 10324–10329.
21. Brooks PC, Stromblad S, Klemke R, *et al.* Anti-integrin αvβ3 blocks human breast cancer growth and angiogenesis in human skin. *J Clin Invest* 1995; **96:** 1815–1822.
22. Chen Q, Manning CD, Millar H, *et al.* CNTO 95, a fully human anti-αv integrin antibody, inhibits cell signaling, migration, invasion, and spontaneous metastasis of human breast cancer cells. *Clin Exp Metast* 2008; **25:** 139–148.
23. Trikha M, Zhou Z, Nemeth JA, *et al.* CNTO 95, a fully human monoclonal antibody that inhibits alphav integrins, has antitumor and anti-angiogenic activity *in vivo*. *Int J Cancer* 2004; **110:** 326–335.
24. Alva A, Slovin S, Daignault S, *et al.* Phase II study of cilengitide (EMD 121974, NSC 707544) in patients with non-metastatic castration resistant prostate cancer, NCI-6735. A study by the DOD/PCF prostate cancer clinical trials consortium. *Invest New Drugs* 2012; **30:** 749–757.
25. Millard M, Odde S, Neamati N. Integrin-targeted therapeutics. *Theranostics* 2011; **1:** 154–188.
26. Delbaldo C, Raymond E, Vera K, *et al.* Phase I and pharmacokinetic study of etaracizumab (Abegrin), a humanized monoclonal antibody against αvβ3 integrin receptor, in patients with advanced solid tumors. *Invest New Drugs* 2008; **26:** 35–43.
27. Hersey P, Sosman J, O'Day S, *et al.* A randomized phase 2 study of etaracizumab, a monoclonal antibody against integrin αvβ3, + or – dacarbazine in patients with stage IV metastatic melanoma. *Cancer* 2010; **116:** 1526–1534.
28. Kim KB, Prieto V, Joseph RW, *et al.* A randomized phase II study of cilengitide (EMD 121974) in patients with metastatic melanoma. *Melanoma Res* 2012; **22:** 294–301.
29. Manegold C, Vansteenkiste J, Cardenal F, *et al.* Randomized phase II study of three doses of the integrin inhibitor cilengitide versus docetaxel as second-line treatment for patients with advanced non-small-cell lung cancer. *Invest New Drugs* 2013; **31:** 175–182.
30. O'Day SJ, Pavlick AC, Albertini MR, *et al.* Clinical and pharmacologic evaluation of two dose levels of intetumumab (CNTO 95) in patients with melanoma or angiosarcoma. *Invest New Drugs* 2012; **30:** 1074–1081.
31. Reardon DA, Fink KL, Mikkelsen T, *et al.* Randomized phase II study of cilengitide, an integrin-targeting arginine–glycine–aspartic acid peptide, in recurrent glioblastoma multiforme. *J Clin Oncol* 2008; **26:** 5610–5617.
32. Sawada K, Ohyagi-Hara C, Kimura T, *et al.* Integrin inhibitors as a therapeutic agent for ovarian cancer. *J Oncol* 2012; **2012:** 915140.
33. Patel SR, Jenkins J, Papadopolous N, *et al.* Pilot study of vitaxin – an angiogenesis inhibitor – in patients with advanced leiomyosarcomas. *Cancer* 2001; **92:** 1347–1348.
34. Friess H, Langrehr JM, Oettle H, *et al.* A randomized multi-center phase II trial of the angiogenesis inhibitor Cilengitide (EMD 121974) and gemcitabine compared with gemcitabine alone in advanced unresectable pancreatic cancer. *BMC Cancer* 2006; **6:** 285.
35. Eckhardt BL, Parker BS, van Laar RK, *et al.* Genomic analysis of a spontaneous model of breast cancer metastasis to bone reveals a role for the extracellular matrix. *Mol Cancer Res* 2005; **3:** 1–13.
36. Kusuma N, Denoyer D, Eble JA, *et al.* Integrin-dependent response to laminin-511 regulates breast tumor cell invasion and metastasis. *Int J Cancer* 2012; **130:** 555–566.
37. Lelekakis M, Moseley JM, Martin TJ, *et al.* A novel orthotopic model of breast cancer metastasis to bone. *Clin Exp Metast* 1999; **17:** 163–170.
38. Denoyer D, Potdevin T, Roselt P, *et al.* Improved detection of regional melanoma metastasis using ^{18}F-6-fluoro-*N*-[2-(diethylamino)ethyl] pyridine-3-carboxamide, a melanin-specific PET probe, by perilesional administration. *J Nucl Med* 2011; **52:** 115–122.
39. Chia J, Kusuma N, Anderson R, *et al.* Evidence for a role of tumor-derived laminin-511 in the metastatic progression of breast cancer. *Am J Pathol* 2007; **170:** 2135–2148.
40. Denoyer D, Kusuma N, Burrows A, *et al.* Bone-derived soluble factors and laminin-511 cooperate to promote migration, invasion and survival of bone-metastatic breast tumor cells. *Growth Factors* 2014; **32:** 63–73.
41. Pouliot N, Nice EC, Burgess AW. Laminin-10 mediates basal and EGF-stimulated motility of human colon carcinoma cells via α3β1 and α6β4 integrins. *Exp Cell Res* 2001; **266:** 1–10.
42. McHugh KP, Hodivala-Dilke K, Zheng MH, *et al.* Mice lacking β3 integrins are osteosclerotic because of dysfunctional osteoclasts. *J Clin Invest* 2000; **105:** 433–440.
43. Paquet-Fifield S, Levy SM, Sato T, *et al.* Vascular endothelial growth factor-δ modulates caliber and function of initial lymphatics in the dermis. *J Invest Dermatol* 2013; **133:** 2074–2084.
44. Arguello F, Baggs RB, Frantz CN. A murine model of experimental metastasis to bone and bone marrow. *Cancer Res* 1988; **48:** 6876–6881.
45. Shaffer MC, Foley TP, Barnes DW. Quantitation of spreading factor in human biologic fluids. *J Lab Clin Med* 1984; **103:** 783–791.
46. Ramos OH, Kauskot A, Cominetti MR, *et al.* A novel αvβ3-blocking disintegrin containing the RGD motive, DisBa-01, inhibits bFGF-induced angiogenesis and melanoma metastasis. *Clin Exp Metast* 2008; **25:** 53–64.
47. Rhodes DR, Kalyana-Sundaram S, Mahavisno V, *et al.* Oncomine 3.0: genes, pathways, and networks in a collection of 18 000 cancer gene expression profiles. *Neoplasia* 2007; **9:** 166–180.

48. Madden SF, Clarke C, Gaule P, *et al.* BreastMark: an integrated approach to mining publicly available transcriptomic datasets relating to breast cancer outcome. *Breast Cancer Res* 2013; **15:** R52.
49. van der P, Vloedgraven H, Papapoulos S, *et al.* Attachment characteristics and involvement of integrins in adhesion of breast cancer cell lines to extracellular bone matrix components. *Lab Invest* 1997; **77:** 665–675.
50. Schneider JG, Amend SR, Weilbaecher KN. Integrins and bone metastasis: integrating tumor cell and stromal cell interactions. *Bone* 2011; **48:** 54–65.
51. Kadowaki M, Sangai T, Nagashima T, *et al.* Identification of vitronectin as a novel serum marker for early breast cancer detection using a new proteomic approach. *J Cancer Res Clin Oncol* 2011; **137:** 1105–1115.
52. Bambace NM, Holmes CE. The platelet contribution to cancer progression. *J Thrombosis Haemostasis* 2011; **9:** 237–249.
53. Honn KV, Tang DG, Crissman JD. Platelets and cancer metastasis: a causal relationship? *Cancer Metast Rev* 1992; **11:** 325–351.
54. Lal I, Dittus K, Holmes CE. Platelets, coagulation and fibrinolysis in breast cancer progression. *Breast Cancer Res* 2013; **15:** 207.
55. Tucker GC. Inhibitors of integrins. *Curr Opin Pharmacol* 2002; **2:** 394–402.
56. Gay LJ, Felding-Habermann B. Contribution of platelets to tumour metastasis. *Nat Rev Cancer* 2011; **11:** 123–134.
57. Liotta LA, Saidel MG, Kleinerman J. The significance of hematogenous tumor cell clumps in the metastatic process. *Cancer Res* 1976; **36:** 889–894.
58. Updyke TV, Nicolson GL. Malignant melanoma cell lines selected *in vitro* for increased homotypic adhesion properties have increased experimental metastatic potential. *Clin Exp Metast* 1986; **4:** 273–284.
59. Estrada J, Nicolson GL. Tumor-cell-platelet aggregation does not correlate with metastatic potential of rat 13762NF mammary adenocarcinoma tumor cell clones. *Int J Cancer* 1984; **34:** 101–105.
60. Wenzel J, Zeisig R, Fichtner I. Inhibition of metastasis in a murine 4T1 breast cancer model by liposomes preventing tumor cell–platelet interactions. *Clin Exp Metast* 2010; **27:** 25–34.
61. MacDonald TJ, Taga T, Shimada H, *et al.* Preferential susceptibility of brain tumors to the anti-angiogenic effects of an αv integrin antagonist. *Neurosurgery* 2001; **48:** 151–157.

SUPPLEMENTARY MATERIAL ON THE INTERNET

The following supplementary material may be found in the online version of this article:

Supplementary materials and methods

Figure S1. Stable suppression of β3 integrin expression induces coordinated down-regulation of αv integrin subunits at the cell surface

Figure S2. Flow-cytometric analysis of the repertoire of integrin subunits following β3 integrin down-regulation

Figure S3. Down-regulation of αvβ3 integrin impairs vitronectin-mediated adhesion and migration and inhibits 4T1.2 spontaneous metastasis to bone and lung

Figure S4. Stromal deletion of β3 integrin does not alter 4T1.2 orthotopic tumour growth and spontaneous metastasis

Figure S5. Suppression of β3 integrin expression or function impairs αvβ3-dependent migration

Figure S6. β3 integrin down-regulation inhibits MMP-9 expression

Figure S7. Differential expression analysis of integrin β3 in ER-positive and -negative human cancer cases

Send Orders for Reprints to reprints@benthamscience.net

Mini-Reviews in Medicinal Chemistry, 2014, *14*, 000-000

[6]-gingerol as a Cancer Chemopreventive Agent: A Review of Its Activity on Different Steps of the Metastatic Process

Juliana Poltronieri[1], Amanda B. Becceneri[1], Angelina M. Fuzer[1], Julio Cesar C. Filho[1], Ana Carolina B.M. Martin[2], Paulo Cézar Vieira[3], Normand Pouliot[4,5] and Márcia R. Cominetti[1]*

[1]*Departamento de Gerontologia, Universidade Federal de São Carlos, São Carlos, SP, Brazil;* [2]*Departamento de Ciências Fisiológicas, Universidade Federal de São Carlos, São Carlos, SP, Brazil;* [3]*Departamento de Química, Universidade Federal de São Carlos, São Carlos, SP, Brazil;* [4]*Metastasis Research Laboratory, Peter MacCallum Cancer Centre, East Melbourne, VIC, Australia;* [5]*Sir Peter MacCallum Department of Oncology and Pathology Department, The University of Melbourne, VIC, Australia*

Abstract: For many years, ginger or ginger root, the rhizome of the plant *Zingiber officinale*, has been consumed as a delicacy, medicine, or spice. Several studies have been conducted on the medicinal properties of ginger against various disorders, including cancer. Cancer is the second leading cause of death, and chemoprevention is defined as the use of natural or synthetic substances to prevent cancer initiation or progression. Evidence that ginger-derived compounds have inhibitory effects on various cancer cell types is increasingly being reported in the scientific literature. In this review we focused on the cancer chemopreventive effects of [6]-gingerol, the major pungent component of ginger, and its impact on different steps of the metastatic process.

Keywords: Apoptosis, cancer, ginger, 6-gingerol, metastasis, natural product.

INTRODUCTION

Ginger (*Zingiber officinale* Roscoe, Zingiberacae) is a native plant from Southeast Asia, that has been used as an important condiment and medicinal agent for more than 2500 years [1]. Several studies have been conducted on the medicinal properties of ginger against various disorders. Ginger has been demonstrated to have anti-inflammatory, hypotensive, antioxidant, antimicrobial, and antiemetic properties and to regulate cholesterol levels [2, 3].

Ginger is composed of volatile oils (flavor and aroma) and non-volatile pungent compounds. The latter include gingerols, shogaols, paradols and zingerone, which are biologically active. Gingerols are found in greater abundance in fresh ginger, and differ in their chemical structure by the length of unbranched alkyl chains [4].

Metastasis is the leading cause of cancer death and can be described as a cascade of events, each being rate-limiting and providing potential opportunities for therapeutic intervention [5]. Normal cells are transformed into tumor cells due to mutations in genes that regulate critical pathways, producing an imbalance between proliferation and cell death that eventually leads to the formation of a primary tumor. Further interactions with the stromal microenvironment surrounding tumor cells, including endothelial cells, fibroblasts, macrophages and extracellular matrix (ECM) proteins, contribute to the formation of new blood and lymphatic vessels [6]. These interactions facilitate tumor cell invasion of surrounding tissues, intravasation through newly formed vessels, and dissemination to other tissues, to form secondary tumors. During the metastatic process, cells must penetrate natural barriers in the microenvironment, survive in circulation as well as invade and populate a new tissue, the latter being helped by the establishment of a pre-metastatic niche [7-9].

The ECM plays a fundamental role in tumor metastasis. The ECM represents the non-cellular component of tissues, and is formed primarily of water, proteins and polysaccharides; however, its precise composition is tissue-specific [10, 11]. Cell-cell and cell-ECM interactions are important regulator of cell adhesion, migration, proliferation and survival. These processes, in turn, play critical roles during both normal physiological and pathological conditions, such as cancer and metastasis.

The aim of this review is to summarize the most recent studies on the cancer chemopreventive action of [6]-gingerol. We will focus on specific steps of the metastatic process, including cell adhesion, migration, invasion and angiogenesis and describe the effects of [6]-gingerol on each of these steps. We will, in particular, discuss the chemopreventive effects of [6]-gingerol focusing on its ability to inhibit tumor cell proliferation, and to induce apoptosis or reactive oxygen species (ROS) production. This review is divided into two parts describing first results from studies performed *in vitro* and then in different animal models *in vivo*. It was prepared using publications reported over the last 10 years (2003 to 2013) on the NLM-Pubmed and TS-Web of Science online bibliographic databases, using the keyword "[6]-gingerol"

*Address correspondence to this author at the Departamento de Gerontologia, Universidade Federal de São Carlos, Rodovia Washington Luís, Km 235, São Carlos, SP, 13565-905, Brazil; Tel: +55 16 3306 6663; Fax; +55 16 3351 9628; E-mail: mcominetti@ufscar.br

1389-5575/14 $58.00+.00

separately matched with the keywords "cancer", "proliferation", "adhesion", "migration", "invasion", "apoptosis", "angiogenesis", "reactive oxygen species", or "*in vivo*", totaling 175 and 147 papers in NLM-Pubmed and Web of Science, respectively. Excluding duplicates and works using other compounds or ginger extracts, a total of 30 articles were consulted for this review.

IN VITRO CANCER CHEMOPREVENTIVE EFFECTS OF [6]-GINGEROL

Effects of [6]-gingerol on Cell Adhesion, Migration, Invasion and Proliferation

Tumors comprise a complex and heterogeneous cellular network that relies on local and systemic cues to execute malignant programs. The importance of cell-cell adhesion relates to the fact that this phenomenon orchestrates large-scale tumor behaviors such as migration, proliferation and invasion [12]. Cell migration is an integral part of invasion allowing cancer cells to escape the primary tumor and to metastasize to distant sites. It is known that invasion of basement membranes is mainly mediated by the gelatinase matrix metalloproteinases, MMP-2 and -9 [13]. Our search of the literature, combining the words "[6]-gingerol" *and* "cell adhesion" identified one publication by Lee and coworkers [14]. In this paper, they demonstrated that 10 μM [6]-gingerol inhibited MDA-MB-231 human breast cancer cell adhesion to fibronectin, an ECM component, without affecting their proliferation. In the same study, MDA-MB-231 cells treated with [6]-gingerol showed a dose-dependent decrease in invasiveness and motility, as well as decreased expression of MMP-2 and -9 [14].

Similar results were found in Hep3B human hepatocarcinoma cells. Treatment of these cells with 10 μM [6]-gingerol resulted in suppression of MMP-2 and -9 activities, concomitant with inhibition of MAPK and PI3K/Akt phosphorylation [15]. In another study, treatment of human HepG2 hepatocarcinoma cells with 5 μM [6]-gingerol for 24 h inhibited their ability to migrate and invade by 22% and 52%, respectively [16]. Similarly, [6]-gingerol (50 μM – 200μM) efficiently blocked invasion of AH109A hepatoma cells *in vitro* [17].

At higher concentrations, [6]-gingerol exerts potent anti-proliferative effects. Park and colleagues [18] showed that [6]-gingerol inhibits the proliferation of HPAC and BxPC-3 pancreatic cancer cells in a dose- and time-dependent manner. The antiproliferative effects ranged from 50 to 800 μM. At the highest concentration, [6]-gingerol showed similar cytotoxicity against BxPC-3 (89.4% inhibition) and HPAC (91.2% inhibition) cells after 72 hours of exposure [18]. Furthermore, exposure to [6]-gingerol (200 μM) for 72 hours inhibited the growth of HCT-116 (28%), SW480 (17%), HT-29 (28%), LoVo (13%) and Caco-2 (8%) colorectal cancer cells [19]. In addition, [6]-gingerol at concentrations varying from 12.5 to 200 μM inhibited AH109A rat hepatoma cell proliferation [17].

[6]-gingerol also mediated direct anti-proliferative effects in non-human tumor cell lines, such as rat YYT colon cancer, inhibiting cell proliferation at all concentrations tested and being most effective at 100 μM [20]. Another group studied the effects of [6]-gingerol in LoVo colon cancer cells and verified that treatments with 10 and 15 μg/mL (35 μM and 50 μM, respectively) decreased cell viability to almost 70 and 25% (24 hours incubation) and 40% and 25% (48 hours incubation) of untreated controls [21].

While there is a broad spectrum of tumor types inhibited by [6]-gingerol, their sensitivity varies considerably between cell lines. It showed moderate cytotoxicity in the human lung cancer cell lines H-1299 (150 μM) [22] and A549 (150 μM) [23], ovarian cancer SK-OV-3 (50 μM) [23], melanoma SK-MEL-2 (70 μM) [23], colon cancer HCT15 (100 μM) [23] and epidermoid carcinoma A431 cells (300 μM) [24]. In another study, however, [6]-gingerol showed only low inhibition of MDA-MB-231 cell proliferation after 72 hours of incubation (IC_{50} =666.2±134.6 μM) [25]. In some cell lines, [6]-gingerol is ineffective at blocking proliferation. A study performed by Liu and colleagues [26] showed that even at concentrations as high as 150 μM, [6]-gingerol did not inhibit the proliferation of ECC-1 and Ishikawa endometrial cancer cells. Similarly, [6]-gingerol was ineffective at inhibiting the proliferation of murine melanoma cells B16F10, at concentrations as high as 100 μM [27]. Also, as cited above, 10 μM [6]-gingerol had no inhibitory effect on MDA-MB-231 cell proliferation when incubated for 24 hours [14].

Taken together, the results above demonstrate the pleiotropic effects of [6]-gingerol on the function of multiple tumor cell types. Inhibition of cell proliferation, adhesion, migration and invasion, observed at concentrations ranging from 5 to 800 μM indicates that [6]-gingerol may have direct anti-tumor or anti-metastatic activity *in vivo*. However, the degree of sensitivity of various cell lines tested in these assays varies considerably, suggesting that some tumor cells may have developed resistance mechanisms against [6]-gingerol.

Effects of [6]-gingerol on Apoptosis

In the metastatic process, only a small proportion (0.04%) of circulating tumor cells successfully colonize secondary sites. Most tumor cells are killed either by the immune system or by apoptosis [5]. Apoptosis or programmed cell death is a basic cellular process critical to the maintenance of tissue homeostasis [28]. Apoptosis is carried out by two major pathways, the receptor (extrinsic) pathway and the mitochondrial (intrinsic) pathway, which eventually result in the activation of caspases, a family of enzymes that act as effector molecules in various forms of cell death [29]. In the extrinsic pathway, binding of the tumor necrosis factor (TNF) superfamily of death receptors by their cognate natural ligands or by agonistic antibodies initiates receptor oligomerization, followed by the recruitment of adaptor molecules such as FADD and caspase-8 to the activated death receptors leading to the activation of caspase-8. Once activated, caspase-8 either directly cleaves and thereby activates effector caspase-3 or, alternatively, cleaves Bid into tBid [30]. Bid is a BH3-only protein of the Bcl-2 family which, upon cleavage, translocates as tBid to mitochondria to stimulate mitochondrial outer membrane permeabilization [31].

In the intrinsic pathway, the release of proteins from mitochondrial inter-membrane space, such as cytochrome c or second mitochondria-derived activator of caspase (Smac)/ direct IAP binding protein with low pI (DIABLO), into the cytosol triggers a common prefinal stage of apoptosis that is characterized by the activation of effector caspases [32]. Cytochrome c promotes caspase-3 activation via formation of the apoptosome complex that contains, besides cytochrome c, Apaf-1 and caspase-9 and results in the activation of caspase-9 and subsequently, caspase-3 [33].

Among their various biological activities, natural products such as [6]-gingerol modulate apoptosis signaling pathways. Lee *et al.* [19] reported that [6]-gingerol increased apoptosis in human colorectal cancer cells, HCT-116, SW480 and LoVo, but not in HT-29 and Caco-2 cells. Flow cytometry analysis showed that the number of apoptotic cells was significantly higher in HCT-116 cells (50, 100 and 200 μM) and in SW480 and LoVo cells (200 μM) after incubation with [6]-gingerol for a period of 72 hours. Cell cycle analysis demonstrated that [6]-gingerol induces G_1 cell cycle arrest in HCT-116 and LoVo cells. To investigate the molecular mechanisms by which [6]-gingerol mediates apoptosis induction and cell cycle arrest, the authors studied the expression of several cell cycle and apoptosis-related genes. They showed that [6]-gingerol (200 μM) suppressed cyclin D1 protein expression in a dose-dependent manner in HCT-116 (100, 150, and 200 μM), SW480 and Caco-2 cells. They also found that treatment with [6]-gingerol (100 - 200 μM) increased NAG-1 protein and mRNA levels in HCT-116 cells and LoVo cells. Suppression of cyclin D1 and induction of NAG-1 by [6]-gingerol appear to require proteolytic degradation and modulation of β-catenin, PKCε, and GSK-3β pathways [19].

On the other hand, Lin and coworkers [21] observed a decrease in G0/G1 phase and an increase in G2/M ratio in LoVo cells treated with 5, 10 and 15 μg/mL (15, 35 and 50 μM respectively) of [6]-gingerol. Monitoring levels of procaspase-3 and caspase-8 in these cells treated with the same concentrations of [6]-gingerol showed no significant changes, but, at concentrations up to 50 μM, increased p53 level, consistent with induction of apoptotic cell death [21].

Another group reported that apoptosis was detected in human hepatocellular carcinoma, HepG2 cells after incubation with [6]-gingerol (0-200 μM) for 24 hours [34]. Hoechst 33342 staining showed that [6]-gingerol-treated HepG2 cells displayed an increased ratio of chromatin condensation and fragmented fluorescent nuclei that was dose-dependent. In a TUNEL assay, the level of apoptotic HepG2 cells treated with [6]-gingerol at concentrations of 50, 100 and 200 μM for 24 hours was significantly higher compared to untreated cells [34]. Chakraborty *et al.* [35] reported that [6]-gingerol induced apoptosis and autophagy in cervix adenocarcinoma HeLa cells. Treatment with 75, 100 and 125 μM [6]-gingerol caused externalization of phosphatidylserine detected by Annexin V binding, and increased the expression of caspase-3 and PARP. The same treatment also increased TUNEL positivity, chromatin condensation and DNA fragmentation, indicative of nuclear DNA degradation and apoptosis.

Nigam and colleagues [24] observed that epidermoid carcinoma cells A431 treated with [6]-gingerol at 250, 300 and 350 μM, presented an increase in sub-G1 population and a decrease in G1 phase of the cell cycle. DNA fragmentation, downregulation of anti-apoptotic Bcl-2 expression and up-regulation of pro-apoptotic Bax, cytochrome-c, Apaf-1, caspase-9 and caspase-3 proteins were also demonstrated by western blotting analysis, indicating that [6]-gingerol induces apoptosis in this cell line [24].

Park *et al.* [18] investigated [6]-gingerol's action on HPAC and BxPC-3 pancreatic tumor cell lines, that express wild-type and mutant forms of p53 respectively. Treatment with [6]-gingerol (400 μM) arrested cell cycle in G1 phase by decreasing cyclin A and cdk expression in both cell lines. This study also showed that [6]-gingerol induced apoptotic death in BxPC-3 but not in HPAC cells, suggesting that [6]-gingerol can bypass p53 mutant resistance to apoptosis. Protein expression analysis demonstrated that NF-kB, AP-1, COX-2, MAPK, pJNK and pERK were inhibited in both cell types after [6]-gingerol treatment. No changes in p85α regulatory subunit of PI3K in both cell lines were observed while AKT phosphorylation was increased in HPAC but not in BxPC-3 cells [18].

Shukla and colleagues [36] reported the modulatory properties of [6]-gingerol on testosterone-induced alterations of apoptosis related proteins in LNCaP human prostate cancer cells. These cells were treated (50 nM) or not with testosterone for 12 hours followed by incubation with [6]-gingerol (50 and 75 μM) for 24 hours. Under both conditions, [6]-gingerol increased sub-G1 cell population and decreased S cell population demonstrating that [6]-gingerol alone is sufficient to induce cell cycle arrest in prostate cancer cells. Testosterone and [6]-gingerol used in combination also decreased mitochondrial membrane potential, increased DNA fragmentation p53 Bax, caspases-3 and -9 expression and restored testosterone-induced upregulation of Bcl-2 to normal levels in LNCaP cells in a dose-dependent manner. Cells treated with [6]-gingerol alone exhibited the same changes, but showed further decrease in anti-apoptotic Bcl-2 protein expression. These observations indicate that [6]-gingerol may be effective to counter the anti-apoptotic effects of testosterone in androgen-dependent prostate cancer.

In contrast, Ishiguro and coworkers [37] found that 50 μg/mL [6]-gingerol (170 μM) alone was insufficient to induce apoptosis in HCG gastric cancer cells. However, co-treatment with TRAIL (40 ng/mL) and [6]-gingerol for 18 hours increased apoptosis in this cell line indicating that [6]-gingerol enhances TRAIL-induced caspase-3 and caspase-7 activation through inhibition of NF-kB activation.

Collectively, the data described above demonstrate that [6]-gingerol acts mainly as a pro-apoptotic molecule in different cell lines and that its pharmacological effects may vary, depending on the cell line. Thus, [6]-gingerol can act on tumor cells by inducing cell cycle arrest or by inhibiting or inducing the expression of anti-apoptotic and pro-apoptotic molecules, respectively, at concentrations ranging from approximately 50 to 400 μM.

Effects of [6]-gingerol on ROS Production

Reactive oxygen species (ROS) are a family of active molecules including superoxide (O_2^-), peroxyl (ROO•), hydroxyl (OH•), and nitric oxide (NO•) that are involved in the modulation of cell functions. However, a large amount or sustained levels of ROS can result in the oxidation of biomolecules, causing cell damage leading to growth arrest, senescence, or death [38]. ROS produced in the body, primarily by mitochondria, play a major role in various cell-signaling pathways. They activate various transcription factors, resulting in the translation of proteins that control inflammation, cellular transformation, tumor cell survival, proliferation, invasion, angiogenesis, and metastasis. Increased intracellular ROS usually leads to DNA damage, and the subsequent phosphorylation of p53 contributes to cell cycle arrest and further apoptosis of cancer cells. Various chemotherapeutic agents used in cancer treatment mediate their effects through the production of ROS, which have been implicated also in the chemo-protective and anti-tumor action of natural products, including gingerols [39]. Paradoxically, increasing evidence suggests that natural product-based compounds with antioxidant activity can effectively neutralize oxidative stress and thus suppress ROS-mediated tumorigenesis in healthy cells. Thus, it appears that natural products have a dual function, either causing ROS-induced tumor cell death or being potent bioactive molecules, protecting healthy cells from oxidative damage.

Indeed, evidence from the literature indicates that [6]-gingerol can act either as a pro-oxidant or as an antioxidant molecule, depending on the experimental approach used. Lin and colleagues [21] demonstrated that 10 and 15 μg/mL (35 and 50 μM, respectively) of [6]-gingerol dose-dependently increased intracellular ROS in LoVo colon cancer cells and this effect was inhibited by pretreatment with *N*-acetylcysteine (NAC), a potent antioxidant. The authors proposed that the increase in p53 levels observed may be attributed to the induction of ROS by [6]-gingerol in this cell line.

Others tested the effect of different concentrations of [6]-gingerol on the induction of ROS using the HepG2 hepatoma cell line [40]. The authors demonstrated that treatment of HepG2 cells with [6]-gingerol at concentrations of 20, 40 and 80 μM resulted in a significant increase in ROS production with a striking decrease of intracellular GSH [40]. Subsequently, the same research group also demonstrated the antioxidant effects of [6]-gingerol. They showed that pretreatment of the same HepG2 cell line with [6]-gingerol (10 μM, 1 hour) produced a significant and dose-dependent reduction of ROS induced by patulin, a mycotoxin produced by several fungi species [41]. More recently, the authors found a significant increase in ROS production in HepG2 cells treated with [6]-gingerol at concentrations of 50, 100 and 200 μM, with a concomitant decrease in intracellular GSH, suggesting that apoptosis may be related to GSH depletion in this cell line [34]. Intracellular ROS levels were also significantly and dose-dependently increased in human epidermoid carcinoma A431 cells treated with [6]-gingerol (250 to 350 μM) [24].

Conversely, Park and coworkers [42] demonstrated that [6]-gingerol decreased the production of ROS in TGF-beta 1-induced nasal polyp-derived fibroblasts, evidencing its antioxidant effect. [6]-gingerol (25-100 μM) also inhibited intracellular ROS production induced by H_2O_2 in a dose dependent pattern in B16F10 murine melanoma cells, protecting them from oxidative injury [43]. Dugasani and colleagues [44] found that [6]-gingerol had the weakest relative scavenging potential when compared to [6]-shogaol, [10]-gingerol and [8]-gingerol but was equipotent to positive control, α-tocopherol as an antioxidant molecule. Additionally, 20 μM [6]-gingerol inhibited the rises in the intracellular peroxide levels concomitant with decreased invasion of AH109A hepatoma cells, suggesting that its antioxidative property may be involved in its anti-invasive action [17]. Additionally, LPS-induced ROS production in the mouse leukaemic monocyte macrophage cell line RAW 264.7 was inhibited by [6]-gingerol treatment at concentrations ranging from 20 to 80 μM [45]. Interestingly, while [6]-gingerol suppressed O_2^- generation in HL-60 cells [46], aframodial, a diterpenoid from *Aframomum* species, had much higher suppressive effects on ROS and reactive nitrogen species generation and on the expression of pro-inflammatory genes than [6]-gingerol. This led the authors to the hypothesis that aframodial, rather than [6]-gingerol, may be the major antioxidant and anti-inflammatory ginger compound.

Effects of [6]-gingerol on Angiogenesis

Angiogenesis refers to the formation of new blood vessels from pre-existing endothelium and is a fundamental process in a variety of physiological and pathological conditions including wound healing, embryonic development, chronic inflammation, and cancer progression and metastasis [47]. Angiogenesis plays an important role not only in primary tumor vascularization but also in metastasis. It is well known that tumors require a microvasculature development in order to grow and metastasize [48]. Tumor angiogenesis is tightly controlled by positive and negative regulators produced by the tumors and neighboring cells. Two angiogenic factors, vascular endothelial growth factor (VEGF) and interleukin-8 (IL-8), are often used as diagnostic markers for tumor metastasis and proliferation [49]. Currently, the most common approach for limiting tumor angiogenesis is VEGF pathway blockade [50].

Recent data showed that [6]-gingerol (5-25 μM) inhibited both VEGF- and bFGF-induced proliferation of human endothelial cells (HUVECs). It also blocked capillary-like tube formation by endothelial cells in response to VEGF, and strongly inhibited sprouting of endothelial cells in rats' aorta and formation of new blood vessel in mice's cornea in response to VEGF at 10 and 25 μM in both assays [51].

In another work, it was demonstrated that at lower doses (starting from 0.8 μM), [6]-gingerol effectively inhibited endothelial cell tube formation by MS1 endothelial cells. The mechanism of action to block tumor growth, as suggested by the authors, could be related to the inhibition of the tumor blood supply [20]. Weng and co-workers [15] showed that [6]-gingerol reduced VEGF and IL-8 secretion in Hep3B hepatocarcinoma cells. Based on these observations, they performed additional tests using HUVEC cells or rat aortas to demonstrate the anti-angiogenic properties of [6]-gingerol.

They observed tube formation retardation and significantly decreased tube lengths that were 81% of the control after treatment with 10 μM [6]-gingerol. Similarly, the outgrowth capillary lengths were significantly reduced to 71% of the untreated control [15].

IN VIVO TUMOR CHEMOPREVENTIVE EFFECTS OF [6]-GINGEROL

The first study investigating the antitumor effects of [6]-gingerol *in vivo* was performed in 2005 by Kim and collaborators [51]. C57BL/6 mice were injected intraperitoneally with [6]-gingerol (3 or 5 mg/kg) prior to intravenous injection of B16F10 melanoma cells. After three weeks, lungs were examined for the presence of metastatic colonies. [6]-gingerol markedly suppressed lung colonization in 50% (3 mg/kg) or almost 100% of animals at higher doses (5 mg/kg) compared to control mice [51]. In the same year, another group [52] aimed to investigate the effects of [6]-gingerol in TPA-induced cyclooxygenase (COX-2) expression in mouse skin. COX-2 is involved in prostaglandin biosynthesis and inflammation, a phenomenon frequently observed in various premalignant and malignant tissues. The authors verified that [6]-gingerol (30 μM) inhibited TPA-induced COX-2 expression in mouse skin *in vivo* by blocking the p38 MAP kinase-NF-kB signaling pathway [52].

The *in vivo* effects of [6]-gingerol were also tested on a model of prostate hyperplasia induced by daily subcutaneous injections of testosterone for a 15 days period. Results showed a significant decrease in prostate weight with supplementation of [6]-gingerol (10 mg/kg) given both prior and post-testosterone administration. [6]-gingerol alone did not cause any significant change in the weight of prostate. The authors conclude that [6]-gingerol shows therapeutic potential for the management of prostate cancer [36].

Jeong and colleagues [53] aimed to investigate the *in vivo* effects of [6]-gingerol on human HCT116 colorectal cancer in nude mice. The authors demonstrated that mice fed by gavage with [6]-gingerol (25 mg/kg) three times a week before being injected with HCT116 cells had fewer measurable tumors and lived longer than untreated control mice. The authors defined a molecular mechanism whereby the suppression of tumor growth *in vivo* is mediated by [6]-gingerol enzymatic inhibition of leukotriene A4 hydrolase, an enzyme implicated in the anchorage-independent growth of HCT116 colon cancer cells [53].

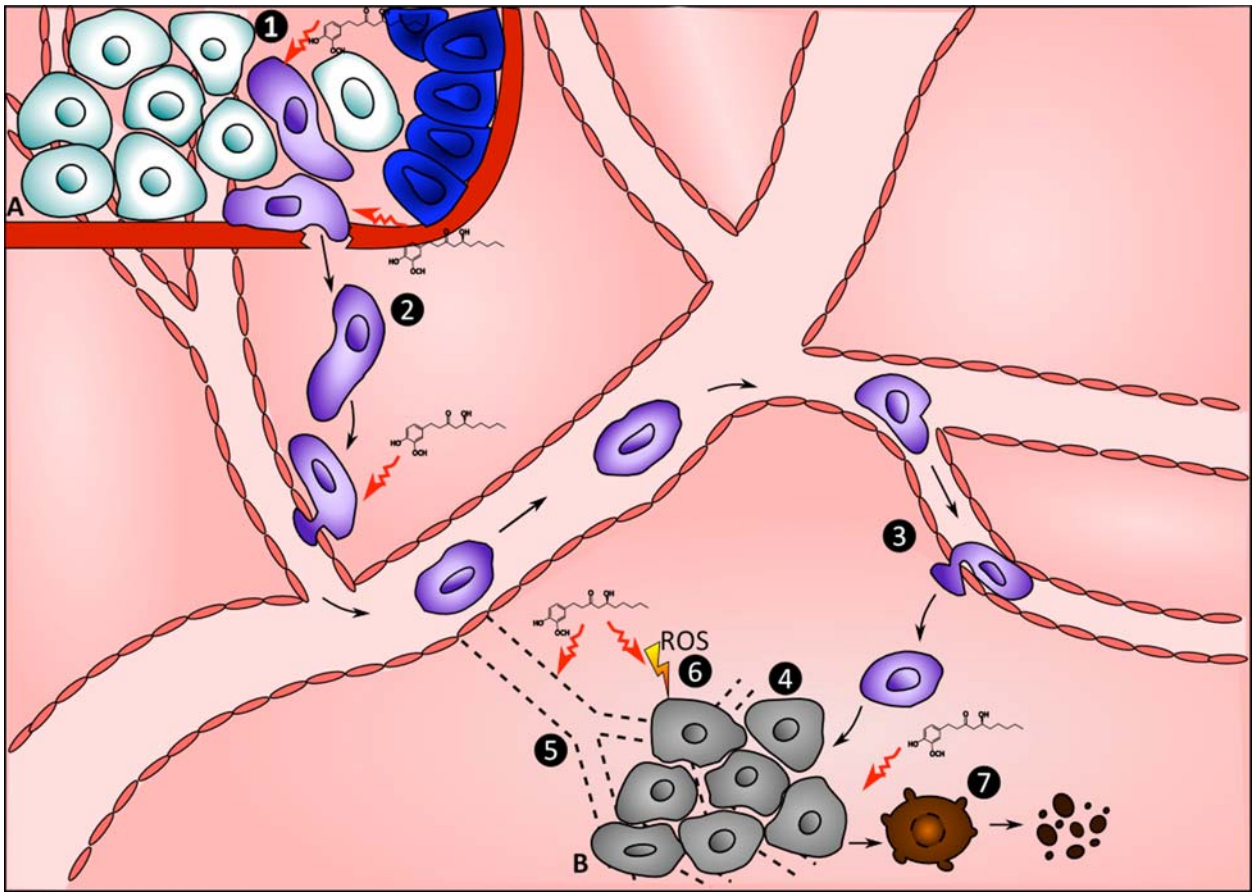

Fig. (1). Effects of [6]-gingerol on different steps of metastatic process. In the scheme it is presented the primary tumor (**A**), the metastatic site, with pre-metastatic niche (**B**), red structures represent blood vessels, blue cells represent normal untransformed cells, green cells represent the primary tumor, purple cells represent tumor transformed cells and grey cells represent metastatic cells at the secondary tumor. [6]-gingerol interferes with metastatic cell adhesion to ECM (❶); inhibits metastatic cell migration (❷); invasion (❸) and proliferation of tumor cells (❹) [6]-gingerol also acts inhibiting angiogenesis at the secondary tumor site (❺), stimulating the production of reactive oxygen species (❻) or stimulating apoptosis and necrosis in tumor cells, in brown (❼). Adapted from [57].

Table 1. Activity of [6]-gingerol in different steps of metastatic process.

***In vitro* assays**			
Cell line	**Concentration (μM)**	**Effect**	**Reference**
Adhesion			
MDA-MB-231	10	-	[14]
Migration			
MDA-MB-231	2.5 to 10	-	[14]
Hep3B	10	-	[15]
HepG2	5		[16]
Invasion			
MDA-MB-231	2.5 to 10	-	[14]
Hep3B	10	-	[15]
AH109A	50 to 200	-	[16]
HepG2	5	-	[16]
Proliferation			
MDA-MB-231	10	No effect	[14]
AH109A	12.5 to 200	-	[17]
BxPC-3, HPAC	50 to 800	-	[18]
HCT-116, SW480, HT-29, LoVo, Caco-2	200	-	[19]
YYT	100	-	[20]
LoVo	35 to 50[1]	-	[21]
H-1299	*150*	-	[22]
A549, SK-OV-3, SK-MEL-2, HCT15	50 to 150[1]	-	[23]
A431	*300*	-	[24]
MDA-MB-231	*666.2±134.6*	-	[25]
ECC-1, Ishikawa	150	No effect	[26]
B16F10	100	No effect	[27]
HepG2	*304.27±13.65*	-	[40]
Apoptosis			
HPAC, BxPC-3	400	+	[18]
HCT-116	50 to 200	+	[19]
SW48, LoVo	200	+	[19]
Lovo	50	+	[21]
A431	250 to 350	+	[24]
HepG2	50 to 200	+	[34]
HeLa	75 to 125	+	[35]
LNCaP	50 and 75	+	[36]
HGC	170[1,2]	+	[37]

(Table 1) Contd….

Cell line	Concentration (μM)	Effect	Reference
Production of ROS			
AH109A	20	-	[17]
LoVo	35 to 50[1]	+	[21]
A431	250 to 350	+	[24]
HepG2	50 to 200	+	[34]
HepG2	20 to 80	+	[40]
HepG2	10	-	[41]
B16F10	25 to 100	-	[43]
RAW264.7	20 to 80	-	[45]
Angiogenesis			
HUVEC	10	-	[15]
MS1	0.8	-	[20]
HUVEC	25 to 50	-	[51]
In vivo assays			
Animal	**Dose/Concentration**	**Effect**	**Reference**
Swiss albino	10 mg/Kg	-	[36]
C57BL/6	3 to 5 mg/Kg	-	[51]
ICR mice	30 μM	-	[52]
Nude mice	25mg/Kg	-	[53]
Swiss albino	2.5 μM	-	[54]
ICR mice	2.5 μM	-	[55]
Balb-c and C57BL/6	0.5 mg/Kg	-	[56]

Italic numbers represents IC_{50} values; symbols (+) or (-) represent induction or inhibition of the process, respectively. [1]Calculated by the authors of this review; [2]Represents co-treatment with TRAIL; Cell lines presented in the table are: MDA-MB-231, human breast cancer cells; Hep3B and HepG2, human hepatocarcinoma; AH109A, rat ascite hepatoma; HCT-116, SW480, HT-29, LoVo, Caco-2, human coloretal cancer; A-549, human lung cancer; SK-OV-3, human ovarian cancer; SK-MEL-2, human skin cancer; HCT15, human colon cancer; A431, epidermoid carcinoma; BxPC-3 and HPAC, human pancreatic cancer cells; YTT, rat colon cancer; H-1299, human lung cancer; B16F10, murine melanome cells; ECC-1 and Ishikawa, human endometrial cancer, HeLa, human cervix adenocarcinoma; LNCaP, human prostate cancer; HGC, human gastric cancer; RAW264.7, murine leukemia; HUVEC, human endothelial cells; MS1, mouse endothelial cells.

More recently Nigam and colleagues [54] used a mouse skin carcinogenesis model in an attempt to evaluate the biological activity of [6]-gingerol. They applied B[a]P (5 μg/animal) topically as a carcinogen to induce mouse skin tumors (squamous cell carcinoma). Mice were untreated (controls) or treated with B[a]P and/or [6]-gingerol (2.5 μM/animal) thrice weekly for 32 weeks. Results revealed a delay of approximately 5 weeks in the onset of tumorigenesis in [6]-gingerol treated groups compared to the B[a]P treated mice. In addition, [6]-gingerol treatment resulted in an increase in the incidence of tumor-free animals and reduction in tumor volume by 51% and 65% in mice receiving topical [6]-gingerol, 30 min prior and postB[a]P, respectively. Regarding cumulative number of tumors, [6]-gingerol treatment caused a decrease of 55% (prior B[a]P injection) and 74% (post B[a]P injection). Suppression of skin tumorigenesis by [6]-gingerol was confirmed histologically. The authors concluded that [6]-gingerol may prevent skin cancer development by directly triggering apoptosis-promoting signaling cascades [54].

Wu and coworkers [55] applied 2.5 μM [6]-gingerol topically twice weekly for 20 weeks in female ICR mice previously treated with DMBA/TPA to induce squamous cell carcinoma formation. The authors found that pre-treatment with [6]-gingerol reduced the number of tumors per mouse as well as the number of animals developing tumors by 70.6% and 28%, respectively. Additionally, [6]-gingerol reduced the number and size of benign papilloma in treated mice. However, in this work the authors compared the

antitumor effects of other compounds and concluded that [6]-shogaol is more effective than [6]-gingerol at inhibiting TPA-induced tumor promotion in mouse skin.

Finally, Ju and coauthors [56], aiming to investigate the number of tumor-infiltrating lymphocytes (TIL) in murine tumors, provided [6]-gingerol in drinking water to Balb/c and C57BL/6 female mice three days after tumor cells inoculation. Results demonstrated that treatment with 0.5 mg/kg/day of [6]-gingerol, resulted in the inhibition of melanoma (B16F1), renal cell carcinoma (Renca) and colon carcinoma (CT26) growth. However, topical [6]-gingerol did not lead to complete eradication of the tumors. In addition, mice treated with [6]-gingerol exhibited a massive increase in the number of TILs with activated characteristics. The authors suggested that [6]-gingerol could be used for tumor immunotherapy to increase the number of TILs [56].

Taken together, these *in vivo* studies show the therapeutic potential of [6]-gingerol for inhibition of tumor growth and metastasis in different animal models. Clearly, more studies should be performed to understand the underlying mechanisms and efficacy of this compound as a cancer chemopreventive agent. The effects of [6]-gingerol on different metastatic steps, as demonstrated through the above studies, are summarized in Table **1** and Fig. (**1**).

CONCLUSIONS

It is possible to conclude that [6]-gingerol acts on different steps of the metastatic process, from tumor cell adhesion to other processes such as cell migration, invasion, proliferation and angiogenesis. The review highlighted a number of *in vitro* and *in vivo* results indicating that [6]-gingerol is a promising and effective molecule, which can be used to block carcinogenesis. Since most modern chemotherapeutic drugs currently available are expensive, toxic, and subject to treatment resistance, it is imperative to investigate thoroughly agents derived from natural sources that are typically less toxic to normal tissues, such as [6]-gingerol, for their use to prevent and/or treat cancer and metastasis. The most common mechanisms of action described in the literature to explain [6]-gingerol inhibitory effects are inhibition of proliferation, induction of apoptosis and regulation of ROS production. However the concentration of [6]-gingerol required for inhibition varies considerably between tumor types, ranging from as low as 0.8 μM up to 800 μM. For example, colon and prostate cancer cells appear to be particularly sensitive to the inhibitory effects of [6]-gingerol whereas breast tumor lines such as MDA-MB-231 are relatively resistant. Furthermore, while inhibition of several signaling pathways was demonstrated in the above studies, the specific molecular target(s) inhibited by [6]-gingerol need to be better defined. Clearly, further studies in patients and in clinically relevant animal models are required to validate the efficacy of this molecule *in vivo*, either alone or in combination with existing therapy and to determine the tumor types most likely to benefit from these interventions. It will be important also in future studies to assess whether [6]-gingerol may be more effective to prevent the development of cancer or for the treatment of established disease.

CONFLICT OF INTEREST

The authors confirm that this article content has no conflicts of interest.

ACKNOWLEDGEMENTS

This work is supported by grants from FAPESP (2008/56758-0), CAPES and CNPq.

REFERENCES

[1] Park, E.J.; Pezzuto J.M. Botanicals in cancer chemoprevention. *Cancer Metastasis Rev*, **2002**, 21(3-4), 231-55.

[2] Ali, B.H.; Blunden, G.; Tanira, M.O.; Nemmar, A. Some phytochemical, pharmacological and toxicological properties of ginger (*Zingiber officinale* Roscoe): a review of recent research. *Food Chem Toxicol*, **2008**, 46(2), 409-20.

[3] Haniadka, R.; Rajeev, A.G.; Palatty, P.L.; Arora, R.; Baliga M.S. *Zingiber officinale* (ginger) as an anti-emetic in cancer chemotherapy: a review. *J Altern Complement Med*, **2012**, 18(5), 440-4.

[4] Shukla, Y.; Singh, M. Cancer preventive properties of ginger: a brief review. *Food Chem Toxicol*, **2007**, 45(5), 683-90.

[5] Perret, G.Y.; Crepin, M. New pharmacological strategies against metastatic spread. *Fundam Clin Pharmacol*, **2008**, 22(5), 465-92.

[6] Joyce, J.A.; Pollard, J.W. Microenvironmental regulation of metastasis. *Nat Rev Cancer*, **2009**, 9(4), 239-52.

[7] Sceneay, J.; Smyth, M.J.; Moller, A. The pre-metastatic niche: finding common ground. *Cancer Metastasis Rev*, **2013,** 32, 449-464.

[8] Peinado, H.; Lavotshkin, S.; Lyden, D. The secreted factors responsible for pre-metastatic niche formation: old sayings and new thoughts. *Semin Cancer Biol*, **2011**, 21(2),139-46.

[9] Psaila, B.; Kaplan, R.N.; Port, E.R.; Lyden, D. Priming the 'soil' for breast cancer metastasis: the pre-metastatic niche. *Breast Dis*, **2006**, 26, 65-74.

[10] Batzios, S.P.; Zafeiriou, D.I.; Papakonstantinou, E. Extracellular matrix components: an intricate network of possible biomarkers for lysosomal storage disorders? *FEBS Lett*, **2013**, 587(8), 1258-67.

[11] Hubmacher, D.; Apte, S.S. The biology of the extracellular matrix: novel insights. *Curr Opin Rheumatol*, **2013**, 25(1), 65-70.

[12] Hale, J.S.; Li, M.; Lathia, J.D. The malignant social network: cell-cell adhesion and communication in cancer stem cells. *Cell Adh Migr*, **2012**, 6(4), 346-55.

[13] Seiki, M.; Yana, I. Roles of pericellular proteolysis by membrane type-1 matrix metalloproteinase in cancer invasion and angiogenesis. *Cancer Sci*, **2003,** 94(7), 569-74.

[14] Lee, H.S.; Seo, E.Y.; Kang, N.E.; Kim, W.K. [6]-Gingerol inhibits metastasis of MDA-MB-231 human breast cancer cells. *J Nutr Biochem*, **2008**, 19(5), 313-9.

[15] Weng, C.J.; Chou, C.P.; Ho, C.T.; Yen, G.C. Molecular mechanism inhibiting human hepatocarcinoma cell invasion by 6-shogaol and 6-gingerol. *Mol Nutr Food Res*, **2012**, 56(8), 1304-14.

[16] Weng, C.J.; Wu, C.F.; Huang, H.W.; Ho, C.T.; Yen, G.C. Anti-invasion effects of 6-shogaol and 6-gingerol, two active components in ginger, on human hepatocarcinoma cells. *Mol Nutr Food Res*, **2010**, 54(11), 1618-1627.

[17] Yagihashi, S.; Miura, Y.; Yagasaki, K. Inhibitory effect of gingerol on the proliferation and invasion of hepatoma cells in culture. *Cytotechnology*, **2008**, 57(2), 129-36.

[18] Park, Y.J.; Wen, J.; Bang, S.; Park, S.W.; Song, S.Y. [6]-Gingerol induces cell cycle arrest and cell death of mutant p53-expressing pancreatic cancer cells. *Yonsei Med J*, **2006**, 47(5), 688-97.

[19] Lee, S.H.; Cekanova, M.; Baek, S.J. Multiple mechanisms are involved in 6-gingerol-induced cell growth arrest and apoptosis in human colorectal cancer cells. *Mol Carcinog*, **2008**, 47(3), 197-208.

[20] Brown, A.C.; Shah, C.; Liu, J.; Pham, J.T.; Zhang, J.G.; Jadus, M.R. Ginger's (*Zingiber officinale* Roscoe) inhibition of rat colonic adenocarcinoma cells proliferation and angiogenesis *in vitro*. *Phytother Res*, **2009**, 23(5), 640-5.

[21] Lin, C.B.; Lin, C.C.; Tsay, G.J. 6-Gingerol Inhibits Growth of Colon Cancer Cell LoVo via Induction of G2/M Arrest. *Evid Based Complement Alternat Med*, **2012**, 326096.

[22] Sang, S.; Hong, J.; Wu, H.; Liu, J.; Yang, C.S.; Pan, M.H.; Badmaev, V.; Ho, C.T. Increased growth inhibitory effects on

human cancer cells and anti-inflammatory potency of shogaols from *Zingiber officinale* relative to gingerols. *J Agric Food Chem*, **2009,** 57(22), 10645-50.

[23] Kim, J.S.; Lee, S.I; Park, H.W.; Yang, J.H.; Shin, T.Y.; Kim, Y.C.; Baek, N.I.; Kim, S.H.; Choi, S.U.; Kwon, B.M.; Leem, K.H.; Jung, M.Y.; Kim, D.K. Cytotoxic components from the dried rhizomes of *Zingiber officinale* Roscoe. *Arch Pharm Res*, **2008**, 31(4), 415-8.

[24] Nigam, N.; Bhui, K.; Prasad, S.; George, J.; Shukla, Y. [6]-Gingerol induces reactive oxygen species regulated mitochondrial cell death pathway in human epidermoid carcinoma A431 cells. *Chem Biol Interact*, **2009**, 181(1), 77-84.

[25] Almada da Silva, J.; Becceneri, A.B.; Sanches, M.H.; Moreno Martin, A.C.; Fernandes da Silva, M.F.; Fernandes, J.B.; Vieira, P.C.; Cominetti, M.R. Purification and differential biological effects of ginger-derived substances on normal and tumor cell lines. *J Chromatogr B Analyt Technol Biomed Life Sci*, **2012**, 903,157-62.

[26] Liu, Y.; Whelan, R.J.; Pattnaik, B.R.; Ludwig, K.; Subudhi, E.; Rowland, H.; Claussen, N.; Zucker, N.; Uppal, S.; Kushner, D.M.; Felder, M, Patankar, M.S.; Kapur, A.Terpenoids from *Zingiber officinale* (Ginger) Induce Apoptosis in Endometrial Cancer Cells through the Activation of p53. *Plos One*, **2012**, 7(12), e53178.

[27] Huang, H.C.; Chiu, S.H.; Chang, T.M. Inhibitory Effect of [6]-Gingerol on Melanogenesis in B16F10 Melanoma Cells and a Possible Mechanism of Action. *Biosci Biotechnol Biochem*, **2011**, 75(6), 1067-1072.

[28] Fulda, S.; Debatin, K.M. Targeting apoptosis pathways in cancer therapy. *Curr Cancer Drug Targets*, **2004**, 4(7), 569-76.

[29] Fulda, S.; Debatin, K.M. Extrinsic versus intrinsic apoptosis pathways in anticancer chemotherapy. *Oncogene*, **2006**, 25(34), 4798-811.

[30] Adams, J.M.; Cory, S. The Bcl-2 apoptotic switch in cancer development and therapy. *Oncogene*, **2007**, 26(9), 1324-37.

[31] Sayers, T.J.; Targeting the extrinsic apoptosis signaling pathway for cancer therapy. *Cancer Immunol Immunother*, **2011**, 60(8), 1173-80.

[32] Kroemer, G.; Galluzzi, L.; Brenner, C. Mitochondrial membrane permeabilization in cell death. *Physiol Rev*, **2007**, 87(1), 99-163.

[33] Saelens, X.; Festjens, N.; Vande Walle, L.; van Gurp, M.; van Loo, G.; Vandenabeele, P. Toxic proteins released from mitochondria in cell death. *Oncogene*, **2004**, 23(16), 2861-74.

[34] Yang, G.; Wang, S.; Zhong, L.; Dong, X.; Zhang, W.; Jiang, L.; Geng, C.; Sun, X.; Liu, X.; Chen, M.; Ma, Y. 6-Gingerol induces apoptosis through lysosomal-mitochondrial axis in human hepatoma G2 cells. *Phytother Res*, **2012**, 26(11), 1667-73.

[35] Chakraborty, D.; Bishayee, K.; Ghosh, S.; Biswas, R.; Mandal, S.K.; Khuda-Bukhsh, A.R. [6]-Gingerol induces caspase 3 dependent apoptosis and autophagy in cancer cells: drug-DNA interaction and expression of certain signal genes in HeLa cells. *Eur J Pharmacol*, **2012**, 694(1-3), 20-9.

[36] Shukla, Y.; Prasad, S.; Tripathi, C.; Singh, M.; George, J.; Kalra, N. *In vitro* and *in vivo* modulation of testosterone mediated alterations in apoptosis related proteins by [6]-gingerol. *Mol Nutr Food Res*, **2007**, 51(12), 1492-502.

[37] Ishiguro, K.; Ando, T.; Maeda, O.; Ohmiya, N.; Niwa, Y.; Kadomatsu, K.; Goto, H. Ginger ingredients reduce viability of gastric cancer cells via distinct mechanisms. *Biochemical and Biophysical Research Communications*, **2007**, 362(1), 218-223.

[38] Finkel, T.; Holbrook, N.J. Oxidants, oxidative stress and the biology of ageing. *Nature*, **2000**, 408(6809), 239-47.

[39] Gupta, S.C.; Hevia, D.; Patchva, S.; Park, B.; Koh, W.; Aggarwal, B.B. Upsides and downsides of reactive oxygen species for cancer: the roles of reactive oxygen species in tumorigenesis, prevention, and therapy. *Antioxid Redox Signal*, **2012**, 16(11), 1295-322.

[40] Yang, G.; Zhong, L.; Jiang, L.; Geng, C.; Cao, J.; Sun, X.; Ma. Y. Genotoxic effect of 6-gingerol on human hepatoma G2 cells. *Chem Biol Interact*, **2010**, 185(1), 12-7.

[41] Yang, G.; Zhong, L.; Jiang, L.; Geng, C.; Cao, J.; Sun, X.; Liu, X.; Chen, M.; Ma, Y. 6-gingerol prevents patulin-induced genotoxicity in HepG2 cells. *Phytother Res*, **2011**, 25(10), 1480-5.

[42] Park, S.A.; Park, I.H.; Cho, J.S.; Moon, Y.M.; Lee, S.H.; Kim, T.H.; Lee, S.H.; Lee, H.M. Effect of [6]-gingerol on myofibroblast differentiation in transforming growth factor beta 1-induced nasal polyp-derived fibroblasts. *Am J Rhinol Allergy*, **2012**, 26(2), 97-103.

[43] Huang, H.C.; Chiu, S.H.; Chang, T.M. Inhibitory effect of [6]-gingerol on melanogenesis in B16F10 melanoma cells and a possible mechanism of action. *Biosci Biotechnol Biochem*, **2011**, 75(6), 1067-72.

[44] Dugasani, S.; Pichika, M.R.; Nadarajah, V.D.; Balijepalli, M.K.; Tandra, S.; Korlakunta, J.N. Comparative antioxidant and anti-inflammatory effects of [6]-gingerol, [8]-gingerol, [10]-gingerol and [6]-shogaol. *J Ethnopharmacol*, **2010,** 127(2), 515-20.

[45] Lee, T.Y.; Lee, K.C.; Chen, S.Y.; Chang, H.H. 6-Gingerol inhibits ROS and iNOS through the suppression of PKC-alpha and NF-kappaB pathways in lipopolysaccharide-stimulated mouse macrophages. *Biochem Biophys Res Commun*, **2009**, 382(1), 134-9.

[46] Wang, C.C.; Chen, L.G.; Lee, L.T.; Yang, L.L. Effects of 6-gingerol, an antioxidant from ginger, on inducing apoptosis in human leukemic HL-60 cells. *In Vivo*, **2003**, 17(6), 641-5.

[47] Folkman, J.; Tumor angiogenesis and tissue factor. *Nat Med*, **1996,** 2(2), 167-8.

[48] Gomes, F.G.; Nedel, F.; Alves, A.M.; Nör, J.E.; Tarquinio, S.B.Tumor angiogenesis and lymphangiogenesis: tumor/endothelial crosstalk and cellular/microenvironmental signaling mechanisms. *Life Sci*, **2013**, 92(2),101-7.

[49] Tartour, E.; Pere, H.; Maillere, B.; Terme, M.; Merillon, N.; Taieb, J.; Sandoval, F.; Quintin-Colonna, F.; Lacerda, K.; Karadimou, A.; Badoual, C.; Tedgui, A.; Fridman, W.H.; Oudard, S. Angiogenesis and immunity: a bidirectional link potentially relevant for the monitoring of antiangiogenic therapy and the development of novel therapeutic combination with immunotherapy. *Cancer Metastasis Rev*, **2011**, 30(1), 83-95.

[50] Kubota, Y. Tumor angiogenesis and anti-angiogenic therapy. *Keio J Med*, **2012**, 61(2), 47-56.

[51] Kim, E.C.; Min, J.K.; Kim, T.Y.; Lee, S.J.; Yang, H.O.; Han, S.; Kim, Y.M.; Kwon, Y.G. [6]-Gingerol, a pungent ingredient of ginger, inhibits angiogenesis *in vitro* and *in vivo*. *Biochem Biophys Res Commun*, **2005**, 335(2), 300-8.

[52] Kim, S.O.; Kundu, J.K.; Shin, Y.K.; Park, J.H.; Cho, M.H.; Kim, T.Y.; Surh, Y.J. [6]-Gingerol inhibits COX-2 expression by blocking the activation of p38 MAP kinase and NF-kappa B in phorbol ester-stimulated mouse skin. *Oncogene*, **2005**, 24(15), 2558-2567.

[53] Jeong, C.H.; Bode, A.M.; Pugliese, A.; Cho, Y.Y.; Kim, H.G.; Shim, J.H.; Jeon, Y.J.; Li, H.; Jiang, H.; Dong, Z. [6]-Gingerol suppresses colon cancer growth by targeting leukotriene A4 hydrolase. *Cancer Res*, **2009**, 69(13), 5584-91.

[54] Nigam, N.; George, J.; Srivastava, S.; Roy, P.; Bhui, K.; Singh, M.; Shukla, Y. Induction of apoptosis by [6]-gingerol associated with the modulation of p53 and involvement of mitochondrial signaling pathway in B[a]P-induced mouse skin tumorigenesis. *Cancer Chemother Pharmacol*, **2010**, 65(4), 687-96.

[55] Wu, H.; Hsieh, M.C.; Lo, C.Y.; Liu, C.B.; Sang, S.; Ho, C.T.; Pan, M.H. 6-Shogaol is more effective than 6-gingerol and curcumin in inhibiting 12-O-tetradecanoylphorbol 13-acetate-induced tumor promotion in mice. *Mol Nutr Food Res*, **2010**, 54(9), 1296-1306.

[56] Ju, S.A.; Park, S.M.; Lee, Y.S.; Bae, J.H.; Yu, R.; An, W.G.; Suh, J.H.; Kim B,S. Administration of 6-gingerol greatly enhances the number of tumor-infiltrating lymphocytes in murine tumors. *Int J Cancer*, **2012**, 130(11), 2618-28.

[57] Geiger, T.R.; Peeper, D.S. Metastasis mechanisms. *Biochim Biophys Acta*, **2009**, 1796(2), 293-308.

Received: November 13, 2013 Revised: February 17, 2014 Accepted: February 19, 2014

Biochimie 95 (2013) 1371–1378

Contents lists available at SciVerse ScienceDirect

Biochimie

journal homepage: www.elsevier.com/locate/biochi

Research paper

ADAM9 silencing inhibits breast tumor cell invasion *in vitro*

Kelli Cristina Micocci [a,1], Ana Carolina Baptista Moreno Martin [a,1], Cyntia de Freitas Montenegro [a,1], Araceli Cristina Durante [a,1], Normand Pouliot [b,c,d,2], Márcia Regina Cominetti [a,*], Heloisa Sobreiro Selistre-de-Araujo [a,1]

[a] Departamento de Ciências Fisiológicas, Rodovia Washington Luís, Km 235, CEP 13565-905, São Carlos, SP, Brazil
[b] Metastasis Research Laboratory, Peter MacCallum Cancer Centre, The University of Melbourne, Melbourne, VIC, Australia
[c] Sir Peter MacCallum Department of Oncology, The University of Melbourne, Melbourne, VIC, Australia
[d] Pathology Department, The University of Melbourne, Melbourne, VIC, Australia

ARTICLE INFO

Article history:
Received 31 October 2012
Accepted 3 March 2013
Available online 14 March 2013

Keywords:
ADAM9
Integrin
RNA silencing
Disintegrin
Cell adhesion
Cancer
Metastasis

ABSTRACT

ADAM9 (A Disintegrin And Metalloproteinase 9) is a member of the ADAM protein family which contains a disintegrin domain. This protein family plays key roles in many physiological processes, including fertilization, migration, and cell survival. The ADAM proteins have also been implicated in various diseases, including cancer. Specifically, ADAM9 has been suggested to be involved in metastasis. To address this question, we generated ADAM9 knockdown clones of MDA-MB-231 breast tumor cells using silencing RNAs that were tested for cell adhesion, proliferation, migration and invasion assays. In RNAi-mediated ADAM9 silenced MDA-MB-231 cells, the expression of ADAM9 was lower from the third to the sixth day after silencing and inhibited tumor cell invasion in matrigel by approximately 72% when compared to control cells, without affecting cell adhesion, proliferation or migration. In conclusion, the generation of MDA-MB-231 knockdown clones lacking ADAM9 expression inhibited tumor cell invasion *in vitro*, suggesting that ADAM9 is an important molecule in the processes of invasion and metastasis.

1. Introduction

Attachment of cells to the extracellular matrix (ECM) depends mainly on a family of glycoproteins known as integrins [1], which are expressed on the cell surfaces of many cultured cell types at specialized adhesion sites known as focal contacts [2]. A number of structural and signaling proteins, such as integrins, cytoskeletal proteins, and kinases are concentrated at these sites and are known to initiate signal transduction pathways [3,4]. The aggregation of integrin receptors, ligand occupancy and tyrosine kinase-mediated phosphorylation are the key events that result in different processes, including cell migration, differentiation, tissue remodeling, cell proliferation, angiogenesis, tumor cell invasion and metastasis [1,5].

Members of the ADAM (an acronym for A Disintegrin And Metalloprotease) protein family are involved in several human diseases such as inflammatory disorders, neurological diseases, asthma and cancer metastasis [6,7]. ADAM9 is a transmembrane protein with a number of characteristic domains, including a pro-domain, a metalloproteinase domain, a disintegrin-like domain, a cysteine-rich region, a transmembrane domain, and a short cytoplasmic tail [8]. The ADAM9 disintegrin domain binds to numerous integrins, such as $\alpha_6\beta_1$ integrins in fibroblasts [9], $\alpha_V\beta_5$ in myeloma cells [10] and $\alpha_V\beta_3$ in MDA-MB-231 breast tumor cells [11]. Mahimkar et al. [12] and Zigrino et al. [13] have demonstrated that the recombinant disintegrin and cysteine-rich domains from human ADAM9 mediate cellular adhesion through β_1 integrins. Furthermore, the disintegrin-like and cysteine-rich domains of ADAM9 mediate interactions between melanoma cells and fibroblasts [14].

Over-expression of ADAM9 has been reported in several human carcinomas, including kidney [15], prostate [16], breast [17], liver [18,19], pancreatic [20], gastric [21], cervix [22] and oral [23]. Expression of ADAM9 is elevated in skin melanoma but is restricted to the invading front [24]. Peduto et al. [25] found a correlation between ADAM9 titer and cancerous changes in mouse models of prostate cancer, especially in well-differentiated tumors. Increased expression of ADAM9 led to increased structural abnormalities and growth of early-stage tumors compared to controls.

* Corresponding author. Present address: Departamento de Gerontologia, Rodovia Washington Luís, Km 235, CEP 13565-905, São Carlos, SP, Brazil. Tel.: +55 16 33066663; fax: +55 16 33519628.
E-mail address: mcominetti@ufscar.br (M.R. Cominetti).
[1] Tel.: +55 16 33518333; fax: +55 16 33518328.
[2] Tel.: +61 3 96561285; fax: +61 3 96561411.

0300-9084
http://dx.doi.org/10.1016/j.biochi.2013.03.001

The ADAM9 protein also appears to interfere with various cell signaling systems. In prostate cancers, the fibroblast growth factor (FGF) signaling pathway is believed to be particularly important [26], with down-regulation of the fibroblast growth factor receptor 2 isoform IIIb (FGFR2IIIb) being a feature of prostrate tumor progression [27]. Transfection of FGFR2IIIb into malignant tumors is enough to inhibit their growth [28]. Therefore, it is potentially significant that over-expression of ADAM9 increases shedding of FGFR2IIIb from cells, which is expected to disrupt FGFR2IIIb signaling and reduce its function [25]. Additionally, over-expression of ADAM9 leads to increased release of epidermal growth factor (EGF) [25], a factor known to induce prostate cancer growth in rat pups [29].

Although ADAM9 is normally considered a transmembrane protein, a soluble form ADAM9-S has been described [30], which is derived from alternative splicing of the gene [31]. The ADAM9-S protein promotes the invasive phenotype of carcinoma cell lines, and ADAM9 is strongly expressed at the invading front of hepatic metastases, although the authors did not distinguish ADAM9 and ADAM9-S [31]. Taken together, these studies suggest that ADAM9 has a significant role in tumorigenesis and metastasis.

To better understand the role of ADAM9 in breast cancer progression, we generated knockdown clones lacking ADAM9 using RNAi in the MDA-MB-231 human breast tumor cell line. As far as we know, this is the first demonstration that decreased ADAM9 expression impaired the invasiveness of this cell line. In addition, the present work demonstrated, for the first time, ADAM9 silencing in a breast tumor cell line and provided evidence that ADAM9 may play an important role in the metastatic progression of human breast cancer.

2. Material and methods

2.1. Cell culture

MDA-MB-231 breast tumor cells were cultivated in DMEM medium (Invitrogen) containing 10% bovine fetal serum (FBS), L-glutamine (2 mM), penicillin (100 U/ml), streptomycin (100 μg/ml) and amphotericin B (250 μg/ml) (Invitrogen) in 5% CO_2 at 37 °C. The anti-ADAM9 antibody was from Abcam (anti-RP2ADAM9) and the anti-β-actin antibody was from Santa Cruz Biotech (sc-1616).

2.2. Design of siRNA primers

Primer set #104056, which targets exon 13 (disintegrin domain) (Silencer® Pre-designed siRNA, Ambion), was selected to ensure that other ADAMs would not be silenced simultaneously. The primer sequences were: sense (5′-rCrCrArGrArGrUrArCrUrGrCrArArUrGrGrUrUrCrUrUrCTC-3′) and antisense (5′-rGrArGrArArGrArArCrCrArUrUrGrCrArGrUrArCrUrCrUrGrGrArA-3′). The negative control (scrambled) used in the assays was *Silencer*® Select Negative Control No. 1 siRNA (Ambion). This sequence does not target any gene product and have no significant sequence similarity to human gene sequences, being essential for determining the effects of siRNA delivery.

2.3. ADAM9 RNA silencing

On the day before transfection, 2×10^5 MDA-MB-231 cells were plated in 5 ml of DMEM medium supplemented with 10% FBS without antibiotics. Ten microliters of lipofectamine were mixed with 490 μl OPTI-MEM serum-free medium (Invitrogen) and incubated at room temperature for 5 min. A total of 10 nM of RNA silencing primer was diluted in OPTI-MEM, added to the lipofectamine/OPTI-MEM mixture and incubated for 20 min at room temperature. This mixture was then added to the cells. The medium was changed 24 h after transfection. Controls comprised of non-treated cells, cells treated with transfection reagent only (lipofectamine), and cells treated with a scrambled primer. Cells were washed in phosphate buffered saline, harvested with Trizol reagent (Invitrogen) according to the manufacturer's protocol, and frozen immediately. For western blotting assays, cells were lysed with Triton X-100 in Hepes buffer [150 mM NaCl, 50 mM Hepes, 1.5 mM $MgCl_2$, 1% Triton X-100, 0.1% SDS, protease inhibitor cocktail (Sigma), 100 mM NaF and 100 mM Na_3VO_4]. Protein concentrations in the lysed samples were determined by the BCA method (Pierce), and 30 μg of each sample was resolved by SDS-PAGE [32]. Protein bands were transferred to nitrocellulose membranes and probed with anti-RP2ADAM9 and anti-β-actin antibodies. Western blots were scanned on an Image Scanner (GE – General Electric). All the assays using ADAM9 knockdown MDA-MB-231 cells were performed after the third day of siRNA transfections.

2.4. Extraction of RNA and synthesis of cDNA

Total RNA was extracted from cells using Trizol reagent (Invitrogen) following the manufacturer's instructions. All samples were treated with DNase I (Deoxyribonuclease I, Amplification Grade, Invitrogen). After quantification, a total of 1 μg of RNA was mixed with 0.5 μl of oligo dT (0.5 μg/μl) (Promega) and nuclease-free water to a volume of 7 μl and incubated at 70 °C for 5 min, followed by 5 min on ice. Next, 0.5 μl of 200 units/μl of Moloney Monkey Leukemia virus (MMLV) reverse transcriptase (Promega), 2.5 μl of 5× MMLV buffer (Promega), and 2.5 μl of 10 mM dNTP mix was added to the reaction. The whole mixture was incubated at 37 °C for 1 h, and was used posteriorly for qPCR.

2.5. Design of qPCR primers

ADAM9 primers targeting the disintegrin domain were designed using Primer3Plus software (http://www.bioinformatics.nl/cgi-bin/primer3plus/primer3plus.cgi). Primers spanned exon boundaries so that only mRNA sequences would be amplified. The primers were ADAM9DF1 (5′CTT GCT GCG AAG GAA GTA CC); and ADAM9DR1 (5′AAC ATC TGG CTG ACA GAA CTG A). Primers targeting HPRT1F1 (5′TGA CAC TGG CAA AAC AAT GCA), HPRT1R1 (5′GGT CCT TTT CAC CAG CAA GCT), GAPDHF1 (5′GAT GCT GGT GCT GAG TAT GT) and GAPDHR1 (5′GTG GTG CAG GAT GCA TTG CT) were used as endogen controls.

2.6. Gene expression

ADAM9 mRNA expression was measured in a Corbett Rotorgene RG 3000 (Corbett Research) using the following thermocycling conditions: 95 °C for 10 min, followed by 40 cycles of amplification at 95 °C for 15 s, 55 °C for 5 s and 72 °C for 20 s. The master mix in each well consisted of 12.5 μl ABsoluteTM QPCR SYBR Green mix (6 mM $MgCl_2$, reaction buffer, DNA polymerase and SYBR green dye) (Advanced Biotechnologies), 1.25 μl each of 5 μM forward and reverse primer and 10.5 μl of nuclease-free water in a total volume of 25 μl.

2.7. Proliferation assays

To measure the effect of RNAi-mediated ADAM9 silencing on cell proliferation the transition of 3-(4,5-dimethylthiazol-2-yl)-2,5-diphenyltetrazolium bromide (MTT) to formazan was used [33]. Cells without any treatment, cells treated only with lipofectamine, and cells transfected with siRNAs were seeded in 96-well plates and left at 37 °C for 24 and 48 h. The cells were then washed with

PBS and incubated in 50 μl of 0.5 mg/ml MTT in culture medium at 37 °C for 4 h. Following the addition of 100 μl of isopropanol, the absorbance was read at 595 nm in an ELISA plate reader. The mean proliferation of cells without any treatment was expressed as 100%.

2.8. Adhesion assays

The effect of RNAi-mediated ADAM9 silencing on the adhesion of MDA-MB-231 cells was analyzed in 96-well plates (Corning). A solution of type I collagen (10 μg) was immobilized on the plates in 0.1% acetic acid. Fibronectin and laminin (10 μg) were dissolved in adhesion buffer (20 mM HEPES, 150 mM NaCl, 5 mM KCl, 1 mM $MgSO_4$ and 1 mM $MnCl_2$ pH 7.35), overnight at 4 °C. On the next day, the wells were blocked with a solution of 1% BSA diluted in adhesion buffer for 1 h. Cells were counted and their concentration was adjusted in proportion to 5×10^6/ml. The blocking solution was removed from the wells and they were washed twice with adhesion buffer (100 μl). After this period the cells were incubated for 45 min on the coatings and subsequently wells were washed in order to remove non-adherent cells. A solution of 70% ethanol (100 μl) was added to the wells and the plate was incubated for 10 min at room temperature. Subsequently, the ethanol was removed and 60 μl of crystal violet (0.5%) was added and incubated for 20 min at room temperature. After this time, the solution containing the crystal was removed and the wells were washed with PBS to remove excess. Finally 100 μl of 1% SDS was added and incubated for 30 min at room temperature. The reading of absorbance was performed at a wavelength of 595 nm, and three treatments were compared, including cells without any treatment, cells treated only with lipofectamine, and cells transfected with siRNAs. The adhesion of control cells to each substrate was determined as 100%.

2.9. Wound healing assay

Wound-healing migration assay is based on the repopulation of wounded cultures. The cells were seeded into 24-well culture plates at 1×10^5 cells/well and the cell monolayer were cultured in medium containing 10% FBS until reach 100% of confluence. The monolayers were carefully wounded using a yellow pipette tip, and any cellular debris present was removed by washing twice with DMEM medium. The wounded monolayers were then incubated in DMEM medium containing 10% FBS. Photographs of the exact wound areas taken initially (0 h) were again taken after 16 and 24 h. The images were compared between three treatments, including cells without any treatment, cells treated only with lipofectamine, and cells transfected with siRNAs, and with or without incubation with the ADAM9D protein [11]. Photographs were analyzed using ImageJ software and the formula of % of wound closure [34].

2.10. Cell migration

Cell migration was assessed in 24 well Boyden chambers (BD Biosciences). MDA-MB-231 (5×10^4) cells were seeded on the upper chamber in FBS-free DMEM medium. DMEM containing FBS (10%) was added to the bottom chamber and acted as a chemoattractant. Tumor cells were allowed to migrate for 22 h at 37 °C and 5% CO_2 in a humidified environment. Then, the cells that remained in the upper chamber were removed using a cotton swab. The cells that migrated to the other side of the upper chamber membrane were fixed with methanol and stained with 1% toluidine blue in 1% borax. Cells were counted using the ImageJ software (public domain software) in 5 fields (100× magnification) per well that essentially covered 80% of the well surface. The average number of cells from each of the triplicates represents the average number of cells that migrated in the different groups. Each experiment had triplicate wells for every treatment group and we repeated each experiment three times. The mean of all results from controls was considered as 100%. After that, the images were compared among three treatments, including cells without any treatment, cells treated only with lipofectamine, and cells transfected with siRNAs.

2.11. Matrigel invasion assay

Cellular invasion assays were carried out using BioCoat Matrigel Invasion Chambers (BD Biosciences) with 8-μm pores in 6-well plates. A total of 2.5×10^4 cells were added to each chamber. Complete medium was used as a chemoattractant in the lower chamber. After incubation for 22 h at 37 °C and 5% CO_2, cell invasion was measured in the same way as performed for migration assay (item 2.10). The invasion of cells without any treatment was determined as 100%.

2.12. Gelatin zymography

The effect of ADAM9 silencing on the proteolytic activity of MDA-MB-231 cells was determined by zymography [35]. MDA-MB-231 cells (2×10^6) in FBS-free DMEM medium were seeded in 6-cm dishes. After incubation for 24 h at 37 °C and 5% CO_2, cells were lysed with a buffer containing Tris–HCl (0.2 M) (pH 7.4) and Triton X-100 (0.2%). The cell lysates were centrifuged (10 min at 13,000× *g* and 4 °C), and the supernatants were separated. The total protein concentration in each sample was measured using the BCA colorimetric detection kit (BCA Protein Assay, Pierce). Protein samples (20 μg) were subjected to electrophoresis under non-reducing conditions in 10% SDS polyacrylamide gels containing 1 mg/ml gelatin. After electrophoresis, gels were washed twice in 2.5% of Triton X-100 to remove SDS and incubated in substrate buffer [50 mM Tris–HCl (pH 8.0); 5 mM of $CaCl_2$ and 0.02% NaN_3] at 37 °C for 20 h. To confirm the metalloproteinase activity, EDTA in a final concentration of 15 mM was added to the samples and substrate buffer. Proteins were stained with Coomassie brilliant blue for 1.5 h and destained with an acetic acid, methanol and water mixture (in a 1:4:5 v:v:v ratio). Gels were photographed with a Canon G6 Power Shot 7.1 machine. Gelatinase activity was visualized as clear bands in the stained gels, and the average band intensities was measured using the Gene Tools v3.06 software (Syngene). MMP-2 and MMP-9 activity were quantified as arbitrary units and compared between three treatments, including cells without any treatment, cells treated only with lipofectamine, and cells transfected with siRNAs.

2.13. Statistical analysis

For all assays, each experiment was repeated three times in triplicate (independent experiments), and standard errors of the mean were calculated. The results were compared statistically using a one-way analysis of variance (ANOVA) and Tukey's test was applied for multiple comparisons. All statistical tests used $p \leq 0.05$ as a cut-off for significance. Cases where $p < 0.05$ were marked as follows: $^{*}p < 0.05$, $^{**}p < 0.01$ and $^{***}p < 0.001$.

3. Results

3.1. ADAM9 silencing is detected at the mRNA and protein levels

ADAM9 gene expression was dramatically decreased in MDA-MB-231 cells treated with siRNAs at both the mRNA and protein (Fig. 1A and B, respectively) levels when compared to the controls (MDA-MB-231 cells without treatment and lipofectamine or

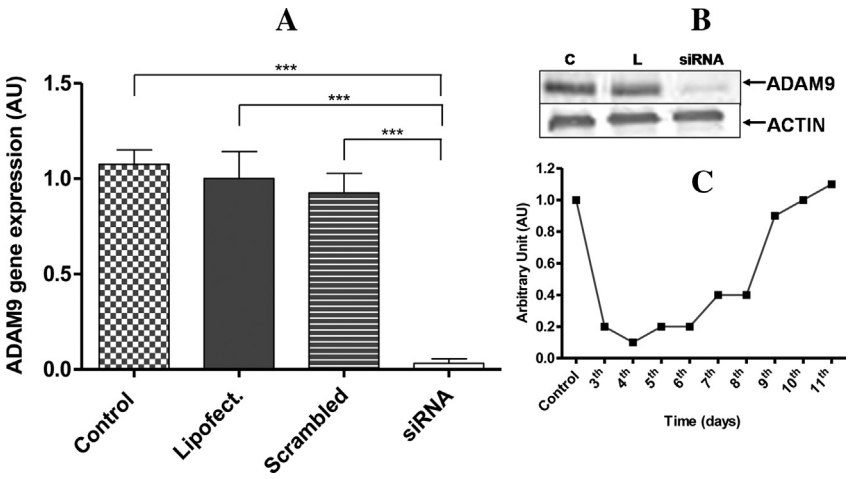

Fig. 1. Silencing of ADAM9. (A) Expression of ADAM9 mRNA in RNAi-mediated ADAM9 silenced MDA-MB-231 cells was analyzed by qPCR. The values are in arbitrary units (AU) and the *p* value was determined using ANOVA with a Tukey's test comparing control, cells treated with lipofectamine, negative control (scrambled) and cells treated with ADAM9 siRNAs (***$p < 0.001$). (B) Western blotting analysis of MDA-MB-231 cell lysates, with three treatments: cells alone (C), lipofectamine alone (L), and ADAM9 siRNAs using anti-ADAM9RP2 primary antibody and goat anti-rabbit IgG as a secondary antibody. β-actin was used as endogen control. (C) The silencing of ADAM9 using siRNAs is transient because it is effective only from the third to the sixth day. The values are in arbitrary units (AU).

scrambled-treated cells). qPCR analysis showed a down regulation of 91.35 ± 6.32% of ADAM9 expression in RNAi-mediated knockdown MDA-MB-231 cells when compared to control cells (Fig. 1A). At the protein level, western blotting analysis using anti-ADAM9 antibody presented similar results (Fig. 1B).

Gene silencing using synthetic duplexes siRNA is transient. As a result, 10 plates (6-cm) containing 2×10^5 MDA-MB-231 cells were silenced. One plate was removed randomly each day to determine the efficiency of ADAM9 silencing over time. RNA knockdown was measured from the third to the eleventh day after transfection and the kinetics of ADAM9 silencing in MDA-MB-231 cells are shown in Fig. 1C. The highest efficiency of ADAM9 silencing was observed from the third to the sixth days, although on the seventh and eighth days, the gene expression still remained low. From the ninth and tenth days onwards, the expression of ADAM9 expression increased exponentially and reached similar levels to those obtained by control cells (Fig. 1C).

3.2. ADAM9 silencing does not affect MDA-MB-231 cell proliferation or adhesion

ADAM9 silencing had no effect on the proliferation of MDA-MB-231 cells on the third (Fig. 2A) or sixth (Fig. 2B) days after silencing in 24 or 48 h of incubation. No significant differences were observed among the groups. ADAM9 silencing also had no effect on the adhesion of MDA-MB-231 cells to different ECM proteins, such as collagen type I, fibronectin or laminin (Fig. 3).

3.3. ADAM9 silencing strongly inhibits MDA-MB-231 cell invasion without affecting cell migration

RNAi-mediated ADAM9 silencing was not able to significantly inhibit the migration of MDA-MB-231 human breast tumor cells when compared with non-transfected cells or with lipofectamine-transfected cells after 16 (Fig. 4A) or 24 h that the wounds were made (Fig. 4B). ADAM9 knockdown cells were incubated with different concentrations of ADAM9D, the disintegrin domain of ADAM9 [11]. ADAM9D in concentrations of 500, 1000 and 2000 nM had no effects in inhibiting ADAM9 knockdown MDA-MB-231 cell migration after 16 (Fig. 4A) or 24 h (Fig. 4B) of incubation. Photographs were taken after 0, 16 or 24 h after wound (Fig. 4C).

To ensure these results we also performed migration assays using Boyden chambers. RNAi-mediated ADAM9 silencing had had no effect on MDA-MB-231 cell migration when compared with control cells or lipofectamine-treated cells after 22 h of incubation (Fig. 5A and B).

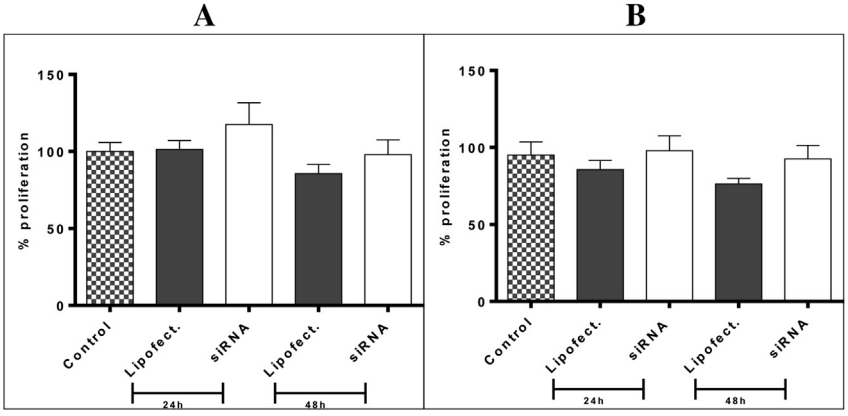

Fig. 2. Proliferation assay. Silencing of ADAM9 had no effect on the proliferation of the MDA-MB-231 cells after three (A) or six days (B) of transfection. After the different times, the cells were incubated with MTT for 24 h or 48 h and compared with control cells or with lipofectamine-treated cells. The absorbance of the samples was measured at 595 nm and the proliferation of control cells was determined as 100%.

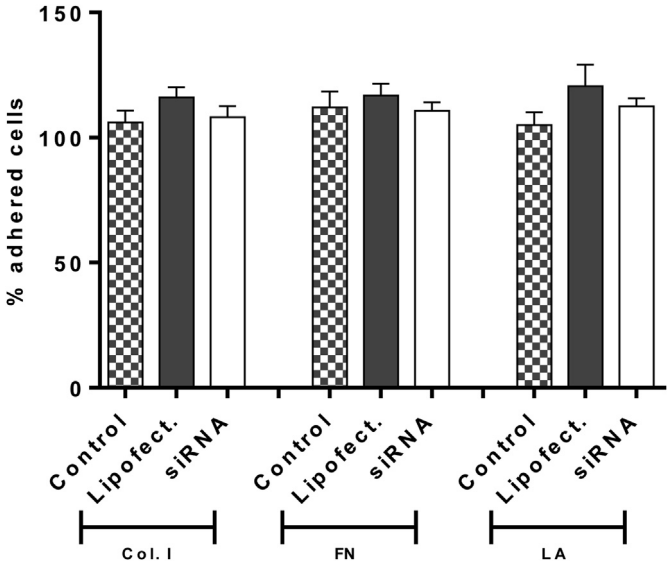

Fig. 3. Adhesion assay. RNAi-mediated ADAM9 silencing had no effect on the adhesion of the MDA-MB-231 under different extracellular matrix proteins, such as collagen I (Col. I), fibronectin (FN) and laminin (LA). The extracellular matrix proteins were coated on the wells of the plate, and on the following day, after the blocking of wells, the cells were allowed to adhere for 45 min. The percentage adhesion was determined as described in the materials and methods. The results were compared using a one-way analysis of variance (ANOVA), followed by a Tukey's post-hoc analysis.

On the other hand, RNAi-mediated ADAM9 knockdown MDA-MB-231 cells strongly inhibited the invasion in an *in vitro* matrigel assay by 71.51 ± 8.02% when compared to control untransfected cells (Fig. 6A). Lipofectamine and negative control-transfected cells (scrambled) remained invasive and no statistically significant differences were observed when compared to untransfected cells (Fig. 6A). Photographs were taken after 22 h of incubation (Fig. 6B).

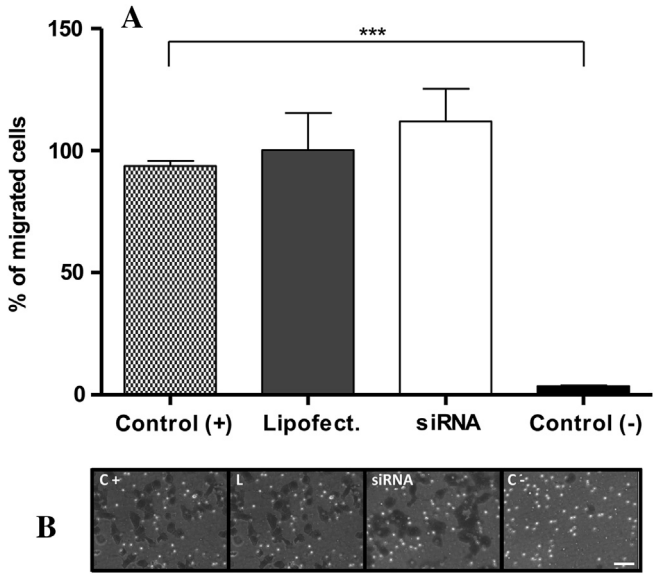

Fig. 5. Effect of RNAi-mediated ADAM9 silencing on migration of MDA-MB-231 cells. (A) A transwell migration assay was used to determine the effect of ADAM9 silencing migration of MDA-MB-231 cells. Control cells, lipofectamine-treated cells or siRNA-ADAM9 cells were allowed to migrate toward medium containing 10% FBS for 22 h. Graphs are representative of three independent experiments. The results were compared using a one-way analysis of variance (ANOVA), followed by a Tukey's post-hoc analysis (***$p < 0.001$). (B) Morphology of cells in the three different treatments: control cells (C+), lipofectamine-treated cells (L), and siRNA-ADAM9 treated cells (siRNA) migrating toward a 10% FBS containing medium. The negative control (C−) was control cells migrating toward a FBS-free medium. Bar represents 10 μm.

3.4. MMP-2 and MMP-9 concentration and activity

In order to investigate the mechanisms involved in the inhibition of the invasion ability of RNAi-mediated ADAM9 silencing of

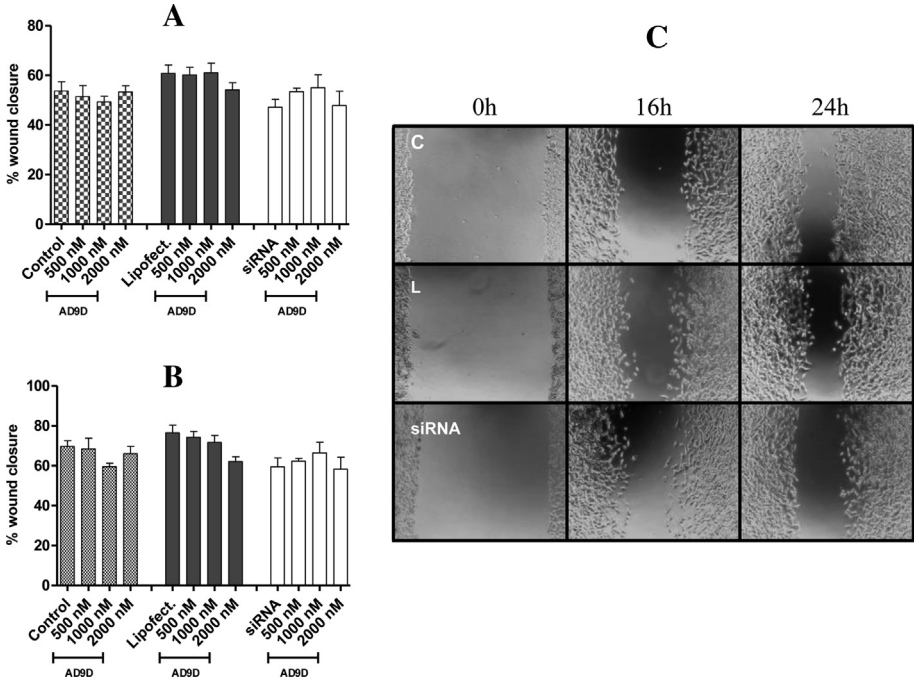

Fig. 4. Migration of MDA-MB-231 cells after wounding. Effects of ADAM9 silencing and ADAM9D recombinant protein on MDA-MB-231 cells migration were plotted as a percentage of wound closure in 16 (A) or 24 h (B) after wounding. Representative photos of wounds were taken at time zero, 16 h, and 24 h after wounding, (C). In these photos we show pictures representing control (C), lipofectamine (L) and siRNA-ADAM9 (siRNA) cells without previous treatment with ADAM9D recombinant protein.

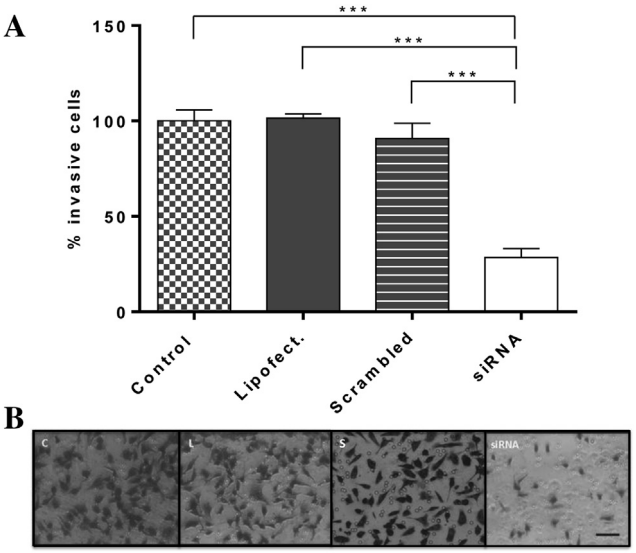

Fig. 6. Effect of RNAi-mediated ADAM9 silencing on the invasion of MDA-MB-231 cells. ADAM9 silencing significantly inhibits the invasion of MDA-MB-231 human breast tumor cells through matrigel compared to the invasion of control cells (A). The cells were plated in wells containing matrigel and FBS was used as a chemoattractant in the lower chamber. The invasive cells were fixed and counted (an average of eight fields from each treatment). The assay was performed in triplicate. The results were compared using a one-way analysis of variance (ANOVA), followed by a Tukey's post-hoc analysis (***$p < 0.001$). (B) Cell morphology in the four different treatments: untreated control (C), lipofectamine-treated cells (L), scrambled siRNA-treated control (S), and siRNA-ADAM9 treated cells (siRNA). Bar represents 10 μm.

MDA-MB-231 cells, we performed zymography assays to evaluate the activity of MMP-2 and MMP-9. There was no variation in the total concentration of MMP-2 or MMP-9 among the three treatment types analyzed in this study, as demonstrated by 1% gelatin-SDS-PAGE (Fig. 7A). The incubation with EDTA resulted in the inhibition of MMP-2 and 9 activities confirming the nature of metalloprotease activity (Fig. 7B). The average activity of MMP-2 and MMP-9 was measured as indicated in Section 2.12 and plotted on a graph (Fig. 7C and D, respectively). This result suggests that RNAi-mediated ADAM9 silencing does not affect the activity of MMP-2 or MMP-9.

4. Discussion

The progression of malignant tumors results from the invasion of the primary tumor to a secondary site, causing metastasis in a multi-step process that requires cell–cell and cell–matrix interactions within the host tissue. These steps can be summarized as follows: cell detachment from the primary tumor, migration into the ECM, intravasation into a blood or lymphatic vessel, survival within the vasculature, adherence of these tumor cells in the endothelium, extravasation, and formation of secondary tumors [36,37]. These interactions lead to the production, release and activation of a variety of cytokines and growth factors and subsequent generation of signals to directly or indirectly promote tumor growth and survival [24]. Different proteases have been implicated in these processes, such as MMPs, ADAMs and ADAMTSs [7,24,38].

Due to the strong involvement of ADAM9 in the metastatic process, in this study we have generated knockdown clones of MDA-MB-231 human breast tumor cells that lack ADAM9 expression and then tested these clones to their ability to adhere, migrate, proliferate and invade through ECM using *in vitro* assays. The RNAi-mediated silencing in MDA-MB-231 cells was very successful, with more than 90% of ADAM9 knocked down, as estimated by quantitative PCR and western blotting analysis. The expression of ADAM9 was easily silenced using a relatively small (10 nM) concentration of ADAM9 siRNAs. A similar result was obtained by other investigators in highly invasive SCC68 cells, a squamous cell carcinoma cell line, but with tenfold higher concentration of siRNAs (100 nM) [39].

Using a matrigel invasion assay, we showed that the ADAM9 silencing significantly inhibited the invasion capacity of MDA-MB-231 human breast cancer cells, which suggests that this protein plays an important role in cell invasion. However, the silencing of ADAM9 had no effect on MDA-MB-231 cell adhesion, migration, proliferation, or MMP-2 and 9 activities. Our results showed that ADAM9 silencing had no impact on MMP-2 and MMP-9 expression or gelatinase activity indicating that reduced invasion in cells

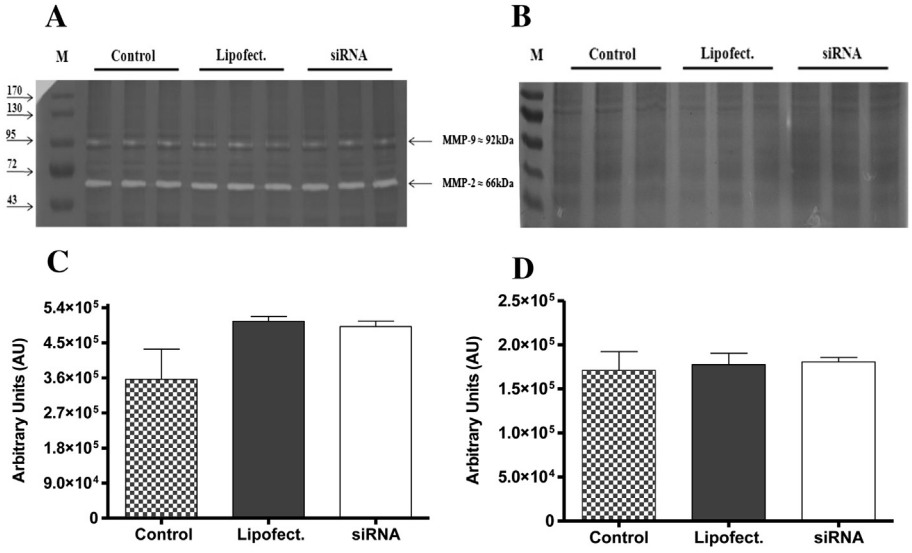

Fig. 7. Analysis of concentration and activity of MMP-2 and MMP-9 in the MDA-MB-231 breast tumor cells. (A) Zymography in 1% gelatin-SDS-PAGE or (B) EDTA-treated samples. Lane 1: molecular mass marker; lanes 2–4: control cells; lanes 5–7: cells treated with lipofectamine; and lanes 8–10: cells treated with ADAM9 siRNAs ($n = 3$; 20 μg of total protein was loaded in each lane). (C) MMP-2 and (D) MMP-9 concentrations were determined by the sum of integrated optical density (IOD) obtained for the intermediate bands. Gels were analyzed by densitometry, and activity was expressed as arbitrary units.

expression ADAM9 siRNA is unlikely to be due to indirect inhibition of MMP-2/9. We propose that ADAM9 proteolytic activity may directly contribute to matrigel invasion by MDA-MB-231 cells since ADAM9 has been reported to cleave laminin [31], a major constituent of matrigel.

Shintani et al. [40] showed that the overexpression of ADAM9 enhances adhesion and cell invasion in lung cancers, via modulation of other adhesion molecules and changes in sensitivity to growth factors. According to this study, ADAM9 may either directly degrade the ECM or induce the activation of other proteases in the ECM, such as matrix MMPs, thereby allowing tumor cell penetration into the brain matrix.

Our results are in agreement with Mazzocca et al. [31] who showed that ADAM9-S, an alternatively spliced variant secreted by activated hepatic stellate cells, induces colon carcinoma cell invasion *in vitro* and that this process requires both protease activity and binding to the $\alpha_6\beta_4$ and $\alpha_2\beta_1$ integrins.

Contradictorily to our results, Fry and Toker [41] demonstrated that the silencing of both soluble (ADAM9-S) and transmembrane (ADAM9-L) isoforms, increased the migration of BT549 breast cancer cells. In this work, they also showed that the overexpression of ADAM9-S is responsible for increasing cell migration in BT549 cells through its metallopeptidase domain. Moreover, they also showed that ADAM9-L is responsible for inhibiting cell migration through its disintegrin domain. Thus, both isoforms have different and opposite responses during cancer progression. Whether MDA-MB-231 cells have ADAM9-S and L isoforms and the effects of isoform silencing in this cell line will be further investigated.

Some ADAMs may induce proliferation by catalyzing the cleavage of growth factors, such as HB-EGF, and its membrane anchored form (proHB-EGF) can act as a negative regulator of proliferation [42,43]. Izumi et al. [44] showed that after induction with TPA (an activator of protein kinase C), ADAM9 interacted with PKCδ and cleaved proHB-EGF; however, we have demonstrated here that ADAM9 is not involved in the proliferation of MDA-MB-231 cells. In another work, RNAi-mediated ADAM9 silencing was responsible by a reduction in adenoid cystic carcinoma metastasis both *in vitro* and *in vivo* [19]. In this work, the authors also demonstrated that ADAM9 is essential for cancer cell proliferation and invasion and that its expression could be used as a prognostic of metastatic risk, since it was elevated in a high metastatic potential cell line (SACC-LM) when compared to a low metastatic potential cell line (SACC-83) [19].

Klessner et al. [39] demonstrated that ADAM9 participates in the shedding of desmoglein 2 (Dsg2), resulting in stronger cell–cell adhesion, which could, in turn, reduce the rate of migration and cell invasion. The ADAMs can also interact with β_1 integrins, and this association facilitates the recognition and location of their substrates for proteolytic shedding [45,46], as reported by Mahimkar et al. [47].

In a recent work, Hamada et al. [48] reported that miR-126 was found to target ADAM9 and that siRNA-based knockdown of ADAM9 in pancreatic cancer cells resulted in reduced cellular migration, invasion, and induction of epithelial marker E-cadherin.

Taken together, the literature results and the data found in the present study suggest that ADAM9 participates in the invasion of tumor cells by either directly degrading the ECM, by inducing activation of other proteases, such as MMPs, by co-localizing with other molecules, such as β_1 integrin, present on the surface of MDA-MB-231 cells (data not shown) or by interacting with other regulators such as miRNAs. A more conclusive demonstration that ADAM9 is a suitable target for metastatic breast cancer will require the use of a stable expression vector *in vivo* and/or inhibitors of this protein alone or in combination with conventional clinical therapies.

5. Conclusions

The results presented in this study reinforce the importance of the ADAM9 role in the invasion of breast tumor cells. Considering the significance of cell invasion in metastatic progression, ADAM9 can be pointed as an interesting target for the design of drugs involved in the treatment or prevention of breast cancers. We conclude that ADAM9 has an essential role in cell invasion and may be involved in metastatic spread. Therefore, it may be an interesting target for anti-metastatic therapy.

Acknowledgments

This work was supported by CAPES (Coordenação de Aperfeiçoamento de Pessoal de Nível Superior), CNPQ (Conselho Nacional de Desenvolvimento Científico e Tecnológico), and FAPESP (Fundação de Amparo à Pesquisa do Estado de São Paulo, Brazil).

References

[1] R.O. Hynes, Integrins: versatility, modulation, and signaling in cell adhesion, Cell 69 (1992) 11–25.
[2] S.H. Lo, L.B. Chen, Focal adhesion as a signal transduction organelle, Cancer Metastasis Rev. 13 (1994) 9–24.
[3] S.E. LaFlamme, K.L. Auer, Integrin signaling, Semin. Cancer Biol. 7 (1996) 111–118.
[4] I.D. Campbell, M.J. Humphries, Integrin structure, activation, and interactions, Cold Spring Harb. Perspect. Biol. 3 (2011) 1–14.
[5] R.L. Juliano, J.A. Varner, Adhesion molecules in cancer: the role of integrins, Curr. Opin. Cell. Biol. 5 (1993) 812–818.
[6] T. Klein, R. Bischoff, Active metalloproteases of the A disintegrin and metalloprotease (ADAM) family: biological function and structure, J. Proteome Res. 10 (2011) 17–33.
[7] N. Rocks, G. Paulissen, M. El Hour, F. Quesada, C. Crahay, M. Gueders, J.M. Foidart, A. Noel, D. Cataldo, Emerging roles of ADAM and ADAMTS metalloproteinases in cancer, Biochimie 90 (2008) 369–379.
[8] T.G. Wolfsberg, P. Primakoff, D.G. Myles, J.M. White, ADAM, a novel family of membrane proteins containing A disintegrin and metalloprotease domain: multipotential functions in cell-cell and cell-matrix interactions, J. Cell. Biol. 131 (1995) 275–278.
[9] D. Nath, P.M. Slocombe, A. Webster, P.E. Stephens, A.J. Docherty, G. Murphy, Meltrin gamma (ADAM-9) mediates cellular adhesion through alpha(6)beta(1)integrin, leading to a marked induction of fibroblast cell motility, J. Cell Sci. 113 (2000) 2319–2328.
[10] M. Zhou, R. Graham, G. Russell, P.I. Croucher, MDC-9 (ADAM-9/meltrin gamma) functions as an adhesion molecule by binding the alpha(v)beta(5) integrin, Biochem. Biophys. Res. Commun. 280 (2001) 574–580.
[11] M.R. Cominetti, A.C. Martin, J.U. Ribeiro, I. Djaafri, F. Fauvel-Lafeve, M. Crepin, H.S. Selistre-de-Araujo, Inhibition of platelets and tumor cell adhesion by the disintegrin domain of human ADAM9 to collagen I under dynamic flow conditions, Biochimie 91 (2009) 1045–1052.
[12] R.M. Mahimkar, O. Visaya, A.S. Pollock, D.H. Lovett, The disintegrin domain of ADAM9: a ligand for multiple beta1 renal integrins, Biochem. J. 385 (2005) 461–468.
[13] P. Zigrino, J. Steiger, J.W. Fox, S. Loffek, A. Schild, R. Nischt, C. Mauch, Role of ADAM-9 disintegrin-cysteine-rich domains in human keratinocyte migration, J. Biol. Chem. 282 (2007) 30785–30793.
[14] P. Zigrino, R. Nischt, C. Mauch, The disintegrin-like and cysteine-rich domains of ADAM-9 mediate interactions between melanoma cells and fibroblasts, J. Biol. Chem. 286 (2011) 6801–6807.
[15] F.R. Fritzsche, K. Wassermann, M. Jung, A. Tolle, I. Kristiansen, M. Lein, M. Johannsen, M. Dietel, K. Jung, G. Kristiansen, ADAM9 is highly expressed in renal cell cancer and is associated with tumour progression, BMC Cancer 8 (2008) 179.
[16] F.R. Fritzsche, M. Jung, A. Tolle, P. Wild, A. Hartmann, K. Wassermann, A. Rabien, M. Lein, M. Dietel, C. Pilarsky, D. Calvano, R. Grutzmann, K. Jung, G. Kristiansen, ADAM9 expression is a significant and independent prognostic marker of PSA relapse in prostate cancer, Eur. Urol. (2007).
[17] C. O'Shea, N. McKie, Y. Buggy, C. Duggan, A.D. Hill, E. McDermott, N. O'Higgins, M.J. Duffy, Expression of ADAM-9 mRNA and protein in human breast cancer, Int. J. Cancer 105 (2003) 754–761.
[18] A. Tannapfel, K. Anhalt, P. Hausermann, F. Sommerer, M. Benicke, D. Uhlmann, H. Witzigmann, J. Hauss, C. Wittekind, Identification of novel proteins associated with hepatocellular carcinomas using protein microarrays, J. Pathol. 201 (2003) 238–249.
[19] K. Tao, N. Qian, Y. Tang, Z. Ti, W. Song, D. Cao, K. Dou, Increased expression of a disintegrin and metalloprotease-9 in hepatocellular carcinoma: implications for tumor progression and prognosis, Jpn. J. Clin. Oncol. 40 (2010) 645–651.
[20] R. Grutzmann, J. Luttges, B. Sipos, O. Ammerpohl, F. Dobrowolski, I. Alldinger, S. Kersting, D. Ockert, R. Koch, H. Kalthoff, H.K. Schackert, H.D. Saeger,

G. Kloppel, C. Pilarsky, ADAM9 expression in pancreatic cancer is associated with tumour type and is a prognostic factor in ductal adenocarcinoma, Br. J. Cancer 90 (2004) 1053–1058.
[21] S. Carl-McGrath, U. Lendeckel, M. Ebert, A. Roessner, C. Rocken, The disintegrin-metalloproteinases ADAM9, ADAM12, and ADAM15 are upregulated in gastric cancer, Int. J. Oncol. 26 (2005) 17–24.
[22] A. Zubel, C. Flechtenmacher, L. Edler, A. Alonso, Expression of ADAM9 in CIN3 lesions and squamous cell carcinomas of the cervix, Gynecol. Oncol. 114 (2009) 332–336.
[23] Q. Xu, X. Liu, Y. Cai, Y. Yu, W. Chen, RNAi-mediated ADAM9 gene silencing inhibits metastasis of adenoid cystic carcinoma cells, Tumour Biol. 31 (2010) 217–224.
[24] P. Zigrino, C. Mauch, J.W. Fox, R. Nischt, Adam-9 expression and regulation in human skin melanoma and melanoma cell lines, Int. J. Cancer 116 (2005) 853–859.
[25] L. Peduto, V.E. Reuter, D.R. Shaffer, H.I. Scher, C.P. Blobel, Critical function for ADAM9 in mouse prostate cancer, Cancer Res. 65 (2005) 9312–9319.
[26] A.I. Evangelou, S.F. Winter, W.J. Huss, R.A. Bok, N.M. Greenberg, Steroid hormones, polypeptide growth factors, hormone refractory prostate cancer, and the neuroendocrine phenotype, J. Cell. Biochem. 91 (2004) 671–683.
[27] B. Naimi, A. Latil, G. Fournier, P. Mangin, O. Cussenot, P. Berthon, Down-regulation of (IIIb) and (IIIc) isoforms of fibroblast growth factor receptor 2 (FGFR2) is associated with malignant progression in human prostate, Prostate 52 (2002) 245–252.
[28] A. Matsubara, M. Kan, S. Feng, W.L. McKeehan, Inhibition of growth of malignant rat prostate tumor cells by restoration of fibroblast growth factor receptor 2, Cancer Res. 58 (1998) 1509–1514.
[29] N. Torring, L.V. Jensen, J.G. Wen, F.B. Sorensen, J.C. Djurhuus, E. Nexo, Chronic treatment with epidermal growth factor induces growth of the rat ventral prostate, Scand. J. Urol. Nephrol. 35 (2001) 339–344.
[30] N. Hotoda, H. Koike, N. Sasagawa, S. Ishiura, A secreted form of human ADAM9 has an alpha-secretase activity for APP, Biochem. Biophys. Res. Commun. 293 (2002) 800–805.
[31] A. Mazzocca, R. Coppari, R. De Franco, J.Y. Cho, T.A. Libermann, M. Pinzani, A. Toker, A secreted form of ADAM9 promotes carcinoma invasion through tumor-stromal interactions, Cancer Res. 65 (2005) 4728–4738.
[32] U.K. Laemmli, Cleavage of structural proteins during the assembly of the head of bacteriophage T4, Nature 227 (1970) 680–685.
[33] T. Mosmann, Rapid colorimetric assay for cellular growth and survival: application to proliferation and cytotoxicity assays, J. Immunol. Methods 65 (1983) 55–63.
[34] P.Y. Yue, E.P. Leung, N.K. Mak, R.N. Wong, A simplified method for quantifying cell migration/wound healing in 96-well plates, J. Biomol. Screen. 15 (2010) 427–433.
[35] J.P. Cleutjens, J.C. Kandala, E. Guarda, R.V. Guntaka, K.T. Weber, Regulation of collagen degradation in the rat myocardium after infarction, J. Mol. Cell. Cardiol. 27 (1995) 1281–1292.
[36] J.D. Hood, D.A. Cheresh, Role of integrins in cell invasion and migration, Nat. Rev. Cancer 2 (2002) 91–100.
[37] S.M. Pontier, W.J. Muller, Integrins in breast cancer dormancy, APMIS 116 (2008) 677–684.
[38] S. Mochizuki, Y. Okada, ADAMs in cancer cell proliferation and progression, Cancer Sci. 98 (2007) 621–628.
[39] J.L. Klessner, B.V. Desai, E.V. Amargo, S. Getsios, K.J. Green, EGFR and ADAMs cooperate to regulate shedding and endocytic trafficking of the desmosomal cadherin desmoglein 2, Mol. Biol. Cell. 20 (2009) 328–337.
[40] Y. Shintani, S. Higashiyama, M. Ohta, H. Hirabayashi, S. Yamamoto, T. Yoshimasu, H. Matsuda, N. Matsuura, Overexpression of ADAM9 in non-small cell lung cancer correlates with brain metastasis, Cancer Res. 64 (2004) 4190–4196.
[41] J.L. Fry, A. Toker, Secreted and membrane-bound isoforms of protease ADAM9 have opposing effects on breast cancer cell migration, Cancer Res. 70 (2010) 8187–8198.
[42] A. Gschwind, S. Hart, O.M. Fischer, A. Ullrich, TACE cleavage of proamphiregulin regulates GPCR-induced proliferation and motility of cancer cells, EMBO J. 22 (2003) 2411–2421.
[43] Q. Zhang, S.M. Thomas, V.W. Lui, S. Xi, J.M. Siegfried, H. Fan, T.E. Smithgall, G.B. Mills, J.R. Grandis, Phosphorylation of TNF-alpha converting enzyme by gastrin-releasing peptide induces amphiregulin release and EGF receptor activation, Proc. Natl. Acad. Sci. U. S. A. 103 (2006) 6901–6906.
[44] Y. Izumi, M. Hirata, H. Hasuwa, R. Iwamoto, T. Umata, K. Miyado, Y. Tamai, T. Kurisaki, A. Sehara-Fujisawa, S. Ohno, E. Mekada, A metalloprotease-disintegrin, MDC9/meltrin-gamma/ADAM9 and PKCdelta are involved in TPA-induced ectodomain shedding of membrane-anchored heparin-binding EGF-like growth factor, EMBO J. 17 (1998) 7260–7272.
[45] L.C. Bridges, R.D. Bowditch, ADAM-integrin interactions: potential integrin regulated ectodomain shedding activity, Curr. Pharm. Des. 11 (2005) 837–847.
[46] J.M. White, L.C. Bridges, D.W. Desimone, M. Tomczuk, T.G. Wolfsberg, The ADAM Family of Proteases: Proteases in Biology and Disease, vol. 4, Springer, The Netherlands, 2005.
[47] R.M. Mahimkar, W.H. Baricos, O. Visaya, A.S. Pollock, D.H. Lovett, Identification, cellular distribution and potential function of the metalloprotease-disintegrin MDC9 in the kidney, J. Am. Soc. Nephrol. 11 (2000) 595–603.
[48] S. Hamada, K. Satoh, W. Fujibuchi, M. Hirota, A. Kanno, J. Unno, A. Masamune, K. Kikuta, K. Kume, T. Shimosegawa, MiR-126 acts as a tumor suppressor in pancreatic cancer cells via the regulation of ADAM9, Mol. Cancer Res. 10 (2012) 3–10.

Journal of Chromatography B, 903 (2012) 157–162

Contents lists available at SciVerse ScienceDirect

Journal of Chromatography B

journal homepage: www.elsevier.com/locate/chromb

Purification and differential biological effects of ginger-derived substances on normal and tumor cell lines

James Almada da Silva[a,1], Amanda Blanque Becceneri[b,2], Hêmily Sanches Mutti[b,2], Ana Carolina Baptista Moreno Martin[c,3], Maria Fátima das Graças Fernandes da Silva[a,1], João Batista Fernandes[a,1], Paulo Cezar Vieira[a,*], Márcia Regina Cominetti[b,**]

[a] Departamento de Química, Rodovia Washington Luís, Km 235, CEP 13565-905, São Carlos, SP, Brazil
[b] Departamento de Enfermagem, Rodovia Washington Luís, Km 235, CEP 13565-905, São Carlos, SP, Brazil
[c] Departamento de Ciências Fisiológicas, Rodovia Washington Luís, Km 235, CEP 13565-905, São Carlos, SP, Brazil

ARTICLE INFO

Article history:
Received 30 March 2012
Accepted 16 July 2012
Available online 20 July 2012

Keywords:
Zingiber officinale
HPLC
Gingerols
Ginger
Cell proliferation
Cancer
MDA-MB-231

ABSTRACT

This study describes an optimization of [6]-, [8]- and [10]-gingerol isolation and purification in semi-preparative HPLC scale and their anti-proliferative activity. The gingerols purification was carried out in HPLC system using a Luna-C_{18} and the best mobile phase evaluated was MeOH/H_2O (75:25, v/v). This new methodology for the gingerols isolation was very effective, since considerable amounts (in the range of milligrams) with a good purity degree (~98%) were achieved in 30 min of chromatographic run. [6]-, [8]- and [10]-Gingerol purified by this methodology inhibited the proliferation of MDA-MB-231 tumor cell line with IC_{50} of 666.2 ± 134.6 μM, 135.6 ± 22.6 μM and 12.1 ± 0.3 μM, respectively. These substances also inhibited human fibroblasts (HF) cell proliferation, however in concentrations starting from 500 μM. In conclusion, our results demonstrate an optimization of gingerols isolation and their specific anti-proliferative activities against tumor cells, suggesting their use as important models for drug design in an attempt to develop new compounds with fewer side effects when compared to conventional chemotherapy.

1. Introduction

Several population-based studies indicate that people in Asian countries have a much lower risk of different cancer types such as colon, gastrointestinal, prostate and breast, when compared to their Western counterparts. It is widely claimed that constituents of their diet such as ginger, garlic, soy, curcumin, onion, tomatoes, cruciferous vegetables, chillies, and green tea contribute to that lower incidence [1]. Therefore, there is increasing interest in naturally occurring cancer chemopreventive agents.

Ginger (*Zingiber officinale* Roscoe) is widely used worldwide as a food, spice and herb [2]. Together with [6]-gingerol, [8]- and [10]-gingerol are the major pungent constituents in the ginger oleoresin from fresh rhizome, being [6]-gingerol the most abundant. Gingerols comprise a series of homologue substances differentiated by the length of their alkyl chains with [6]-, [8]- and [10]-gingerol having 10, 12 and 14 carbons in their unbranched alkyl chains, respectively [3].

Regarding [6]-gingerol a variety of pharmacological characteristics was already described, including analgesic, antipyretic, cardiotonic, hypothermia inducing and cancer preventing effects [4–6]. However, the effects on tumor cell proliferation for [8]- and [10]-gingerol are still scarce.

Breast cancer is the third most frequent cancer in the world and one of the most common malignant diseases in women worldwide. In developing countries, it is the second highest cause of death in women after cervical cancer [7]. To treat breast and many other cancer types, chemotherapy is one of the most extensively studied methods. However, its efficacy and safety remain a primary concern as well as its toxicity and other side effects [8,9]. Another reason for concern regarding this method is the development of chemotherapy resistance, which is a major obstacle to the effective treatment of many tumor types, including breast cancer [8]. Tumor cells are found to adopt multiple mechanisms to resist drugs, such as decreased uptake, and/or enhanced efflux and altered drug

* Corresponding author. Tel.: +55 16 33518206; fax: +55 16 33518350.
** Corresponding author. Tel.: +55 16 33519442; fax: +55 16 33518334.
E-mail addresses: dpcv@ufscar.br (P.C. Vieira), mcominetti@ufscar.br (M.R. Cominetti).
[1] Tel.: +55 16 33518206; fax: +55 16 33518350.
[2] Tel.: +55 16 33066663; fax: +55 16 33519628.
[3] Tel.: +55 16 33518333; fax: +55 16 33518328.

1570-0232/$ – see front matter © 2012 Elsevier B.V. All rights reserved.
http://dx.doi.org/10.1016/j.jchromb.2012.07.013

metabolism. Alteration in drug targets, activation of detoxification systems, enhanced DNA repair ability, and inhibition of apoptosis are also cancer cell strategies to resist against chemotherapy drugs [10].

Many anticancer therapies can temporarily stop tumor growth; it means that, in most cases, the effect is not permanent. In this way, there is a significant need for new agents with low susceptibility to common drug resistance mechanisms in order to improve response rates and potentially prolong patient's survival. Approximately 30% of the women diagnosed with early-stage disease progress to metastatic breast cancer. To these women, therapeutic options are still limited. Current recommendations for first-line chemotherapy include anthracycline-based and taxanes treatments (paclitaxel and docetaxel) [8]. Taxanes – which are taxol derivatives that were first described as microtubule stabilizing agents [11] and then had their antineoplasic effects confirmed [12,13] – are the first example of natural product derivatives used in antitumor therapy. Therefore, the search for new natural products that may be used as an additional alternative to the chemotherapy in an attempt to develop more effective drugs with fewer side effects is of great interest [14]. Based on this assumption it is important to develop an effective method for the isolation of these compounds.

The aim of this work was to search a faster, efficient and productive procedure for isolation of [6]-, [8]- and [10]-gingerol by reverse phase HPLC operating under overloading conditions and to test their anti-proliferative activity on MDA-MB-231 breast cancer tumor line and normal human fibroblasts (HF), a non tumor cell line. The results presented in this study showed a more specific anti-proliferative activity for [8]- and [10]-gingerol against breast cancer compared to HF and suggest their use as important models for anti-cancer therapy in an attempt to develop new drugs with fewer side effects when compared to conventional chemotherapy.

2. Materials and methods

2.1. Chemicals

[6]-, [8]- and [10]-Gingerol were isolated from the ethanol extract of the ginger rhizome (purchased locally) by liquid chromatography. The structures were elucidated by ^{1}H NMR using a Bruker DRX200 instrument (Bruker, USA), operating at 200 MHz for ^{1}H spectra, with TMS as internal standard, GC–MS on a Shimadzu QP 5000 and comparison with literature data. The purity was determined by elemental analysis on an EA 1108, CHNS-O (Fisons). HPLC grade acetonitrile and methanol were purchased from JTBaker Company (Netherland). Water was deionised. All other analytical grade reagents were from Sigma–Aldrich (St. Louis, MO, USA).

2.2. [6]-, [8]- and [10]-Gingerol isolation

The fresh ginger rhizome was thin sliced, dried at 40 °C and ground to powder. The powder was extracted with ethanol for 72 h, three times. The solvent was evaporated under reduced pressure at 40 °C. The extraction of ginger (0.4 kg dry weight) yielded 21.2 g of crude extract (5.3%). The extract was stored at −4 °C for the later fractionation.

In order to isolate [6]-, [8]- and [10]-gingerol, dry ginger rhizome crude ethanol extract was chromatographed on SiO_2 (70–230 mesh) column with bed height 20 cm (20 cm × 8 cm i.d.), using initially *n*-hexane (1 L), to eliminate the lipids. After, *n*-hexane/ethyl acetate 50:50 (v/v, 2.5 L) was used as eluent resulting in 5 fractions (A1-5), where the fractions A1, A2, A3 and A4 (68.9%, 14.6 g), rich in [6]-, [8]- and [10]-gingerols, were joined resulting in the fraction A1–4. Part of this fraction (5.5 g) was re-chromatographed on SiO_2 column (28 cm × 5 cm i.d.) using *n*-hexane/ethyl acetate 60:40 (v/v, 2.4 L). Forty eight fractions (50 mL each) were collected and combined after monitoring by TLC resulting in six sub-fractions with the following volumes: 250 mL (B1), 400 mL (B2), 150 mL (B3), 800 mL (B4), 200 mL (B5) and 600 mL (B6). The gingerols were the main constituent on the fraction B4 (800 mL, 2.8 g, yellow oil).

Analytical and semi-preparative HPLC were carried out using a Shimadzu SCL-10AVP system with an SPD-10AVP UV–vis detector with a flow cell analytical or flow cell preparative, according with the HPLC mode (analytical or semi-preparative), and a Shimadzu LC-6AD pump. The isolation optimization was carried out on a Luna-C_{18} column (250 mm × 4.6 mm i.d., 10 μm, homemade, UFSCar, São Carlos, SP, Brazil) and the column was maintained at 25 °C, the detection wavelength was set at 282 nm and the flow rate at 1.0 mL/min. The mobile phases consisted of isocratic binary mixtures (v/v) of MeOH/H_2O (80:20; 75:25; 70:30) and ACN/H_2O (67:33). Forty microlitres of methanol containing 0.156 mg, 5 mg, 7.5 mg, 15 mg and 30 mg of B4 sample were injected. In the column scale-up reverse phase semi-preparative, a Luna-C_{18} column (300 mm × 10 mm i.d., 10 μm, homemade, UFSCar, São Carlos, SP, Brazil) was used. This column was maintained at 25 °C, the detection wavelength was set at 254 nm (lower absorbance wavelength for the gingerols) and the flow rate at 6.0 mL/min. The best mobile phase was MeOH/H_2O 75:25 (v/v) and the scale-up factor was calculated using Eq. (1) below, where *S*, *R*, *L*, $_P$, $_A$ are scale-up factor, column radius, column length, semi-preparative and analytical columns, respectively. The maximum amount of fraction B4 injected in the semi-preparative column was 170.1 mg diluted to final volume of 400 μL.

$$S = \frac{R_P^2 x L_P}{R_A^2 x L_A} \quad (1)$$

2.3. Cell line and culture

MDA-MB-231 human breast tumor and HF cell lines, obtained from ATCC (Manassas, VA, USA), were maintained at 37 °C in 5% CO_2 in Dulbecco's modified Eagle's medium (DMEM, Cultilab – Campinas; SP, Brazil) containing 10% of FBS (fetal bovine serum), penicillin (100 UI/mL), streptomycin (100 mg/mL) and L-glutamine (2 mM). Cell cultures and experiments were conducted in a humidified environment with 5% CO_2 at 37 °C.

2.4. Proliferation assays

Cell lines were prepared at a concentration of 5×10^4 cells/200 μL, in appropriate medium with 10% of FBS, and plated on sterile 96-well plates for 5 h. After cell adhesion to the plates, the DMEM medium was replaced by DMEM medium without FBS and cells were maintained for 14–18 h at 37 °C and 5% CO_2 in a cell culture incubator. This procedure, known as starvation, was used to synchronize the cell cycle. After starvation, the culture medium was removed from the wells and a new one, supplemented with 10% of FBS, containing different concentrations of the tested compounds was added to the wells. The cells were incubated for 24 and 48 h under the same conditions as described above. Cell proliferation assay was performed in comparison to the wells where the vehicle compound (2.5% DMSO) was added instead of the tested compounds. After incubation, the culture medium of each well was removed and a solution containing MTT (0.5 mg/mL) was added (100 μL/well). The plates were then kept at 37 °C for 4 h and the formed crystals were dissolved in isopropyl alcohol. The absorbance was read on an ELISA plate reader at a wavelength of 595 nm. Doxorubicin was used as a positive control for inhibition of cell proliferation [15].

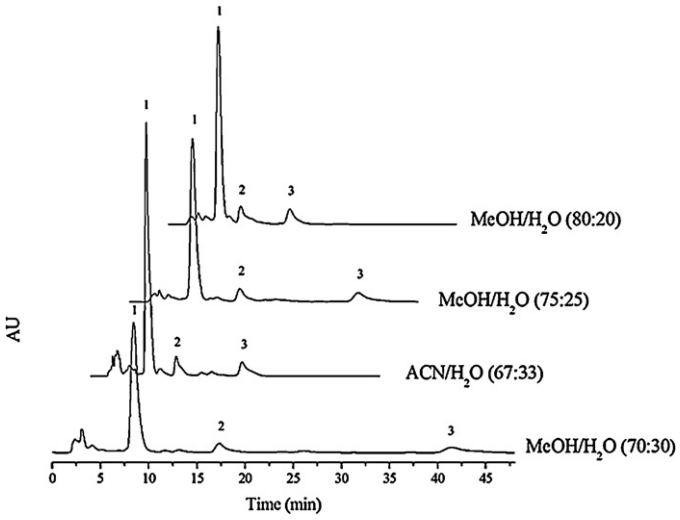

Fig. 1. Chromatograms of fraction enriched in [6]-gingerol (peak 1), [8]-gingerol (peak 2) and [10]-gingerol (peak 3), obtained from HPLC in analytical scale. The fraction was injected in a C_{18} (250 mm × 4.6 mm i.d., 10 μm) column maintained at 25 °C with MeOH/H_2O 80:20; MeOH/H_2O 75:25, ACN/H_2O 67:23 and MeOH/H_2O 70:30, UV detection at 282 nm and flow rate at 1.0 mL/min. The injection volume was 40 μL.

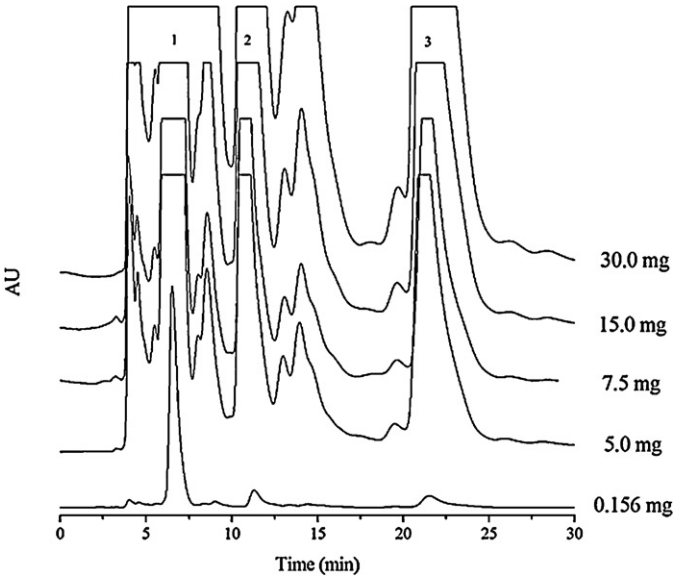

Fig. 2. Overload chromatograms of fraction enriched in [6]-gingerol (peak 1), [8]-gingerol (peak 2) and [10]-gingerol (peak 3), obtained from HPLC in analytical scale. The fraction was injected in a C_{18} (250 mm × 4.6 mm i.d., 10 μm) column maintained at 25 °C with MeOH/H_2O 75:25, UV detection at 282 nm and flow rate at 1.0 mL/min. The injected masses were 0.156 mg, 5 mg, 7.5 mg, 15 mg and 30 mg. The injection volume was 40 μL.

2.5. Statistical analysis

Each experiment was repeated three times in triplicate and a standard error mean was calculated. Shapiro–Wilk's *W* test was used to verify data normality. As normal distribution was present, the results were compared statistically with a two-way analysis of variance (ANOVA). Since the ANOVA tests showed significant differences (acceptable P level < 0.05), Bonferroni's significant difference *post hoc* analyses were performed to determine differences between simple and grouped main-effect means, respectively. The data were analyzed by using Statistica software (version 8.0; Stat Soft Inc., Tulsa, USA) and IC_{50} calculations were made using Hill's equation in the Origin software (version 8.5; OriginLab Corporation, Northampton, MA, USA).

3. Results

3.1. [6]-, [8]- and [10]-Gingerol isolation

Four different conditions were carried out on analytical C_{18} column HPLC to achieve the best separation of [6]-, [8]- and [10]-gingerol. The best separation condition was achieved using MeOH/H_2O 75:25 (v/v), where a good separation of three gingerols in a single run of 30 min was obtained (Fig. 1).

The injection volume (400 μL) was larger than the usual size of an injection volume and also it was not the one that was calculated by the scale up formula. This occurred because of the sample viscosity, which would be very high if 170.1 mg were diluted in 230 μL (calculated volume) that would impair the chromatographic separation. For column overloading with the sample, increasing amounts of fraction B4 (0.156 mg, 5 mg, 7.5 mg, 15 mg and 30 mg diluted to final volume 40 μL) were injected in a C_{18} analytical column. Using the detector at 282 nm electronic saturation was observed when 5 mg of sample was injected, although the peaks were still visible for isolation of gingerols until 15 mg. With the injection of 30 mg of sample, the electronic saturation hindered the visualization of peaks closer to peak 1 (Fig. 2). To solve this problem, on the semi-preparative mode, the detector was set at 254 nm and in this condition it was possible to identify the three gingerols present in the fraction.

Using Eq. (1) for the determination of scale-up factor, the value 5.67 was obtained, consequently the maximum amount of B4 fraction that could be injected in a semi-preparative column was 170.1 mg (Fig. 3). However, to make the adjustment of the flow rate easier we decided to use 6.0 mL/min instead of 5.67 mL/min, and by working in this condition the results obtained were satisfactory.

The mass of each gingerol obtained from 170.1 mg of fraction B4 was: 94 mg ([6]-gingerol), 22 mg ([8]-gingerol) and 17 mg ([10]-gingerol). The purity of gingerols was calculated based on the elemental analysis of each gingerol. The purification yields based on the fresh ginger weight were 1027, 241 and 187 ppm for [6]-, [8]- and [10]-gingerol, respectively. The purity obtained was 94.4, 99 and 97.3% for [6]-, [8]- and [10]-gingerol, respectively.

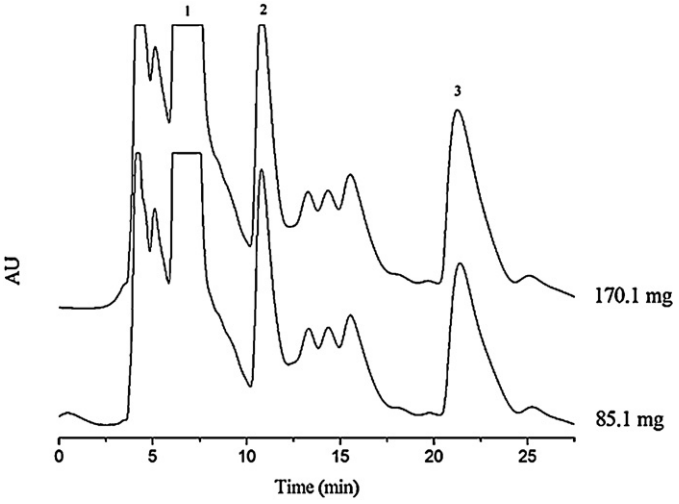

Fig. 3. Scale-up chromatograms of fraction enriched in [6]-gingerol (peak 1), [8]-gingerol (peak 2) and [10]-gingerol (peak 3), obtained from HPLC in analytical scale. The fraction was injected in a C_{18} (300 mm × 10 mm i.d., 10 μm) column maintained at 25 °C with MeOH/H_2O 75:25, UV detection at 254 nm and flow rate at 6.0 mL/min. The injected masses were 85.1 mg, 170.1 mg. The injection volume was 400 μL.

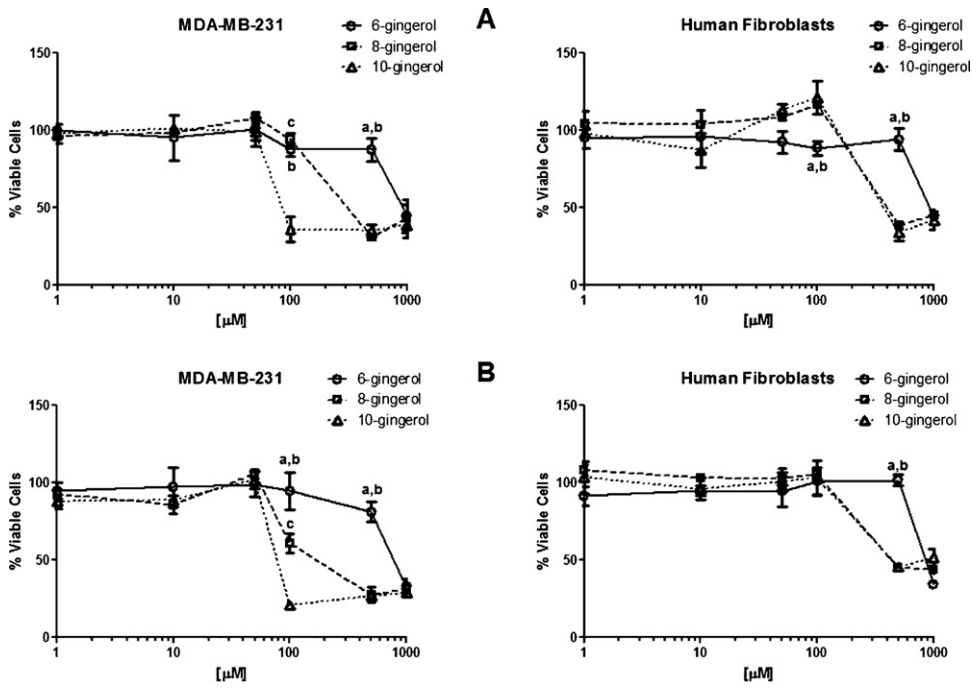

Fig. 4. Effects of [6]-, [8]- and [10]-gingerol on MDA-MB-231 and Human Fibroblasts cell proliferation. MDA-MB-231 tumor cells or Human Fibroblasts were plated at a density of 5×10^4 cells/200 μL in a 96-well plate containing DMEM medium with 10% of FBS (fetal bovine serum) for 5 h. After cell adhesion to the plates, the DMEM medium was replaced by DMEM medium without FBS and cells were maintained for 14–18 h at 37 °C and 5% CO_2 in a cell culture incubator. This procedure, named starvation, was used to synchronize the cell cycle. After starvation the monolayers were incubated with different concentrations of [6]-, [8]- or [10]-gingerol in DMEM medium, supplemented with 10% of FBS. The cells were incubated for 24 (A) or 48 (B) hours. Viable cells were estimated by the MTT assay. Results are mean ± SD of three independent assays in triplicate (a = [6]-gingerol *vs.* [8]-gingerol $P < 0.05$; b = [6]-gingerol *vs.* [10]-gingerol $P < 0.01$; c = [8]-gingerol *vs.* [10]-gingerol $P < 0.001$).

3.2. Identification of [6], [8] and [10]-gingerol

The gingerols were identified based on the ^{1}H NMR and MS spectra data compared with literature [16,17].

3.2.1. [6]-Gingerol

Yellow oil; $C_{17}H_{26}O_4$. MS *m/z* 294 $[M]^{+\bullet}$ (9), 276 (4), 205 (8), 194 (13), 179 (4), 150 (26), 137 (100), ^{1}H NMR (200 MHz, $CDCl_3$): δ 0.88 (t, 3H, t, *J* = 6.0 Hz, H-10), 1.22–1.48 (8H, m, H-6 to H-9), 2.47–2.90 (2H, m, H-4), 2.78 (4H, m, H-1, H-2), 3.85 (3H, s, —OCH_3), 4.02 (1H, q, H-5), 6.64 (1H, dd, *J* = 8.0, 2.0 Hz, H-6′), 6.67 (1H, d, *J* = 2.0 Hz, H-2′), 6.82 (1H, d, *J* = 8.0 Hz, H-5′).

3.2.2. [8]-Gingerol

Brown oil; $C_{19}H_{30}O_4$, MS *m/z* 322 $[M]^{+\bullet}$ (3), 304 (5), 205 (9), 194 (23), 179 (2), 150 (13), 137 (100). ^{1}H NMR (200 MHz, $CDCl_3$): δ 0.88 (t, 3H, t, *J* = 6.0 Hz, H-10), 1.22–1.48 (12H, m, H-6 to H-11), 2.47–2.90 (2H, m, H-4), 2.78 (4H, m, H-1, H-2), 3.86 (3H, s, —OCH_3), 4.02 (1H, q, H-5), 6.64 (1H, dd, *J* = 8.0, 2.0 Hz, H-6′), 6.67 (1H, d, *J* = 2.0 Hz, H-2′), 6.82 (1H, d, *J* = 8.0 Hz, H-5′).

3.2.3. [10]-Gingerol

Colorless powder; $C_{21}H_{34}O_4$, MS *m/z* 351.2 $[M+1]^+$, *m/z* 373.3 $[M+23]^+$, 389.2 $[M+39]^+$ ^{1}H NMR (200 MHz, $CDCl_3$): δ 0.88 (t, 3H, t, *J* = 6.0 Hz, H-10), 1.22–1.48 (14H, m, H-6 to H-13), 2.47–2.90 (2H, m, H-4), 2.78 (4H, m, H-1, H-2), 3.87 (3H, s, —OCH_3), 4.02 (1H, q, H-5), 6.64 (1H, dd, *J* = 8.0, 2.0 Hz, H-6′), 6.67 (1H, d, *J* = 2.0 Hz, H-2′), 6.82 (1H, d, *J* = 8.0 Hz, H-5′).

3.3. Effects of [8] and [10]-gingerol on normal and tumor cell proliferation

The effects of isolated compounds, [6]-, [8]-, and [10]-gingerol, were compared to their effects on HF, a normal (non tumor) cell line (Figs. 4A and B and 5). In these assays, the controls were made by incubating the cells in a normal medium, supplemented with 10% of FBS (+FBS), in a medium without FBS (−FBS), adding DMSO (final concentration of 2.5%) to the medium supplemented with 10% of FBS (DMSO) and finally, in doxorubicin (1.5 μM), a compound used in breast cancer chemotherapy, as a positive control for cell proliferation inhibition [15].

The results showed that [8]-gingerol affects MDA-MB-231 cell proliferation after 24 h of incubation, with 500 and 1000 μM inhibiting approximately 75% and 50% of tumor cell proliferation, respectively (Fig. 4A and B). After 48 h of incubation with [8]-gingerol 100 μM there was approximately 60% of MDA-MB-231 cell proliferation inhibition (Fig. 4B). At the same incubation period with [8]-gingerol 500 and 1000 μM, MDA-MB-231 inhibition remained in a rate of 75% compared to control cells (+FBS). [8]-Gingerol 1, 10 and 50 μM had no effects on MDA-MB-231 cell proliferation (Fig. 4A and B).

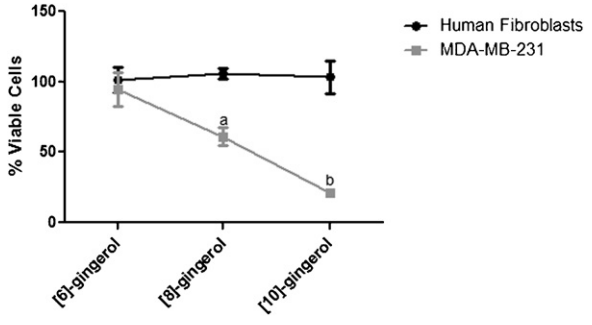

Fig. 5. Differential effects of [6]-, [8]- and [10]-gingerol 100 μM on MDA-MB-231 and Human Fibroblasts cell proliferation after 48 h of incubation. Results are mean ± SD of three independent assays in triplicate (a = MDA-MB-231 *vs.* HF $P < 0.01$; b = MDA-MB-231 *vs.* HF $P < 0.001$).

For [10]-gingerol, a concentration of 100 μM was significantly effective in inhibiting MDA-MB-231 cell proliferation at 24 h of incubation in a rate of 75%, compared to cells seeded on normal medium (+FBS). The same pattern was observed after 48 h of [10]-gingerol incubation; there was a cell proliferation inhibition of about 90% (Fig. 4B).

HF were used in order to compare the effects of both [6]-, [8]- and [10]-gingerol in a non tumor cell line (Figs. 4A and B and 5). No significant differences in MDA-MB-231 cell proliferation using 1, 10, 50 and 100 μM for [6]-, [8]- and [10]-gingerol in 24 or 48 h of incubation were verified. However, 500 and 1000 μM concentrations were effective in this inhibition, but in an approximate rate of only 50% (Fig. 4A and B).

The differential effects of [8]- and [10]-gingerol 100 μM after 48 h of incubation with HF and MDA-MB-231 tumor cell line are demonstrated in Fig. 5. These compounds were more effective in inhibiting tumor cell proliferation (MDA-MB-231) when compared to normal cell proliferation (HF). The IC_{50} values for [6]-, [8]- and [10]-gingerol on MDA-MB-231 cell proliferation were calculated. The results showed that these compounds inhibited the proliferation of MDA-MB-231 tumor cell line with IC_{50} of 666.2 ± 134.6 μM; 135.6 ± 22.6 μM and 12.1 ± 0.3 μM, respectively. These substances also inhibit HF cell proliferation, nevertheless, we were not able to calculate the IC_{50} values for this cell line, since the initial concentration that had an effect was 500 μM for [6]-, [8] and [10]-gingerol.

4. Discussion

Studies of isolation and purification of gingerols are scarce in the literature. Considering the interesting biological activities and the potential of these compounds to the medical area it is imperative to develop new methodologies to achieve an optimization of gingerol separation and purification. The isolation of gingerols ([6]-, [8]- and [10]-gingerol) described in this work was achieved satisfactorily, once it was possible to obtain relatively high mass and a good degree of gingerols purity. To our knowledge, only one work about isolation of gingerols using HPLC system was published [18]. In this work, the authors isolated the major gingerols from the crude dichloromethane extract of ginger rhizome by normal phase HPLC. A low purity degree (calculated by the percentage of peak area) for both, [8]-gingerol (86%) and [10]-gingerol (84%) was achieved, while for the [6]-gingerol the purity was 99%. The purity degree obtained for each gingerol does not represent the real one, because HPLC system using UV detection does not guarantee the absence of other components in the sample. In a recent work, the isolation of [6]-, [8]- and [10]-gingerol was carried out using counter-current chromatography (CCC). In this study gingerols were obtained with high purity degree (99%), however the time of chromatographic run was very length (240 min) [19]. In another work regarding isolation of gingerols from crude extract of ginger rhizome using CCC the time of chromatographic run was again very extensive, and the purity was about 98% [20].

Electronic saturation is a factor that considerable limits the increasing of injected mass in the semi-preparative scale. In our work, this factor had limited injections of samples with higher masses, even at a wavelength of low absorption of gingerols (254 nm) (Fig. 3). However, the gingerols were isolated in significant quantities and with a good purity degree. To avoid the electronic saturation we could use either a less sensitive flow cell or make the adjustment of the wavelength well off the lambda max. We have not tried a less sensitive cell, however all the experiment conditions were tested in the lower absorption wavelength for the gingerols, and we still obtained electronic saturation. It may be possible to use other detectors even though we have only used UV.

The effects of [6]-gingerol on tumor cell proliferation are already well documented [5,21–23], however, the effects of [8]- and [10]-gingerol on tumor cells are still scarce. In fact, among all the ginger constituents, much more attention has been given to [6]-gingerol in order to explore its pharmacological properties and action mechanisms. In this sense, besides [6]-gingerol effects, those of [8]- and [10]-gingerol on *in vitro* tumor cell proliferation using MDA-MB-231 and HF cell lines were also investigated.

The overall results suggest that the higher the alkyl chain, the greater the effectiveness of gingerol in inhibiting tumor cell proliferation, probably due to the manner in which these substances enter the cells through their plasma membrane. In general, with increasing alkyl chain lengths, there is an increase in lipophilic character (log *P*) of compounds, and this can be quantified by the partition coefficient (*P*) in an n-octanol/water system. It is also known that the higher the log *P* value, to a certain extent, the higher will be the permeation in biological membranes [24,25]. This can be extended to compounds such as gingerols, which represent a homologous series of substances.

Similar effects of gingerols and other ginger-derived substances were already described in the literature. Tjendraputra et al. [26] demonstrated that the inhibition of COX-2 by ginger constituents and synthetic analogs was structure-dependent. The lipophilicity and the functional group substitution on the alkyl side chain, as well as the aromatic moiety were the main aspects influencing COX-2 inhibition. Similar correlations between the side-chain length of gingerols and their activities of apoptosis induction and neuronal cells protection from β-amyloid insult have already been demonstrated [27,28].

The cytotoxic effect of [8]- and [10]-gingerol has been investigated by a few authors [27,29]. Kim and coworkers [29] have tested the effects of [8] and [10]-gingerol in a variety of human tumor cells lines including A-549 (lung cancer), SK-OV-3 (ovarian cancer), SK-MEL-2 (skin cancer) and HCT15 (colon cancer). They found an IC_{50} ranging from approximately 4.52 μg/mL (13 μM) to 12.57 μg/mL (40 μM), with [10]-gingerol being more effective than [8]-gingerol in decreasing the viability of these tumor cell lines [29]. Wei and coworkers [27] found an IC_{50} of 87.9 ± 3.5 μM and 56.5 ± 6.0 μM for [8]- and [10]-gingerol, respectively, in the inhibition of HL-60 proliferation, a human leukemia tumor cell line. These data are in accordance with the findings in this work on MDA-MB-231 cells, revealing the same activity dependence on the chain length size pattern.

Kuo and collaborators [30] working with SW480 cells, a lineage of colorectal cancer, observed that [10]-gingerol caused a significant concentration-dependent and sustained $[Ca^{2+}]_i$ rise, suggesting that this elevation can alter cellular functions, leading to cell death. They found a cytotoxic effect of [10]-gingerol 50, 75 and 100 μM [30]. It is important to notice that the methodology in the present study was different, even though, similar effects were found in MDA-MB-231 tumor cell line.

Our findings demonstrate a specificity of [8]- and [10]-gingerol on the inhibition of breast tumor cell proliferation when compared to non tumor human fibroblast cell line. The findings of other authors corroborate with our results. Kazi et al. [31] described the effects of antibiotics derived from β-lactam, lactam 1 and 12 on normal and tumor cells. They show that lactam 1 selectively induces apoptosis in human leukemic Jurkat T, but not in the non transformed, immortalized human natural killer cells. Furthermore, the authors demonstrated that lactam 12 induces apoptosis selectively in Jurkat T and simian virus 40-transformed, but not in non transformed NK and parental normal fibroblast cells. The authors propose that these N-thiolated β-lactams act by inducing DNA damage that leads to apoptosis preferentially in cancer and transformed over normal/non transformed cells. Another example includes pancratistatin, a natural compound isolated from the

spider lily, which is an efficient inducer of apoptosis in human lymphoma (Jurkat) cells, with minimal effect on normal nucleated blood cells. The authors discuss that this selective effect could be due to the expression of the Fas receptors, which are found to be greater in blood lymphoma cells than normal blood cells. Furthermore, in fast-dividing cancer cells, the plasma membrane tends to run short of lipids, perhaps changing the fluidity of the membrane [32]. Ovadje et al. [33] demonstrate that dandelion root extract is capable of inducing apoptosis at low concentrations specifically in cancer cells with no toxicity to peripheral blood mononuclear cells (PBMCs). Finally, Mathen et al. [34] working with extracts from *Calotropis gigantea*, the giant milkweed, traditionally used for the treatment of cancer and in Ayurvedic medicine and *Poecilocerus pictus*, an orthopteran insect, which feeds on *C. gigantea*, demonstrated that both the insect and the plant extracts induce concentration-dependent apoptosis and differentiate between human cancer cells and normal cells and exhibit species specificity.

The chemopreventive mechanisms of gingerols are not well understood however, are thought to involve proapoptotic [27,35–37], antioxidant [38], anti-inflammatory [6,39–41], and anti-angiogenic [42] activities. Further investigation will be done in order to determine the mechanisms by which [8]- and [10]-gingerol act inhibiting with more specificity the MDA-MB-231 cell proliferation.

5. Conclusion

In conclusion, this work presents a new methodology for the isolation of gingerols, which proved to be effective, once considerable amounts with a good purity degree in a relatively short time of chromatographic run were achieved from these important bioactive compounds, mainly [8]-gingerol (99%) and [10]-gingerol (97.3%). This is the first report on the separation of these compounds with such a purity degree using HPLC semi-preparative scale. Optimizations in the separation process regarding column overloading can still be made so that the electron saturation be not reached, which can be achieved by using other less sensitive detectors. The gingerols isolated through this methodology, demonstrate an anti-proliferative activity of [8]- and [10]-gingerol specifically on MDA-MB-231 breast cancer cells when compared to HF normal cells. As far as we know, this is the first report regarding a specific cell effect of ginger derivatives. The results also suggest the use of [8]- and [10]-gingerol as important models for anti-cancer therapy and drug design in an attempt to develop new compounds with fewer side effects when compared to conventional chemotherapy.

References

[1] T. Dorai, B.B. Aggarwal, Cancer Lett. 215 (2004) 129.
[2] S. Dugasani, M.R. Pichika, V.D. Nadarajah, M.K. Balijepalli, S. Tandra, J.N. Korlakunta, J. Ethnopharmacol. 127 (2010) 515.
[3] S. Sang, J. Hong, H. Wu, J. Liu, C.S. Yang, M.H. Pan, V. Badmaev, C.T. Ho, J. Agric. Food Chem. 57 (2009) 10645.
[4] A.M. Bode, W.Y. Ma, Y.J. Surh, Z. Dong, Cancer Res. 61 (2001) 850.
[5] H.S. Lee, E.Y. Seo, N.E. Kang, W.K. Kim, J. Nutr. Biochem. 19 (2008) 313.
[6] K.K. Park, K.S. Chun, J.M. Lee, S.S. Lee, Y.J. Surh, Cancer Lett. 129 (1998) 139.
[7] A. Stuckey, Clin. Obstet. Gynecol. 54 (2011) 96.
[8] E. Rivera, H. Gomez, Breast Cancer Res. 12 (Suppl. 2) (2010) S2.
[9] J. Prouse, Clin. J. Oncol. Nurs. 14 (2010) 206.
[10] L. Froidevaux-Klipfel, F. Poirier, C. Boursier, R. Crepin, C. Pous, B. Baudin, A. Baillet, Proteomics 11 (2011) 3877.
[11] K. Tsuji, A. Ueno, T. Ide, Cell Struct. Funct. 17 (1992) 139.
[12] M.H. Bartoli, M. Boitard, H. Fessi, H. Beriel, J.P. Devissaguet, F. Picot, F. Puisieux, J. Microencapsul. 7 (1990) 191.
[13] Y. Kalechman, A. Shani, S. Dovrat, J.K. Whisnant, K. Mettinger, M. Albeck, B. Sredni, J. Immunol. 156 (1996) 1101.
[14] A.L. Demain, P. Vaishnav, Microb. Biotechnol. 4 (2010) 687.
[15] G.P. Sartiano, W.E. Lynch, W.D. Bullington, J. Antibiot. (Tokyo) 32 (1979) 1038.
[16] S.D. Jolad, R.C. Lantz, G.J. Chen, R.B. Bates, B.N. Timmermann, Phytochemistry 66 (2005) 1614.
[17] M.C. Rho, S.W. Lee, J.H. Lim, M.S. Kim, J.H. Jeong, G.Y. Song, W.S. Lee, Food Chem. 128 (2011) 778.
[18] R.D. Hiserodt, S.G. Franzblau, R.T. Rosen, J. Agric. Food Chem. 46 (1998) 2504.
[19] K. Zhan, K. Xu, H. Yin, Food Chem. 126 (2011) 1959.
[20] X. Wang, Z.J. Zheng, X.F. Guo, J.P. Yuan, C.C. Zheng, Food Chem. 125 (2011) 1476.
[21] A.A. Oyagbemi, A.B. Saba, O.I. Azeez, Biofactors 36 (2010) 169.
[22] C.H. Jeong, A.M. Bode, A. Pugliese, Y.Y. Cho, H.G. Kim, J.H. Shim, Y.J. Jeon, H. Li, H. Jiang, Z. Dong, Cancer Res. 69 (2009) 5584.
[23] S.Y. Song, Y.J. Park, J. Wen, S. Bang, S.W. Park, Yonsei Med. J. 47 (2006) 688.
[24] C. Hansch, K.H. Kim, R.H. Sarma, J. Am. Chem. Soc. 95 (1973) 6447.
[25] C. Hansch, T. Fujita, J. Am. Chem. Soc. 86 (1964) 1616.
[26] E. Tjendraputra, V.H. Tran, D. Liu-Brennan, B.D. Roufogalis, C.C. Duke, Bioorg. Chem. 29 (2001) 156.
[27] Q.Y. Wei, J.P. Ma, Y.J. Cai, L. Yang, Z.L. Liu, J. Ethnopharmacol. 102 (2005) 177.
[28] D.S. Kim, J.Y. Kim, Bioorg. Med. Chem. Lett. 14 (2004) 1287.
[29] J.S. Kim, S.I. Lee, H.W. Park, J.H. Yang, T.Y. Shin, Y.C. Kim, N.I. Baek, S.H. Kim, S.U. Choi, B.M. Kwon, K.H. Leem, M.Y. Jung, D.K. Kim, Arch. Pharm. Res. 31 (2008) 415.
[30] S.Y. Kuo, C.Y. Chen, Y.W. Li, Molecules 14 (2009) 959.
[31] A. Kazi, R. Hill, T.E. Long, D.J. Kuhn, E. Turos, Q.P. Dou, Biochem. Pharmacol. 67 (2004) 365.
[32] N. Kekre, C. Griffin, J. McNulty, S. Pandey, Cancer Chemother. Pharmacol. 56 (2005) 29.
[33] P. Ovadje, S. Chatterjee, C. Griffin, C. Tran, C. Hamm, S. Pandey, J. Ethnopharmacol. 133 (2011) 86.
[34] C. Mathen, S.M. Peter, B.P. Hardikar, J. Environ. Pathol. Toxicol. Oncol. 30 (2011) 83.
[35] E. Lee, Y.J. Surh, Cancer Lett. 134 (1998) 163.
[36] Y. Shukla, N. Nigam, J. George, S. Srivastava, P. Roy, K. Bhui, M. Singh, Cancer Chemother. Pharmacol. 65 (2010) 687.
[37] C.Y. Chen, C.H. Chen, C.H. Kung, S.H. Kuo, S.Y. Kuo, J. Nat. Prod. 71 (2008) 137.
[38] R.S. Ahmed, V. Seth, S.T. Pasha, B.D. Banerjee, Food Chem. Toxicol. 38 (2000) 443.
[39] P. Karna, S. Chagani, S.R. Gundala, P.C. Rida, G. Asif, V. Sharma, M.V. Gupta, R. Aneja, Br. J. Nutr. (2011) 1.
[40] H. Ling, H. Yang, S.H. Tan, W.K. Chui, E.H. Chew, Br. J. Pharmacol. 161 (2010) 1763.
[41] Y. Shukla, M. Singh, Food Chem. Toxicol. 45 (2007) 683.
[42] E.C. Kim, J.K. Min, T.Y. Kim, S.J. Lee, H.O. Yang, S. Han, Y.M. Kim, Y.G. Kwon, Biochem. Biophys. Res. Commun. 335 (2005) 300.

UNIVERSIDADE ESTADUAL DE CAMPINAS
Comissão de Ética no Uso de Animais

CEUA/UNICAMP

Protocolo para uso de animais em pesquisa	
Dados do remetente	
Nome	Maria Cristina Cintra Gomes Marcondes
E-mail	cintgoma@unicamp.br
1 Informações gerais sobre o projeto	
1.1 Protocolo	3224-1
1.2 Finalidade do projeto	Pesquisa
1.3 Título do projeto	Investigando a eficacia do [10]-gingerol contra metastases de cancer de mama
1.4 Área de conhecimento (inserção) do projeto	Área do conhecimento Citologia e Biologia Celular Número (código) da área 2.06.01.00-0
1.5 Período do projeto	**Início** 01/2014 **Término** 02/2015
1.6 Responsável pelo projeto	
1.6.1 Nome completo	Maria Cristina Cintra Gomes Marcondes / Docente
1.6.2 Departamento / setor	Biologia estrutural e Funcional
1.6.3 Unidade	IB - Instituto de Biologia
1.6.4 Telefone / ramal	35216194
1.6.5 Fax	35216185
1.6.6 E-mail	cintgoma@unicamp.br
1.7 Agência Financiadora	FAPESP
2 Executores	
2.1 Nome completo	Ana Carolina Baptista Moreno Martin
2.2 Telefone / Ramal	(16)33518333
2.3 Fax	(16)33518327
2.4 E-mail	martin.acbm@gmail.com
2.5 Nível acadêmico	Mestrado
2.6 Nome do orientador / supervisor	Heloísa Sobreiro Selistre de Araujo
2.7 Departamento	Ciencias Fisiológicas
2.8 Unidade	Centro de Ciencias Biológicas e da Saúde - Ufscar
2.1 Nome completo	Rebeka Tomasin
2.2 Telefone / Ramal	35216193
2.3 Fax	35216185
2.4 E-mail	rebekatomasin@hotmail.com
2.5 Nível acadêmico	Mestrado

2.6 Nome do orientador / supervisor	Maria Cristina Cintra Gomes Marcondes
2.7 Departamento	Biologia Estrutural e Funcional
2.8 Unidade	IB - Instituto de Biologia
3 Colaboradores	
3.1 Nome	Márcia Regina Cominetti
3.2 Nível acadêmico	Docente (Pós-doutorado)
3.3 Departamento	Gerontologia
3.4 Faculdade / Instituto	Centro de Ciencias Biológicas e da Saúde
3.5 Instituição	Universidade Federal de São Carlos
3.6 Vínculo formal com a Unicamp	Não
3.7 Telefone / Ramal	(16)33066663
3.8 Fax	(16)33518327
3.9 E-mail	mcominetti@ufscar.br
3.1 Nome	Normand Pouliot
3.2 Nível acadêmico	Pós-Doc Senior
3.3 Departamento	Oncology/Patology
3.4 Faculdade / Instituto	Peter MacCallum Cancer Centre - Melbourne /Australia
3.5 Instituição	University of Melbourne
3.6 Vínculo formal com a Unicamp	Não
3.7 Telefone / Ramal	+610396561285
3.8 Fax	+610396562740
3.9 E-mail	normand.pouliot@petermac.org
4. Objetivo(s) principal(is) da pesquisa	
4.1 Descrição geral da pesquisa ou da aula	Esse projeto visa estudar a ação do [10]-gingerol, uma substancia derivada do gengibre, sobre uma linhagem celular de câncer de mama triplo-negativo que forma metástases cerebrais (4T1Br4cl6). Uma vez que este tipo de câncer apresenta maior resistência aos tratamentos usuais, há poucos medicamentos e intervenções possíveis. Sabendo-se que produtos naturais são capazes de cruzar a barreira hematocefálica devido seu tamanho e estrutura química, e que o [10]-gingerol apresentam estruturas e características químicas similares a alguns destes compostos, podemos sugerir que ele atravesse a barreira cerebral.
4.2 Objetivo da pesquisa ou da aula	Verificar o papel do [10]-gingerol, um produto natural proveniente do gengibre, na progressão tumoral de câncer de mama in vivo.
4.3. Principal impacto/relevância da pesquisa ou da aula	Identificação de moléculas menos tóxicas e que atravessem a barreira hemato-encefálica para o tratamento de cancer de mama e metástases, sobretudo cerebrais.
4.4 Justifique a impossibilidade de adotar métodos alternativos	Embora os estudo in vitro sejam importantes e contribuam para o desenvolvimento terapêutico, estes estudos possuem limitações e necessitam de complementação com estudos in vivo, que possibilitam uma compreensão mais abrangente e real do funcionamento das substancias em questão no organismo como um todo.
4.5 Informe as	Almada da Silva J, Becceneri AB, Sanches Mutti H, Moreno Martin AC, Fernandes da Silva MF, Fernandes JB, Vieira PC, Cominetti MR. Purification and differential biological effects of ginger-derived substances on normal and tumor cell lines. J Chromatogr B Analyt Technol Biomed Life Sci. Aug 15;903:157-62, 2012.

publicações que a equipe tem nesta linha de pesquisa (autores, título, revista, volume, página, ano)	Tomasin R, Gomes-Marcondes MC. Oral administration of Aloe vera and honey reduces Walker tumour growth by decreasing cell proliferation and increasing apoptosis in tumour tissue. Phytother Res. Apr;25(4):619-23, 2011. Sloan EK, Pouliot N, Stanley KL, Chia J, Moseley JM, Hards DK, Anderson RL. Tumor-specific expression of alphavbeta3 integrin promotes spontaneous metastasis of breast cancer to bone. Breast Cancer Res. 8(2):R20. Epub 2006 Apr 11, 2006.
5 Qualificação da equipe	
5.1 Experiência do responsável pelo projeto (orientador/supervisor)	A profa. Maria Cristina possui ampla experiencia em modelos de câncer in vivo tanto em camundongos quanto em ratos.
Executor: Ana Carolina Baptista Moreno Martin	
5.2. Treinamento do executor (técnico ou aluno de IC, M, D ou PD)	Aluna de doutorado com treinamento e experiencia com o modelo a ser utilizado
a. Tipo de treinamento	Capacitação feita durante estágio sanduiche no Peter Mac/Australia
b. Quanto tempo?	1 ano
Executor: Rebeka Tomasin	
5.2. Treinamento do executor (técnico ou aluno de IC, M, D ou PD)	Aluna de doutorado com ampla prática no manuseio de animais de laboratório
a. Tipo de treinamento	Capacitação feira na Unesp (2005), novamente na Unicamp (2006) e no Peter Mac/Australia 2012
b. Quanto tempo?	Experiencia de 8 anos
Colaborador: Márcia Regina Cominetti	
5.3 Treinamento do colaborador	Pos doutora, docente da Ufscar, com experiencia no manuseio de animais de laboratorio
a. Tipo de treinamento	capacitação do INSERN/França
b. Quanto tempo?	6 meses
Colaborador: Normand Pouliot	
5.3 Treinamento do colaborador	Pos-doc senior, desenvolveu o modelo a ser utilizado
a. Tipo de treinamento	capacitação
b. Quanto tempo?	acima de 20 anos de experiencia
6 Informações sobre o modelo animal experimental	
6.1 Descrição do modelo	
6.1.1 Descrição dos grupos	

Grupo	Espécie	Linhagem	Sexo / Quantidade		Idade	Peso	Grau de invasividade
			Nº exemplares Machos	Nº exemplares Fêmeas			
1	Camundongo isogênico	Balb/C		30	7.00 Semanas	25.00 Gramas	2
	Descrição	Grupo controle tumor: não recebera [10]-gingerol e o tumor primario será removido com 0.5g (21 dias aprox.)					
	Camundongo isogênico	Balb/C		15	7.00 Semanas	25.00 Gramas	2

2	**Descrição**	Grupo tumor [10]-gingerol: recebera [10]-gingerol assim que o tumor primario estiver palpável e o tumor primario será removido com 0.5g (21 dias aprox.)

3	Camundongo isogênico	Balb/C		15	7.00 Semanas	25.00 Gramas	2
	Descrição	Grupo tumor [10]-gingerol pós cirurgia: recebera [10]-gingerol após a remoção do tumor primario (0.5g, 21 dias aprox.)					

	Total Machos	**Total Fêmeas**	**Total Geral**	
	0	**60**	**60**	

6.1.2 Haverá a utilização de animais geneticamente modificados nestes experimentos?	Não
6.1.3 Haverá a utilização de animais selvagens nestes experimentos?	Não
6.1.4 Procedência dos animais	CEMIB/Unicamp
6.1.5 Padrão sanitário	SPF
6.1.6 Planejamento estatístico e delineamento experimental	O grupo de pesquisa que desenvolveu o modelo experimental (prof. Robin L Anderson, Dr. Normand Pouliot, Melbourne/Australia) consultou um estatístico que analisando os dados concluiu que o numero de animais por grupo deveria estar entre 15 e 20.
6.1.7 Haverá compartilhamento de material biológico destes animais em outros projetos?	Não
6.2 Condições de manutenção	
6.2.1 Local (biotério, aviário, canil, fazenda, etc.) onde serão mantidos os animais	Bioterio do Laboratório de Nutrição e Cancer
6.2.2 Número de animais por ambiente de contenção	5
6.2.3 Exaustão do ar	Sim
6.2.4 Ambiente de contenção	Gaiola
6.2.5 Tipo de cama	Maravalha
6.2.6 Água	

Filtrada	Sim	**Clorada**	Sim
Autoclavada	Não	**Destilada**	Não

6.2.7 Alimentação	
Ração industrial	Nuvital
Suplemento	Não
Dieta específica	Não
7. Procedimentos Experimentais	

7.1 Jejum	Não
7.2 Restrição hídrica	Não
7.3 Imobilização do animal	Não
7.4 Anestesia	Sim

Anestésico	Dose e unidades	Via de administração
quetamina	100mg/kg	intraperitonial
isoflurano	2mL/10 segundos	inalação

7.5 Uso de bloqueador (relaxante) muscular	Sim

Relaxante/bloqueador	Dose e unidades	Via de administração
xilasina	16mg/kg	intraperitonial

7.6 Cirurgia	Única - Remoção do tumor primário (localizado na glandula
7.7 Recuperação pós-clínica	12.00 hora(s)
7.8 Utilização de analgésico	Sim

Analgésico	Dose e unidades	Via de administração	Frequência	Duração do uso
carprofeno	40mg/kg	subcutaneo	1 x após cirurgia	1 dia

7.9 Utilização de antibiótico	Não
Justificativa do não uso do antibiótico	Os procedimentos são feitos de maneira estéril, não havendo risco de infecção.
7.10 O experimento é específico para	
a. Dor	Não
b. Anorexia	Não
c. Estresse	Não
7.11 Exposição a agentes biológicos, químicos, físicos ou mecânicos?	Não
7.12 Extração de fluídos	Não
7.13 Extração de órgãos	pulmão, femur, coluna vertebral, fígado, baço e cerebro
7.14 Inoculação de substâncias, drogas, medicamentos ou outros	Sim

Nome	Via de administração	Dose (indicar unidades)	Frequência
[10]-gingerol	intraperitonial	10mg/kg	diariamente

8 Destino dos Animais	
8.1 Reaproveitamento	Não
8.2 Morte	Outro - Overdose de Isoflurano (inalado)
8.3 Forma de descarte dos animais	Incineração/Lixo sanitario
9. Resumo do Procedimento Experimental	
	Um dos modelos a ser utilizado será o modelo de metástase espontânea singênico ortotópico. Neste modelo 1x10^5 células/20µL/camundongo

Resumo	serão injetadas no tecido adiposo da quarta mama de camundongos Balb/c (6-8 semanas). Assim que o tumor se tornar palpável os camundongos serão tratados diariamente com [10]-Gingerol (1mg/kg), através de injeções intra-peritoniais, invertendo os lados das injeções para evitar lesões devido ao tratamento diário. Após trintas dias da injeção tumoral os camundongos serão sacrificados. Durante esse período os camundongos serão monitorados através do peso corporal e seu tumor primário será quantificado com o uso de um paquímetro. No sacrifício serão avaliadas as metástases visíveis, e dependendo da linhagem utilizada órgãos específicos serão coletados (já que as formações das metástases nesse modelo dependem da linhagem celular utilizada) para análise da RTB (Relative Tumor Burden). Para a linhagem 4T1Br4, que naturalmente ocorre metástases para o cérebro, serão coletados: pulmão, fêmur, espinha e cérebro para análise da RTB. Os tumores primários, baço, fígado e pulmão também serão pesados para avaliar de forma indireta indícios de metástases (qPCR).

10. Termo de Responsabilidade

Eu asseguro à CEUA/UNICAMP que:

10.1. Li os Princípios Éticos para Uso de Animais de Laboratório (disponível no endereço: http://www.cobea.org.br/), elaborado pela SBCAL - Sociedade Brasileira da Ciência em Animais de Laboratório - e concordo plenamente com suas exigências durante a vigência deste protocolo; assim como a legislação nacional vigente - Lei no 11.794, de 8 de outubro de 2008 (http://www.planalto.gov.br/ccivil_03/_ato2007-2010/2008/lei/l11794.htm).

10.2. Este estudo não é desnecessariamente duplicativo, tem mérito científico e que a equipe que participa deste projeto foi treinada e é competente para executar os procedimentos descritos nesse protocolo;

10.3. Comprometo-me a solicitar nova aprovação deste protocolo sempre que ocorra alteração significativa nos experimentos aqui descritos;

10.4. Tudo o que foi declarado nesse protocolo é a absoluta expressão da verdade. Estou ciente que o não cumprimento das condições aqui especificadas é de minha total responsabilidade (pesquisador principal) e que estarei sujeito às punições previstas na legislação em vigor.

Nome do Executor: _____

Data: ___/___/_____ Assinatura: _____

Nome do Orientador: _____

Data: ___/___/_____ Assinatura: _____

DECISÃO DA CEUA/UNICAMP

Data da Reunião: ___/___/_____

☐ Aprovado ☐ Aprovado com recomendação ☐ Com pendências ☐ Reprovado

_____
Membro da CEUA

Reservado aos membros do CEUA/UNICAMP para anotações referentes a recomendações e pendências.

CEUA/UNICAMP
Caixa Postal 6109
13083-970 Campinas, SP - Brasil

Telefone: (19) 3521-6359
Telefax: (19) 3289-3124
E-mail: comisib@unicamp.br
http://www.ib.unicamp.br/ceea